

Synthetic, Spectroscopic and Electrochemical  
Studies of Ruthenium and Osmium Complexes.

by

Robert M. Christie

Thesis presented for the Degree of

Dr of Philosophy

University of Edinburgh

1989



To my Mother, Father and Gran.

## Declaration

Except where specific reference is made to other sources, the work presented in this thesis is the original work of the author. It has not been submitted, in whole or part, for any other degree.

R. M. CHRISTIE

### Acknowledgements

I am deeply indebted to my present supervisors Dr. M. Schröder and Dr. L. J. Yellowlees who have been unceasing in their help and encouragement since the departure of Dr. G. A. Heath and the premature death of Dr. T. A. Stephenson, my initial supervisors. I also wish to thank Dr. A. J. Blake for *data collection* and extensive help with the X-Ray structural analyses, Dr. T. Hyde for running e.s.r. spectra and solving the structure of  $[\text{RuCl}(\text{MeCN})(\text{PPh}_3)(\text{[9]aneS3})](\text{PF}_6)$  in conjunction with Dr. A. J. Blake and also Stuart MacGregor for help with the electrosynthesis of  $[\text{Ru}_2\text{Cl}_8(\text{Py})](\text{TBA})_2$ .

My thanks to Dr. S. G. D. Henderson for his instruction on the use of the Joel  $^{31}\text{P}$  n.m.r. instruments and along with John Miller and Miss Heather Grant for running various other n.m.r. spectra. In addition I would like to thank Mrs Elaine McDougall and Mr A. T. Taylor for performing the elemental analysis and mass spectral measurements respectively. I am indebted also to the S.E.R.C. for financial support, the University of Edinburgh for the use of facilities and Johnson-Matthey for generous loans of platinum metals. My thanks are also due to Tami Martin for the careful typing of this thesis.

Finally I would like to thank all the members of the inorganic chemistry research group, particularly Ruth, Ken, Alan and Stuart, for their encouragement and support during this work.

## A B S T R A C T

Chapter 1 gives a brief outline of general aspects of ruthenium and osmium chemistry.

Chapter 2 outlines the development of macrocyclic co-ordination chemistry, the origins of the macrocyclic effect and the synthesis and complexes of the trithiamacrocyclic [9]aneS<sub>3</sub>. A discussion is then given on the complexation of [9]aneS<sub>3</sub> to Ru(II) and Os(II) centres to yield the new complexes [(RuX(EPh<sub>3</sub>)([9]aneS<sub>3</sub>))(BF<sub>4</sub>)<sub>2</sub>] (X=Cl<sup>-</sup>, E=P, As; X=Br<sup>-</sup>, E=P) and [M(L)(L')(L'')( [9]aneS<sub>3</sub>)]<sup>n+</sup> (M=Ru, Os; L, L', L''=H<sup>-</sup>, Cl<sup>-</sup>, Br<sup>-</sup>, PR<sub>3</sub>, AsPh<sub>3</sub>, N-donors, CO, CS; n=1, 0). The complex [RuH(CO)(PPh<sub>3</sub>)([9]aneS<sub>3</sub>)](PF<sub>6</sub>) is found to be unstable in oxygenated solvents, in CH<sub>2</sub>Cl<sub>2</sub> one of the species formed is [RuCl(CO)(PPh<sub>3</sub>)([9]aneS<sub>3</sub>)](PF<sub>6</sub>) via what is thought to be an oxygenated species. The single crystal X-Ray structures of [RuCl(PEtPh<sub>2</sub>)<sub>2</sub>([9]aneS<sub>3</sub>)](PF<sub>6</sub>), [RuCl(MeCN)(PPh<sub>3</sub>)([9]aneS<sub>3</sub>)](PF<sub>6</sub>) and [OsH(CO)(PPh<sub>3</sub>)([9]aneS<sub>3</sub>)](PF<sub>6</sub>) confirms that [9]aneS<sub>3</sub> is fully co-ordinated. Analysis of the M-S (macrocyclic) bond lengths suggest a M→3dS bonding interaction. A high yield synthesis and the single crystal X-Ray structure of [Os([9]aneS<sub>3</sub>)<sub>2</sub>](PF<sub>6</sub>)<sub>2</sub> is also reported.

Chapter 3 details the electrochemical studies carried out on the ruthenium complexes discussed in Chapter 2, many of which exhibit a chemically reversible (II)/(III) couple. This allowed spectroscopic studies to be carried out in both the (II) and the (III) oxidation states via spectroelectrochemical techniques. Analysis of the results showed that the sulphur lone pairs of [9]aneS3 not involved in the Ru-S  $\sigma$ -bond are able to donate electron density to the metal centre. The energy and intensity of these transitions ( $\Pi S \rightarrow Ru$ ) are dependant on the trans ligand set L, L' and L".

Chapter 4 initially discusses the different classes of metal-metal interaction in mixed-valence complexes with particular reference to the family  $[L_{(3-x)}Cl_yRuCl_3RuCl_xL_{(3-x)}]^{n+/-}$ . Subsequent to this the electrochemical and chemical synthesis of the new complex  $[Cl_3RuCl_3RuCl_2(Py)](TBA)_2 (I^{2-})$  is detailed. From electrochemical studies it was found that two mixed-valence species could be generated and studied i.e.  $I^{3-} (Ru_2(II)(III))$  and  $I^- (Ru_2(III)(IV))$ . The two metal centres, from spectroscopic studies, were found to be strongly interacting in  $I^{3-}$  (Class IIIA) and weakly interacting in  $I^-$  (Class II).

Chapter 5 reports the synthesis of the heterotrimetallic complexes  $(\text{PEtPh}_2)_2\text{XRuX}_3\text{RuX}(\text{PEtPh}_2)_2\cdot\text{M}(\text{PEtPh}_2)$  ( $\text{X}=\text{Cl}^-$ ,  $\text{M}=\text{Cu}$ ,  $\text{HgCl}$ ;  $\text{X}=\text{Br}^-$ ,  $\text{M}=\text{Ag}$ ). The mercury complex is found to be unstable in solution yielding the species  $((\text{PEtPh}_2)_2\text{ClRuCl}_3\text{RuCl}(\text{PEtPh}_2)_2\cdot\text{HgCl})_2$ . A single crystal X-Ray structure of the copper complex reveals that the  $[\text{Cu}(\text{PEtPh}_2)]^+$  fragment is bound via one terminal and two bridging chlorides of the  $[(\text{PEtPh}_2)_2\text{ClRuCl}_3\text{RuCl}(\text{PEtPh}_2)_2]^-$  moiety.

Appendix 1 gives a short description of the electrochemical techniques employed in this work.

## Table of Contents

Chapter	Page
1 A General Survey of the Oxidation States Exhibited by Ruthenium and Osmium	1
1.1 Introduction	2
The (VIII) $d^0$ , (VII) $d^1$ and (VI) $d^2$ Oxidation States	5
The (V) $d^3$ Oxidation State	9
The (IV) $d^4$ Oxidation State	10
The (III) $d^5$ Oxidation State	15
The (II) $d^6$ Oxidation State	21
The (I) $d^7$ Oxidation State	27
The (0) $d^8$ Oxidation State	29
The (-I) $d^9$ and (-II) $d^{10}$ Oxidation States	30
References	32
2 Synthesis of Half Sandwich Complexes of Ru(II) and Os(II) with the Macrocyclic [9]aneS <sub>3</sub> .	44
2.1 Introduction	45
2.1.2 The Macrocyclic Effect	48
2.1.3 Synthesis and Complexes of [9]aneS <sub>3</sub>	52
Mo	56
Fe, Ru, Os	56
Co, Rh, Ir	58
Ni, Pd, Pt	60
Cu, Ag, Au	62
2.2 Results and Discussion	67
2.2.1 Achiral Bisphosphine Complexes:	



Chapter	Page
$[\text{RuX}(\text{PR}_3)_2([\text{9}] \text{aneS3})](\text{PF}_6)$	
a/x = $\text{Cl}^-$ , $\text{PR}_3 = \text{PMe}_2\text{Ph}$	67
b/x = $\text{Cl}^-$ , $\text{PR}_3 = \text{PEt}_2\text{Ph}$	69
c/x = $\text{Cl}^-$ , $\text{PR}_3 = \text{PMePh}_2$	71
d/x = $\text{Cl}^-$ , $\text{Br}^-$ ; $\text{PR}_3 = \text{PEtPh}_2$	71
2.2.2 Achiral Bishalo Complexes:	
$\text{RuX}_2(\text{EPh}_3)([\text{9}] \text{aneS3})$	77
2.2.3 Bis-Halo Dimers:	
$[(\text{RuX}(\text{EPh}_3)([\text{9}] \text{aneS3}))_2(\text{BF}_4)_2$	80
(X = $\text{Cl}^-$ , E = P, As; X = $\text{Br}^-$ , E = P)	
2.2.4 Chiral Complexes: $[\text{RuX}(\text{L})(\text{EPh}_3)([\text{9}] \text{aneS3})]^+$	81
2.2.5 Chiral Chlorocarbonyl and Chlorothiocarbonyl Complexes: $[\text{RuCl}(\text{EC})(\text{PR}_3)([\text{9}] \text{aneS3})](\text{PF}_6)$	
a/E = O, $\text{PR}_3 = \text{PPh}_3$	90
b/E = O, $\text{PR}_3 = \text{PEtPh}_2$	90
c/E = S, $\text{PR}_3 = \text{PPh}_3$	92
2.2.6 Chiral Hydridocarbonyl Complexes:	
$[\text{M}(\text{H})(\text{CO})(\text{PPh}_3)([\text{9}] \text{aneS3})](\text{PF}_6)$	
a/M = Ru	93
b/M = Os	101
2.2.7 $[\text{Os}([\text{9}] \text{aneS3})_2](\text{PF}_6)_2$	109
2.3 Conclusions	113
2.4 Experimental	114
References	137
3 Spectroscopic and Electrochemical Studies of Complexes of (9)aneS3	143
3.1 Introduction	144

Chapter	Page
1/ d-d Transitions or Ligand-field Transitions	145
2/ Ligand to Metal Charge Transfer (LMCT)	146
3/ Metal to Ligand Charge Transfer (MLCT)	148
4/ Intra-Ligand Transitions	150
3.2 Results and Discussion	150
3.2.1 UV/Vis/NIR Spectra in the (II) Oxidation State	150
3.2.2 Electrochemical Experiments	154
3.2.3 UV/Vis/NIR Spectra in the (III) Oxidation State	158
3.3 Conclusions	189
3.4 Experimental	190
References	192
4 Synthesis and Characterisation of $[\text{Ru}_2\text{Cl}_8(\text{Py})]^{n-}$ in Differing Oxidation States	193
4.1 Introduction	194
4.1.1 Class IIIA Behaviour	203
4.1.2 Class II Behaviour	207
4.1.3 Class I Behaviour	209
4.2 Results and Discussion	212
4.2.1 Electroreduction of $[\text{Ru}_2\text{Cl}_9]^{3-}$ in the Presence of Py	215
4.2.2 Purification of the Electrogenerated $[\text{Ru}_2\text{Cl}_8(\text{Py})]^{2-}$	216
4.2.3 Chemical Synthesis of $[\text{Ru}_2\text{Cl}_8(\text{Py})]^{2-}$	219
4.2.4 Spectroelectrochemical Synthesis of $[\text{Ru}_2\text{Cl}_8(\text{Py})]^{3-}$	223

Chapter	Page
4.2.5 Spectroelectrochemical Synthesis of $[\text{Ru}_2\text{Cl}_8(\text{Py})]^-$	230
4.3 Conclusions	233
4.4 Experimental	235
References	237
5 Heterotrimetallic Complexes of Ru(II)	239
5.1 Introduction	240
5.2 Results and Discussion	244
5.2.1 CuCl	244
5.2.2 HgCl <sub>2</sub>	250
5.2.3 AgBr	255
5.3 Conclusions	258
5.4 Experimental	259
References	262
Appendix 1 Electrochemical and Spectroelectrochemical Techniques	263
A.1.1 Electrochemical Techniques	
a/ Cyclic Voltammetry (c.v.)	264
b/ Stirred Linear Sweep Voltammetry	263
c/ Linear Sweep A.C. Voltammetry	263
A.1.2 Electrosynthesis	271
A.1.3 Spectroelectrosynthesis	273
References	275
Appendix 2 Abbreviations	276
Lecture Courses and Meetings Attended.	279

## List of Figures

	Page
Figure 2.1 Some Examples of Cyclic Polyethers	49
Figure 2.2 Some Examples of Cryptands	49
Figure 2.3 Conformation of Some Polythia Macrocycles	55
Figure 2.4 [9]aneS3 and Analogous 6e Donor Ligands	66
Figure 2.5 $^1\text{H}$ n.m.r. Spectrum of [RuCl(PMe <sub>2</sub> Ph) <sub>2</sub> ([9]aneS3)](PF <sub>6</sub> ) in CD <sub>3</sub> NO <sub>2</sub>	70
Figure 2.6 Ortep Plot of [RuCl(PEtPh <sub>2</sub> ) <sub>2</sub> ([9]aneS3)] <sup>+</sup>	73
Figure 2.7 $^{31}\text{P}$ -( $^1\text{H}$ ) n.m.r. Spectrum of [RuCl(PPh <sub>3</sub> )(PMe <sub>2</sub> Ph)([9]aneS3)](BF <sub>4</sub> ) in CDCl <sub>3</sub>	83
Figure 2.8 Ortep Plot of [RuCl(MeCN)(PPh <sub>3</sub> )([9]aneS3)] <sup>+</sup>	85
Figure 2.9 I.R. Spectrum (in the Region 1500–2100cm <sup>-1</sup> ) of the Product Mixture on Reacting RuCl <sub>2</sub> (CO)(DMF)(PEtPh <sub>2</sub> ) <sub>2</sub> with [9]aneS3	91
Figure 2.10 Synthesis of RuCl(CO)(PPh <sub>3</sub> )(C <sub>5</sub> H <sub>5</sub> ) from RuH(CO)(PPh <sub>3</sub> )(C <sub>5</sub> H <sub>5</sub> ) via Chloride Abstraction from CHCl <sub>3</sub>	94
Figure 2.11 I.R. Spectrum of [RuH(CO)(PPh <sub>3</sub> )([9]aneS3)](PF <sub>6</sub> ) in the Region 1800–2100cm <sup>-1</sup>	95
Figure 2.12 $^{31}\text{P}$ -( $^1\text{H}$ ) n.m.r. of [RuH(CO)(PPh <sub>3</sub> )([9]aneS3)](PF <sub>6</sub> )	97
Figure 2.13 UV/Vis/NIR Spectra of [RuH(CO)(PPh <sub>3</sub> )([9]aneS3)](PF <sub>6</sub> ) after 2 hours in Non-degassed Acetone (a) and Methylenechloride (b)	99
Figure 2.14 E.S.R. Spectrum of	

	Page
[RuH(CO)(PPh <sub>3</sub> )([9]aneS3)](PF <sub>6</sub> ) after 2 hours in Non-degassed Methylenechloride	100
Figure 2.15 I.R. Spectrum of [OsH(CO)(PPh <sub>3</sub> )([9]aneS3)](PF <sub>6</sub> ) in the Region 1800-2100cm <sup>-1</sup>	103
Figure 2.16 Ortep Plot of [OsH(CO)(PPh <sub>3</sub> )([9]aneS3)] <sup>+</sup>	105
Figure 2.17 Ortep Plot of [Os([9]aneS3) <sub>2</sub> ] <sup>2+</sup>	110
Figure 3.1 Possibility of $\pi S \rightarrow M$ CT Transitions in M(SR <sub>2</sub> ) Complexes via the Lone Pair not Involved in the $\sigma$ -Bond	144
Figure 3.2 $\pi L \rightarrow M$ CT Transitions in Low Spin d <sup>6</sup> and d <sup>5</sup> Octahedral Complexes	147
Figure 3.3 $M \rightarrow \pi L$ CT Transition in a Low Spin d <sup>7</sup> Octahedral Complex	149
Figure 3.4 UV/Vis/NIR Spectrum of RuCl <sub>2</sub> (PPh <sub>3</sub> )([9]aneS3) at 238K in CH <sub>2</sub> Cl <sub>2</sub>	153
Figure 3.5 Electrochemical Response of [RuCl(Py)(PPh <sub>3</sub> )([9]aneS3)] <sup>+</sup> at 238K in CH <sub>2</sub> Cl <sub>2</sub> /0.5M(TBA)(BF <sub>4</sub> )	157
Figure 3.6 Electrochemical Response of [RuCl(CO)(PPh <sub>3</sub> )([9]aneS3)] <sup>+</sup> at 238K in CH <sub>2</sub> Cl <sub>2</sub> /0.5M(TBA)(BF <sub>4</sub> )	159
Figure 3.7 Spectroelectrochemical Oxidation of [RuCl(Py)(AsPh <sub>3</sub> )([9]aneS3)]BF <sub>4</sub>	161
Figure 3.8 UV/Vis/NIR Spectrum of [RuCl <sub>2</sub> (PPh <sub>3</sub> )([9]aneS3)] <sup>+</sup> at 238K in CH <sub>2</sub> Cl <sub>2</sub>	162
Figure 3.9 UV/Vis/NIR Spectrum of [RuBr <sub>2</sub> (PPh <sub>3</sub> )([9]aneS3)] <sup>+</sup> at 238K in CH <sub>2</sub> Cl <sub>2</sub>	163

- Figure 3.10 UV/Vis/NIR Spectrum of  
 $[\text{RuCl}_2(\text{AsPh}_3)([\text{9}] \text{aneS3})]^+$  at 238K in  $\text{CH}_2\text{Cl}_2$  164
- Figure 3.11 UV/Vis/NIR Spectrum of  
 $[\text{RuCl}(\text{PEtPh}_2)_2([\text{9}] \text{aneS3})]^{2+}$  at 238K in  
 $\text{CH}_2\text{Cl}_2$  166
- Figure 3.12 UV/Vis/NIR Spectrum of  
 $[\text{RuBr}(\text{PEtPh}_2)_2([\text{9}] \text{aneS3})]^{2+}$  at 238K in  
 $\text{CH}_2\text{Cl}_2$  167
- Figure 3.13 UV/Vis/NIR Spectrum of  
 $[\text{RuCl}(\text{PMe}_2\text{Ph})_2([\text{9}] \text{aneS3})]^{2+}$  at 238K in  
 $\text{CH}_2\text{Cl}_2$  168
- Figure 3.14 UV/Vis/NIR Spectrum of  
 $[\text{RuCl}(\text{Py})(\text{PPh}_3)([\text{9}] \text{aneS3})]^{2+}$  at 238K in  
 $\text{CH}_2\text{Cl}_2$  170
- Figure 3.15 UV/Vis/NIR Spectrum of  
 $[\text{RuBr}(\text{Py})(\text{PPh}_3)([\text{9}] \text{aneS3})]^{2+}$  at 238K in  
 $\text{CH}_2\text{Cl}_2$  171
- Figure 3.16 UV/Vis/NIR Spectrum of  
 $[\text{RuCl}(\text{Py})(\text{AsPh}_3)([\text{9}] \text{aneS3})]^{2+}$  at 238K in  
 $\text{CH}_2\text{Cl}_2$  172
- Figure 3.17 UV/Vis/NIR Spectrum of  
 $[\text{RuBr}(\text{PMe}_2\text{Ph})(\text{PPh}_3)([\text{9}] \text{aneS3})]^{2+}$  at 238K in  
 $\text{CH}_2\text{Cl}_2$  174
- Figure 3.18 UV/Vis/NIR Spectrum of  
 $[\text{RuBr}(\text{PMe}_2\text{Ph})(\text{PPh}_3)([\text{9}] \text{aneS3})]^{2+}$  at 238K in  
 $\text{CH}_2\text{Cl}_2$  175

	Page
Figure 3.19 UV/Vis/NIR Spectrum of $[\text{RuBr}(\text{PMe}_2\text{Ph})(\text{AsPh}_3)([\text{9}]\text{aneS3})]^{2+}$ at 238K in $\text{CH}_2\text{Cl}_2$	176
Figure 3.20 UV/Vis/NIR Spectrum of $[\text{RuCl}(\text{P}(\text{OMe})_2\text{Ph})(\text{PPh}_3)([\text{9}]\text{aneS3})]^{2+}$ at 238K in $\text{CH}_2\text{Cl}_2$	173
Figure 3.21 UV/Vis/NIR Spectrum of $[\text{RuCl}(\text{PhCN})(\text{PPh}_3)([\text{9}]\text{aneS3})]^{2+}$ at 238K in $\text{CH}_2\text{Cl}_2$	179
Figure 3.22 Halide $\Pi$ -orbital Interaction in cis-dihalide Complexes	181
Figure 3.23 UV/Vis/NIR Spectra of $[\text{RuX}_2(\text{PPh}_3)([\text{9}]\text{aneS3})]^+$ ( $\text{X}=\text{Cl}^-, \text{Br}^-$ ) in the Region $30000\text{-}45000\text{cm}^{-1}$	183
Figure 3.24 UV/Vis/NIR Spectra of $[\text{RuX}(\text{PEtPh}_2)_2([\text{9}]\text{aneS3})]^{2+}$ ( $\text{X}=\text{Cl}^-, \text{Br}^-$ ) in the Region $10000\text{-}30000\text{cm}^{-1}$	184
Figure 3.25 UV/Vis/NIR Spectra of $[\text{RuX}_2(\text{PPh}_3)([\text{9}]\text{aneS3})]^+$ ( $\text{X}=\text{Cl}^-, \text{Br}^-$ ) in the Region $30000\text{-}45000\text{cm}^{-1}$	188
Figure 4.1 Confacial Bioctahedral Geometry Adopted by the Family of Complexes $[\text{L}_3\text{RuCl}_3\text{RuL}_3]^{n+/-}$	194
Figure 4.2 Some Examples of Triply Bridged Ruthenium Binuclear Complexes	196
Figure 4.3 Synthetic Routes to Mixed Valence Ruthenium Binuclear Complexes	197
Figure 4.4 Energy Configurational Co-ordinate Diagram for Valence Interchange in Symmetric Complexes	201

	Page
Figure 4.5 Energy Configurational Co-ordinate Diagram for Valence Interchange Taking into Consideration Polarised Solvent and Terminal Ligand Asymmetry	202
Figure 4.6 Visible/NIR Spectrum of $[(\text{NH}_3)_3\text{RuCl}_3\text{Ru}(\text{NH}_3)_3]^{2+}$ in MeCN	205
Figure 4.7 Schematic Representation of Metal Bonding Orbitals in Symmetric Triple Bridged Binuclear Ruthenium Complexes	206
Figure 4.8 $^{31}\text{P}$ -( $^1\text{H}$ ) n.m.r. Spectra of $(\text{PPh}_3)_2(\text{CO})\text{RuCl}_3\text{RuCl}(\text{PPh}_3)_2$ Before and After Oxidation	211
Figure 4.9 Proposed Scheme for the Electrosynthesis of $[\text{Ru}_2\text{Cl}_8\text{L}]^{n+/-}$	213
Figure 4.10 AC and Stirred Linear Sweep Responses of the Product Solution from a Typical Electroreduction/oxidation of $[\text{Ru}_2\text{Cl}_9]^{3-}$ in the Presence of Py	217
Figure 4.11 AC Response of the Reaction Solution During the Chemical Synthesis of $[\text{Ru}_2\text{Cl}_8(\text{Py})](\text{TBA})_2$	221
Figure 4.12 UV/Vis/NIR Spectrum of $[\text{Ru}_2\text{Cl}_8(\text{Py})](\text{TBA})_2$ in $\text{CH}_2\text{Cl}_2$	224
Figure 4.13 CV and AC Response of $[\text{Ru}_2\text{Cl}_8(\text{Py})](\text{TBA})_2$ in $\text{CH}_2\text{Cl}_2/0.5\text{M}(\text{TBA})(\text{BF}_4)$ at 238K	225
Figure 4.14 UV/Vis/NIR Spectra of $[\text{Ru}_2\text{Cl}_8(\text{Py})]^{2-/3-}$ in $\text{CH}_2\text{Cl}_2$ at 238K	226



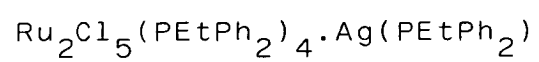
	Page
Figure 4.15 UV/Vis/NIR Spectra of $[\text{Ru}_2\text{Cl}_8(\text{Py})]^{2-/-1-}$ in $\text{CH}_2\text{Cl}_2$ at 238K	231
Figure 4.16 Plot of Eop vs $(1/n^2 - 1/D)$ for $[\text{Ru}_2\text{Cl}_8(\text{Py})]^-$ in Various Solvents	232
Figure 5.1 $^{31}\text{P}$ -( $^1\text{H}$ ) n.m.r. Spectrum of $\text{Ru}_2\text{Cl}_5(\text{PEtPh}_2)_4 \cdot \text{Ag}(\text{PEtPh}_2)$ at 183K in $\text{CD}_2\text{Cl}_2$	242
Figure 5.2 $^{31}\text{P}$ -( $^1\text{H}$ ) n.m.r. Spectrum of $\text{Ru}_2\text{Cl}_5(\text{PEtPh}_2)_4 \cdot \text{Cu}(\text{PEtPh}_2)$ at 184K in $\text{CD}_2\text{Cl}_2$	243
Figure 5.3 $^{31}\text{P}$ -( $^1\text{H}$ ) n.m.r. Spectrum of $\text{Ru}_2\text{Cl}_5(\text{PEtPh}_2)_4 \cdot \text{Cu}(\text{PEtPh}_2)$ at 184K in $\text{CD}_2\text{Cl}_2$	245
Figure 5.4 Ortep Plot of $\text{Ru}_2\text{Cl}_5(\text{PEtPh}_2)_4 \cdot \text{Cu}(\text{PEtPh}_2)$	247
Figure 5.5 $^{31}\text{P}$ -( $^1\text{H}$ ) n.m.r. Spectrum of $\text{Ru}_2\text{Cl}_5(\text{PEtPh}_2)_4 \cdot \text{HgCl}(\text{PEtPh}_2)$ at 183K and Ambient Temperature in $\text{CD}_2\text{Cl}_2$	252
Figure 5.6 $^{31}\text{P}$ -( $^1\text{H}$ ) n.m.r. Spectrum at 183K on Leaving $\text{Ru}_2\text{Cl}_5(\text{PEtPh}_2)_4 \cdot \text{HgCl}(\text{PEtPh}_2)$ at Ambient Temperature for Three Weeks in $\text{CD}_2\text{Cl}_2$	254
Figure 5.7 $^{31}\text{P}$ -( $^1\text{H}$ ) n.m.r. Spectrum of $\text{Ru}_2\text{Br}_5(\text{PEtPh}_2)_4 \cdot \text{Ag}(\text{PEtPh}_2)$ at 182K in $\text{CD}_2\text{Cl}_2$	257
Figure A.1 Standard Three-electrode Electrochemical Cell	264
Figure A.2 Cyclic and Stirred Linear Sweep Voltammograms of a Reversible and an Irreversible Charge Transfer Process	266
Figure A.3 Linear Sweep A.C. Voltammogram	270
Figure A.4 Typical Electrogeneration Current/Time Plot	272

	Page
Figure A.5 Modified Three-electrode Cell Used for Preparative-scale Electrosynthesis	272
Figure A.6 O.T.T.L.E. Cell	274

## List of Schemes

	Page
Scheme 1.1 Some Reactions of $\text{MO}_4$ (M = Ru, Os)	6
Scheme 1.2 Bonding in the Trans-dioxo $\text{MO}_2$ (VI) Moiety	8
Scheme 1.3 Some Reactions of $[\text{OsCl}_6]^{2-}$	11
Scheme 1.4 Some Reactions of $\text{RuCl}_3 \cdot 3\text{H}_2\text{O}$	16
Scheme 1.5 Some Reactions of $\text{RuCl}_3 \cdot 3\text{H}_2\text{O}$ with Trialkyl Phosphines and Arsines	17
Scheme 1.6 Some Reactions of $\text{RuCl}_2(\text{PPh}_3)_3$	25
Scheme 1.7 Some Reactions of $\text{Ru}_3(\text{CO})_{12}$	31
Scheme 2.1 Reaction of Trisethylenediaminenickel (II) with Acetone	46
Scheme 2.2 Reaction of 2,3-Octanedionebis-(mercaptoethylimino) nickel (II) with Dibromo-o-xylene	46
Scheme 2.3 The Metal Template Condensation of o-aminobenzaldehyde	46
Scheme 2.4 Molybdenum Template Synthesis of $[\text{9}]_{\text{aneS3}}$	53
Scheme 2.5 Formation of $[\text{Ru}_2\text{Cl}_3(\text{PMe}_2\text{Ph})_6] \text{Cl}$ from $\text{RuCl}_2(\text{PMe}_2\text{Ph})_4$	68
Scheme 2.6 Synthetic routes to $\text{RuCl}_2(\text{PPh}_3)([\text{9}]_{\text{aneS3}})$	79
Scheme 2.7 Formation of $\{\text{RuCl}(\text{PPh}_3)(\text{C}_6\text{H}_6)\}_2(\text{PF}_6)_2$ from $\text{RuCl}_2(\text{PPh}_3)([\text{9}]_{\text{aneS3}})$	82
Scheme 2.8 Synthetic Routes to the Chiral Complexes $[\text{RuCl}(\text{L})(\text{PPh}_3)([\text{9}]_{\text{aneS3}})]^+$	89
Scheme 2.9 Synthetic Routes to $[\text{RuCl}(\text{CO})(\text{PPh}_3)([\text{9}]_{\text{aneS3}})]^+$	102
Scheme 4.1 Proposed Scheme for the Electrosynthesis of $[\text{Ru}_2\text{Cl}_8\text{L}]^{n-}$ and $[\text{Ru}_2\text{Cl}_7\text{L}_2]^{n-}$	214

Scheme 5.1 Postulated Pathways for the Synthesis of



## List of Tables

	Page
Table 1.1 The Oxidation States of Ru and Os	4
Table 1.2 Some Complexes Containing the $\mu$ -Nitride Ligand	13
Table 2.1 Thermodynamics of Cu(II) Complex Formation with Tetraamine Ligands in Water	50
Table 2.2 Kinetic Data for Cu(II) Complexes	52
Table 2.3 Selected Bond Lengths (Å) with Standard Deviations for $[\text{RuCl}(\text{PEtPh}_2)_2([\text{9}]aneS3)]^+$	74
Table 2.4 Selected Angles ( $^\circ$ ) with Standard Deviations for $[\text{RuCl}(\text{PEtPh}_2)_2([\text{9}]aneS3)]^+$	74
Table 2.5 Selected Torsion Angles with Standard Deviations for $[\text{RuCl}(\text{PEtPh}_2)_2([\text{9}]aneS3)]^+$	75
Table 2.6 Selected Structural Parameters for $[\text{9}]aneS3$ Complexes of Ru(II)	76
Table 2.7 Some Experimental Parameters of the Chiral Complexes $[\text{RuX}(\text{L})(\text{ER}_3)([\text{9}]aneS3)](\text{BF}_4)$	85
Table 2.8 Selected Bond Lengths (Å) with Standard Deviations for $[\text{RuCl}(\text{PEtPh}_2)_2([\text{9}]aneS3)]^+$	87
Table 2.9 Selected Angles ( $^\circ$ ) with Standard Deviations for $[\text{RuCl}(\text{PEtPh}_2)_2([\text{9}]aneS3)]^+$	87
Table 2.10 Selected Torsion Angles ( $^\circ$ ) with Standard Deviations for $[\text{RuCl}(\text{PEtPh}_2)_2([\text{9}]aneS3)]^+$	88
Table 2.11 Selected Bond Lengths (Å) with Standard Deviations for $[\text{OsH}(\text{CO})(\text{PPh}_3)([\text{9}]aneS3)]^+$	106
Table 2.12 Selected Angles ( $^\circ$ ) with Standard Deviations for $[\text{OsH}(\text{CO})(\text{PPh}_3)([\text{9}]aneS3)]^+$	106

	Page
Table 2.13 Selected Torsion Angles ( $^{\circ}$ ) with Standard Deviations for $[\text{OsH}(\text{CO})(\text{PPh}_3)([\text{9}]\text{aneS3})]^+$	107
Table 2.14 Selected Structural Parameters for $[\text{9}]$ aneS3 Complexes of Os(II)	108
Table 2.15 Selected Bond Lengths (A) with Standard Deviations for $[\text{Os}([\text{9}]\text{aneS3})_2]^{2+}$	111
Table 2.16 Selected Angles ( $^{\circ}$ ) with Standard Deviations for $[\text{Os}([\text{9}]\text{aneS3})_2]^{2+}$	111
Table 2.17 Selected Torsion Angles ( $^{\circ}$ ) with Standard Deviations for $[\text{Os}([\text{9}]\text{aneS3})_2]^{2+}$	112
Table 2.18 $^{31}\text{P}$ -( $^1\text{H}$ ) and $^1\text{H}$ n.m.r. Spectra of the new $[\text{9}]$ aneS3 Complexes in d6-acetone Unless Otherwise Stated	135
Table 3.1 Variation of $\Pi\text{L}\rightarrow\text{M}$ CT Transition on Changing M, its Oxidation State and L	147
Table 3.2 Variation of $\text{M}\rightarrow\Pi\text{L}$ CT Transition on Changing M and its Oxidation State	149
Table 3.3 Spectral Data for $[\text{9}]$ aneS3 Complexes in the (II) Oxidation State at 238K in $\text{CH}_2\text{Cl}_2$	151
Table 3.4 Electrode Potentials for some $[\text{9}]$ aneS3 Complexes $E_{1/2}$ (volts) at 238K in $\text{CH}_2\text{Cl}_2/0.5\text{M}$ (TBA)( $\text{BF}_4$ )	155
Table 3.5 Variation of $\Delta E_p$ with Scan Rate for $[\text{RuCl}(\text{Py})(\text{PPh}_3)([\text{9}]\text{aneS3})]^+$ at 238K in $\text{CH}_2\text{Cl}_2/0.5\text{M}$ (TBA)( $\text{BF}_4$ )	156
Table 3.6 Spectral Data for $[\text{RuX}_2(\text{EPh}_3)([\text{9}]\text{aneS3})]^+$ ( $\text{X}=\text{Cl}^-$ , $\text{E}=\text{P}$ , $\text{As}$ ; $\text{X}=\text{Br}^-$ , $\text{E}=\text{P}$ ) at 238K in	

	Page
	165
Table 3.7	169
Table 3.8	173
Table 3.9	177
Table 3.10	180
Table 3.11	190
Table 4.1	198
Table 4.2	200
Table 4.3	210
Table 4.4	228
Table 4.5	229
Table 4.6	232

	Page
Table 5.1 Selected Bond Lengths (Å) with Standard Deviations for $\text{Ru}_2\text{Cl}_5(\text{PEtPhg}_2)_4\cdot\text{Cu}(\text{PEtPh}_2)$	248
Table 5.2 Selected Bond Angles ( $^\circ$ ) with Standard Deviations for $\text{Ru}_2\text{Cl}_5(\text{PEtPh}_2)_4\cdot\text{Cu}(\text{PEtPh}_2)$	248
Table 5.3 Selected Torsion Angles ( $^\circ$ ) with Standard Deviations for $\text{Ru}_2\text{Cl}_5(\text{PEtPh}_2)_4\cdot\text{Cu}(\text{PEtPh}_2)$	249
Table 5.4 Selected Bond Lengths (Å) and Bond Angles ( $^\circ$ ) for $\text{Ru}_2\text{Cl}_5(\text{PEtPh}_2)_4\cdot\text{M}(\text{PEtPh}_2)$ (M=Ag, Cu)	251
Table A.1 Cyclic Voltammetry Reversibility Criteria	267
Table A.2 A.C Voltammetry Reversibility Criteria	270



Chapter 1

A General Survey of the Oxidation States  
Exhibited by Ruthenium and Osmium

## Chapter 1.1

The work presented in this thesis deals with the preparation, characterisation and properties of a series of neutral, anionic and cationic complexes of ruthenium (Ru) and osmium (Os). These complexes mostly in the (II) and (III) oxidation states, range from macrocyclic compounds (Chapters 2 and 3) to binuclear (Chapter 4) and heterotrimetallic species (Chapter 5). A short review of Ru and Os co-ordination chemistry is given below.

### Introduction

Iron (Fe), ruthenium (Ru) and osmium (Os) form the first triad of the Group VIII transition elements with an outer electron configuration of  $nd^7 (n + 1)s^1$  ( $n = 3, 4$  and  $5$  respectively). The properties of Ru are found to be more closely related to those of Os than to its lighter congener Fe. This stems from the similarity in the atomic and ionic radii (and hence the ionisation potentials) of the two elements - a consequence of the lanthanide contraction that occurs between Ru and Os. Two of the most notable differences between Ru and Os and their lighter congener are:-

1. The high oxidation state complexes of Ru and Os are far more prevalent and stable than those of Fe. For instance Ru and Os both form complexes in the (VIII) oxidation state ( $d^0$ ) such as  $MO_4$  ( $M = Ru, Os$ ) for which iron has no counterpart. The (VI)

oxidation state ( $d^2$ ) is the highest found for Fe eg.  $[\text{FeO}_4]^{2-}$ .

2. Both Ru and Os form low spin complexes. This stems from the increased size of the 4d and 5d orbitals which lowers the energy required to pair electrons and also, for a given set of ligands, the ligand field splitting parameter,  $\Delta$ , is greater than for Fe. For example, all Ru and Os  $d^6$  and  $d^5$  complexes are low spin whereas those of Fe exhibit both low and high spin configurations.

A wide range of oxidation states is exhibited by complexes of Ru and Os ((VIII)  $\longrightarrow$  (-II)) with the (III) and (II) being the most common (see Table 1.1). As would be expected the observed oxidation state is dependent on the donor/acceptor properties of the ligand set. Thus, the high oxidation states are stabilised by  $\sigma$  and  $\Pi$ -donating ligands such as  $\text{F}^-$ ,  $\text{O}^{2-}$  and  $\text{N}^{3-}$ , while for the lowest oxidation states  $\sigma$  donor  $\Pi$ -acceptor ligands such as  $\text{PR}_3$  and  $\text{CO}$  are prevalent.

Ligands such as  $\text{H}_2\text{O}$  and  $\text{NH}_3$  which are good  $\sigma$ -donors but have little or no  $\Pi$ -acceptor or  $\Pi$ -donor properties are usually associated with the (III) and (II) states.

Table 1.1 The Oxidation States of Ru and Os

<u>Oxidation State</u>	<u>Examples</u>
(-II)	$[\text{Ru}(\text{PF}_3)_4]^{2-}$ , $[\text{Os}(\text{CO})_4]^{2-}$
(0)	$\text{Os}_3(\text{CO})_{11}(\text{MeCN})$ , $\text{Ru}(\text{CO})_4(\text{C}_2\text{H}_4)$
(I)	$\text{Ru}_2(\text{CO})_8(\text{SnMe}_3)_2$ , $(\text{Os}(\text{CO})_4\text{X})_2$
(II)	$\text{OsH}_2(\text{CO})(\text{PPh}_3)$ , $\text{Ru}(\text{C}_5\text{H}_5)_2$
(III)	$\text{Ru}(\text{sacsac})_3$ , $\text{mer-OsCl}_3(\text{Py})_3$
(IV)	$[\text{Ru}_2(\text{N})(\text{en})_5]^{5+}$ , $[\text{Os}(\text{C}_5\text{H}_5)_2(\text{OH})]^+$
(V)	$\text{Os}_2\text{Cl}_{10}$ , $\text{Ru}_2(\text{O})_2(\text{CH}_2\text{SiMe}_3)_6$
(VI)	$[\text{OsN}(\text{Me})_4]^-$ , $[\text{Ru}(\text{O})_2\text{Cl}_4]^{2-}$
(VII)	$\text{OsF}_7$ , $[\text{RuO}_4]^-$
(VIII)	$\text{RuO}_4$ , $[\text{Os}(\text{O})_4(\text{OH})_2]^{2-}$

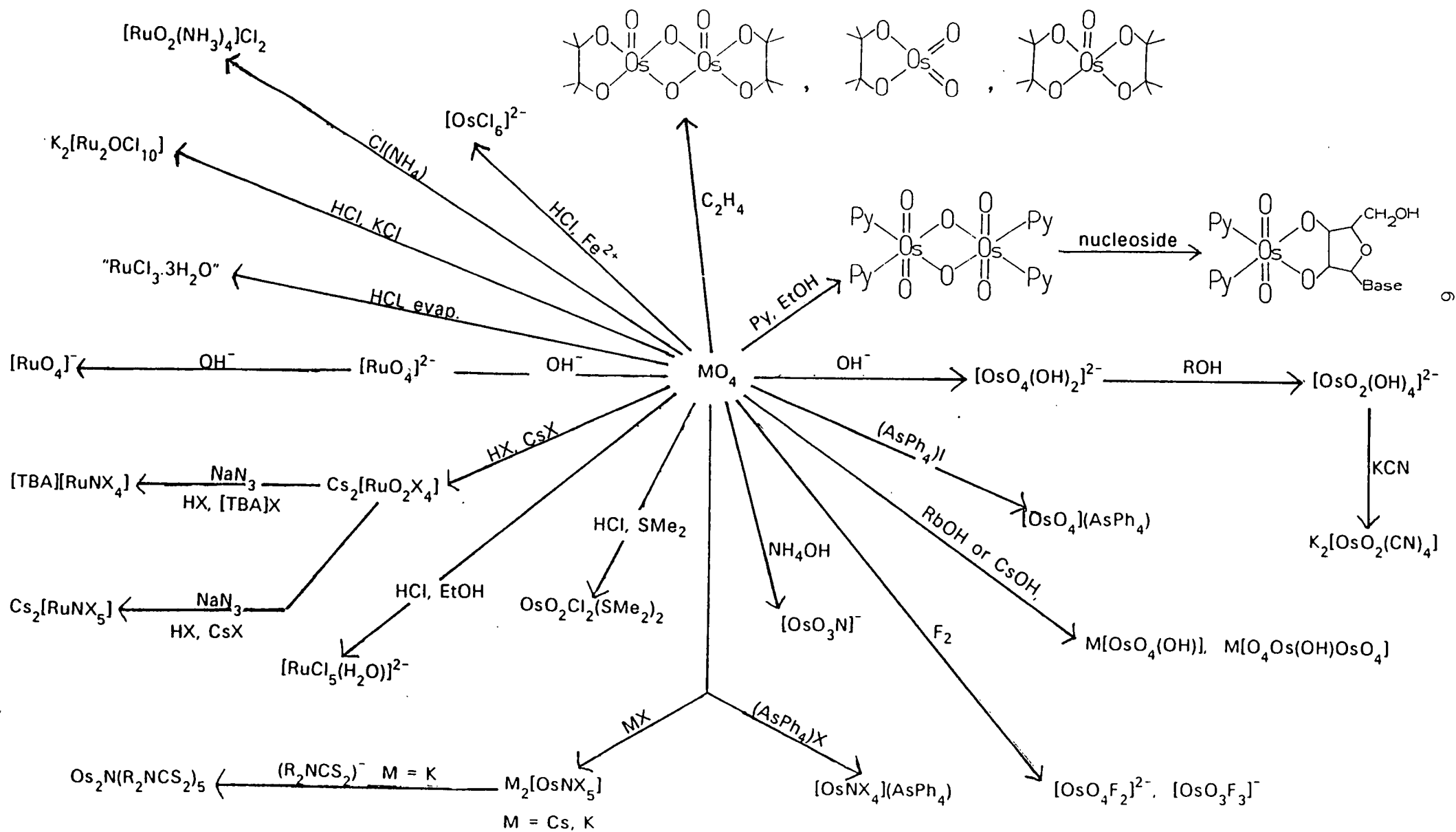
The (VIII)  $d^0$ , (VII)  $d^1$  and (VI)  $d^2$  Oxidation States.

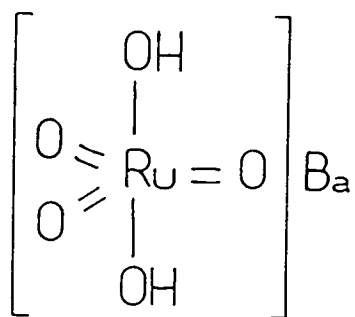
High valent complexes are dominated by small, electronegative ligands such as  $N^{3-}$ ,  $F^-$  but particularly  $O^{2-}$ , and it is therefore convenient to discuss these oxidation states as a group.

The tetrahedral tetroxides,  $MO_4$ , are poisonous, volatile crystalline solids and as can be seen from Scheme 1.1, are useful synthetic reagents.  $RuO_4$  is more sensitive to light and temperature, decomposing explosively above  $180^\circ$  to give  $RuO_2$  and  $O_2$ . Both tetroxides are powerful oxidising agents and are extensively used in organic synthesis. For instance, in the presence of  $ClO_3^-$ ,  $OsO_4$  can be used to catalytically convert olefins into cis-diols (via 1,2-diolato complexes - see Scheme 1.1)<sup>(1)</sup>.

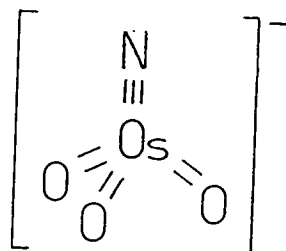
Contrasting behaviour is observed on dissolving the tetroxides in alkaline solution.  $RuO_4$  is initially reduced to  $[RuO_4]^-$ , which has a distorted tetrahedral structure<sup>(2)</sup>, then to  $[RuO_4]^{2-}$ . However, the single crystal structure of the barium salt of  $[RuO_4]^{2-}$  shows the complex to be  $Ba[RuO_3(OH)_2]^{(3)}$  [1].  $OsO_4$ , on the other hand, forms the perosmate ion  $[OsO_4(OH)_2]^{2-}$ <sup>(4)</sup>. Addition of concentrated ammonia to  $[OsO_4(OH)_2]^{2-}$  affords the nitrido complex  $[OsO_3N]^{-}$ <sup>(5)</sup> [2].

Scheme 1.1. Some Reactions of  $MO_4$  (M=Ru, Os).

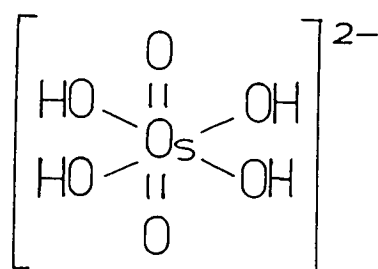




[1]



[2]

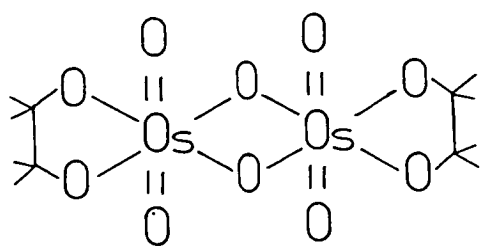
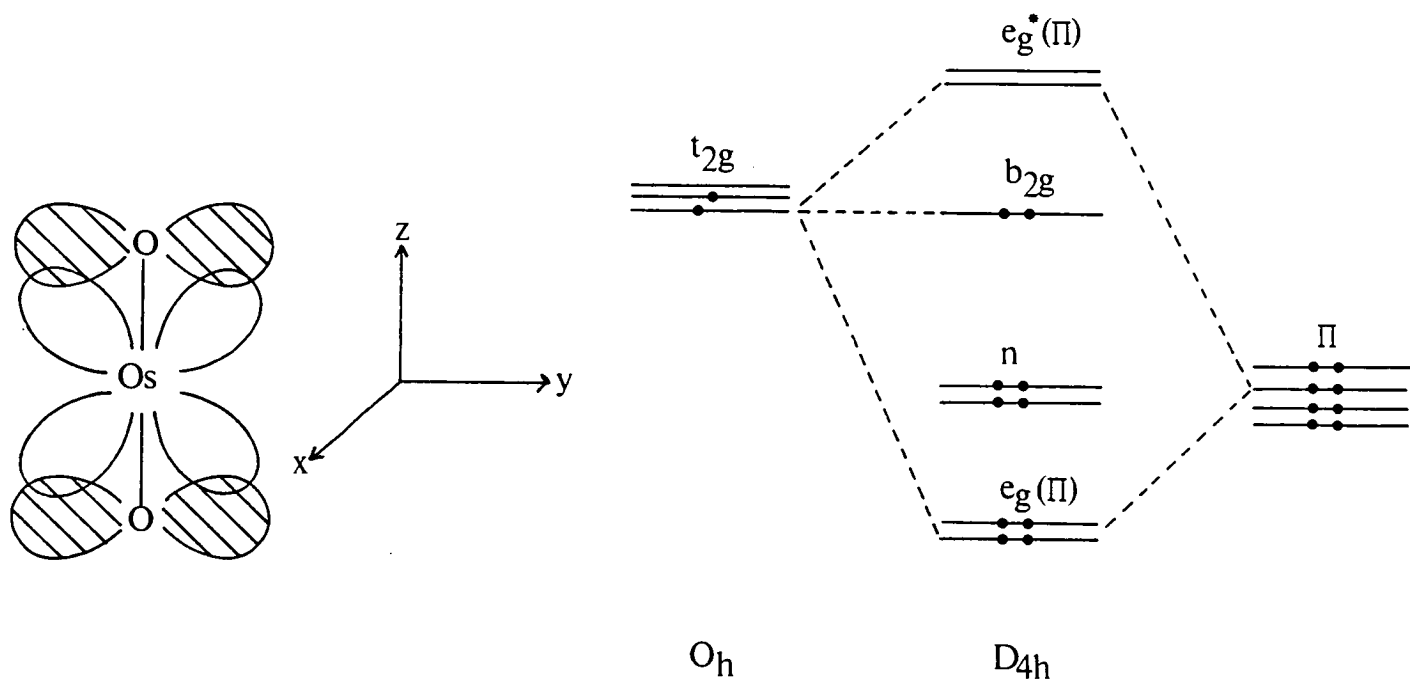


[3]

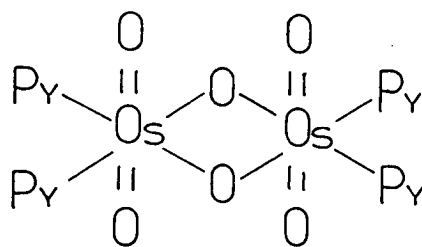
On reducing  $[\text{OsO}_4(\text{OH})_2]^{2-}$  with EtOH the osmate ion  $[\text{OsO}_2(\text{OH})_4]^{2-}$  is formed<sup>(6)</sup> [3]. This, along with its analogues such as  $[\text{OsO}_2\text{Cl}_4]^{2-}$ <sup>(7)</sup>,  $\text{OsO}_2\text{X}_2(\text{SMe}_2)_2$  (X=Cl, Br)<sup>(8)</sup>,  $\text{RuO}_2(\text{Py})_2(\text{OAc})_2$ <sup>(9)</sup> and  $\text{RuO}_2(\text{TMC})$ <sup>(10)</sup> possess a trans-dioxo group. The nature of the  $\Pi$ -bonding in the trans  $\text{MO}_2$  moiety is such that the symmetry of the d-orbitals is lowered to an extent that spin pairing becomes energetically favourable and thus these complexes are diamagnetic<sup>(11)</sup> (see Scheme 1.2).

Other oxo compounds include 1,2 diolato complexes such as  $\text{OsO}_2(1,2-\text{O}_2\text{C}_2\text{H}_4)$  and  $\text{trans}-(1,2-\text{O}_2\text{C}_2\text{Me}_4)\text{OsO}(\text{O})_2\text{OsO}(1,2-\text{O}_2\text{C}_2\text{Me}_4)$ <sup>(12)</sup> [4], the pyridine complex  $(\text{Py})_2\text{O}_2\text{Os}(\text{O})_2(\text{Py})_2$ <sup>(13)</sup> [5] and the hydroxide complexes  $[\text{OsO}_4(\text{OH})]^-$  and  $[\text{O}_4\text{Os}(\text{OH})\text{OsO}_4]^-$ <sup>(14)</sup> [6].

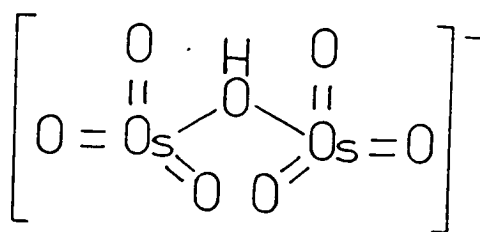
Scheme 1.2. Bonding in the Trans-dioxo  $\text{MO}_2$  (VI) Moiety.



[4]



[5]



[6]

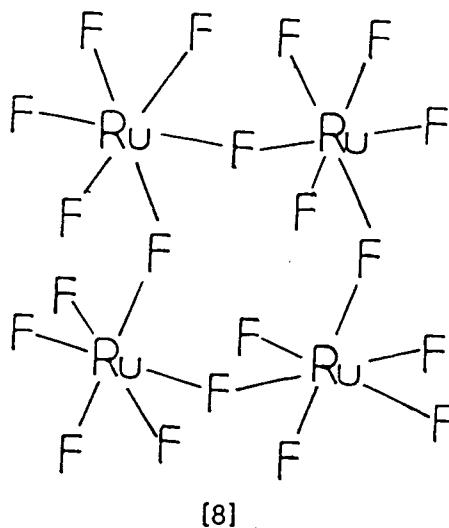
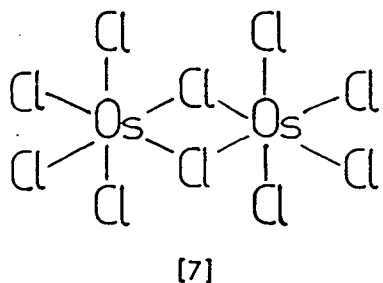


Halonitrido complexes such as  $[\text{MNX}_4]^-$  and  $[\text{MNX}_5]^{2-}$  ( $\text{M}=\text{Ru}, \text{Os}$ ;  $\text{X}=\text{Cl}^-, \text{Br}^-$ )<sup>(15)</sup> can be synthesised (see Scheme 1.1) and these are useful precursors for other nitrido complexes. For instance  $[\text{RuNCl}_4]^-$  reacts with  $\text{EPh}_3$  to yield  $\text{RuNCl}_3(\text{EPh}_3)$  ( $\text{E}=\text{As}$ <sup>(16)</sup>,  $\text{Sb}$ <sup>(17)</sup>) while  $[\text{OsNCl}_4]^-$  and its derivative  $[\text{OsN}(\text{OSiMe}_3)_4]^-$  will react with  $\text{MgR}_2$ ,  $\text{AlR}_3$  or  $\text{XMgR}$  to give complexes such as  $\text{OsNCl}_2(\text{CH}_2\text{SiMe}_3)_2$  (cis and trans) and  $[\text{OsNR}_4]^-$  ( $\text{R}=\text{CH}_2\text{SiMe}_3, \text{CH}_2\text{Ph}, \text{CH}_2\text{CMe}_3, \text{Me}$ )<sup>(18)</sup>.

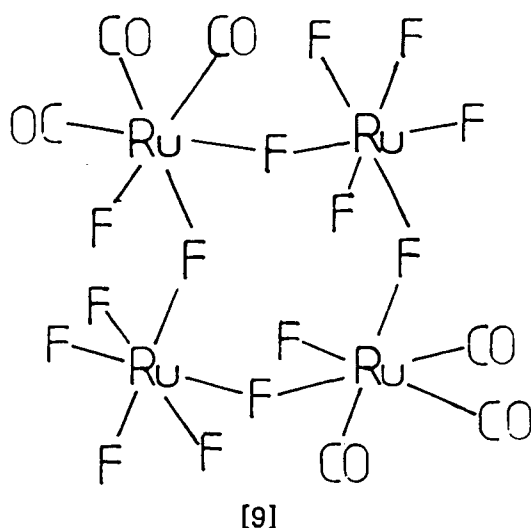
Finally fluoro complexes such as  $[\text{OsO}_4\text{F}_2]^-$ ,  $[\text{OsO}_3\text{F}_3]^-$ <sup>(19)</sup>,  $\text{RuF}_6$ <sup>(20)</sup> and  $\text{OsF}_7$ <sup>(21)</sup>, the latter two formed by direct fluorination of the metal, are also known.

### The (V) $d^3$ Oxidation State

Very few Ru and Os complexes are found in the (V) oxidation state. These include  $[\text{Os}(\text{O})_2(\text{TMC})]^+$ <sup>(22)</sup>,  $\text{Na}_3[\text{RuO}_4]$ <sup>(23)</sup>,  $\text{Ru}_2(\text{O})_2(\text{R})_6$ ,  $\text{Ru}_2(\text{NPh})_2(\text{R})_6$  ( $\text{R}=\text{CH}_2\text{SiMe}_3$ )<sup>(24)</sup> and some halide species such as  $[\text{MF}_6]^-$ ,  $[\text{OsCl}_5]_2$ <sup>(25)</sup> [7] and  $[\text{RuF}_5]_4$ , the Ru-F-Ru linkages being non-linear<sup>(26)</sup> [8].



$[\text{RuF}_5]_4$ , will react with  $\text{XeF}_2$  (2:1) to yield the dimer  $(\text{XeF})[\text{Ru}_2\text{F}_{11}]$  (27) and with CO or  $\text{Ru}_3(\text{CO})_{12}$  to yield the mixed Ru(V)-Ru(II) complex  $[\text{RuF}_2(\text{CO})_3 \cdot \text{RuF}_5]_2$  which is proposed to have a tetranuclear structure from IR and magnetic measurements [9] (28)



### The (IV) $d^4$ Oxidation State

Ru (IV) and Os (IV) complexes usually have an octahedral or distorted octahedral co-ordination sphere with a low spin  $t_{2g}^4$  configuration. A number of neutral halide complexes are known such as  $\text{RuF}_4$ , however it is the hexahalogeno anions  $[\text{MX}_6]^{2-}$  ( $\text{M}=\text{Ru}$ ,  $\text{X}=\text{F}^-, \text{Cl}^-, \text{Br}^-$ ;  $\text{M}=\text{Os}$ ,  $\text{X}=\text{F}^-, \text{Cl}^-, \text{Br}^-, \text{I}^-$ ) which are the more synthetically useful. For instance  $[\text{OsCl}_6]^{2-}$  reacts with a wide range of substrates some examples of which are given in Scheme 1.3.

Scheme 1.3 Some Reactions of  $[\text{OsCl}_6]^{2-}$

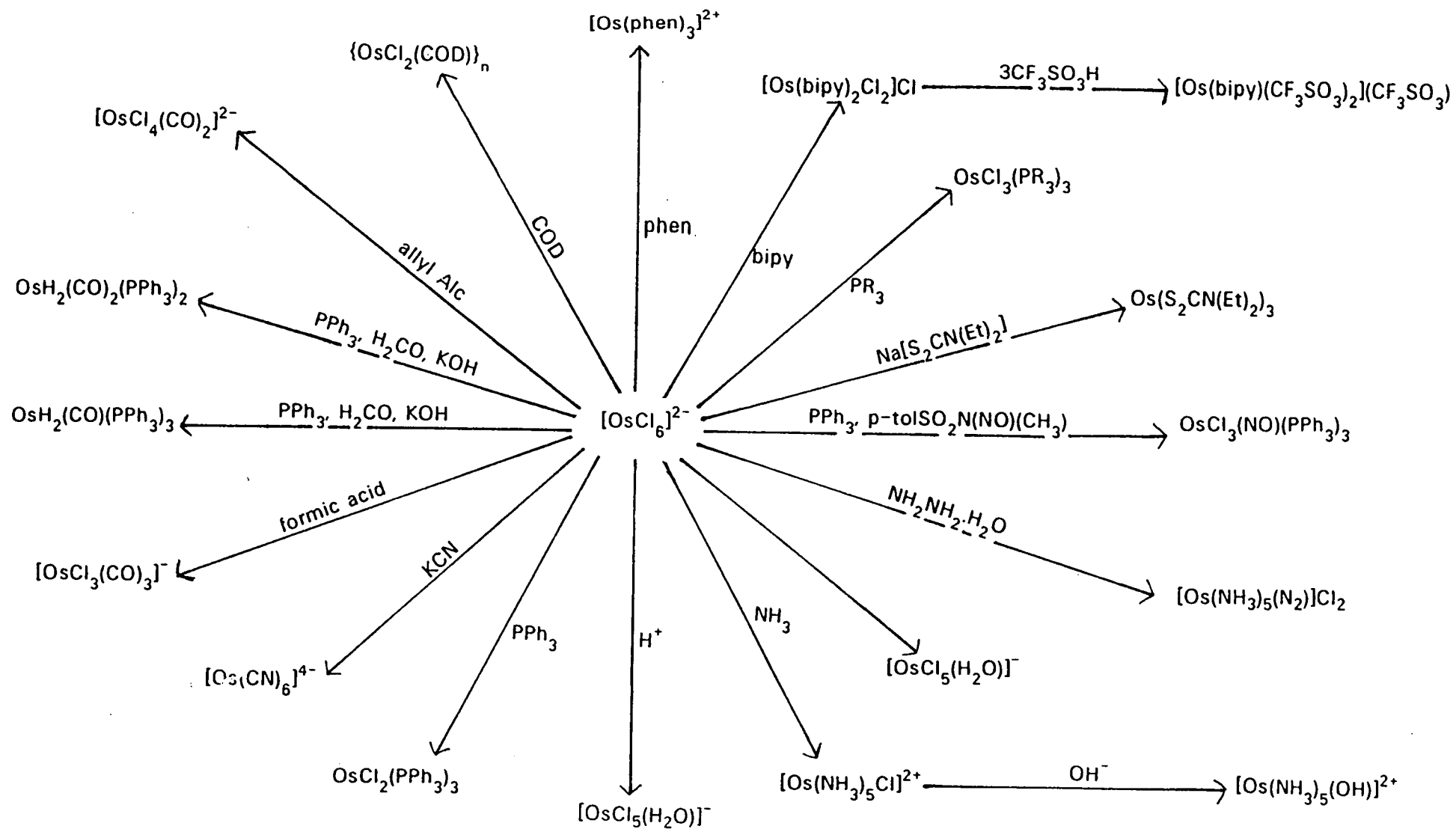
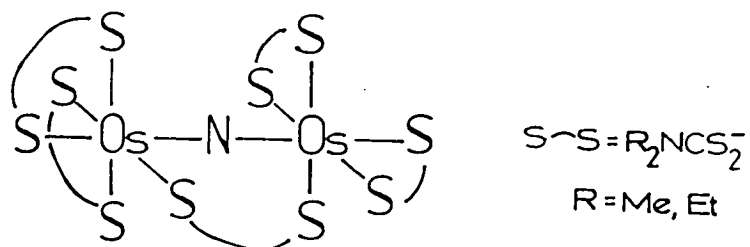
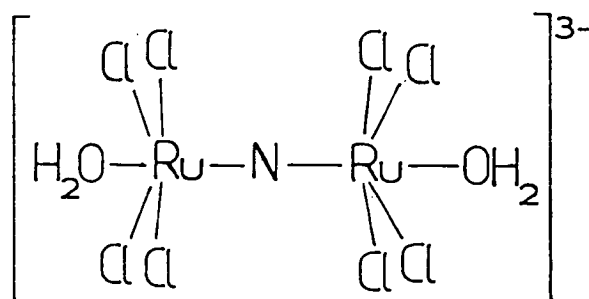




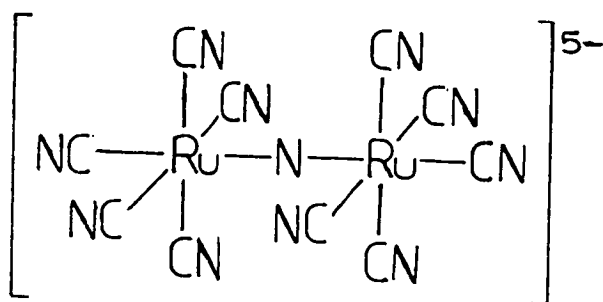
Table 1.2. Some Complexes Containing the  $\mu$ -Nitrido Ligand.



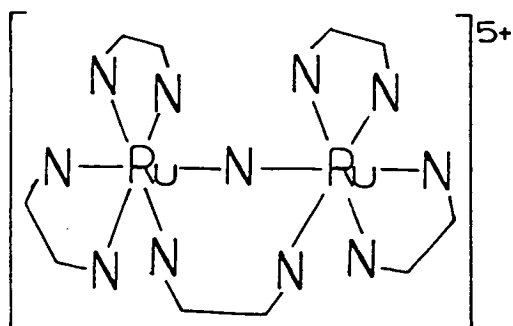
ref 35



ref 36



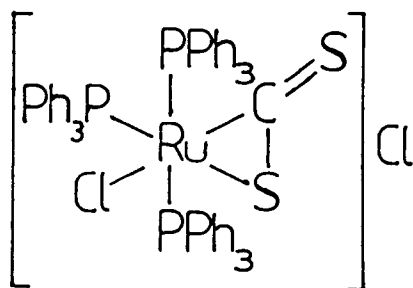
ref 37



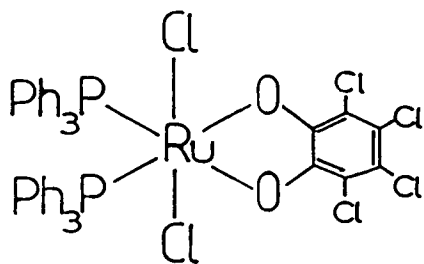
ref 38

of a simple molecular orbital treatment similar to that given by Dunitz and Orgel for  $[\text{Ru}_2\text{OCl}_{10}]^{4-}$  (39).

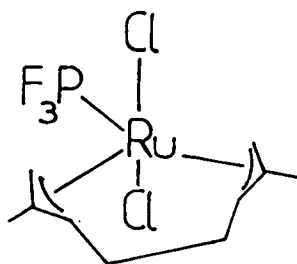
Other complexes containing N-donor ligands include  $\text{trans-RuCl}_4(\text{Py})_2$  (40),  $\text{RuCl}_4(\text{bipy})$  (41) and  $\text{RuCl}_3(\text{NMe}_2\text{Ph})(\text{AsPh}_3)_2$ , formed by the reaction of  $\text{RuNCl}_3(\text{AsPh}_3)_2$  with  $\text{PMe}_2\text{Ph}$  (42). A number of trialkyl phosphine and arsine complexes are formed e.g.  $[\text{RuH}_3(\text{PMe}_2\text{Ph})_4](\text{PF}_6)$  (43),  $[\text{Os}(\text{diars})_2\text{Cl}_2]^{2+}$  (44),  $[\text{RuCl}(\text{CS})(\text{PPh}_3)_3]\text{Cl}$  (45) [12] and  $\text{Ru}(1,2\text{-O}_2\text{C}_6\text{Cl}_4)(\text{PPh}_3)_2\text{Cl}_2$  [13] (45), formed by the reaction of  $\text{RuCl}_2(\text{PPh}_3)_3$  and tetrachloro-1, 2-benzoquinone in propanone.



[12]



[13]



[14]

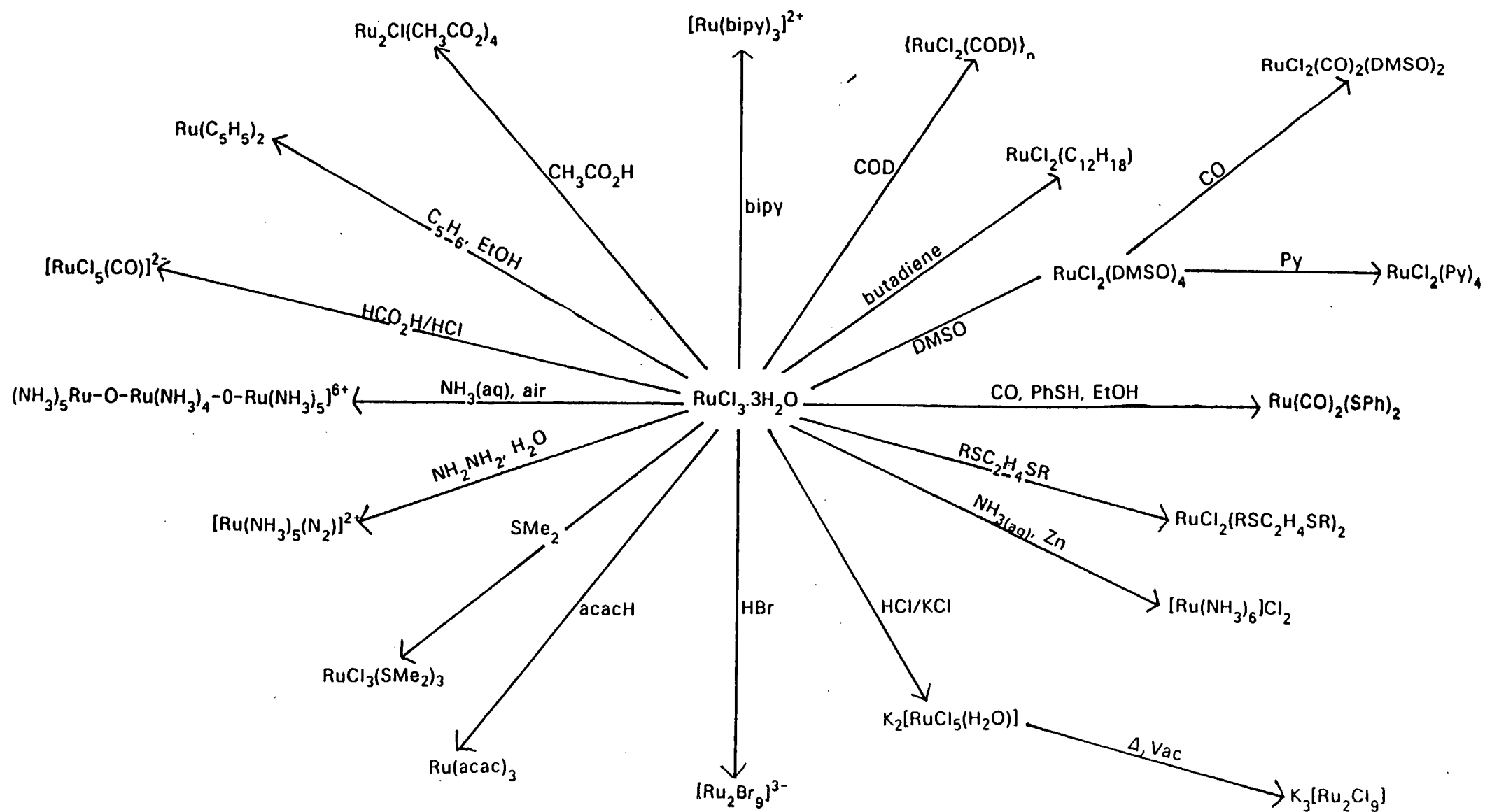
Finally a number of group IVB complexes such as  $[\text{RuCl}_2(\text{C}_{10}\text{H}_{16})]_2$  (47),  $\text{RuCl}_2(\text{PF}_3)(\text{C}_{10}\text{H}_{16})$  (48) [14],  $[\text{Os}(\text{C}_5\text{H}_5)_2(\text{OH})](\text{PF}_6)$  (49) and  $\text{RuH}_3(\text{SiR}_3)(\text{PPh}_3)_3$  ( $\text{SiR}_3 = \text{SiEt}_3$ ,  $\text{SiMe}_2\text{Ph}$ ,  $\text{SiPh}_3$  etc) (50,51,52) have been synthesised.

### The (III) $d^5$ Oxidation State

Most Ru and Os complexes in the (III) oxidation state are octahedral with a low spin  $t_{2g}^5$  configuration. As it is one of the two commonest oxidation states for the two metals (the other being the (II) state) a full survey cannot be given.

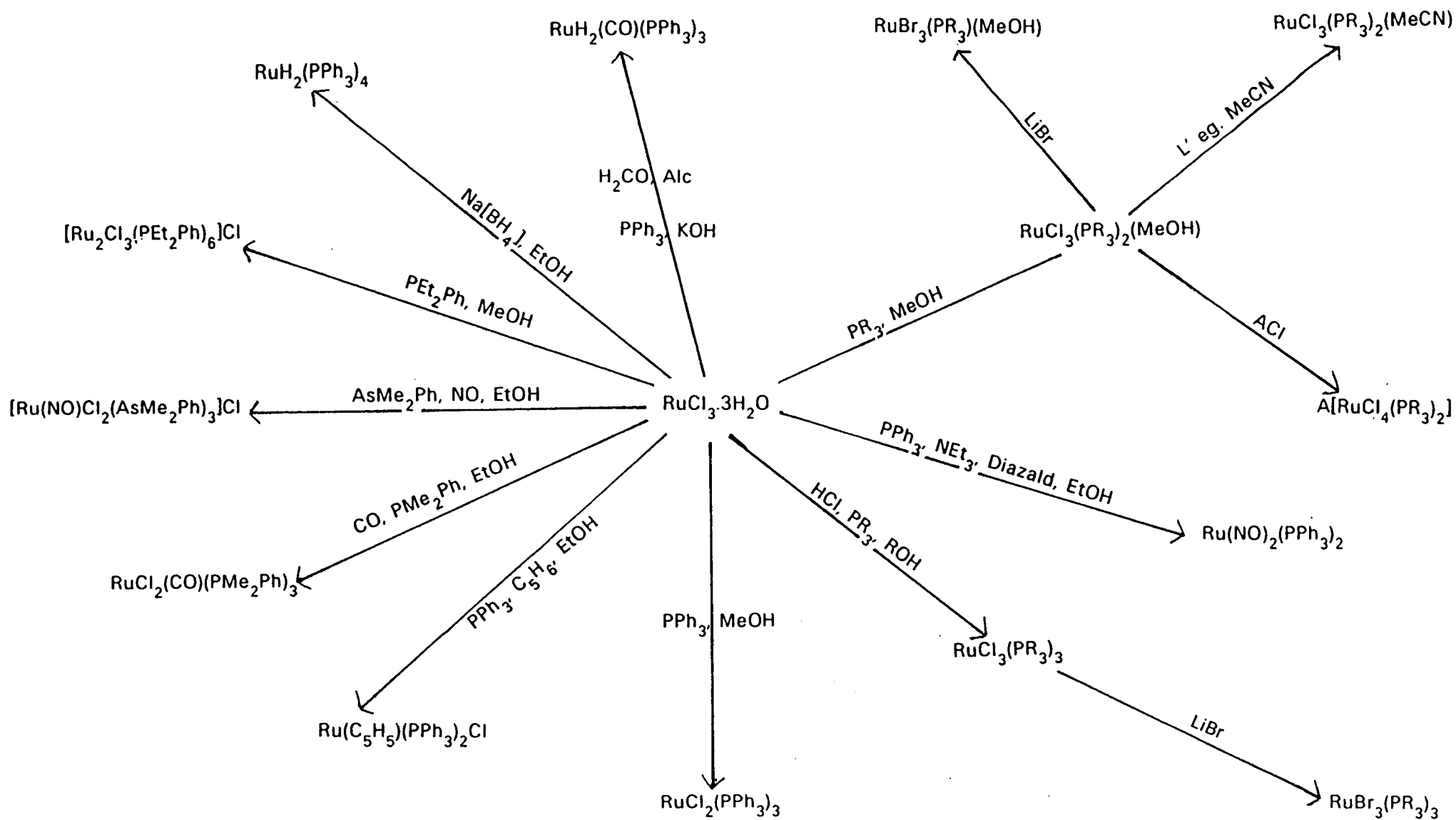
In addition to hexahalo anions such as  $[\text{RuCl}_6]^{3-}$  a number of trihalides,  $\text{MX}_3$  ( $\text{M} = \text{Ru}$ ,  $\text{X} = \text{F}^-$ ,  $\text{Cl}^-$ ,  $\text{Br}^-$ ,  $\text{I}^-$ ;  $\text{M} = \text{Os}$ ,  $\text{X} = \text{Cl}^-$ ,  $\text{Br}^-$ ,  $\text{I}^-$ ), are also known.  $\text{RuCl}_3$  is commercially available as  $\text{RuCl}_3 \cdot 3\text{H}_2\text{O}$  (in fact a mixture of Ru(III) and Ru(IV)) and is a common starting reagent, some general reactions of which are shown in Scheme 1.4. This is further demonstrated by its reactions to form trialkyl phosphine and arsine complexes as shown in Scheme 1.5.

Scheme 1.4. Some Reactions of  $\text{RuCl}_3 \cdot 3\text{H}_2\text{O}$ .



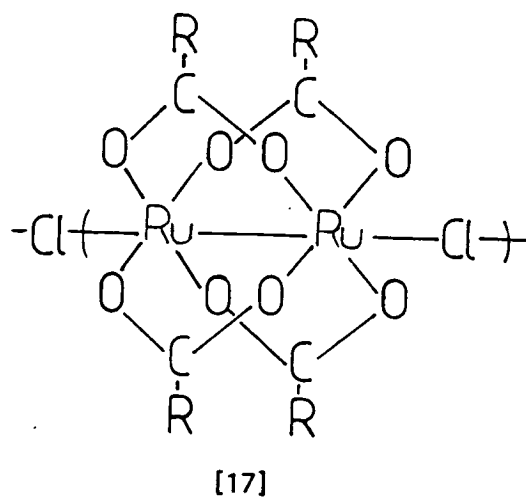
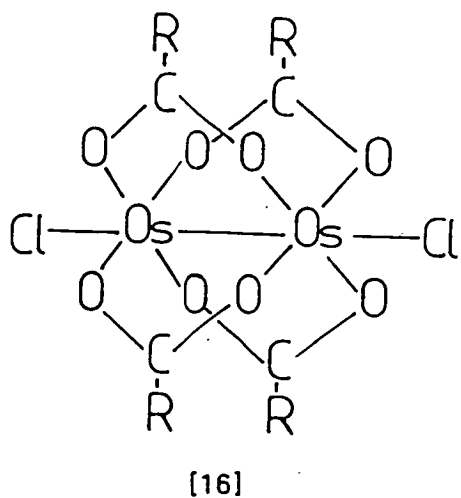
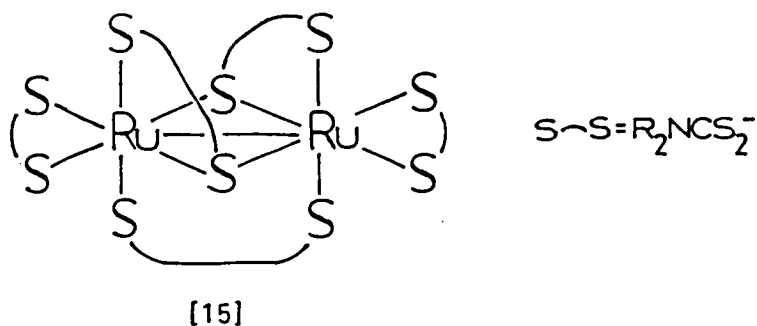


Scheme 1.5. Some Reactions of  $\text{RuCl}_3 \cdot 3\text{H}_2\text{O}$  with Trialkyl Phosphines and Arsines.



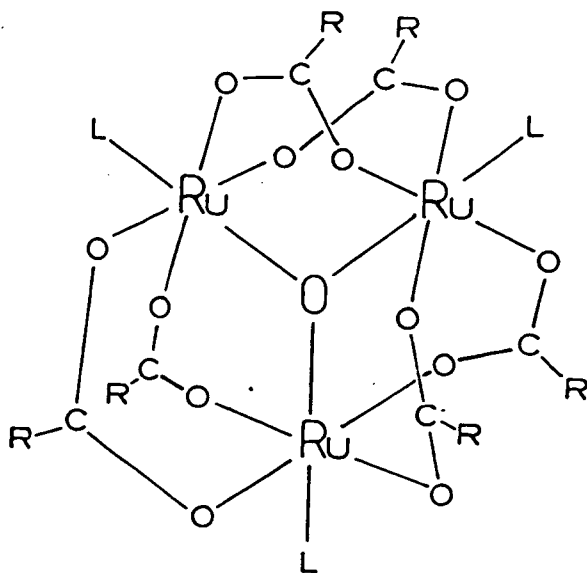
The reaction conditions are usually critical, for instance  $\text{RuCl}_3 \cdot 3\text{H}_2\text{O}/\text{PPh}_3$  stirred in MeOH yields  $\text{RuCl}_3(\text{PPh}_3)_2(\text{MeOH})$  whereas if the reaction is carried out under reflux  $\text{RuCl}_2(\text{PPh}_3)_3$  is formed.

Both Ru and Os form a number of complexes containing monodentate oxygen and sulphur donor ligands (see Schemes 1.3 and 1.4 for some examples). However, perhaps the more interesting complexes are formed by chelating ligands of these Group VIB donors.



Such ligands not only form monomers e.g.  $\text{Ru}(\text{acac})_3$  (53),  $\text{Os}(\text{sacsac})_3$  (54) and  $[\text{Ru}(\text{ox})_2(\text{Py})_2]^-$  (55) but also a number of binuclear and some higher nuclearity species. These include  $[\text{Ru}_2(\text{SCNR}_2)_5](\text{BF}_4)$  ( $\text{R}=\text{Me}, \text{Et}, \text{benzyl}$ ) (56) [15], which due to the formation of a metal-metal bond is diamagnetic,  $\text{Os}_2(\text{RCO}_2)_4\text{Cl}_2$  (e.g.  $\text{R}=\text{Me}, \text{Pr}^n, \text{But}^n$ ) (57) [16] and the mixed valence,  $\text{Ru}_2(\text{III})(\text{II}), \text{complex } \text{Ru}_2(\text{RCO}_2)\text{Cl}$  (e.g.  $\text{Me}, \text{Et}, \text{Pr}^n$ ) [17] (58). Interestingly the latter mixed-valence complexes (from magnetic moment measurements of between 4.0 and 4.6 BM) are thought to contain three unpaired electrons.

A number of trinuclear carboxylate complexes are known that have the  $\mu^3\text{O}$  centred structure  $[\text{Ru}_3\text{O}(\text{L})_3(\text{O}_2\text{CR})_6]^{n+}$  (18) (e.g.  $n=1, \text{L}=\text{H}_2\text{O}, \text{Py}, \text{R}=\text{CH}_3, \text{C}_2\text{H}_5, \text{C}_3\text{H}_7$ ;  $n=1, \text{L}=\text{H}_2\text{O}, \text{Py}, \text{R}=\text{CH}_3$ ) (59) this being confirmed by an X-Ray study carried out on the  $\text{PPh}_3$  analogue  $\text{Ru}_3\text{O}(\text{PPh}_3)_2(\text{O}_2\text{CMe})_6$  (60). A similar structure to [18] is probably present for the complexes  $\text{Ru}_3(\text{L})_3(\text{O}_2\text{CMe})_6$  ( $\text{L}=\text{H}_2\text{O}, \text{Py}$ ) (59) which do not possess the  $\mu^3\text{O}$  moiety.



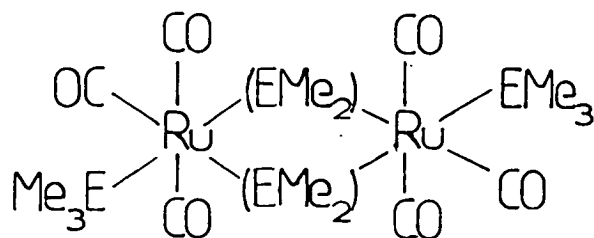
[18]

Complexes containing group VB donors are very common. For example both metals form a variety of ammine and amine complexes such as  $[\text{Ru}(\text{NH}_3)_6]^{3+}$  (61),  $[\text{Ru}(\text{NH}_3)_5(\text{L})]^{2+}$  (e.g.  $\text{L}=\text{N}_3^-$ ,  $\text{OH}^-$ ,  $\text{MeCO}_2^-$ ,  $\text{NCSe}^-$ ,  $\text{NCS}^-$ ,  $\text{NCO}^-$ ) (62,63,64) synthesised from  $[\text{Ru}(\text{NH}_3)_5\text{Cl}]^{2+}$ ,  $[\text{M}(\text{en})_2\text{Cl}_2]^+$   $[\text{MCl}_2(\text{cyclam})]^+$  ( $\text{M}=\text{Ru}$  (65),  $\text{Os}$  (66)) and  $[\text{Ru}(\text{en})_3]^{3+}$  (67). There are also a large number of heterocyclic aromatic N-donor complexes e.g.  $\text{mer-RuCl}_3(\text{Py})_3$  (68),  $[\text{Os}(\text{phen})_3]^{3+}$  (69) and  $[\text{Ru}(\text{bipy})(\text{acac})(\text{Py})_2]^{2+}$  (70).

As well as monomers, a number of binuclear complexes such as  $[(\text{NH}_3)_n\text{Ru-B-Ru}(\text{NH}_3)_n]^{n+}$  (e.g.  $n=5$ ,  $\text{B}=\text{py}$  (71);  $n=4$ ,  $\text{B}=(\text{NH}_2^-)_2$  (72)) and  $[(\text{phen})_2\text{ClRu}(\text{pz})\text{RuCl}(\text{phen})_2]^{3+}$  (73) are known.

Particular attention is given to the formally mixed valence state,  $\text{M}_2(\text{III})(\text{II})$ , of these complexes, if it can be generated, in order to determine the interaction between the two metal centres with respect to the "odd" electron (see Chapter 4).

Complexes containing trialkyl phosphine and arsine ligands are common with many being directly synthesised from  $\text{RuCl}_3 \cdot 3\text{H}_2\text{O}$  or  $[\text{OsCl}_6]^{2-}$  (see Schemes 1.3 and 1.5). They can be monomeric e.g.  $\text{OsCl}_3(\text{PEt}_2\text{Ph})_3$  (74),  $[\text{RuBr}_4(\text{AsPh}_3)_2](\text{AsPh}_4)$  (75),  $\text{RuCl}_3(\text{PPh}_3)_2(\text{L})$  (e.g.  $\text{L}=\text{MeOH}$ ,  $\text{DMSO}$ ,  $\text{SMe}_2$ ,  $\text{CS}_2$ ) (76) or binuclear species such as  $(\text{PMe}_3)_3\text{Ru}(\text{CH}_2)_3\text{Ru}(\text{PMe}_3)_3$  (77) and  $\text{Os}_2\text{Cl}_5(\text{EPh}_3)_4$  ( $\text{E}=\text{P}$ ,  $\text{As}$ ) (78).



[19]

Carbonyl complexes are also known such as  $\text{Ru}(\text{CO})_3\text{F}_3$  (79) formed by the action of an excess of  $\text{XeF}_2$  on  $\text{Ru}_3(\text{CO})_{12}$ ,  $\text{Cs}_2[\text{Ru}(\text{CO})\text{X}_5]$  ( $\text{X}=\text{Cl}^-$ ,  $\text{Br}^-$ ) (80),  $[\text{OsX}_4(\text{CO})_2](\text{Et}_4\text{N})$  ( $\text{X}=\text{Cl}^-$ ,  $\text{Br}^-$ ,  $\text{I}^-$ ) (81) and  $\text{Ru}_2(\text{CO})_6(\text{EMe}_3)_2(\text{EMe}_2)_2$  ( $\text{E}=\text{Si}$  (82),  $\text{Ge}$  (83),  $\text{Sn}$  (84)) [19]. In addition some organometallic compounds have been reported e.g.  $\text{Ru}_2\text{R}_6$  ( $\text{R}=\text{CH}_2\text{SiMe}_3$ ,  $\text{CH}_2\text{CMe}_3$ ),  $\text{Os}_2\text{R}_4(\text{O}_2\text{CMe})_2$  ( $\text{R}=\text{CH}_2\text{SiMe}_3$ ,  $\text{CH}_2\text{CMe}_3$ ) and  $\text{Os}(\text{C}_3\text{H}_5)_2(\text{CH}_2\text{CMe}_3)_4$  (24).

### The (II) $d^6$ Oxidation State

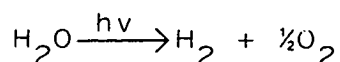
$\text{Ru}$  and  $\text{Os}$  complexes in the (II) oxidation state are nearly always octahedral with a  $t_{2g}^6$  configuration. A large number of  $\text{M}(\text{II})$  complexes can be prepared directly from commercial  $\text{RuCl}_3 \cdot 3\text{H}_2\text{O}$ ,  $[\text{OsCl}_6]^{2-}$  (see Schemes 1.3-1.5) or their halide analogues.

Both metals form a number of complexes containing Group VIB donors. These include  $[\text{Ru}(\text{H}_2\text{O})_6]^{2+}$  (85),  $\text{Ru}(\text{acac})_2\text{L}_2$  ( $\text{L}=\text{CO}$  (86),  $\text{PPh}_3$  (87)),  $[\text{Ru}(\text{O}-\text{DMSO})_2(\text{S}-\text{DMSO})_4](\text{BF}_4)_2$  (88),

$[(\text{NH}_3)_4\text{Ru}(\text{SO}_2)\text{Cl}]\text{Cl}$  (89),  $\text{Os}(\text{PyS})_2(\text{CO})(\text{PPh}_3)$  (90),  
 $\text{Os}(\text{O}_2\text{CCF}_3)(\text{CO})_2(\text{PPh}_3)_2$  (91) and  $\text{Ru}_2(\text{S}_2\text{CNR}_2)_4(\text{CO})_2$  (R=Me,  
 Et) (92).  $\text{RuCl}_2(\text{DMSO})_4$ , prepared by the reduction of  $\text{RuCl}_3 \cdot 3\text{H}_2\text{O}$   
 in DMSO at  $80^\circ\text{C}$  with dihydrogen, further reacts to form  
 complexes such as  $\text{Ru}(\text{S}_2\text{CNEt}_2)_2(\text{DMSO})_2$ ,  $\text{Ru}(\text{Py})_4\text{Cl}_2$ ,  
 $\text{RuCl}_2(\text{CO})_2(\text{DMSO})_2$ ,  $\text{Ru}(\text{NO})(\text{DMSO})_2\text{Cl}_3$  and  $\text{Ru}(\text{SnCl}_3)_2(\text{DMSO})_4$  (93).

An extensive range of complexes of Group VB donor ligands are  
 known. For instance ammine, amine and heterocyclic N-donor  
 complexes are numerous e.g.  $[\text{Ru}(\text{NH}_3)_6]^{2+}$  (94),  
 $[\text{Ru}(\text{NH}_3)_5(\text{Py})]^{2+}$  (95), (cis,trans)  $[\text{Ru}(\text{NH}_3)_4(\text{H}_2\text{O})(\text{CO})]^{2+}$  (96)  
 $[\text{M}(\text{phen})_3]^{2+}$  (M=Ru (97), Os (98)),  $[\text{Ru}(\text{bipy})_2(\text{H})(\text{L})]^+$   
 (L=CO,  $\text{PPh}_3$ ,  $\text{AsPh}_3$ ) (99) and  $[(\text{Py})_4\text{Ru}(\text{C}_2\text{O}_4)\text{Ru}(\text{Py})_4](\text{BF}_4)_2$   
 (100).

The tris-bipy complexes  $[\text{M}(\text{bipy})_3]^{2+}$  (M=Ru (101), Os (102))  
 and their derivatives possess a unique combination of chemical  
 stability, electrochemical and photochemical properties. The  
 use of these complexes for the photocatalytic decomposition of  
 water i.e.

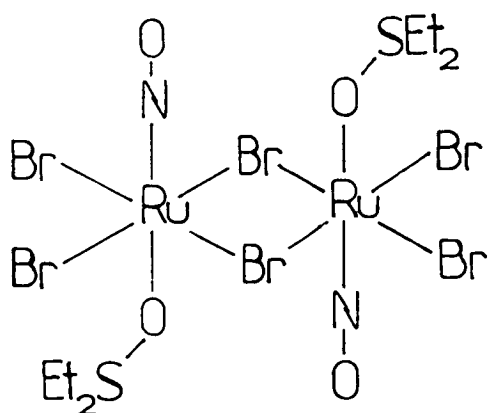


has been proposed (103).

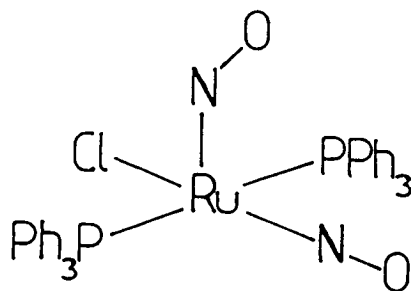
An important feature of the (II) oxidation state is the number  
 of nitrosyl complexes formed especially for Ru e.g.  
 $[\text{Ru}(\text{NO})\text{Cl}_2(\text{AsMe}_2\text{Ph})_3]\text{Cl}$  (104),  $\text{Ru}(\text{NO})(\text{S}_2\text{NR}_2)_3$  (R=Me,Et) (105),

$\text{RuCl}_3(\text{NO})(\text{MeCN})_2$  (106),  $\text{Ru}(\text{NO})\text{Cl}(\text{SO}_4)(\text{PPh}_3)_2$  (107),  
 $\text{OsH}(\text{O}_2\text{CCF}_3)(\text{NO})(\text{PPh}_3)_2$  (108) and  $\text{Ru}_2(\text{NO})_2(\text{OSet}_2)(\text{Br})_6$  (109)

[20]. In general the NO ligand is quite stable to attack or substitution, with the M-N-O moiety generally linear, though for the (0) oxidation state complex  $[\text{RuCl}(\text{NO})_2(\text{PPh}_3)_2](\text{PF}_6)$  (21) there is unusually a linear and a bent M-N-O linkage (110) [21].



[20]



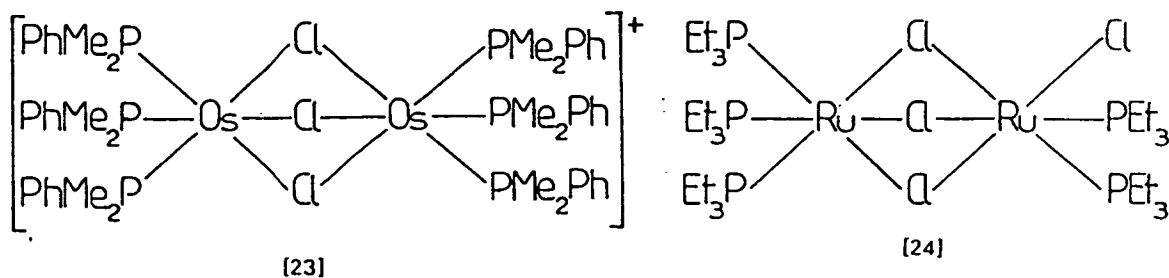
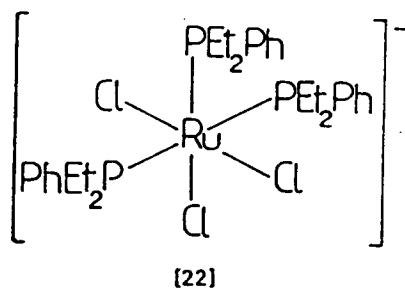
[21]

Other N-donor complexes include a number of dinitrogen species such as the monomers  $\text{OsCl}_2(\text{N}_2)(\text{PMe}_2\text{Ph})_3$  formed on the electrochemical reduction of  $\text{OsCl}_3(\text{PMe}_2\text{Ph})_3$  (111),  $[\text{Ru}(\text{en})_2(\text{N}_3)(\text{N}_2)]^+$  (112) and  $[\text{M}(\text{N}_2)(\text{NH}_3)_5]^{2+}$  (M=Ru (113), Os (114)). In addition some complexes containing bridging dinitrogen have been synthesised e.g.  $[(\text{NH}_3)_5\text{Ru}(\text{N}_2)\text{Ru}(\text{NH}_3)_5]^{4+}$  (115),  $[(\text{NH}_3)_5\text{Ru}(\text{N}_2)\text{Os}(\text{NH}_3)_5]^{4+}$  (116) and  $(\text{PPh}_3)_3(\text{H})_2\text{Ru}(\text{N}_2)\text{B}_{10}\text{H}_8(\text{SMe}_2)$  (117) which can be prepared from

$\text{Ru}(\text{H})_2(\text{N}_2)(\text{PPh}_3)_3$  and  $\text{B}_{10}\text{H}_8(\text{N}_2)(\text{SMe}_2)$ .

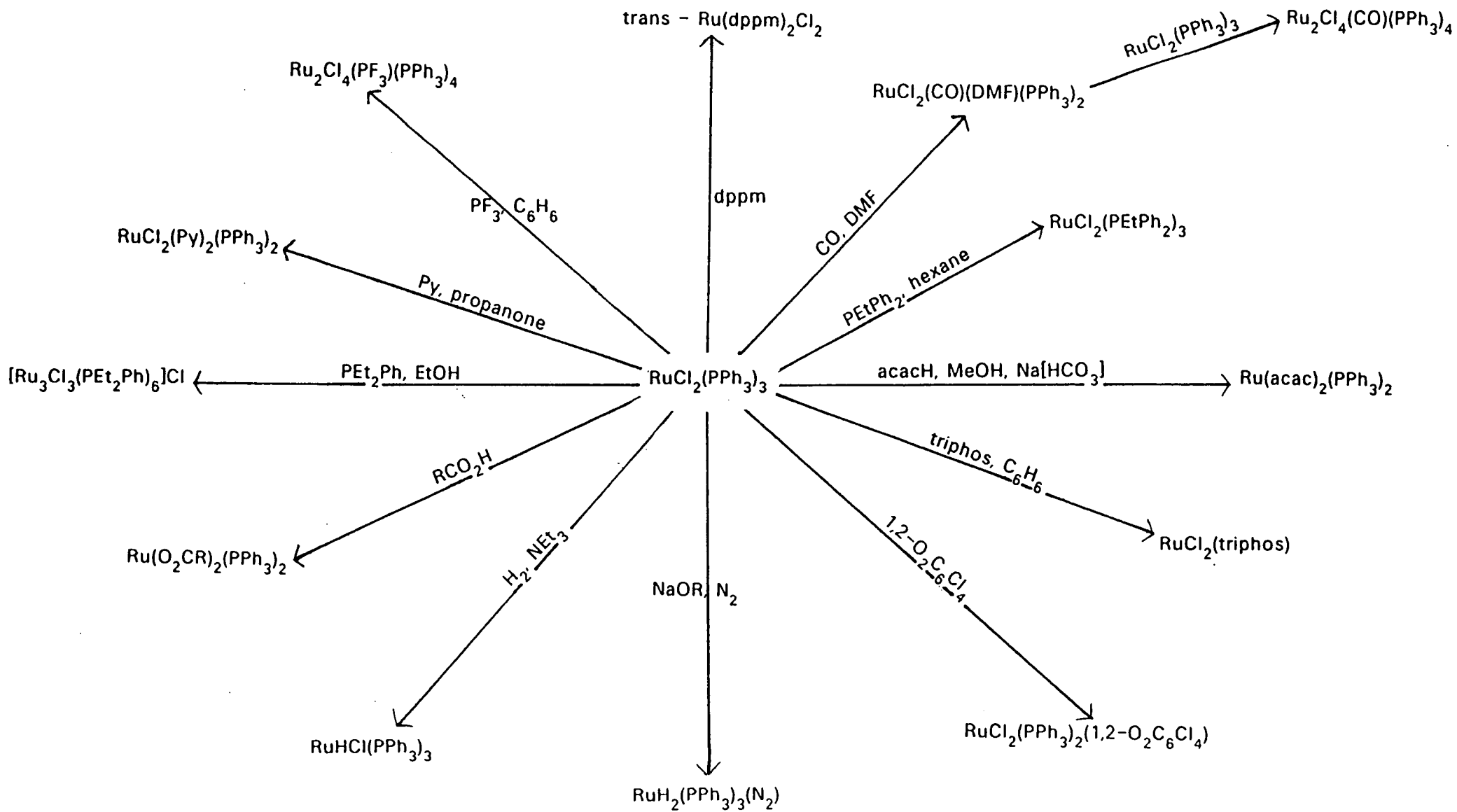
A large number of halo complexes containing  $\text{PR}_3$ ,  $\text{AsR}_3$  (and  $\text{SbR}_3$ ) have been synthesised. These range from monomers such as  $\text{MX}_2(\text{ER}_3)_3$  (e.g.  $\text{M}=\text{Ru}$ ,  $\text{X}=\text{Cl}^-$ ,  $\text{Br}^-$ ,  $\text{ER}_3=\text{PPh}_3$ ,  $\text{PEtPh}_2$  etc) (118, 119),  $\text{MX}_2(\text{ER}_3)_4$  (e.g.  $\text{M}=\text{Os}$ ,  $\text{X}=\text{Cl}^-$ ,  $\text{Br}^-$ ,  $\text{ER}_3=\text{AsPh}_3$ ,  $\text{SbPh}_3$  etc) (120, 121),  $\text{mer}[\text{RuCl}_3(\text{PEt}_2\text{Ph})_3]^-$  (122) [22] and  $[\text{RuCl}(\text{P}(\text{OR})_3)_5](\text{BPh}_4)$  ( $\text{R}=\text{Me}$ ,  $\text{Et}$ ) (123) to dimers e.g.  $[\text{M}_2\text{Cl}_3(\text{ER}_3)_6]^+$  (e.g.  $\text{M}=\text{Os}$ ,  $\text{ER}_3=\text{PEt}_2\text{Ph}$ ,  $\text{PMe}_2\text{Ph}$ ) (124) [23] and  $\text{M}_2\text{Cl}_4(\text{ER}_3)_5$  (e.g.  $\text{M}=\text{Ru}$ ,  $\text{ER}_3=\text{PMe}_2\text{Ph}$ ,  $\text{PEt}_3$ ) (68) [24].

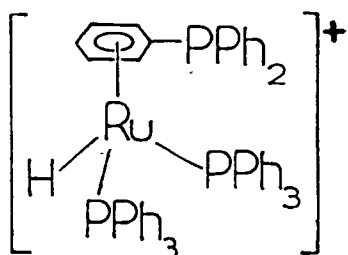
Some of these complexes, particularly the 5 co-ordinate species  $\text{RuCl}_2(\text{PPh}_3)_3$  (the 6th site is blocked by an agostic hydrogen of one of the phenyl rings) (125), are useful starting materials for a number of other complexes (see Scheme 1.6).



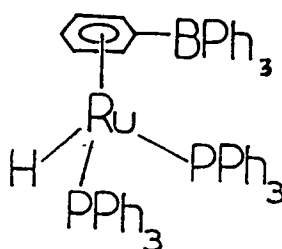


Scheme 1.6. Some Reactions of  $\text{RuCl}_2(\text{PPh}_3)_3$





[25]

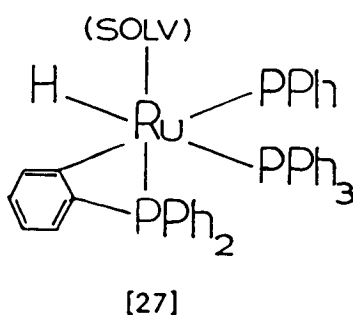


[26]

Hydridophosphine complexes are also known such as  $[\text{RuH}(\text{PPh}_2\text{H})_5](\text{PF}_6)$  (126) formed by the reaction of  $\text{RuHCl}(\text{PPh}_2\text{H})_4$  with  $\text{PPh}_2\text{H}$  in the presence of  $\text{K}(\text{PF}_6)$ ,  $[\text{RuH}(\text{dppb})_2](\text{PF}_6)$  (127) and  $[\text{RuH}(\text{PPh}_3)_4]^+$  (128). On heating a solution of  $[\text{RuH}(\text{PPh}_3)_4]^+$  the ion  $[\text{RuH}(\text{PPh}_3)_3]^+$  can be isolated and this was found to have the remarkable structure [25] (129). The analogous complex  $\text{RuH}(\text{PPh}_3)_2(\text{BPh}_4)$  [26] is also known (130).

A large number of carbonyl containing complexes is also known e.g.  $[\text{RuF}_2(\text{CO})]_4$  (131),  $\text{M}(\text{H})_2(\text{CO})(\text{PPh}_3)_3$  (132),  $\text{Os}(\text{CO})(\text{PMe}_2\text{Ph})_2(\text{S}_2\text{PMe}_2)_2$  (133),  $[\text{OsCl}(\text{CO})_3(\text{PEt}_2\text{Ph})_2]^+$  (134),  $\text{Os}(\text{OC}(\text{CF}_3)_2)(\text{CO})_2(\text{PMe}_2\text{Ph})_2$  (135) and  $\text{RuR}(\text{Cl})(\text{CO})_2(\text{PMe}_2\text{Ph})$  ( $\text{R}=\text{Me}, \text{Et}, \text{Ph}$ ) (136). Other organometallic compounds include  $\text{M}[\text{C}_5\text{H}_5]_2$  ( $\text{M}=\text{Ru}$  (137),  $\text{Os}$  (138)),  $(\text{C}_6\text{H}_6)\text{XRu}(\text{X})_2\text{RuX}(\text{C}_6\text{H}_6)$  ( $\text{X}=\text{Cl}^-$ ,  $\text{Br}^-$ ,  $\text{I}^-$ ) (139) and  $\text{RuH}(\text{C}_6\text{H}_4\text{PPh}_2)(\text{PPh}_3)_2(\text{solv})$  ( $\text{solv}=\text{Et}_2\text{O}, \text{THF}$ ) [27] which can be synthesised by the reaction

of  $\text{RuHCl}(\text{PPh}_3)_3$  with alkyllithium reagents ( $\text{RLi}$ ) (140).



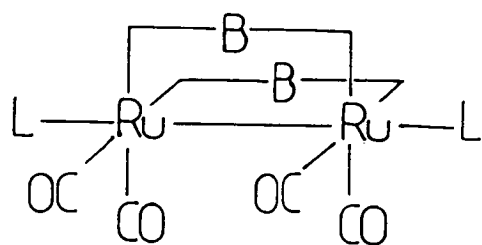
Finally other Group IVB donor complexes include  $[\text{RuCl}(\text{SnCl}_3)_5](\text{Et}_3\text{NH})_4$  (141),  $(\text{CO})_3\text{Ru}(\text{X})_3\text{Ru}(\text{CO})_2(\text{SnX}_3)$  ( $\text{X}=\text{Cl}^-$ ,  $\text{Br}^-$ ) (142),  $\text{cis-}[\text{Ru}(\text{CO})_4(\text{ECl}_3)_2]$  ( $\text{E}=\text{Ge}$  (143),  $\text{Si}$  (144)) and  $\text{Ru}(\text{CO})_2(\text{PEt}_3)_2(\text{SiMe}_3)_2$  (145).

### The (I) $d^7$ Oxidation State

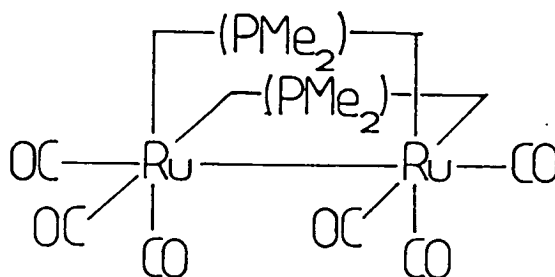
Although complexes such as  $\{\text{Ru}(\text{NO})(\text{I})_2(\text{L})_2\}_n$  ( $\text{L}=\frac{1}{2}\text{bipy}$ ,  $\text{AsMePh}_2$  and  $\text{Py}$ ) (146) and the dimer  $(\text{PMe}_3)_3\text{Ru}(\text{H})(\text{OH})\text{Ru}(\text{PMe}_3)_3$  (147) have been reported the vast majority of complexes in the (I) state are metal-metal bonded dimers containing a number of carbonyl ligands.

Many of the Group VB, VIB and VIIB complexes have the general structure [28] e.g.  $\text{L}=\text{CO}$ ,  $\text{B} = \text{MeCO}_2^-$  (148),  $\text{SEt}^-$  (149),

$\text{PMe}_2^-$  (150) [29] ;  $\text{L}=\text{P}(\text{CMe}_3)_2(\text{C}_6\text{H}_4\text{Me})$ ,  $\text{B}=\text{Cl}^-$ ,  $\text{Br}^-$ ,  $\text{I}^-$  (151).

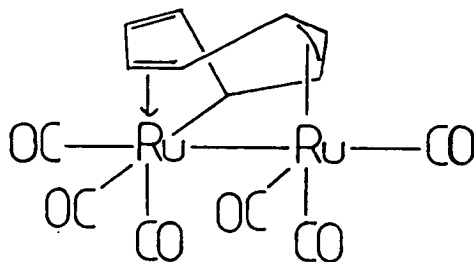


[28]



[29]

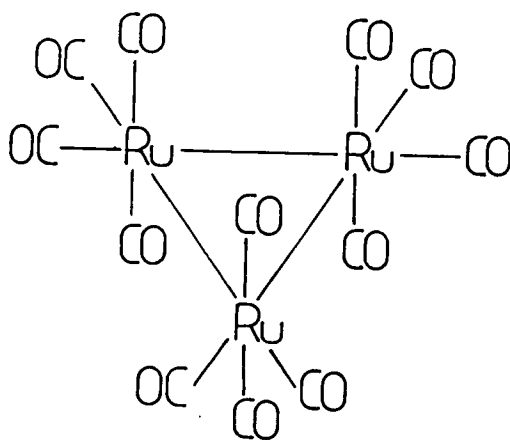
A number of Group IVB donor complexes is also known e.g.  $(\text{Me}_3\text{E})(\text{CO})_4\text{Ru}-\text{Ru}(\text{CO})_4(\text{EMe}_3)$  ( $\text{E}=\text{Si}$  (152),  $\text{Ge}$  (143),  $\text{Sn}$  (153)),  $\text{M}_2(\text{CO})_4(\text{C}_5\text{H}_5)_2$  ( $\text{M}=\text{Ru}$  (154),  $\text{Os}$  (155)),  $\text{Ru}_2(\text{CO})_6(\text{C}_8\text{H}_8)$  (156) [30] etc.



[30]

### The (0) $d^8$ Oxidation State

The vast majority of compounds in the (0) oxidation state are carbonyl or carbonyl derivatives. The homoleptic carbonyls can be monomeric e.g.  $M(CO)_5$  or of higher nuclearity such as  $Os_5(CO)_{16}$  <sup>(157)</sup> and  $Os_7(CO)_{21}$  <sup>(158)</sup>. The trinuclear species  $M_3(CO)_{12}$ , in particular, have an extensive chemistry. For instance  $Ru_3(CO)_{12}$  [31] can undergo substitution reactions with or without concomitant fragmentation of the cluster e.g. reaction with  $PPh_3$  can yield a mixture of  $Ru(CO)_4(PPh_3)$  and  $Ru(CO)_3(PPh_3)_2$  <sup>(159)</sup> or  $Ru_3(CO)_9(PPh_3)_3$  <sup>(160)</sup> depending on the conditions.



[31]

Some other representative examples of the reactions of  $Ru_3(CO)_{12}$  are given in Scheme 1.7. This contains some examples of the many hydrocarbon complexes known in the (0)

oxidation state, osmium examples of which include  $\text{Os}(\text{C}_6\text{Me}_6)(1,4\text{-COT})$  (161) and the cluster complex  $\text{Os}_3(\text{CO})_{10}(\text{C}_4\text{H}_6)$  (162).

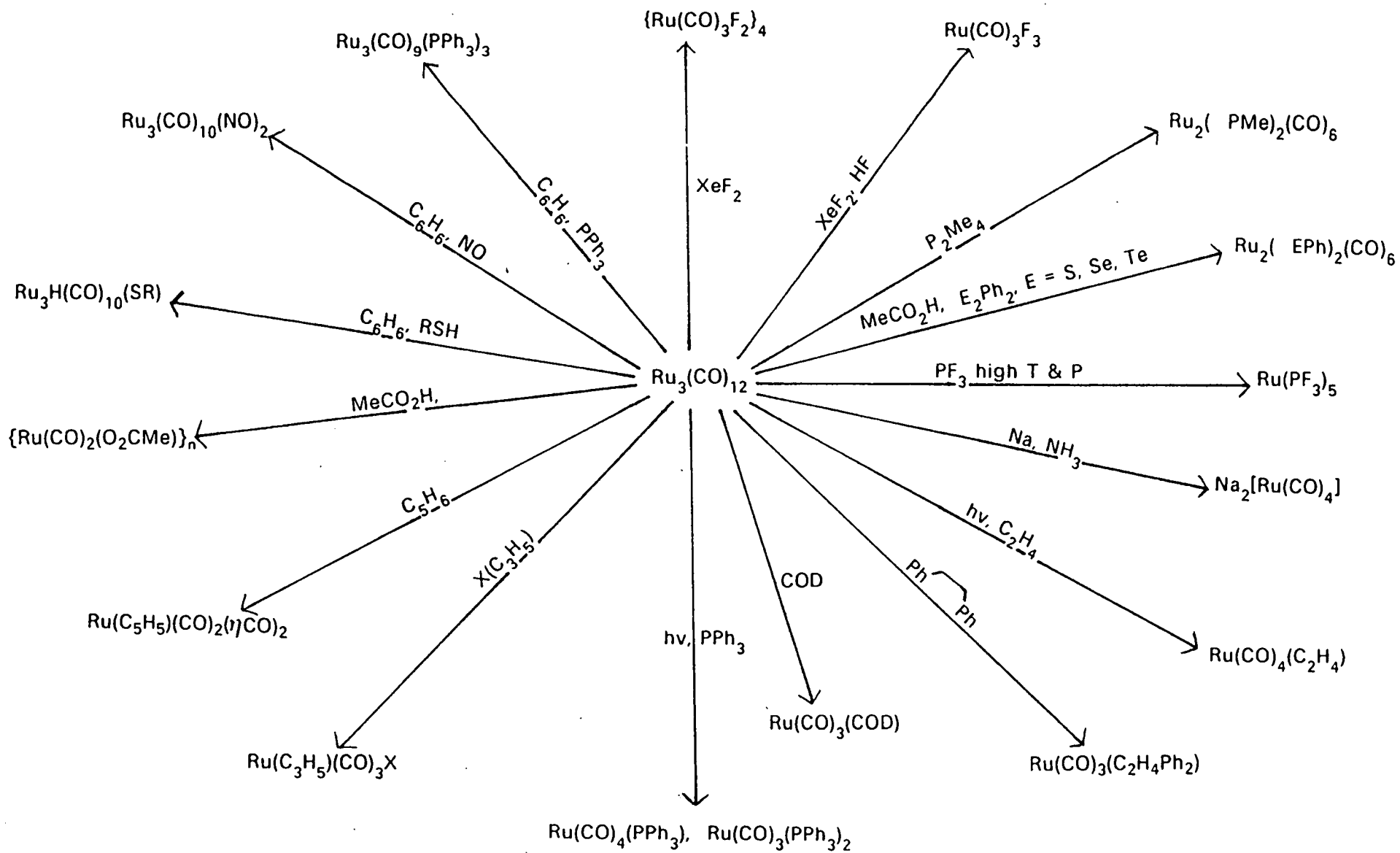
Other synthetic routes to (0) oxidation state complexes includes the reduction of M(II) complexes. For example Na/Hg reduction of  $\text{RuCl}_2(\text{CNCMe}_3)_4$  and  $[\text{Os}(\text{C}_6\text{H}_6)_2]^{2+}$  yields  $\text{Ru}(\text{CNCMe}_3)_5$  (163) and  $\text{Os}(\text{C}_6\text{H}_6)(\eta^4\text{C}_6\text{H}_6)$  (164) respectively.

Conversely M(II) complexes can be synthesised by the oxidative addition of various moieties to M(0) compounds. For instance from  $\text{Ru}(\text{CO})_3(\text{PPh}_3)_2$ , complexes such as  $\text{Ru}(\text{H})_2(\text{CO})_2(\text{PPh}_3)_2$  (165),  $\text{Ru}(\text{CO})_2(\text{PPh}_3)_2(\text{O}_2\text{C}_6\text{Cl}_4)$  (166) and  $[\text{RuI}(\text{CO})_3(\text{PPh}_3)](\text{SnI}_3)$  (167) can be synthesised.

### The (-I) $d^9$ and (-II) $d^{10}$ Oxidation States

Few examples of these unfavourable oxidation states of Ru and Os are known. However several anionic species such as  $[\text{Ru}(\text{PF}_3)_4]^{2-}$  (168) and  $[\text{M}(\text{CO})_4]^{2-}$  (169) have been reported and may prove to be synthetically useful. For instance  $[\text{Ru}(\text{CO})_4]^{2-}$  has been used to synthesise a number of mixed hydridocarbonyl clusters such as  $\text{H}_4\text{Ru}_2\text{Os}_2(\text{CO})_{12}$  and  $\text{H}_4\text{RuOs}_3(\text{CO})_{12}$  (170).

Scheme 1.7. Some Reactions of  $\text{Ru}_3(\text{CO})_{12}$



References

1. K. A. Hofmann, Chem. Ber., 1912, 45, 3329.
2. A. Zalkin and D. H. Templeton, J Chem. Phys., 1964, 40, 501.
3. G. Nowogrocki, F. Abraham, J. Tréhoux and D. Thomas, Acta Crystallogr., Sect. B, 1976, 32, 2413.
4. F. Krauss and D. Wilken, Z. anorg. Chem., 1925, 145, 156.
5. A. F. Clifford and C. S. Kobayashi, Inorg. Synth., 6, 204.
6. Muller, Z. Electrochem., 1922, 28, 307.
7. L. Wintrebert, Ann. Chim. Phys., 1903, 28(7), 15.
8. S. K. Harbron and W. Levason, J Chem. Soc., Chem. Commun., 1985, 205.
9. T. C. Lau and J. K. Kochi, J Chem. Soc., Chem., Commun., 1987, 798.
10. T. C. W. Mak, C-M. Che and K-Y. Wong, J Chem. Soc., Chem Commun., 1985, 987.
11. K. A. K. Lott and M. C. R. Symons, J Chem. Soc., 1960, 973.
12. F. L. Phillips and A. C. Skapski, J Chem. Soc., Dalton Trans., 1975, 2586.
13. W. P. Griffith and R. Rossetti, J Chem. Soc., Dalton Trans., 1972, 1449.
14. H.C. Jewiss, W. Levasson, M. Tajik, M. Webster and N.P.C. Walker, J Chem. Soc., Dalton Trans., 1985 199.
15. W.P. Griffith and D. Pawson, J Chem. Soc., Dalton Trans., 1973, 1315.



16. L.N. Lomakina, A.I. Busev and G.K. Zhuravleva, Vest. Mosk. Univ., Khim., 1972, 13, 684.
17. J.M. Longo and J.A. Kafalas, Mater. Res. Bull., 1968, 3, 687.
18. P.A. Belmonte and Z-Y Own, J. Am. Chem. Soc., 1984, 106, 7493.
19. P.J. Jones, W. Levasson, M. Tajik, J. Fluorine. Chem., 1984, 25(2), 195.
20. H.H. Classen, H. Selig, J.M. Malm, C.I. Chernick and B.W. Weinstock, J. Am. Chem. Soc., 1961, 83, 2390.
21. O. Glemser, H.W. Roesky, K-H. Hellberg and H-U Werther, Ber., 1966, 99, 2652.
22. C-M. Che and Wing-Kin Cheng, J. Chem. Soc., Chem. Commun., 1986, 1519.
23. J. Darriet and A. Vidal, C.R. Acad. Sci., Ser C, 1973, 277, 1235.
24. R.P. Trooze, G. Wilkinson, M. Motevalli and M.B. Hursthouse, J. Chem. Soc., Dalton Trans., 1986, 2711.
25. R. C. Burns and T. A. O'Donnell, Inorg. Chem., 1979, 18, 3081.
26. J. H. Holloway, R. D. Peacock and R. W. H. Small, J Chem. Soc., 1964, 644.
27. U. Schindewolf, Ber. Bunsenges. Phys Chem., 1963, 67, 219.
28. A. J. Hewitt, J. H. Holloway, R. D. Peacock, J. B. Raynor and I. L. Wilson, J Chem. Soc., Dalton Trans., 1976, 579.
29. D. P. Mellor, J proc. Roy. Soc. N.S. Wales, 1943, 77, 145.
30. D. Hewkin and W. P. Griffith, J Chem. Soc., A, 1966, 472.

31. A. M. Mathieson, D. P. Mellor and N. C. Stephenson, Acta Cryst., 1952, 5, 185.
32. R. R. Miano and C. S. Garner, Inorg. Chem., 1965, 4, 337.
33. J. R. Campbell, R. J. H. Clark, W. P. Griffith and J. P. Hall J Chem. Soc., Dalton Trans., 1980, 2228 and references therein.
34. P. M. Smith, T. Fealey, J. E. Earley and J. V. Silverton, Inorg. Chem., 1971, 10, 1943.
35. K. W. Given, S. H. Wheeler, B. S. Jick, L. J. Haheu and L. H. Pignolet, Inorg. Chem., 1979, 18, 1261.
36. M. Ciechanowicz and A. C. Skapski, J Chem. Soc., A, 1971, 1792.
37. W. P. Griffith and D. Pawson, J Chem. Soc., Dalton Trans., 1973 1315.
38. W. P. Griffith, N. T. McManus and A. C. Skapso, J Chem. Soc., Chem Commun., 1984, 434.
39. J. D. Dunitz and L. E. Orgel, J Chem. Soc., 1953, 2594.
40. R. Charronat, Ann. Chim. (Paris), 1931, 16(10), 179, 188, 235.
41. F. P. Dwyer, H. A. Goodwin and E. C. Gyarfás, Aust. J Chem., 1963, 16, 42, 544.
42. D. Pawson and W. P. Griffith, J Chem. Soc., Dalton Trans., 1975, 417.
43. T. V. Ashworth and E. Singleton, J Chem. Soc., Chem. Commun., 1976, 705.
44. R. S. Nyholm and G. J. Sutton, J Chem. Soc., 1958, 572.
45. J. D. Gilbert, M. C. Baird and G. Wilkinson, J Chem. Soc., A, 1968, 2198.

46. A. Y. Girgis, Y. S. Sohn and A. L. Balch, Inorg Chem., 1975, 14 2327.
47. A. Colombo and G. Allegra, Acta Crystallogr., Sect. B, 1971, 27, 1653.
48. P. B. Hitchcock, J. F. Nixon and J. Sinclair, J Organomet. Chem., 1975, 86, C34.
49. E. O. Fischer and H. Grubert, Ber., 1959, 92, 2302.
50. H. Kono, and Y. Nagai, Chem. Lett., 1974, 931.
51. H. Kono, N. Wakao, K. Ito and Y. Nagai, J Organomet. Chem., 1977, 132, 53.
52. Y. Nagai and H. Kohno, Japan. Kokai, 7616617, 1976.
53. G. A. Barbieri, Atti Acad. Linc., 1914, 23(5), I, 336.
54. F. P. Dwyer and A. M. Sargeson, J Am. Chem. Soc., 1955, 77, 1285.
55. K. Brodersen, F. Moers and H. G. Schnering, Naturwiss., 1965, 52, 205.
56. B. M. Mattson, J. R. Heinan and L. H. Pignolet, Inorg. Chem., 1976, 15, 564.
57. T. A. Stephenson, D. A. Tocher and M. D. Walkinshaw, J Organometal. Chem., 1982, 232, C51.
58. T. A. Stephenson and G. Wilkinson, J Inorg. Nucl. Chem., 1966, 28, 2285.
59. A. Spencer and G. Wilkinson, J Chem. Soc., Dalton Trans., 1972, 1570.
60. F. A. Cotton and J. G. Norman, Jr., Inorg. Chim. Acta, 1972 6, 411.
61. H. C. Stynes and J. A. Ibers, Inorg. Chem., 1971, 10, 2304.

62. J. A. Broomhead, F. Basolo and R. G. Pearson, Inorg. Chem., 1964, 3, 826.
63. L. A. P. Kane-Maguire, P. S. Sheridan, F. Basolo and R. G. Pearson, J Am. Chem. Soc., 1970, 92, 5865.
64. S-W Lin and A. F. Schreiner, Inorg. Chim. Acta, 1971 5, 290.
65. P. K. Chan, D. A. Isabirge and C. K. Poon, Inorg. Chem., 1975, 14, 2579.
66. C-K Poon, C-M Che, T-W Tang, J Chem. Soc., Dalton Trans., 1981, 1697.
67. H. J. Peresie and J. A. Stanko, J Chem. Soc., D, 1970, 1674.
68. J. Lewis, F. E. Mabbs and R. A. Walton, J Chem. Soc., A, 1967, 1366.
69. F. P. Dwyer and E. C. Gyarfas, J Am. Chem. Soc., 1952, 74, 4699.
70. F. P. Dwyer, H. A. Goodwin and E. C. Gyarfas, Aust. J Chem., 1963, 16, 42.
71. C. Creutz and H. Taube, J Am. Chem. Soc., 1969, 91, 3988.
72. M. T. Flood, R. F. Ziolo, J. E. Earley and H. B. Gray, Inorg. Chem., 1973, 12, 2153.
73. K. K. Cloninger and R. W. Callahan, Inorg. Chem., 1981, 20, 1611.
74. J. Chatt, G. J. Leigh, D. M. P. Mingos and R. J. Paske, J Chem. Soc., A, 1968, 2636.
75. T. A. Stephenson, J Chem. Soc., A, 1970, 889.
76. L. Ruiz-Ramirez, T. A. Stephenson, and E. Switkes, J Chem. Soc., Dalton Trans., 1973, 1770.

77. M. B. Hursthouse, R. A. Jones, K. M. Abdul Malik and G. Wilkinson, J Am. Chem. Soc., 1979, 101, 4128.
78. R. A. Contreras-Zarate, Ph.D. Thesis, University of Edinburgh, 1981.
79. A. J. Hewitt, J. H. Holloway, R. D. Peacock, J. B. Raynor and I. L. Wilson, J Chem. Soc., Dalton Trans., 1976, 579.
80. R. Cotton and R. H. Farthing, Aust. J. Chem., 1971, 24, 903.
81. F. H. Johannsen, W. Preetz and A. Scheffler, J Organomet. Chem., 1975, 102, 527.
82. A. Brooks, S. A. R. Knox and F. G. A. Stone, J Am. Chem. Soc., A, 1971, 3468.
83. S. A. R. Knox and F. G. A. Stone, J Chem. Soc., A, 1971, 2874.
84. J. D. Cotton, S. A. R. Knox and F. G. A. Stone, J Chem. Soc., A, 1968, 2758.
85. E. E. Mercer and R. R. Buckley, Inorg. Chem., 1965, 4, 1692.
86. F. Calderazzo, C. Floriani, R. Henzi and F. L'Eplattenier, J Chem. Soc., A, 1969, 1378
87. J. D. Gilbert, G. Wilkinson, J Chem. Soc., A, 1969 1749
88. A. R. Davies, F. W. B. Einstein, N. P. Farrel, B. R. James and R. S. McMillan, Inorg. Chem., 1978, 17, 1965.
89. L. H. Vogt Jr., J. L. Katz, and S. E. Wiberly, Inorg. Chem., 1965, 4, 1157.
90. P. Mura, B. G. Olby and S. D. Robinson, J Chem. Soc., Dalton Trans., 1985, 2101.

91. A. Dobson, S. D. Robinson and M. F. Utley, J Chem. Soc., Dalton Trans., 1975, 370.
92. J. V. Kingston and G. Wilkinson, J Inorg. Nucl. Chem., 1966 28, 2709.
93. I. P. Evans, A. Spencer and G. Wilkinson, J Chem. Soc., Dalton Trans, 1973, 204.
94. F. M. Lever and A. R. Powell, Chem. Soc. Spec. Pub., 1959, 13, 135.
95. P. Ford, De F. P. Rudd, R. Gaunder and H. Taube, J Am. Chem. Soc., 1968, 90, 1187.
96. A. D. Allen, T. Eliades, R. O. Harris and P. Reinsalu, Can. J Chem., 1969, 47, 1605.
97. F. P. Dwyer and E. C. Gyarfas, J Proc. Roy. Soc. N S Wales, 1949, 83, 170, 174.
98. F. P. Dwyer, N. A. Gibson and E. C. Gyarfas, J Proc. Roy. Soc. N S Wales, 1950, 84, 68.
99. J. M. Kelly and J. G. Vos, J Chem. Soc., Dalton Trans., 1986, 1045.
100. P-T Cheng, B. R. Loesher and S. C. Nyburg, Inorg. Chem., 1971, 10, 1275.
101. F. H. Burstall, J Chem. Soc., 1936, 173.
102. F. H. Burstall, F. P. Dwyer and E. C. Gyarfas, J Chem. Soc., 1950, 953.
103. C. Creutz and N. Sutin, Proc. Natl. Acad. Sci. U S A., 1975 72, 2858.
104. R. E. Townsend and K. J. Coskran, Inorg. Chem., 1971, 10, 1661.

105. L. Cambi and L. Malatesta, Rend. 1st. Lomb. Accad. Sci. Lett. A, 1938, 71, 118.
106. J. Chatt and B. L. Shaw, J Chem. Soc., A, 1966, 1811.
107. J. Reed, S. L. Soled and R. Eisenberg, Inorg. Chem., 1974, 13, 3001.
108. E. B. Boyar, A. Dobson, S. D. Robinson, B. L. Haymore and J. C. Huffman, J Chem. Soc., Dalton Trans., 1985, 621.
109. J. E. Ferguson, C. T. Page and W. T. Robinson, Inorg. Chem., 1976, 15, 2270.
110. C. G. Pierpont and R. Eisenberg Inorg. Chem., 1972, 11, 1088.
111. V. T. Coombe, G. A. Heath, T. A. Stephenson, J. D. Whitelock and L. J. Yellowlees, J Chem. Soc., Dalton Trans., 1985, 947.
112. B. R. Davis and J. A. Ibers, Inorg. Chem., 1970, 9, 2768.
113. A. D. Allen and C. V. Senoff, J Chem. Soc. Chem. Commun., 1965, 621.
114. A. D. Allen and J. R. Stevens, J Chem. Soc., Chem. Commun., 1967, 1147.
115. I. M. Treitel, M. T. Flood, R. E. Marsh and H. B. Gray, J Am. Chem. Soc., 1969, 91, 6512.
116. C. M. Elso, J. Gulens and J. A. Page, Can. J Chem., 1971, 49, 207.
117. K. D. Schramm and J. A. Ibers, Inorg. Chem., 1977, 16, 3287.
118. T. A. Stephenson and G. Wilkinson, J Inorg. Nucl. Chem., 1966, 28, 945.

119. P. W. Armit and T. A. Stephenson, J Organometal. Chem., 1973, 57, C80.
120. L. Vaska, Chem. Ind. (London), 1961, 1402.
121. F. P. Dwyer, R. S. Nyholm and B. T. Tyson, J Proc. Roy. Soc. N S Wales, 1947, 81, 272.
122. K. A. Raspin, J Chem. Soc., A, 1969, 461.
123. D. A. Couch and S. D. Robinson, Inorg. Chim Acta, 1974, 9, 39.
124. J. Chatt and R. G. Hayter, J Chem. Soc., 1961, 896, 2605; 1963, 6017.
125. S. J. La Placa and J. A. Ibers, Inorg. Chem., 1965, 4, 778.
126. J. R. Sanders, J Chem. Soc., Dalton Trans., 1972, 1333.
127. T. V. Ashworth and E. Singleton, J Chem Soc., Chem. Commun., 1976, 705.
128. J. R. Sanders, J Chem. Soc., Dalton Trans., 1973, 743.
129. J. C. McConway, A C Skapski, L Phillips, R J Young and G Wilkinson, J Chem. Soc., Chem. Commun., 1974, 327.
130. J. J. Hough and E. Singleton, J Chem. Soc., Chem. Commun., 1972, 371.
131. C. J. Marshall, R. D. Peacock, D. R. Russell and I. L. Wilson, J Chem. Soc., D, 1970, 1643.
132. N. Ahmad, J. J. Levison, S. D. Robinson and M. F. Uttley, Inorg. Synth., 15, 45.
133. D. J. Cole-Hamilton and T. A. Stephenson, J Chem. Soc., Dalton Trans., 1976, 2396.



134. W. Hieber, V. Frey and P. John, Chem. Ber., 1967, 100, 1961.
135. M. Cooke, M. Green and T. A. Kuc, J Chem. Soc., A, 1971, 1200.
136. C. F. J. Barnard, J. A. Daniels and R. J. Mawby, J Chem. Soc., Dalton Trans., 1976, 961.
137. E. O. Fisher and H. Grubert, Ber., 159, 92, 2302.
138. D. E. Bulbitz, W. E. McEwan and J. Kleinberg, Org. Syn., 1961, 41, 96.
139. M. A. Bennett and A. K. Smith, J Chem. Soc., Dalton Trans., 1974, 233.
140. D. J. Cole-Hamilton and G. Wilkinson, J Chem. Soc., Dalton Trans., 1977, 797.
141. H. Okuno, T. Ishimori, K. Mizumachi and H. Ihochi, Bull. Chem. Soc. Jpn., 1971, 44, 415.
142. M. Elder and D. Hall, J Chem. Soc., A, 1970, 245.
143. S. A. R. Knox and F. G. A. Stone, J Chem. Soc., A, 1971, 2874.
144. R. K. Pomeroy, R. S. Gay, G. O. Evans and W. A. G. Graham, J Am. Chem. Soc., 1972, 94, 272.
145. J. D. Cotton, M. I. Bruce and F. G. A. Stone, J Chem. Soc., A, 1968, 2162.
146. R. J. Irving and P. G. Laye, J Chem. Soc., A, 1966, 161.
147. R. A. Jones, G. Wilkinson, I. J. Colquhoun, W. McFarlane, A. M. R. Galas and M. B. Hursthouse, J Chem. Soc., Dalton Trans., 1980, 2480.
148. G. R. Crooks, B. F. G. Johnson, J. Lewis, I. G. Williams and G. Gamlen, J Chem. Soc., A, 1969, 2761.

149. G. Cetini, O. Gambino, E. Sappa and M. Valle, J Organomet. Chem., 1969, 17, 437.
150. J. P. Candlin, K. K. Joshi, and D. T. Thompson, Chem. Ind. (London), 1966, 1960.
151. D. F. Gill, B. E. Mann and B. L. Shaw, J Chem. Soc., Dalton Trans., 1973, 311.
152. J. D. Cotton, S. A. R. Knox and F. G. A. Stone, J Chem. Soc., D, 1967, 965.
153. J. A. K. Howard, S. C. Kellett and P. Woodward, J Chem. Soc., Dalton Trans., 1975, 2332.
154. O. S. Mills and J. P. Nice, J Organomet. Chem., 1967, 9, 339.
155. E. O. Fischer and K. Bittler, Z Naturforsch., Teil B, 1962 17, 274.
156. F. A. Cotton and W. T. Edwards, J Am. Chem. Soc., 1968, 90, 5412.
157. B. E. Reichert and G. M. Sheldrick, Acta Crystallogr. B., 1977, 33, 173.
158. C. R. Eady, B. F. G. Johnson and J. Lewis, J Chem. Soc., Chem. Commun, 1977, 385.
159. R. Whyman, J Organomet. Chem., 1973, 56, 339.
160. F. Piacenti, M. Bianchi, E. Benedetti and G. Sbrana, J Inorg. Nucl. Chem., 1967, 29, 1389.
161. M. A. Bennett, T. W. Matheson, G. B. Robertson, A. K. Smith and P A Tucker, Inorg. Chem., 1980, 1014.
162. C. G. Pierpont, Inorg. Chem., 1978, 1976.

163. G. K. Barker, A. M. R. Galas, M. Green, J. A. K. Howard, F. G. A. Stone, T. W. Turney, A. J. Welsh and P. Woodward J Chem. Soc., Chem. Commun., 1977, 256.
164. E. O. Fisher and J. Muller, Ber., 1963, 96, 3217.
165. F. L'Eplattenier and F. Calderazzo, Inorg. Chem., 1968, 7, 1290.
166. A. L. Balch and Y. S. Sohn, J Organomet. Chem., 1971, 30, C31.
167. H. B. Kuhnhen, J Organomet. Chem. 1977, 129, 215.
168. Th. Kruck, Angew. Chem., Int. Ed. Engl., 1967, 7, 53.
169. J. D. Cotton, M. I. Bruce and F. G. A. Stone, J Chem. Soc., A, 1968, 2162.
170. G. L. Geoffroy and W. L. Gladfelter, J Am. Chem. Soc., 1977, 99, 7565.

Chapter 2

Synthesis of Half-sandwich Complexes of Ru(II) and Os(II)  
with the Macrocyclic [9]aneS3.

## 2.1 Introduction

This chapter describes an investigation into the complexation of the trithia macrocycle [9]aneS<sub>3</sub> to Ru(II) and Os(II) centres to yield half sandwich complexes of the general formula

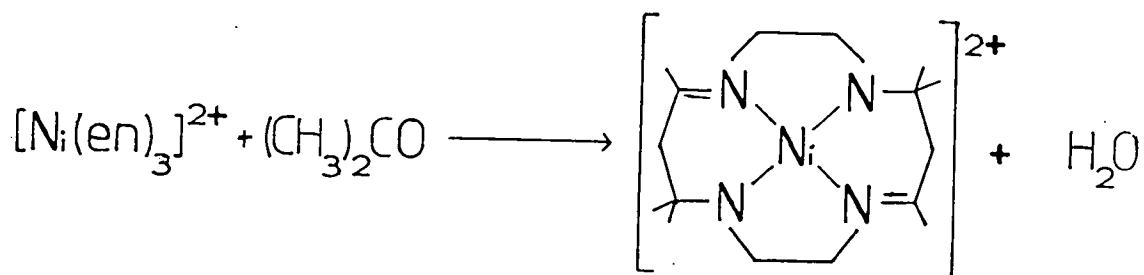
$$[M(L)(L^1)(L^{11})[9]aneS_3]^{n+}$$

(M=Ru,Os; L, L<sup>1</sup>, L<sup>11</sup>=Cl<sup>-</sup>, Br<sup>-</sup>, H<sup>-</sup>, PR<sub>3</sub>, N-donors, CO etc; n=1,0).

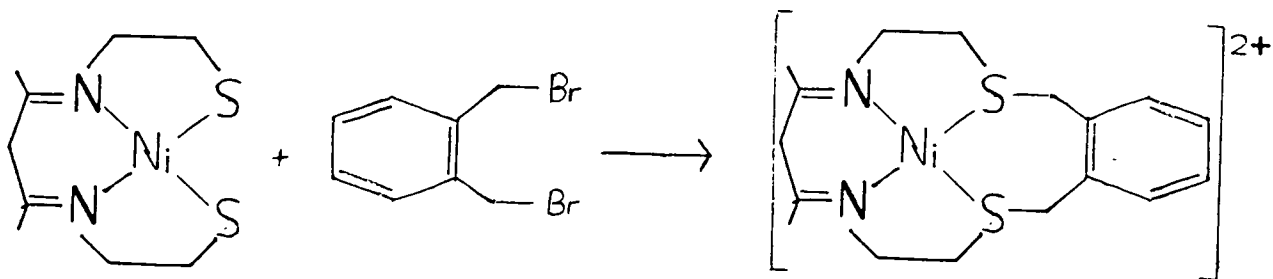
Before describing this work in detail some background information on macrocycles and then [9]aneS<sub>3</sub> in particular is given below.

Although co-ordination compounds containing macrocyclic ligands have been known and studied since the early 1900s real interest in developing the co-ordination chemistry of macrocycles stems from reports made in the early 1960s. The first report by Curtis<sup>(1)</sup> outlined the reaction between [Ni(en)<sub>3</sub>](ClO<sub>4</sub>)<sub>2</sub> and acetone. The product was initially thought to be a Schiff-base co-ordination complex, however it was subsequently assigned to a Ni(II) centre bound to a tetradentate ligand as shown in scheme 2.1.<sup>(2)</sup> The reaction was found to be a general one leading to the synthesis of a series of complexes.<sup>(3)</sup> About the same time Thompson and Busch<sup>(4,5)</sup> achieved the first deliberate synthesis of a compound containing a new macrocyclic ligand via the reaction shown in scheme 2.2. From these reports and others such as the self condensation of o-aminobenzaldehyde<sup>(6)</sup> (see scheme 2.3) modern macrocyclic co-ordination chemistry developed.

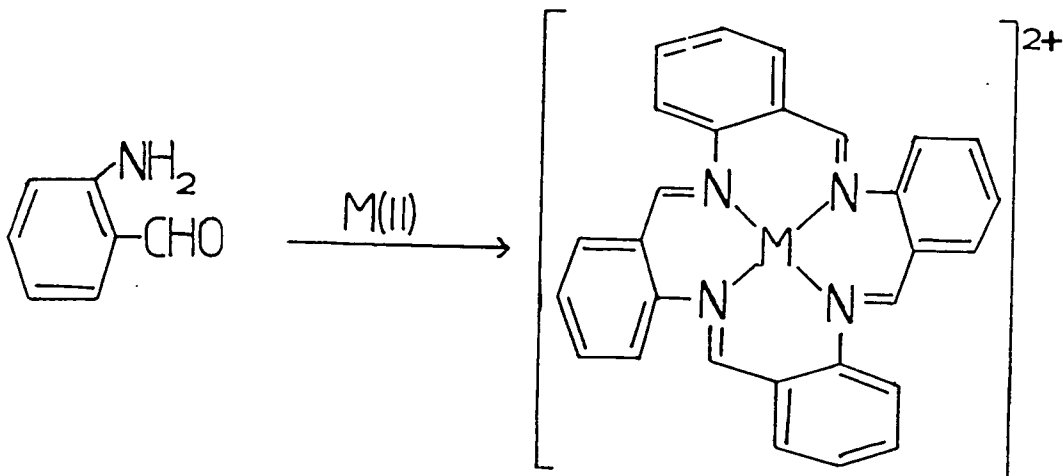
Scheme 2.1: Reaction of Trisethylenediaminenickel (II) with Acetone



Scheme 2.2: Reaction of 2,3-Octanedionebis (mercaptoethylimino) nickel (II) with, Dibromo-o-xylene



Scheme 2.3: The Metal Template Condensation of o-aminobenzaldehyde



In 1967 the synthesis of cyclic polyethers (see Figure 2.1) was reported by Pederson (7). These ligands were found to bind strongly and in some cases selectively (depending on the ring size) to alkali metals. Since then, new donor atoms such as sulphur and nitrogen have been introduced into the ring in place of the original oxygens, which opens up further avenues of investigation (8).

Shortly after Pederson's report of cyclic polyethers Lehn and co-workers reported the synthesis of the cryptands (macropolycyclic polyethers - see Figure 2.2) which can form inclusion complexes with metal ions of suitable size (9). These original cryptands are bicycles, ligands containing larger numbers of cycles being unknown till 1977 (10).

Thus resulting from these reports numerous ligands and their co-ordination complexes have been synthesised and studied. There are a number of reasons for the continuing and expanding interest in macrocyclic chemistry and these include:

1. Understanding the nature and origin of the macrocyclic effect (see section 2.1.2).
2. Modelling biological systems such as the tetrapyrrole macrocycles containing iron, magnesium and cobalt which are involved in many biologically important systems. For example, the iron complexes are used to transport  $O_2$  (Haemoglobin and Myoglobin) and as one electron carriers (Cytochromes) linking the oxidation of

- substrates to the reduction of  $O_2$ .
3. Investigation of metal binding properties such as the complexation of alkali metals by cyclic polyethers.
  4. Study of the electron transfer and redox properties of the macrocyclic complexes possibly leading to the characterisation of unusual oxidation states for the metal centres.
  5. Possible use of macrocyclic complexes in catalysis, where the macrocyclic ligand acts as a protecting group to the active metal centre.

### 2.1.2 The Macrocyclic Effect

From the study of macrocyclic complexes it became apparent that they exhibit the "macrocyclic effect" <sup>(11)</sup>. The effect is defined as the enhanced stability of the complex compared to that of its open chain analogue. The open chain complex in turn being more stable than the complex formed from the donor fragments which is termed the "chelate effect".

The increase in stability for chelates over monodentate ligands is mainly due to the entropy difference of the chelate system compared to the non-chelated one, which is large and positive. The stability of complexes containing macrocycles rather than chelates (see Table 2.1) is however not so readily explained and has been the cause of considerable controversy.



Figure 2.1: Some Examples of Cyclic Polyethers

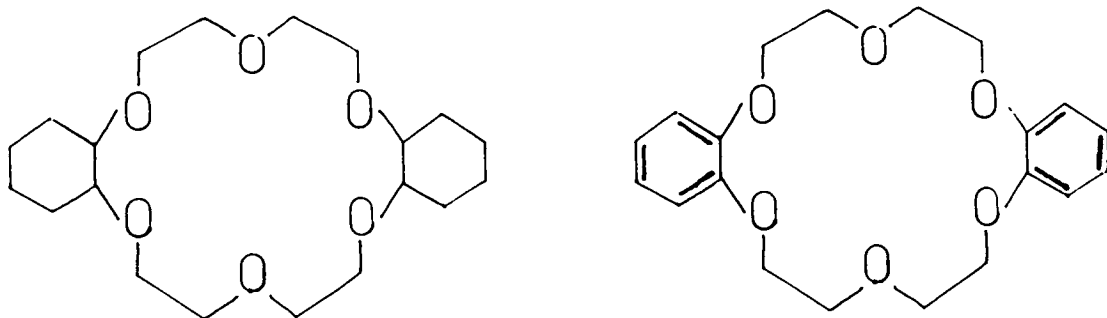


Figure 2.2: Some Examples of Cryptands

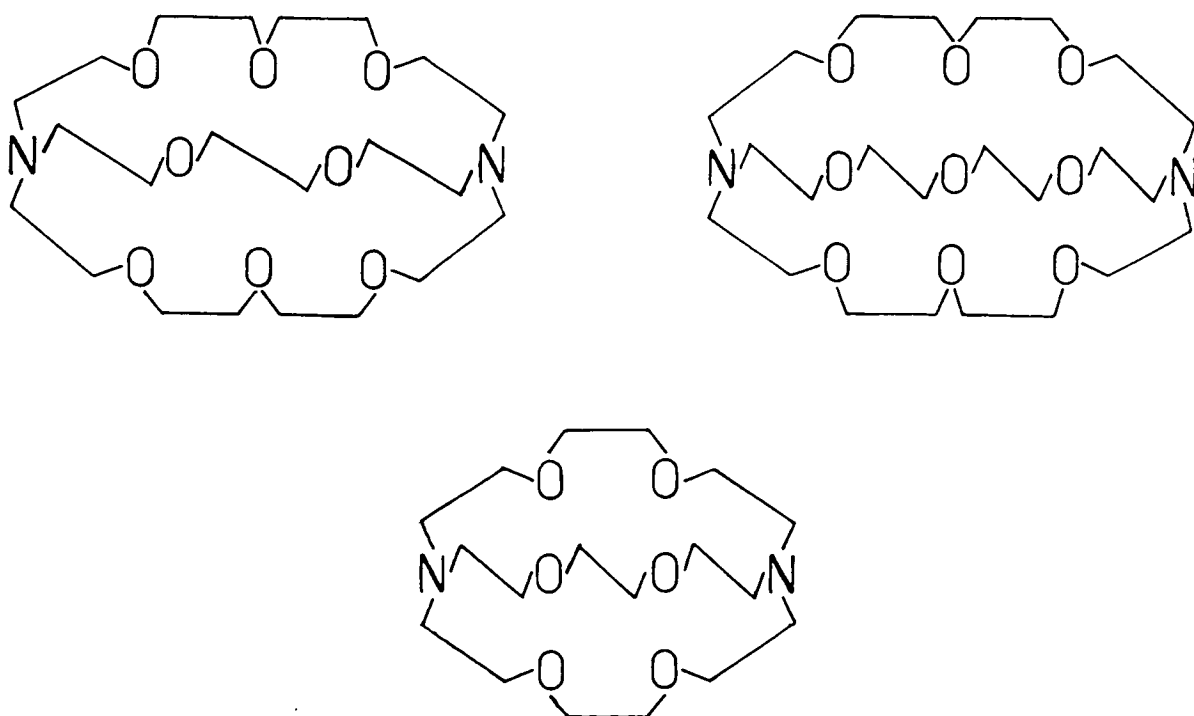
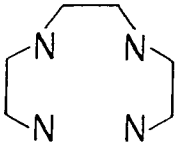
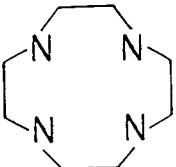


Table 2.1: Thermodynamics of Cu(II) Complex Formation with  
Ligands in Water (12)

	$\Delta H$ (K cal mol <sup>-1</sup> )	T $\Delta S$ (K cal mol <sup>-1</sup> )	$\Delta G$ (K cal mol <sup>-1</sup> )	log K
	-21.6	5.8	-27.4	20.1
	-18.3	15.3	-33.6	24.8

Initial studies by Hinz and Margerum <sup>(13)</sup> claimed the effect was due totally to enthalpy consideration but Kodama and Kimura <sup>(14)</sup> reached the opposite conclusion; that is that entropy was solely responsible. Later studies such as that of Anichini et al <sup>(15)</sup> indicate that entropy will always favour the formation of the macrocyclic complex due to the configurational entropy difference between the macrocycle and its relatively floppy open chain analogue. In contrast enthalpy terms in the macrocyclic effect can be favourable or unfavourable (see Table 2.1).

The variation in the enthalpy term is thought to arise from a combination of the following:-

1. The differences in the degree and nature of

- solvation of the free and complexed ligand.
2. The matching of the metal ion to the hole size of the strain free macrocycle.
  3. The ability of the macrocycle to match the preferred stereochemistry of the metal ion.
  4. Pre-organisation of the macrocyclic ligand for complexation.

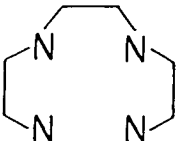
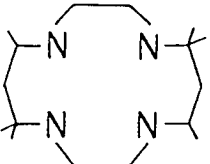
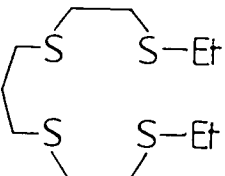
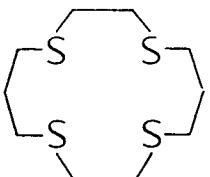
A further consideration in explaining the observed effect comes from kinetic work carried out by Cabbiness and Margerum (16) and later by Jones et al (17). They determined the formation and dissociation rates of macrocyclic complexes versus their open chain analogues, some of the results of which are summarised in Table 2.2. These reveal that the dissociation rate,  $K_d$ , is much slower for the macrocyclic complex, compared to its chelate analogue, however this more than compensates for its less favourable formation rate,  $K_f$ . The difference in dissociation rates was attributed to the contrasting mechanisms involved. Chelates undergo successive  $S_n1$  replacement of the donor atoms by solvent molecules at one or both ends. The cyclic ligand, having no ends, cannot be displaced in such a simple manner and the proposed mechanism involves initial distortion, so weakening a bond, which is then eventually cleaved on attack by solvent.

Thus the combination of dissociative constraints and the enthalpy and entropy terms generally leads to the enhanced stability of the macrocyclic complex over its open chain



analogue.

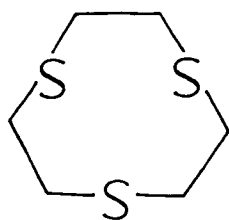
Table 2.2: Kinetic Data for Cu(II) Complexes at 298K

	Solvent	$K_f$ ( $m^{-1}s^{-1}$ )	$K_d$ ( $s^{-1}$ )
	H <sub>2</sub> O <sup>(15)</sup>	$8.9 \times 10^4$	4.1
	H <sub>2</sub> O <sup>(15)</sup>	$5.8 \times 10^{-2}$	$3.6 \times 10^{-7}$
	80% MeOH <sup>(16)</sup>	$4.1 \times 10^5$	$3.0 \times 10^4$
	80% MeOH <sup>(16)</sup>	$2.8 \times 10^4$	9

### 2.1.3 Synthesis and complexes of [9]aneS3

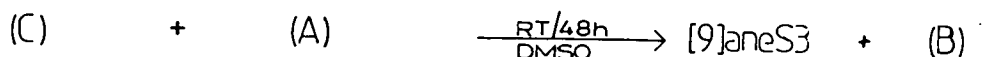
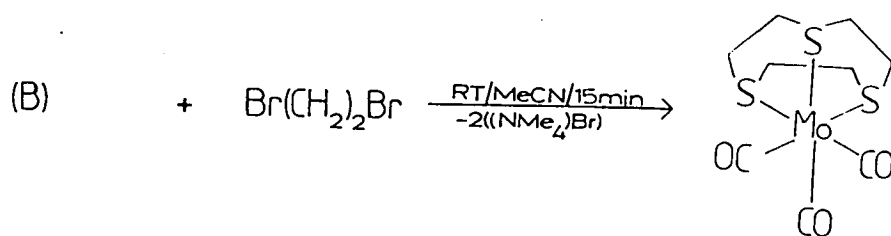
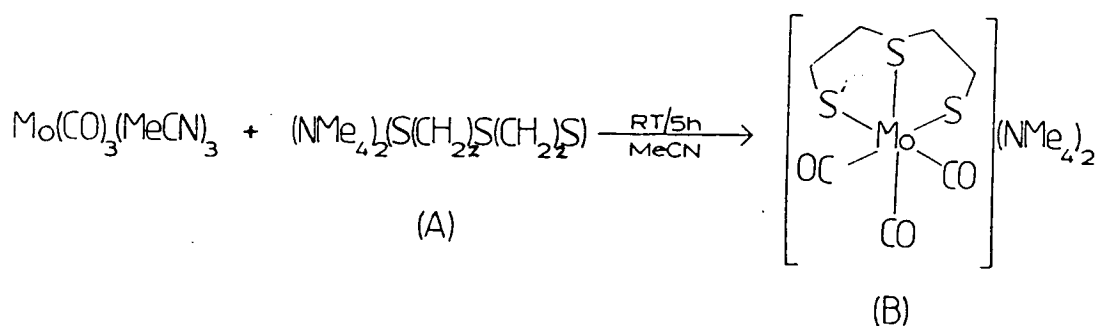
The work described in this chapter involves the complexation of [9]aneS3 [32] to Ru(II) and Os(II) centres. [9]aneS3 was first synthesised, though in low yield (0.04%), by Gerber et al<sup>(18)</sup> in 1977. This work showed that Ray had earlier synthesised p-dithiane and not [9]aneS3 as claimed in his

paper of 1920.



[32]

Scheme 2.4: Molybdenum Template synthesis of [9]aneS3



This low yield was later improved by Setzer et al (20) in 1986 to 4.4% and further, by a modified method, to 20% by Hartman and Cooper (21). In 1987 Sellman and Zaff (22) reported a high yield (60%) template synthesis which is outlined in scheme 2.4. Finally a high yield, one step synthesis that

required no chromatography step was reported by Blower and Cooper (23) in 1987. Their method used the cesium carbonate mediated cyclisation first reported by Butler and Kellogg (24,25). The exact role of cesium carbonate in favouring cyclisation over polymerisation is unclear but it has been suggested (22) that there is ion pairing occurring between  $\text{Cs}^{2+}$  and  $\text{RS}^-$  which under high dilution gives the observed product.

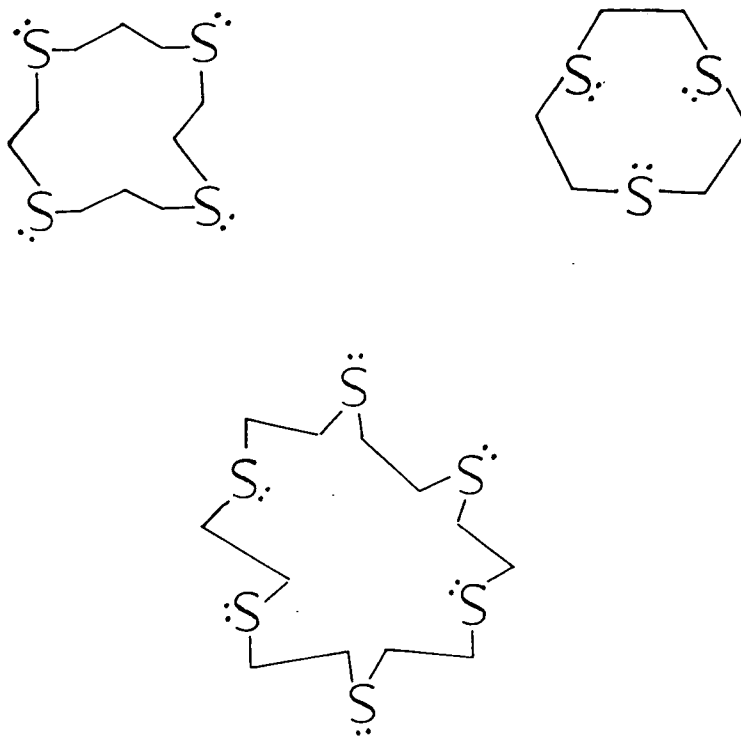
Crystallographic (26) and gaseous (27) studies showed that [9]aneS3 has  $\text{C}_3$  symmetry. This conformation is different from its oxygen analogue which is asymmetric from n.m.r. and IR studies (29). The single crystal x-Ray diffraction study revealed that the intra-molecular S-S distance was  $3.45\text{\AA}$  (the S-S Van Der Waals contact distance is  $3.70\text{\AA}$  (29)) which indicates that further investigation is required such as an ED study to see if this is a solid state effect.

The following factors should lead to the formation of [9]aneS3 complexes which are unusually stable:-

1. The sulphurs are all rigidly held so that no preorganisation of the ligand is required before coordination unlike other polythia macrocycles such as [12]aneS4 (30) or [18]aneS6 (31) (see Figure 2.3).
2. The relative spacial positions of the sulphurs are suitable for tridentate co-ordination to a metal center with little or no change to the internal conformation of the ligand.

3. There will be a decrease in the dipole-dipole repulsion between the sulphur donors on co-ordination.

Figure 2.3: Conformation of Some Polythia Macrocycles



To date several complexes of [9]aneS<sub>3</sub> have been reported, but these are mainly concerning species of the type  $[M([9]aneS_3)_2]^{n+}$ . In most cases these exhibit novel coordination and/or redox properties, a brief summary of which is given in the following pages.

Mo

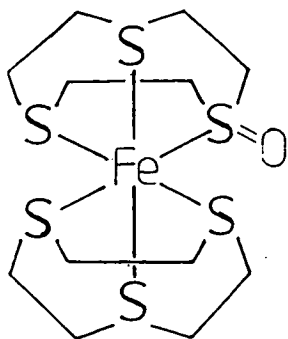
The complex  $\text{Mo}(\text{CO})_3([\text{9}]aneS3)$  (22,32) has been prepared as shown in scheme 2.3, that is, as an intermediate in the synthesis of the free macrocycle. The chloride analogue,  $\text{MoCl}_3([\text{9}]aneS3)$ , prepared by treating  $\text{MoCl}_3(\text{THF})_3$  with  $[\text{9}]aneS3$ , has also been reported (33).

Fe, Ru, Os

All three species of the type  $[\text{M}([\text{9}]aneS3)_2]^{2+}$  ( $\text{M}=\text{Fe}$  (34),  $\text{Ru}$  (35-38) and  $\text{Os}$  (35), have been reported with X-Ray diffraction studies carried out on the  $\text{Fe}$  (34) and  $\text{Ru}$  (35-38) complexes. These studies revealed that both metals have a distorted octahedral geometry and in the case of  $\text{Ru}$  the solvent of crystallisation seemed to exhibit some inclusion behaviour (35).

The electrochemical behaviour of  $[\text{Fe}([\text{9}]aneS3)_2]^{2+}$  in  $\text{MeCN}$  shows a reversible  $\text{Fe}(\text{II})/(\text{III})$  couple at 0.982V vs  $\text{Fc}^+/\text{Fc}$  (34). The complex was subsequently chemically oxidised with the resulting product dependent on the oxidant used (39). The chemical oxidant  $\text{PbO}_2$  generates  $[\text{Fe}([\text{9}]aneS3)_2]^{3+}$ , however  $\text{S}_2\text{O}_8^{2-}$  affords the species  $[\text{Fe}([\text{9}]aneS3)([\text{9}]aneS3(\text{O}))]^{2+}$  [33] i.e. the ligand rather than the metal has been oxidised. The oxidation potential of the free ligand is +0.99V vs  $\text{Fc}^+/\text{Fc}$  (39) which is close to that of the metal-based (II)/(III) couple of the parent complex.





[33]

The Ru(II) complex is more stable than its Fe analogue with a quasi reversible Ru(II)/(III) couple observed at +1.41V vs  $\text{Fc}^+/\text{Fc}$  in MeCN. Such a positive potential reflects the degree to which [9]aneS3 meets the electronic and stereochemical requirements of Ru(II). This is emphasised in that the closely related complex  $[\text{Ru}([\text{12]aneS3})_2]^{2+}$  exhibits a Ru(II)/(III) couple at a potential 0.33V more cathodic than that of the [9]aneS3 complex (38).

The synthesis of the complex  $[\text{Os}([\text{9]aneS3})_2]^{2+}$  has been achieved in Edinburgh in very low yield ( $< 5\%$ ) (35); one of the aims of this research was to develop a realistic synthetic route to this compound and fully characterise it.

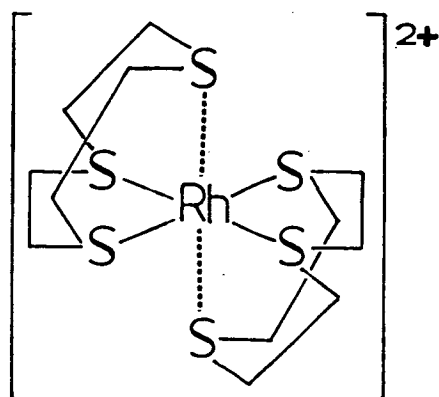
Other complexes containing [9]aneS3 are  $[\text{Ru}([\text{9]aneS3})(\text{C}_6\text{Me}_6)]^{2+}$ ,  $[\text{Os}([\text{9]aneS3})(4\text{-MeC}_6\text{H}_4^i\text{Pr})]^{2+}$  (36),  $[\text{Fe}(\text{C}_5\text{H}_5)([\text{9]aneS3})]^+$  (40),  $\text{MCl}_3([\text{9]aneS3})(\text{M}=\text{Fe})$  (34),  $\text{Ru}$  (36) and  $[\text{RuCl}(\text{DMSO})_2([\text{9]aneS3})](\text{PF}_6)$  (35).

Co, Rh and Ir

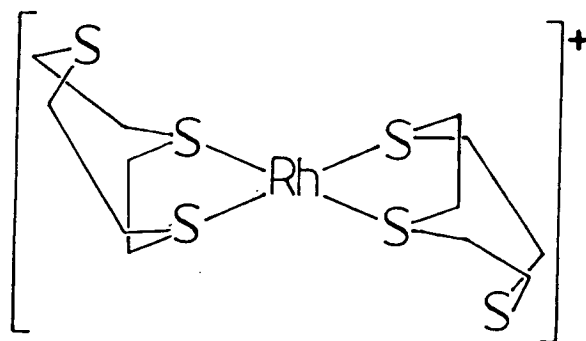
All three  $[M([9]aneS3)_2]^{n+}$  species have been reported. The stable Co(II) complex synthesised by Setzer et al (20) was found to have a slightly distorted octahedral co-ordination sphere (Co-S 2.356, 2.240 and 2.367Å). An electrochemical study of  $[Co([9]aneS3)_2]^{2+}$  in MeCN (34) shows two reversible one-electron processes at -0.013V(ox) and -0.86V(red) vs  $Fc^+/Fc$  i.e. the Co(II)/(III) and Co(II)/(I) couples respectively. These results are interesting in that Co(II)/(III) couples are generally electrochemically irreversible due to changes in the spin state (high  $\longrightarrow$  low) and the Co-L bond lengths. This can however be explained as from magnetic studies  $[Co([9]aneS3)_2]^{2+}$  is found to be low spin and Wieghardt et al (41) have shown that the Co-S distances in the chemically generated  $[Co([9]aneS3)_2]^{3+}$  are on average only 0.068Å shorter than those of the parent complex.

The analogous Rh complex  $[Rh([9]aneS3)_2]^{3+}$  has been shown to have near octahedral geometry (42,43) (Rh-S 2.345, 2.348 and 2.331Å). Electrochemical studies of the complex in MeCN reveal two separate and chemically reversible one-electron reductions at -0.71 and -1.08V vs  $Fs^+/Fc$  (43) which parallels the electrochemistry exhibited by the Co complex. The stable nature of the Rh(II) species formed on the first reduction contrasts with the normally elusive nature of monomeric Rh(II) species which tend to dimerise in solution (43). This must reflect the continued interaction of all 6 donor atoms,

probably via a tetragonal elongation [34] to accommodate the Jahn-Teller distorted geometry generally exhibited by  $d^7$  centres.



[34]



[35]

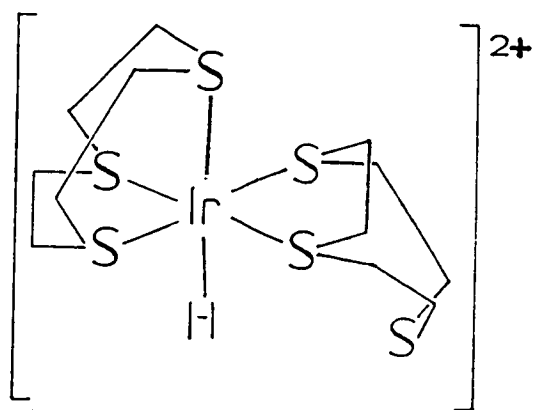
The second reduction to the Rh(I) species although chemically reversible has a large  $\Delta E_p$  value (127mV cf Rh(III)/(II)  $\Delta E_p=71\text{mV}$  at 293K) which probably reflects a gross change in the co-ordination sphere about the Rh centre. This change is probably due to the adoption of the square planar geometry generally favoured by Rh(I)  $d^8$  species [35].

The Ir analogue,  $[\text{Ir}([\text{9}]aneS3)_2]^{3+}$  (44), has also been synthesised and was found to have a near perfect octahedral co-ordination sphere (Ir-S 2.342, 2.341 and 2.338Å; S-Ir-S' 88.3-89.1° S and S' of the same macrocycle).

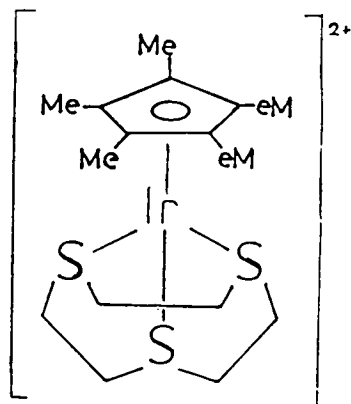
Interestingly, the complex was synthesised upon the action of nitric acid on the hydride complex  $[\text{Ir}(\text{H})([\text{9}]aneS3)_2]^{2+}$  (44) [36]. The hydride complex has one [9]aneS3 bound by three

sulphurs while the other is bound only by two. The Ir-S bond trans to the hydride is significantly longer (0.155Å) than the other four (2.321Å average).

The complexes  $[M([9]aneS3)(C_5Me_5)]^+$  (M=Rh, Ir) [37] and  $IrCl_3([9]aneS3)$  (36) have also been synthesised.



[36]

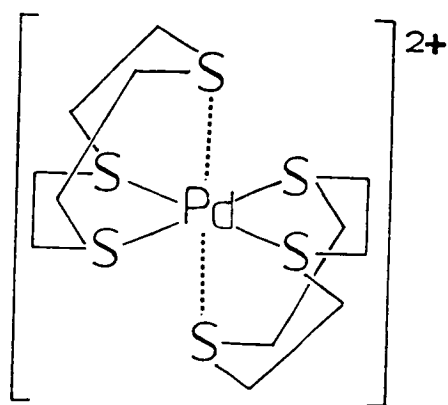


[37]

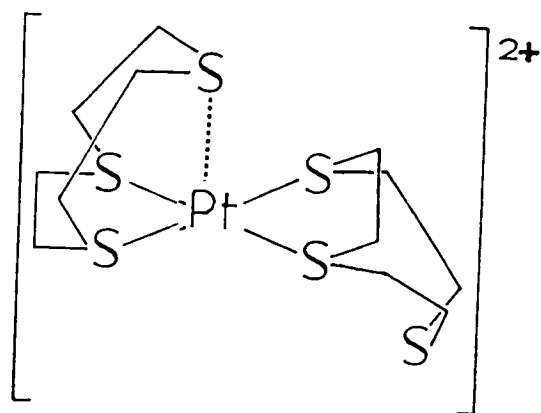
### Ni, Pd and Pt.

The complex  $[Ni([9]aneS3)_2]^{2+}$  was first reported by Setzner et al (20) in 1983 and found to have a slightly distorted octahedral co-ordination sphere (Ni-S 2.377, 2.380 and 2.400Å). Later Wieghardt et al (34) showed that the complex exhibited a quasi-reversible one electron oxidation at +0.97V vs  $Fc^+/Fc$  in MeCN. However further work is necessary to prove that this is a Ni(II)/(III) couple rather than a quasi-reversible oxidation of the ligand in the presence of the metal centre (an irreversible oxidation at +0.99V vs  $Fc^+/Fc$  is observed for the free ligand).

The analogous Pt(II) and Pd(II) species have co-ordination geometries which are different from that of their lighter congener Ni and also to the normal square planar geometry expected for these  $d^8$  centres. In the case of Pd(II) (45,46) all 6 sulphurs interact with the metal centre, four in an approximate square plane (Pd-S 2.332 and 2.311Å) with the other two exhibiting significant apical interactions (Pd-S 2.952Å) [38] (45). The Pt(II) analogue in contrast has only one apically interacting sulphur (Pt-S 2.9Å), the remaining S is non-bonding being on average 4.11Å from the Pt(II) centre [39] (47).



[38]



[39]

The Pd(II) complex exhibits a reversible one-electron oxidation at +0.605V vs  $Fc^+/Fc$  in MeCN ( $\Delta E_p=84mV$  at 293K) with e.s.r. studies of the electrochemically oxidised species confirming that the oxidation is metal based. This oxidation product was isolated via chemical oxidation, thus allowing a full x-Ray analysis which was the first to be carried out on a mononuclear Pd(III) centre. This showed that all 6 S-donor atoms interact with the Pd(III) centre to yield a tetragonally

elongated octahedral co-ordination (Pd-S 2.3558, 2.3692 and 2.5448Å) consistent with a Jahn-Teller distorted  $d^7$  complex. This is achieved by the apically interacting donor atoms of the parent complex moving towards the Pd centre on oxidation while the others move slightly outwards due to the restrictive conformation of the macrocycle.

The Pt(II) species also exhibits an oxidation this time at +0.39V vs  $Fc^+/Fc$  in MeCN (47) with the larger value of  $\Delta E_p$  (145mV at 293K) reflecting the more extensive rearrangement necessary to achieve a geometry which would be expected to be similar to that of the Pd(III) species. Further oxidation of Pt(III) to Pt(IV) is also observed (49).

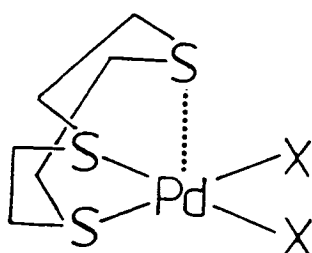
Other [9]aneS3 complexes of Pd(II) and Pt(II) have also been reported:-  $MCl_2([9]aneS3)$ ,  $[M(PPh_3)_2([9]aneS3)](PF_6)$  (M=Pd, Pt) (45) and  $PdBr_2([9]aneS3)$  (46). X-Ray diffraction studies carried out on  $PdX_2([9]aneS3)$  ( $X^- = Cl^-$  (50),  $Br^-$  (46)), both exhibit an apical interaction of the third sulphur donor ( $X^- = Cl^-$ , Pd-S=3.140;  $X^- = Br^-$ , Pd-S=3.00Å) [40] to the Pd(II) centre in what otherwise might be considered to be a planar complex.

### Cu, Ag and Au.

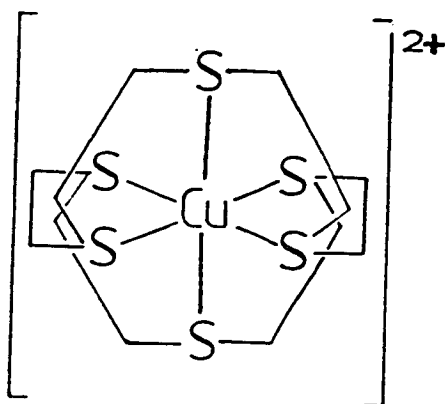
The complex  $[Cu([9]aneS3)_2]^{2+}$  was found to have a slightly distorted octahedral stereochemistry (20) (Cu-S 2.419, 2.426 and 2.459Å) which is a common feature of the first row

complexes of this type. Its electrochemical behaviour in  $\text{MeNO}_2$  consists of a quasi-reversible  $\text{Cu(II)/(I)}$  couple at  $+0.16\text{V}$  vs SCE (34).

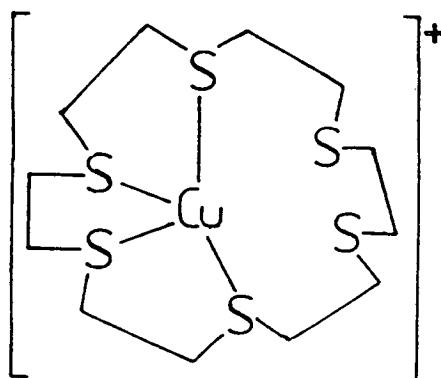
The single crystal X-Ray structures of  $[\text{Cu}(\text{[18]aneS6})]^{n+}$  ( $n=2,1$ ) (21) have been determined and a dramatic change in co-ordination between  $\text{Cu(II)}$ , distorted octahedral [41], and  $\text{Cu(I)}$ , severely distorted tetrahedral [42], was found. It would seem reasonable to suggest that a similar change in co-ordination occurs for the [9]aneS3 complex. The lower  $\text{Cu(II)/(I)}$  potential of the [9]aneS3 complex compared to that for  $[\text{Cu}(\text{[18]aneS6})]$  ( $+0.72\text{V}$  vs SCE), and the latter's reversibility, must imply the comparative inability of the [9]aneS3 complex to stabilise  $\text{Cu(I)}$ , presumably via a tri- and a monodentate ligand.



[40]

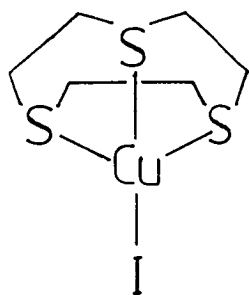


[41]

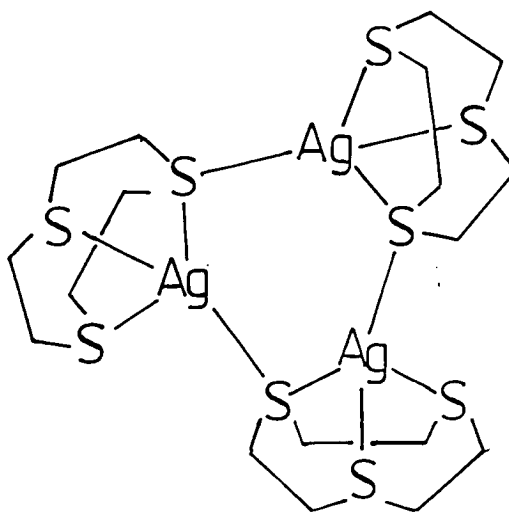


[42]

The tetrahedral geometry required by Cu(I) is evident in complexes such as  $\text{CuI}([\text{9}]\text{aneS3})$  [43] (51),  $[\text{Cu}(\text{PPh}_2)([\text{9}]\text{aneS3})]^+$  (52) and  $[\text{Cu}_2([\text{18}]\text{aneS6})(\text{MeCN})_2]^{2+}$  (53). For complexes such as  $\text{Ag}(\text{NO}_3)([\text{9}]\text{aneS3})$  and  $\text{Cu}(\text{ClO}_4)([\text{9}]\text{aneS3})$  (51) Wieghardt et al proposed that a similar structure to  $[\text{Ag}_3([\text{9}]\text{aneS3})_3]^{3+}$  [44] is formed, this latter complex being the first example of a bridging crown thioether (51).



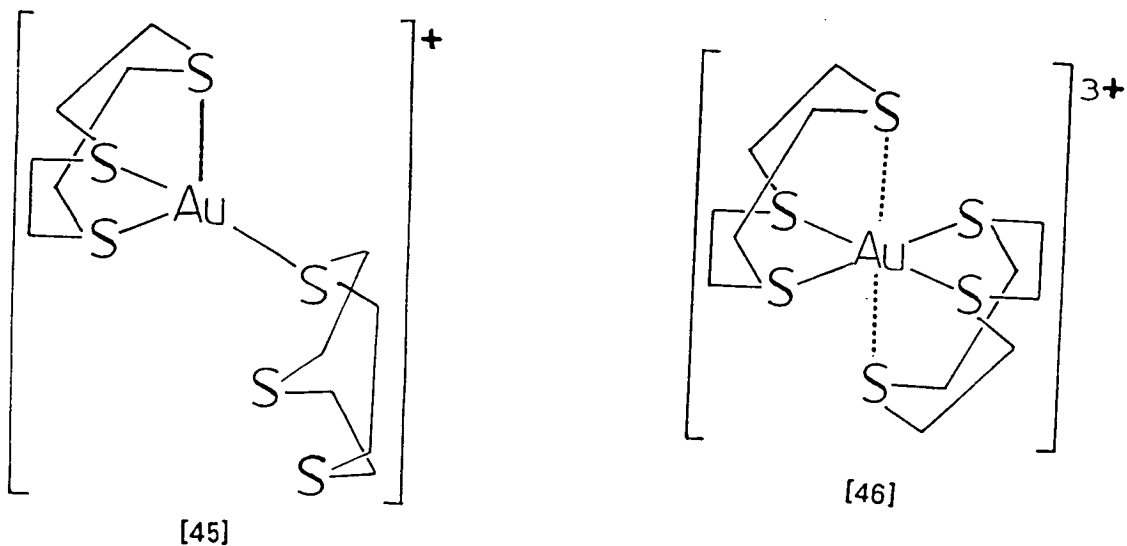
[43]



[43]

The complex  $[\text{Ag}([\text{9}]\text{aneS3})_2]^+$  (54) has regular octahedral symmetry (Ag-S 2.696-2.753Å) which contrasts with other structurally characterised silver thioether complexes - found to be two co-ordinate (55) or irregular and polymeric (56-58).

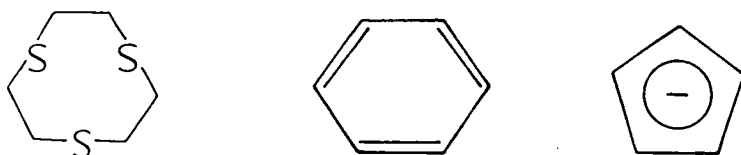




The electrochemistry of  $[\text{Ag}(\text{[9]aneS3})_2]^+$  in  $\text{MeNO}_2$  consists of a reversible one-electron oxidation at +1.30V vs NHE. The reversible nature of the process, which is uncommon, again reflects the ability of [9]aneS3 to adapt to the stereochemical requirements of differing oxidation states.

An X-Ray analysis has been carried out on both  $[\text{Au}(\text{[9]aneS3})_2]^+$  [45] and  $[\text{Au}(\text{[9]aneS3})_2]^{3+}$  [46] (59). For  $[\text{Au}(\text{[9]aneS3})_2]^+$ , one ligand is bound asymmetrically (Au-S 2.350, 2.733 and 2.825Å) while the other is only co-ordinated via one of the sulphurs (Au-S 2.302Å cf the suggested structure for  $[\text{Cu}(\text{[9]aneS3})_2]^+$ ) and is the first example of [9]aneS3 acting as a monodentate ligand. In contrast  $[\text{Au}(\text{[9]aneS3})_2]^{3+}$  exhibits a tetragonally elongated octahedral geometry (Au-S 2.348, 2.354 and 2.926Å) analogous to the Pd(II) complex.

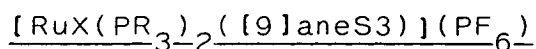
Figure 2.4: [9]aneS3 and Analogous 6e<sup>-</sup> Donor Ligands



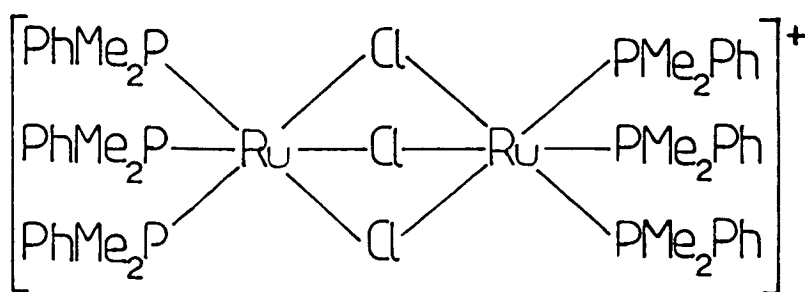
As mentioned in section 2.1.1 a number of areas of interest concerning macrocyclic complexes exist. The present study set out to investigate the use of [9]aneS<sub>3</sub> as a protecting group to Ru(II) and Os(II) metal centres. For this purpose [9]aneS<sub>3</sub>, analogous to other 6e<sup>-</sup> donor ligands such as arenes (see Figure 2.4), should be ideal as it is able to co-ordinate facially to these metal centres via all three sulphur donors with little or no conformational change. This should result in the strong complexation of the ligand to the metal centre and hence fulfil its desired role as a protecting group.

## 2.2 Results and Discussion

### 2.2.1 Achiral Bisphosphine Complexes:



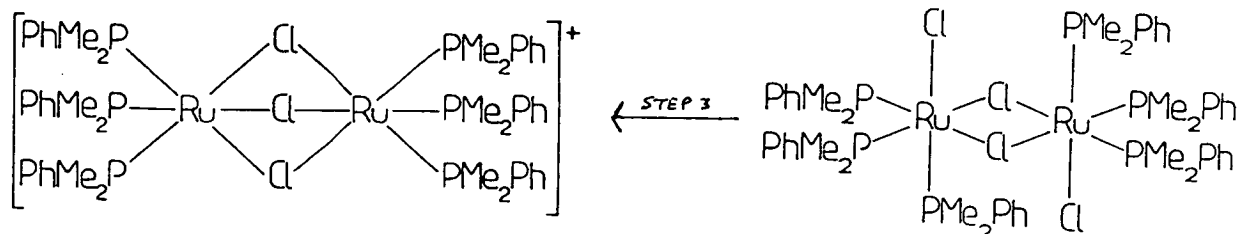
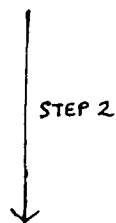
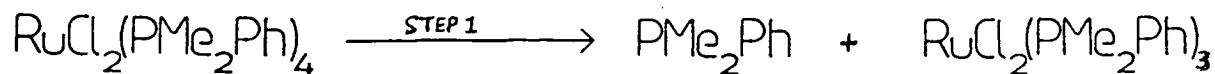
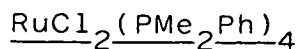
Reaction of  $RuCl_2(PMe_2Ph)_4$  with one molar equivalent of [9]aneS3 in refluxing EtOH yielded a light yellow solution. Addition of an excess of  $NH_4PF_6$  afforded a light yellow precipitate. The  $^{31}P-(^1H)$  spectrum, however revealed that the product was the already known binuclear species  $[Ru_2Cl_3(PMe_2Ph)_6](PF_6^-)$  [47]. The same product was also formed if  $CH_2Cl_2$  was used instead of EtOH.



[47]

The proposed mechanism for the formation of [47] involves dissociation of  $PMe_2Ph$  to give  $RuCl_2(PMePh)_3$ , dimerisation then occurs with subsequent loss of chloride (see scheme 2.5).

Scheme 2.5: Formation of  $[\text{Ru}_2\text{Cl}_3(\text{PMe}_2\text{Ph})_6]\text{Cl}$  from



It seems likely that further ligand dissociation (either  $\text{Cl}^-$  or  $\text{PMe}_2\text{Ph}$ ) would be required after step 1 for initial co-ordination of [9]aneS3 due to steric considerations. Obviously, this does not occur, possibly exacerbated by the presence of free  $\text{PMe}_2\text{Ph}$  on forming  $\text{RuCl}_2(\text{PMe}_2\text{Ph})_3$ , and thus the binuclear species [47] is the sole product.

A light yellow solution was obtained after 4 hours on treating the Ru(III) monomer  $\text{RuCl}_3(\text{PMe}_2\text{Ph})_3$  with one molar equivalent of [9]aneS3 in refluxing  $\text{CH}_2\text{Cl}_2$ . On removal of the solvent, addition of a small volume of EtOH and an excess of  $\text{NH}_4\text{PF}_6$  a light yellow precipitate formed. Apart from resonances

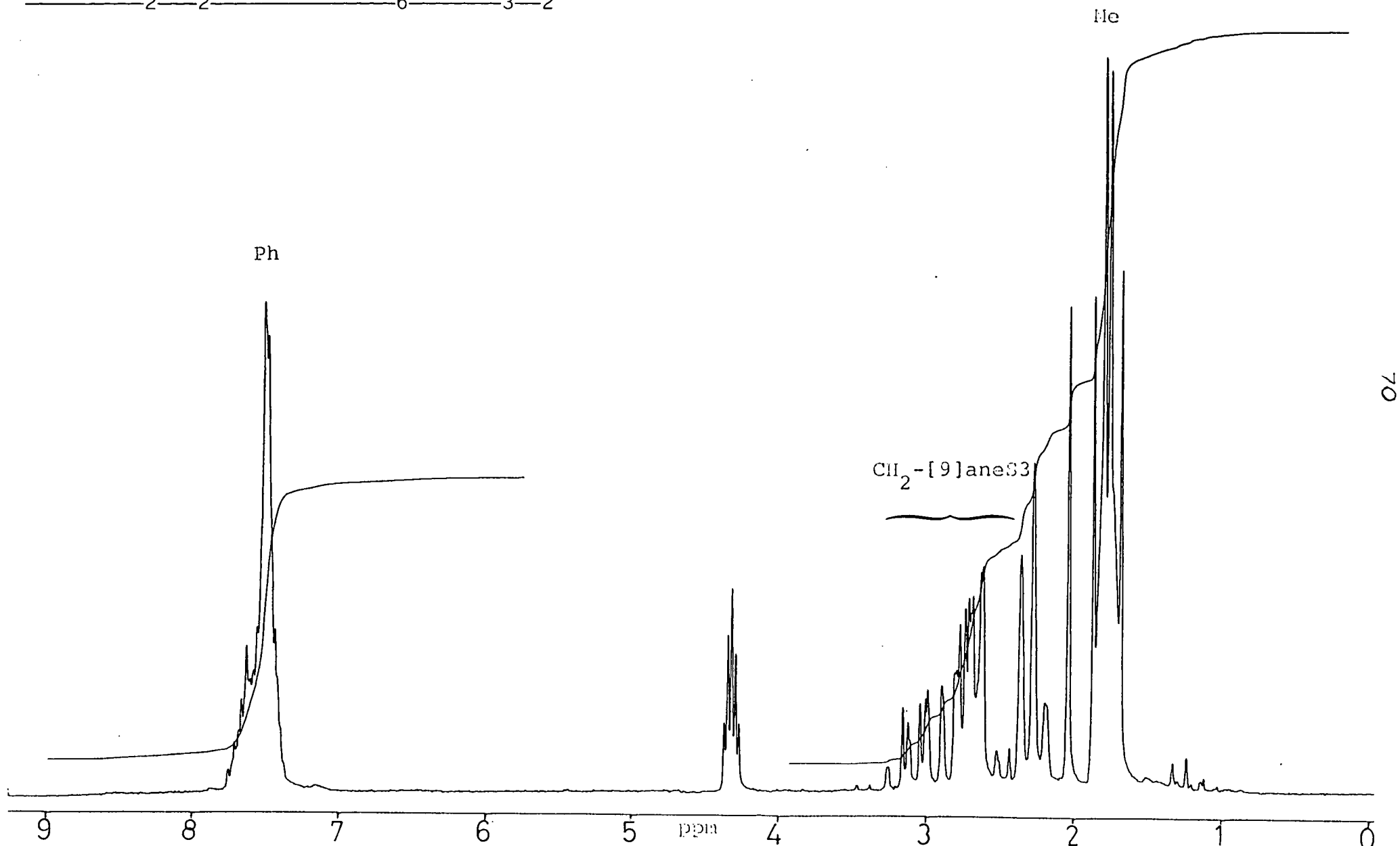
associated with the counterion,  $(PF_6)^-$ , only one other resonance was observed in the  $^{31}P-(^1H)$ n.m.r. spectrum. This resonance at 4.84 p.p.m. was not however due to the binuclear species (47). The  $^1H$  n.m.r. spectrum indicated that [9]aneS3 had been incorporated by a series of resonances between 2.18 and 3.25 p.p.m. (see Figure 2.5). The ratio of [9]aneS3:  $PMe_2Ph$  of 2:1, along with analytical and FAB mass spectral data indicated that the isolated complex was  $[RuCl(PMe_2Ph)_2([9]aneS3)](PF_6)$  [48].

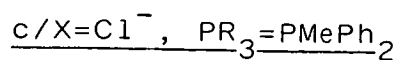
As [48] is the sole product it suggests that  $RuCl_2(PMe_2Ph)_3$  is not formed and that the reaction proceeds via the co-ordination of [9]aneS3 to a Ru(III) centre. Reduction to form [48] may result from the concomitant oxidation of  $Cl^-$  or  $PMe_2Ph$ .

$b/X=Cl^-$ ,  $PR_3=PEt_2Ph$

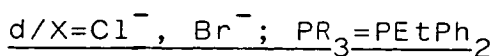
The complex  $[RuCl(PEt_2Ph)_2([9]aneS3)](PF_6)$  can also be synthesised by treating  $RuCl_3(PEt_2Ph)_3$  with one molar equivalent of [9]aneS3 in refluxing  $CH_2Cl_2$ . A resonance for co-ordinated  $PEt_2Ph$  is observed at 21.30p.p.m. in the  $^{31}P-(^1H)$  n.m.r. spectrum while the  $^1H$  n.m.r. spectrum indicates the co-ordination of the macrocycle. Elemental and FAB mass spectral data confirm the formulation.

Figure 2.5:  $^1\text{H}$  n.m.r. Spectrum of  
 $[\text{RuCl}(\text{PMe}_2\text{Ph})_2\{[9]\text{aneS3}\}](\text{PF}_6)$  in  $\text{CD}_3\text{NO}_2$





Only the starting materials were recovered on treating  $RuCl_3(PMePh_2)_3$  with [9]aneS3 in refluxing  $CH_2Cl_2$  even for prolonged periods (24 hours). If EtOH or methoxyethanol are used instead of  $CH_2Cl_2$  only the binuclear species  $[Ru_2Cl_3(PMePh_2)_6]^+$  [49] was formed. This is indicative of reduction of  $RuCl_3(PMePh_2)_3$  by these reducing solvents to give  $RuCl_2(PMePh_2)_3$  which quickly dimerises to give [49] (cf scheme 2.4).



Reaction of  $RuCl_2(PEtPh_2)_3$  with one molar equivalent of [9]aneS3 in refluxing EtOH for 10 minutes yielded a light yellow solution. Addition of an excess of  $NH_4PF_6$  afforded a light yellow precipitate. The  $^{31}P-(^1H)$  n.m.r. spectrum of the complex consisted of a resonance at 24.46 p.p.m. (not due to  $[Ru_2Cl_3(PEtPh_2)_6]^+$ ) as well as the usual multiplet for  $(PF_6)^-$ .

Direct evidence for the incorporation of [9]aneS3 was provided by the  $^1H$  n.m.r. spectrum which clearly showed resonances for the co-ordinated ligand between 1.84 and 3.20 p.p.m., the relative ratio of [9]aneS3:  $PEtPh_2$  was found to be 1:2.

The formulation of the complex as  $[RuCl(PEtPh_2)_2([9]aneS3)](PF_6)$  [50] was confirmed by FAB mass spectral data and elemental analysis.

The analogous bromide complex  $[RuBr(PEtPh_2)_2([9]aneS3)](PF_6)$  may also be prepared by reaction of  $RuBr_2(PEtPh_2)_3$  with [9]aneS3 in refluxing  $CH_2Cl_2$ .

It is interesting to note that in refluxing EtOH the other phosphine monomers will only form binuclear complexes such as [47]. This may be due to ligand dissociation (either  $X^-$  or  $PEtPh_2$ ) from  $RuX_2(PEtPh_2)_3$  being a facile process in comparison to the other monomers thus yielding [50] instead of a binuclear product.

To confirm the proposed octahedral co-ordination of the complexes  $[RuX(PR_3)_2([9]aneS3)](PF_6)$  ( $X=Cl^-$ ;  $PR_3=PEt_2Ph$ ,  $PEtPh_2$ ,  $PMe_2Ph$ ;  $X=Br^-$ ,  $PR_3=PEtPh_2$ ) and to obtain data on M-L bond lengths, bright yellow crystals of [50] were grown by the slow diffusion of  $Et_2O$  into a  $CH_2Cl_2$  solution of the complex. Details of the structural solution, which converged to give a final R factor of 5.84%, are given in the experimental section. An ortep plot of the structure is given in Figure 2.6 while selected bond lengths, bond angles and torsion angles are given in Tables 2.3-5.

As expected the Ru(II) centre is in an octahedral environment, bound to a chloride, two  $PEtPh_2$  ligands and all three sulphur donor atoms of [9]aneS3. The Ru-S bond lengths are not all the same due to the differing ligands trans to them. The Ru-S bond trans to chloride ( $2.294(4)\text{\AA}$ ) being  $0.08\text{\AA}$  shorter (average of  $2.387(4)$  and  $2.369(4)\text{\AA}$ ) than those trans to the  $PEtPh_2$  ligands. Thus from this and the other structurally determined [9]aneS3 complexes of Ru(II)  $[(RuCl(MeCN)(PPh_3)([9]aneS3)](PF_6)$  [51] (see section 2.2.4) and  $[Ru([9]aneS3)_2]^{2+}$  [52] <sup>(35)</sup> -see table 2.6)



Figure 2.6: Ortep Plot of  $[\text{RuCl}(\text{PEtPh}_2)_2(\text{[9]aneS3})]^+$

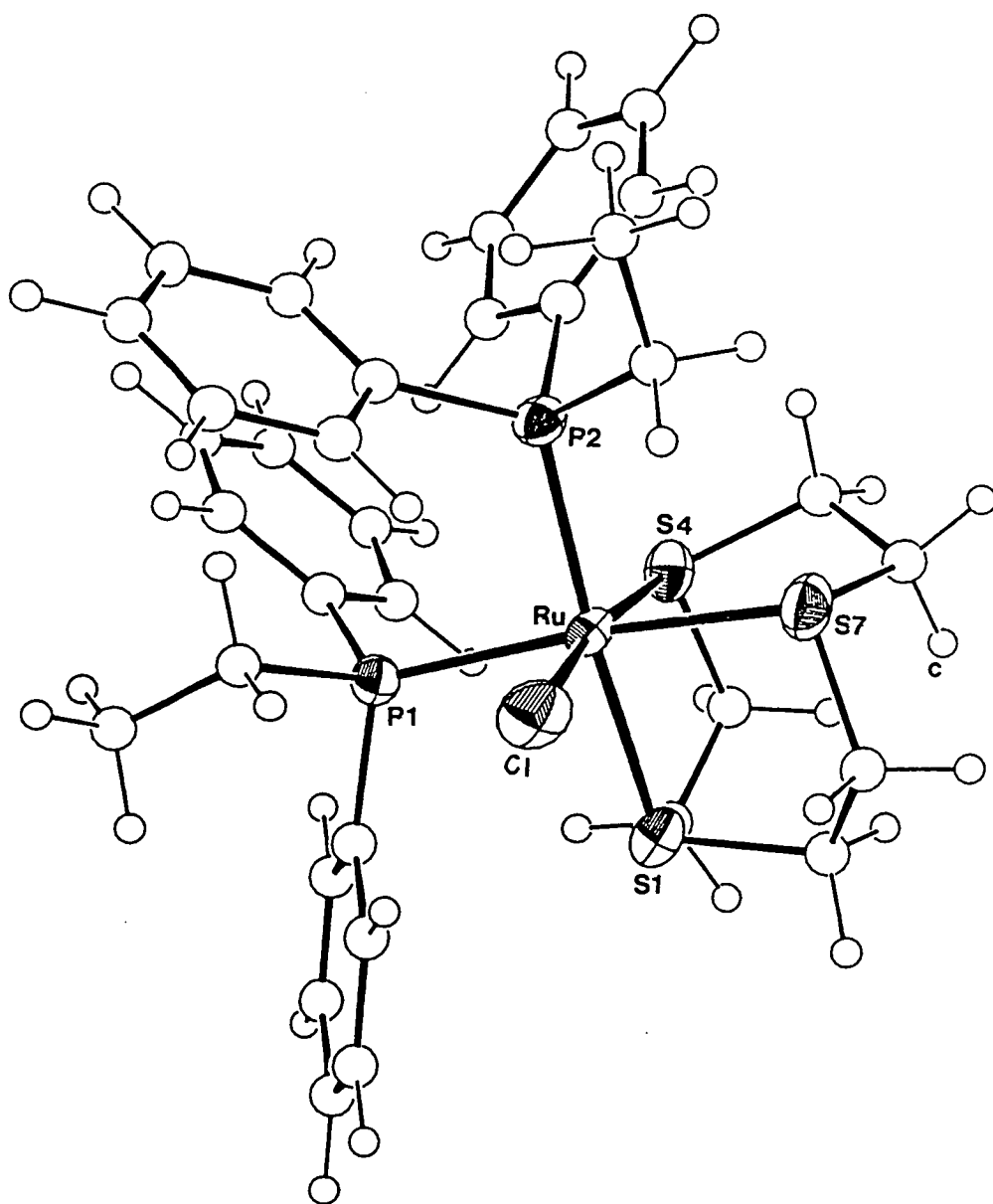


Table 2.3: Selected Bond Lengths (Å) with Standard Deviations  
for [RuCl(PEtPh<sub>2</sub>)<sub>2</sub>([9]aneS3)]<sup>+</sup>

R(u) - Cl	2.453( 4)	C(2S) -C(3S)	1.516(20)
R(u) - S(1)	2.387( 4)	C(3S) - S(4)	1.878(14)
R(u) - S(4)	2.294( 4)	S(4) -C(5S)	1.829(14)
R(u) - S(7)	2.369( 4)	C(5S) -C(6S)	1.543(19)
R(u) - P(1)	2.378( 4)	C(6S) - S(7)	1.835(15)
R(u) - P(2)	2.383( 4)	S(7) -C(8S)	1.823(15)
S(1) -C(2S)	1.826(15)	C(8S) -C(9S)	1.506(21)
S(1) -C(9S)	1.829(15)		

Table 2.4: Selected Angles (°) with Standard Deviations for  
[RuCl(PEtPh<sub>2</sub>)<sub>2</sub>([9]aneS3)]<sup>+</sup>

Cl - R(u) - S(1)	87.57(14)	R(u) - S(1) -C(2S)	102.4( 5)
Cl - R(u) - S(4)	170.86(15)	R(u) - S(1) -C(9S)	106.8( 5)
Cl - R(u) - S(7)	85.20(14)	C(2S) - S(1) -C(9S)	101.6( 7)
Cl - R(u) - P(1)	89.94(14)	S(1) -C(2S) -C(3S)	115.3(10)
Cl - R(u) - P(2)	91.26(14)	C(2S) -C(3S) - S(4)	111.5(10)
S(1) - R(u) - S(4)	87.45(15)	R(u) - S(4) -C(3S)	107.9( 4)
S(1) - R(u) - S(7)	85.26(15)	R(u) - S(4) -C(5S)	104.8( 4)
S(1) - R(u) - P(1)	89.74(14)	C(3S) - S(4) -C(5S)	99.5( 6)
S(1) - R(u) - P(2)	174.74(15)	S(4) -C(5S) -C(6S)	113.8( 9)
S(4) - R(u) - S(7)	86.75(14)	C(5S) -C(6S) - S(7)	110.0( 9)
S(4) - R(u) - P(1)	97.70(14)	R(u) - S(7) -C(6S)	107.1( 5)
S(4) - R(u) - P(2)	92.99(14)	R(u) - S(7) -C(8S)	103.4( 5)
S(7) - R(u) - P(1)	173.16(15)	C(6S) - S(7) -C(8S)	100.8( 7)
S(7) - R(u) - P(2)	89.54(14)	S(7) -C(8S) -C(9S)	113.4(10)
P(1) - R(u) - P(2)	95.38(14)	S(1) -C(9S) -C(8S)	111.6(10)

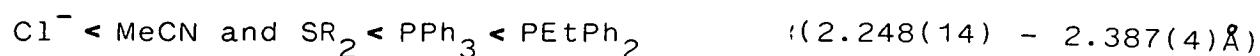
Table 2.5: Selected Torsion Angles ( $^{\circ}$ ) with StandardDeviations for  $[\text{RuCl}(\text{PEtPh}_2)_2([\text{9]aneS3})]^+$ 

Cl - R(u) - S(1) -C(2S)	167.8( 5)	S(1) - R(u) - S(7) -C(8S)	-20.5( 5)
Cl - R(u) - S(1) -C(9S)	-85.8( 5)	S(4) - R(u) - S(7) -C(6S)	-2.3( 5)
S(4) - R(u) - S(1) -C(2S)	-19.9( 5)	S(4) - R(u) - S(7) -C(8S)	-108.2( 5)
S(4) - R(u) - S(1) -C(9S)	86.5( 5)	P(1) - R(u) - S(7) -C(6S)	128.5(13)
S(7) - R(u) - S(1) -C(2S)	-106.8( 5)	P(1) - R(u) - S(7) -C(8S)	22.6(14)
S(7) - R(u) - S(1) -C(9S)	-0.5( 5)	P(2) - R(u) - S(7) -C(6S)	-95.3( 5)
P(1) - R(u) - S(1) -C(2S)	77.9( 5)	P(2) - R(u) - S(7) -C(8S)	158.7( 5)
P(1) - R(u) - S(1) -C(9S)	-175.8( 5)	R(u) - S(1) -C(2S) -C(3S)	41.2(11)
P(2) - R(u) - S(1) -C(2S)	-114.9(17)	C(9S) - S(1) -C(2S) -C(3S)	-69.1(12)
P(2) - R(u) - S(1) -C(9S)	-8.5(18)	R(u) - S(1) -C(9S) -C(8S)	27.3(11)
Cl - R(u) - S(4) -C(3S)	58.6(11)	C(2S) - S(1) -C(9S) -C(8S)	134.3(10)
Cl - R(u) - S(4) -C(5S)	-46.7(11)	S(1) -C(2S) -C(3S) - S(4)	-43.0(13)
S(1) - R(u) - S(4) -C(3S)	1.5( 5)	C(2S) -C(3S) - S(4) - R(u)	22.3(11)
S(1) - R(u) - S(4) -C(5S)	-103.8( 5)	C(2S) -C(3S) - S(4) -C(5S)	131.3(10)
S(7) - R(u) - S(4) -C(3S)	86.9( 5)	R(u) - S(4) -C(5S) -C(6S)	42.5(10)
S(7) - R(u) - S(4) -C(5S)	-18.5( 5)	C(3S) - S(4) -C(5S) -C(6S)	-68.9(10)
P(1) - R(u) - S(4) -C(3S)	-87.9( 5)	S(4) -C(5S) -C(6S) - S(7)	-46.3(12)
P(1) - R(u) - S(4) -C(5S)	166.8( 5)	C(5S) -C(6S) - S(7) - R(u)	27.3(10)
P(2) - R(u) - S(4) -C(3S)	176.2( 5)	C(5S) -C(6S) - S(7) -C(8S)	135.2(10)
P(2) - R(u) - S(4) -C(5S)	70.9( 5)	R(u) - S(7) -C(8S) -C(9S)	45.3(11)
Cl - R(u) - S(7) -C(6S)	173.4( 5)	C(6S) - S(7) -C(8S) -C(9S)	-65.4(11)
Cl - R(u) - S(7) -C(8S)	67.4( 5)	S(7) -C(8S) -C(9S) - S(1)	-48.9(13)
S(1) - R(u) - S(7) -C(6S)	85.4( 5)		

Table 2.6: Selected Structural Parameters for [9]aneS3 complexes of Ru(II)

	[RuCl(PEtPh <sub>2</sub> ) <sub>2</sub> ([9]aneS3)] <sup>+</sup>	[RuCl(MeCN)(PPh <sub>3</sub> )([9]aneS3)] <sup>+</sup>	[Ru([9]aneS3) <sub>2</sub> ] <sup>2+</sup>
Ru - Cl	2.453Å	2.493(13)Å	
Ru - P	2.378(4), 2.383(4)Å	2.360(14)Å	
Ru - N		2.01(4)Å	
Ru - S trans to Cl	2.294(4)Å	2.248(14)Å	
Ru - S trans to P	2.378(4), 2.369(4)Å	2.348(16)Å	
Ru - S trans to N		2.332(15)Å	
Ru - S (av.)			2.335Å
∑ S - Ru - S	259.46	263.7	263.33

a rough series of the Ru-S bond lengths as a function of the trans ligand can be obtained i.e.



As the Ru-S bond is shortened by a trans  $\text{Cl}^-$  (a  $\Pi$ -donor) and lengthened by a trans trialkyl phosphine (a  $\Pi$ -acceptor) compared to a trans  $\text{SR}_2$  group, it seems that this is direct evidence for [9]aneS3 acting as a  $\Pi$ -acceptor via the sulphur empty low-lying d orbitals. Also of note is <sup>that</sup> the sum of the S-Ru-S bond angles for [50] is less than that of the other two complexes and its Ru-Cl bond length is significantly longer (0.045 $\text{\AA}$ ) than for [51]. This tends to suggest that there is steric crowding about the Ru(II) centre in [50] due to the bulky  $\text{PEtPh}_2$  ligands.

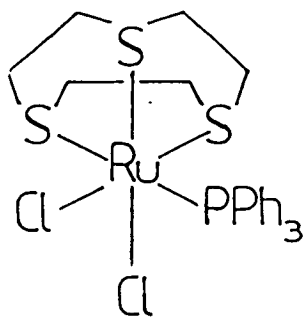
### 2.2.2 Achiral Bishalo Complexes: $\text{RuX}_2(\text{EPh}_3)([\text{9]aneS3})$

Reaction of  $\text{RuCl}_2(\text{PPh}_3)_3$  with one molar equivalent of [9]aneS3 in refluxing EtOH for 10 minutes yielded a bright yellow precipitate. The  $^{31}\text{P}$ -( $^1\text{H}$ ) n.m.r. spectrum consisted of a singlet at 22.96 p.p.m. for co-ordinated  $\text{PPh}_3$ . Incorporation of [9]aneS3 was confirmed by the  $^1\text{H}$  n.m.r. spectrum, with the ratio of [9]aneS3:  $\text{PPh}_3$  found to be 1:1. Elemental analysis and FAB mass spectral data confirmed the formulation of the complex as being  $\text{RuCl}_2(\text{PPh}_3)([\text{9]aneS3})$  [53]. The complex, [53] may also be formed by

1. The use of  $\text{CH}_2\text{Cl}_2$  instead of EtOH.
2. Reaction of  $\text{RuCl}_3(\text{NO})(\text{PPh}_3)_2$  with [9]aneS3 in

refluxing  $\text{CH}_2\text{Cl}_2$ .

3. Reaction of  $[\text{RuCl}_2(\text{CS})(\text{PPh}_3)_2]_2$  with [9]aneS3 in refluxing EtOH.



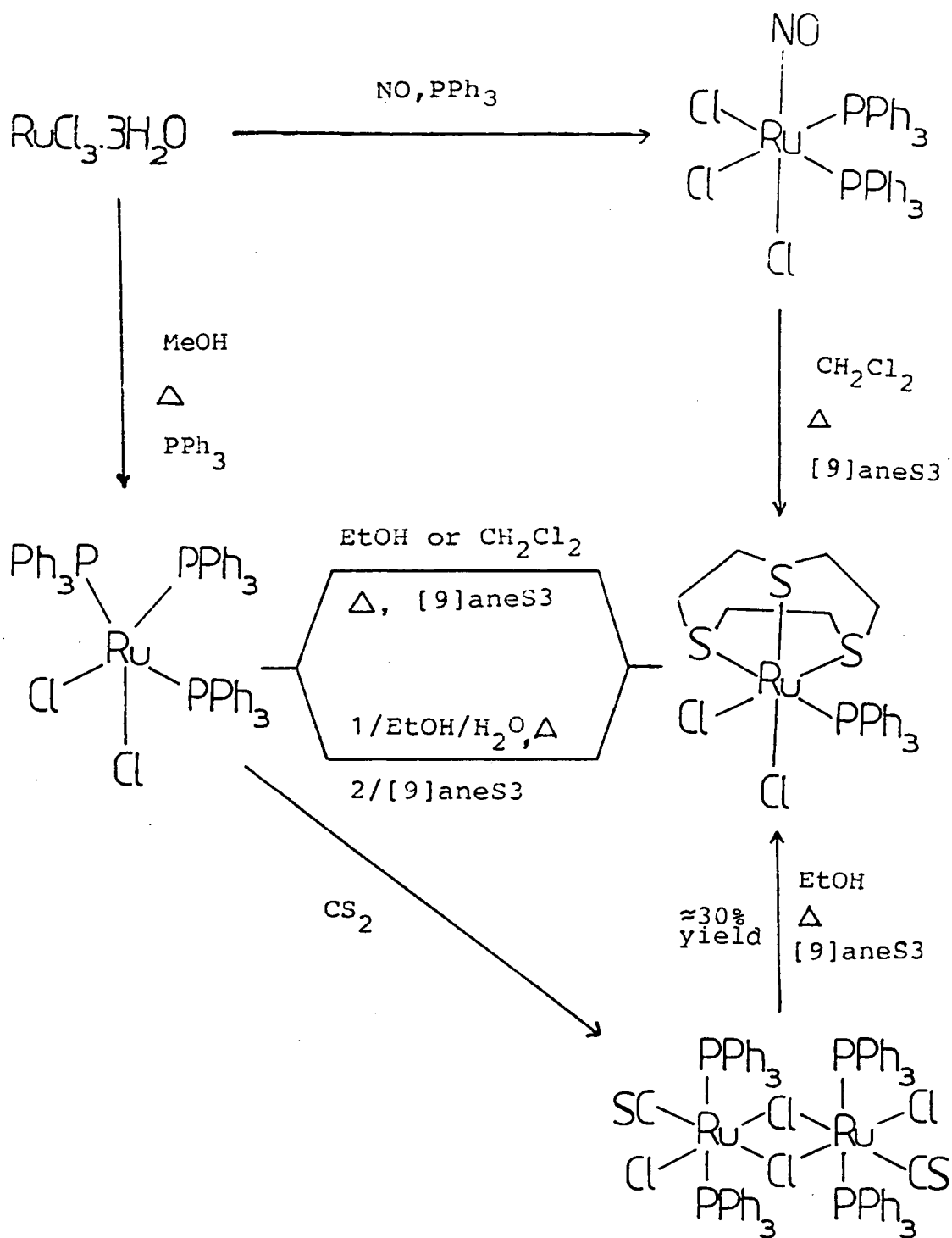
[53]

These preparative routes are summarised in scheme 2.6 and apart from method 3 (30%) the complex was obtained in high yield.

The analogous bromide complex  $\text{RuBr}_2(\text{PPh}_3)([\text{9]aneS3})$  can be prepared by reaction of  $\text{RuBr}_2(\text{PPh}_3)_3$  with one molar equivalent of [9]aneS3 in refluxing EtOH, the resulting precipitate being a slightly darker yellow than its chloride analogue [53].

Although no comparable  $\text{AsPh}_3$  complex such as  $\text{RuCl}_2(\text{AsPh}_3)_3$  is known the bright yellow complex  $\text{RuCl}_2(\text{AsPh}_3)([\text{9]aneS3})$  can be prepared by treating  $\text{RuCl}_3(\text{AsPh}_3)_2(\text{MeOH})$  with one molar equivalent of [9]aneS3 in refluxing EtOH for 15 hours.

Scheme 2.6: Synthetic routes to  $\text{RuCl}_2(\text{PPh}_3)([9]\text{aneS}_3)$



No evidence for the formation of complexes of the type  $[\text{RuX}(\text{EPh}_3)_2([\text{9}] \text{aneS3})]^+$  was found; this may be due to the electronic and/or steric factors (cf  $[\text{RuCl}(\text{PEtPh}_2)_2([\text{9}] \text{aneS3})]^+$  which seemed to exhibit steric crowding). Complexes such as  $\text{RuCl}(\text{PPh}_3)_2(\text{C}_5\text{H}_5)$  (60) and  $[\text{RuCl}(\text{EPh}_3)_2(\text{C}_6\text{H}_6)]^+$  (61) are known (as well as  $\text{RuCl}_2(\text{PPh}_3)(\text{C}_6\text{H}_6)$  (62), however it should be noted that the metal  $\text{C}_5\text{H}_5/\text{C}_6\text{H}_6$  cone angles are smaller than that for  $[\text{9}] \text{aneS3}$ .

2.2.3 Bis -Halo Dimers:  $[(\text{RuX}(\text{EPh}_3)([\text{9}] \text{aneS3}))_2(\text{BF}_4)_2$  (X=Cl<sup>-</sup>, E=P, As; X=Br<sup>-</sup>, E=P)

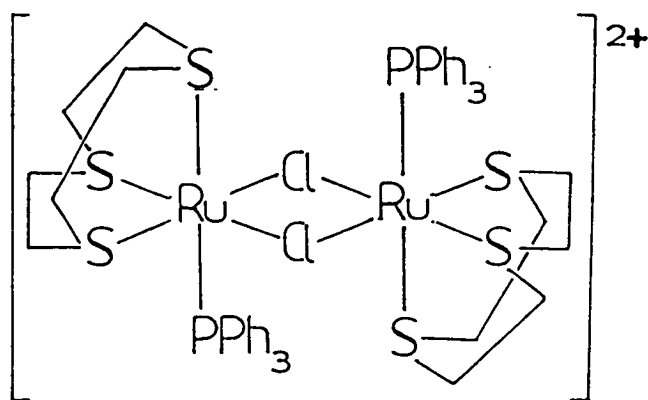
Attempts to synthesise  $[\text{RuCl}(\text{PPh}_3)_2([\text{9}] \text{aneS3})](\text{BF}_4)$  from  $\text{RuCl}_2(\text{PPh}_3)([\text{9}] \text{aneS3})$  in the presence of one equivalent of  $\text{Tl}(\text{BF}_4)$  and an excess of  $\text{PPh}_3$  (1:4) in refluxing  $\text{CH}_2\text{Cl}_2$  for 15 hours failed. The orange precipitate formed was found to be insoluble in cold solvents such as  $\text{CHCl}_3$ , MeCN,  $\text{CH}_3\text{NO}_2$ , acetone, benzene etc. However on addition to refluxing MeCN a yellow solution and a white precipitate was observed to form. The white precipitate was found to be  $\text{TlCl}$  while the yellow species proved to be  $[\text{RuCl}(\text{MeCN})(\text{PPh}_3)([\text{9}] \text{aneS3})]^+$  (see section 2.2.4). This suggests that removal of chloride from  $\text{RuCl}_2(\text{PPh}_3)([\text{9}] \text{aneS3})$  by  $\text{Tl}^+$  (to give  $\text{TlCl}$ ) affords an insoluble ruthenium salt in preference to  $[\text{RuCl}(\text{PPh}_3)_2([\text{9}] \text{aneS3})](\text{BF}_4)$ . This insoluble species, also formed in the absence of  $\text{PPh}_3$ , is assigned as the



chloride-bridged binuclear complex

$[\text{RuCl}(\text{PPh}_3)([\text{9}]\text{aneS3})]_2(\text{BF}_4)_2$  which would be expected to adopt a trans configuration to minimise steric strain [54].

The complexes  $[\text{RuBr}(\text{PPh}_3)([\text{9}]\text{aneS3})]_2(\text{BF}_4)_2$  and  $[\text{RuCl}(\text{AsPh}_3)([\text{9}]\text{aneS3})]_2(\text{BF}_4)_2$  can also be prepared in an analogous manner.



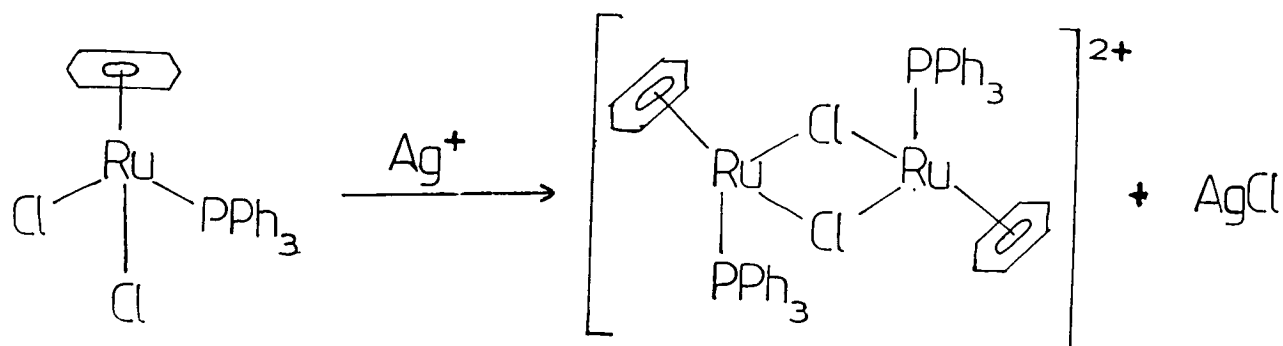
[54]

Although no conclusive evidence for the binuclear nature of [54] could be obtained due to its insolubility and the presence of  $\text{TlCl}$  the analogous arene complex has been characterised and was prepared in a similar manner (63) (see scheme 2.7).

#### 2.2.4 Chiral Complexes: $[\text{RuX}(\text{L})(\text{EPh}_3)([\text{9}]\text{aneS3})]^+$

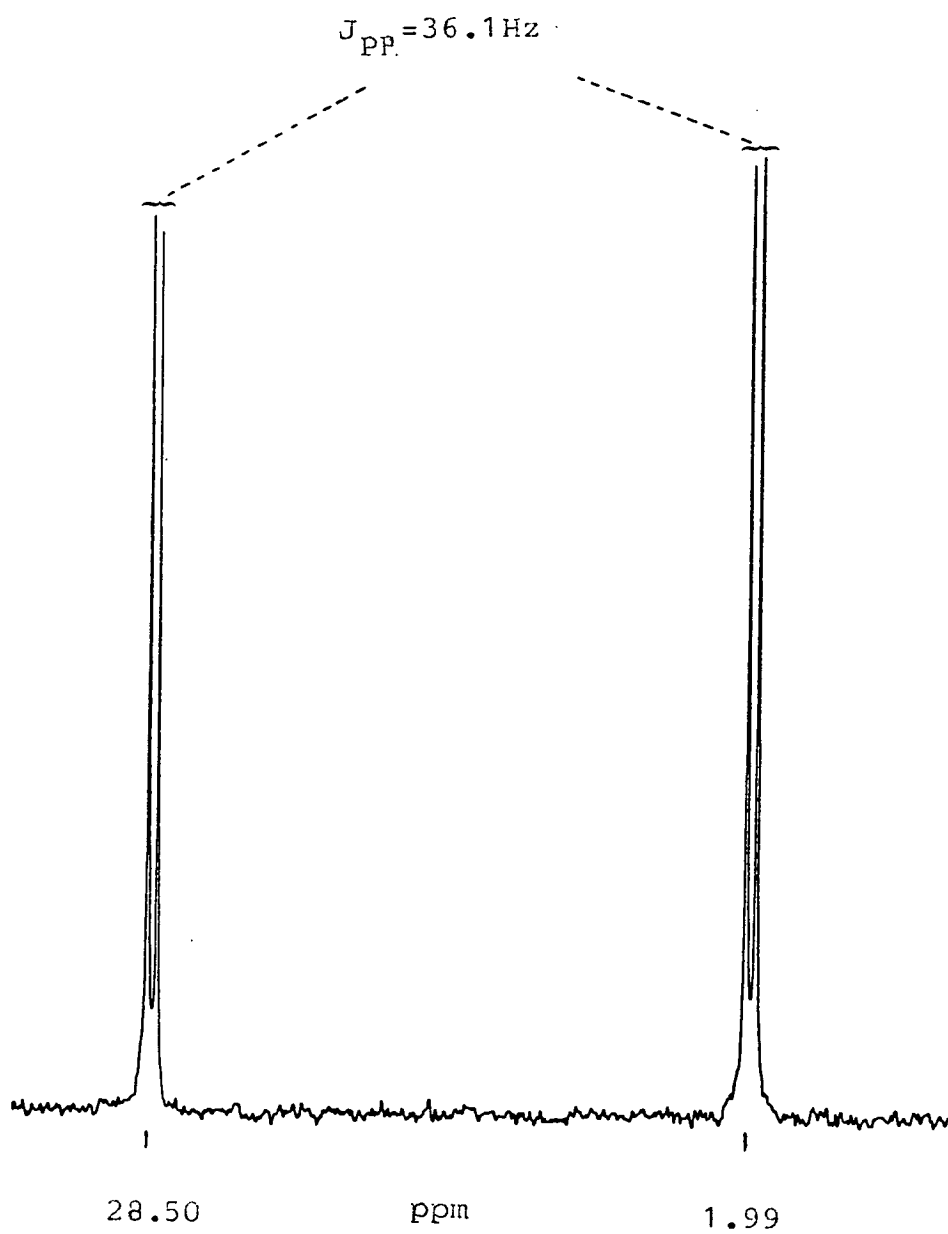
Although treatment of  $\text{RuCl}_2(\text{PPh}_3)([\text{9}]\text{aneS3})$  with one molar equivalent of  $\text{Tl}(\text{BF}_4)$  and an excess of  $\text{PPh}_3$  had yielded the binuclear complex [54], other ligands, L, were found to co-ordinate to give chiral complexes of the general formula  $[\text{RuCl}(\text{L})(\text{PPh}_3)([\text{9}]\text{aneS3})]^+$ .

Scheme 2.7: Synthesis of  $[\text{RuCl}(\text{PPh}_3)(\text{C}_6\text{H}_6)]_2(\text{PF}_6)_2$



For instance reaction of  $\text{RuCl}_2(\text{PPh}_3)([\text{9]aneS3})$  with one molar equivalent of  $\text{Tl}(\text{BF}_4)$  and  $\text{PMe}_2\text{Ph}$  in refluxing  $\text{CH}_2\text{Cl}_2$  for 15 hours under  $\text{N}_2$ , affords a light yellow solution and  $\text{TlCl}$  as a white precipitate. On filtration, partial removal of the solvent followed by addition of an excess of  $\text{Et}_2\text{O}$  a light yellow precipitate formed. The  $^{31}\text{P}$ - $(^1\text{H})$  n.m.r. spectrum of this product consisted of two doublets centred at 28.50 ( $\text{PPh}_3$ ) and 1.99 p.p.m ( $\text{PMe}_2\text{Ph}$ ) with  $J_{\text{PH}}=36.1\text{Hz}$  (see figure 2.7). This is consistent with the formation of  $[\text{RuCl}(\text{PMe}_2\text{Ph})(\text{PPh}_3)([\text{9]aneS3})](\text{BF}_4)$  which was confirmed by elemental analysis and FAB mass spectral data.

Figure 2.7:  $^{31}\text{P}$ -( $^1\text{H}$ ) n.m.r. Spectrum of  
 $[\text{RuCl}(\text{PPh}_3)(\text{PMe}_2\text{Ph})(\text{[9]andS3})(\text{BF}_4)]$  in  $\text{CDCl}_3$



Some experimental parameters for these chiral complexes synthesised mainly from  $\text{RuCl}_2(\text{PPh}_3)([9]\text{aneS3})$  but also from  $\text{RuBr}_2(\text{PPh}_3)([9]\text{aneS3})$  and  $\text{RuCl}_2(\text{AsPh}_3)([9]\text{aneS3})$  are given in Table 2.7. In the preparation of the MeCN complex  $[\text{RuCl}(\text{MeCN})(\text{PPh}_3)([9]\text{aneS3})]^+$ ,  $\text{Tl}(\text{PF}_6)$  rather than  $\text{Tl}(\text{BF}_4)$  was used, thus yielding the  $(\text{PF}_6)^-$  salt. Crystals of this complex suitable for a structural determination could be grown by the slow diffusion of  $\text{Et}_2\text{O}$  into a MeCN solution of the complex. Details of the structural solution, which converged to give a final R factor of 9.24%, is given in the experimental section. An Ortep plot of the structure is given in Figure 2.8 while selected bond lengths, bond angles and torsion angles are given in Tables 2.8-10.

The Ru(II) centre is in an octahedral environment, bound to a  $\text{Cl}^-$ ,  $\text{PPh}_3$ , MeCN and all three sulphur donor atoms of the macrocycle. The Ru-S bond lengths, in the context of the trans ligation, have previously been discussed in section 2.2.1c.

The complex  $[\text{RuCl}(\text{CO})(\text{PPh}_3)([9]\text{aneS3})]^+$ , identified by its characteristic  $\nu_{\text{CO}}$  stretching vibration at  $2010\text{cm}^{-1}$  (see section 2.2.5), may also be synthesised by treating  $\text{RuCl}_2(\text{PPh}_3)([9]\text{aneS3})$  with one molar equivalent of  $\text{Tl}(\text{BF}_4)$  in refluxing  $\text{CH}_2\text{Cl}_2$  under an atmosphere of CO. This, however is a very inefficient synthetic method as the major product is the insoluble dimer [54], possibly reflecting the low solubility of CO in  $\text{CH}_2\text{Cl}_2$ . A summary of the chiral complexes synthesised from  $\text{RuCl}_2(\text{PPh}_3)([9]\text{aneS3})$  is given in scheme 2.8.

Table 2.7: Some Experimental Parameters of the Chiral  
Complexes [RuX(L)(ER<sub>3</sub>)([9]aneS3)](BF<sub>4</sub>)

X	L	E	I.R (cm <sup>-1</sup> )	<sup>31</sup> P - { <sup>1</sup> H} n.m.r. (p.p.m.)
Cl	py	PPh <sub>3</sub>	V <sub>(C=C)</sub> = 1602	34.41 <sup>(a, 1)</sup>
Cl	py	AsPh <sub>3</sub>	V <sub>(C=C)</sub> = 1604	
Br	py	PPh <sub>3</sub>	V <sub>(C=C)</sub> = 1608	33.92 <sup>(a, 1)</sup>
Cl	PMe <sub>2</sub> Ph	PPh <sub>3</sub>		28.50 (PPh <sub>3</sub> ), 1.99 (PMe <sub>2</sub> Ph) J <sub>pp</sub> <sup>2</sup> = 36Hz <sup>(b, 2)</sup>
Cl	PMe <sub>2</sub> Ph	AsPh <sub>3</sub>		2.69 (PMe <sub>2</sub> Ph) <sup>(a, 1)</sup>
Br	PMe <sub>2</sub> Ph	PPh <sub>3</sub>		27.76 (PPh <sub>3</sub> ), -0.74 (PMe <sub>2</sub> Ph) J <sub>pp</sub> <sup>2</sup> = 35Hz <sup>(b, 2)</sup>
Cl	PhCN	PPh <sub>3</sub>	V <sub>(C=N)</sub> = 2240	32.72 <sup>(a, 1)</sup>
Cl	MeCN	PPh <sub>3</sub>	V <sub>(C=N)</sub> = 2041	35.44 <sup>(c, 2)</sup>
Cl	P(OMe) <sub>2</sub> Ph	PPh <sub>3</sub>		32.0 (PPh <sub>3</sub> ), 113.0 (P(OMe) <sub>2</sub> Ph) J <sub>pp</sub> <sup>2</sup> = 44Hz <sup>(a, 1)</sup>

a - (CD<sub>3</sub>)<sub>2</sub>CO, b - CDCl<sub>3</sub>, c - CD<sub>3</sub>CN

1 - Joel FXQ90, 2 - Bruker WP80SY

Figure 2.8: Ortep Plot of  $[\text{RuCl}(\text{MeCN})(\text{PPh}_3)(\text{[9]aneS3})]^+$

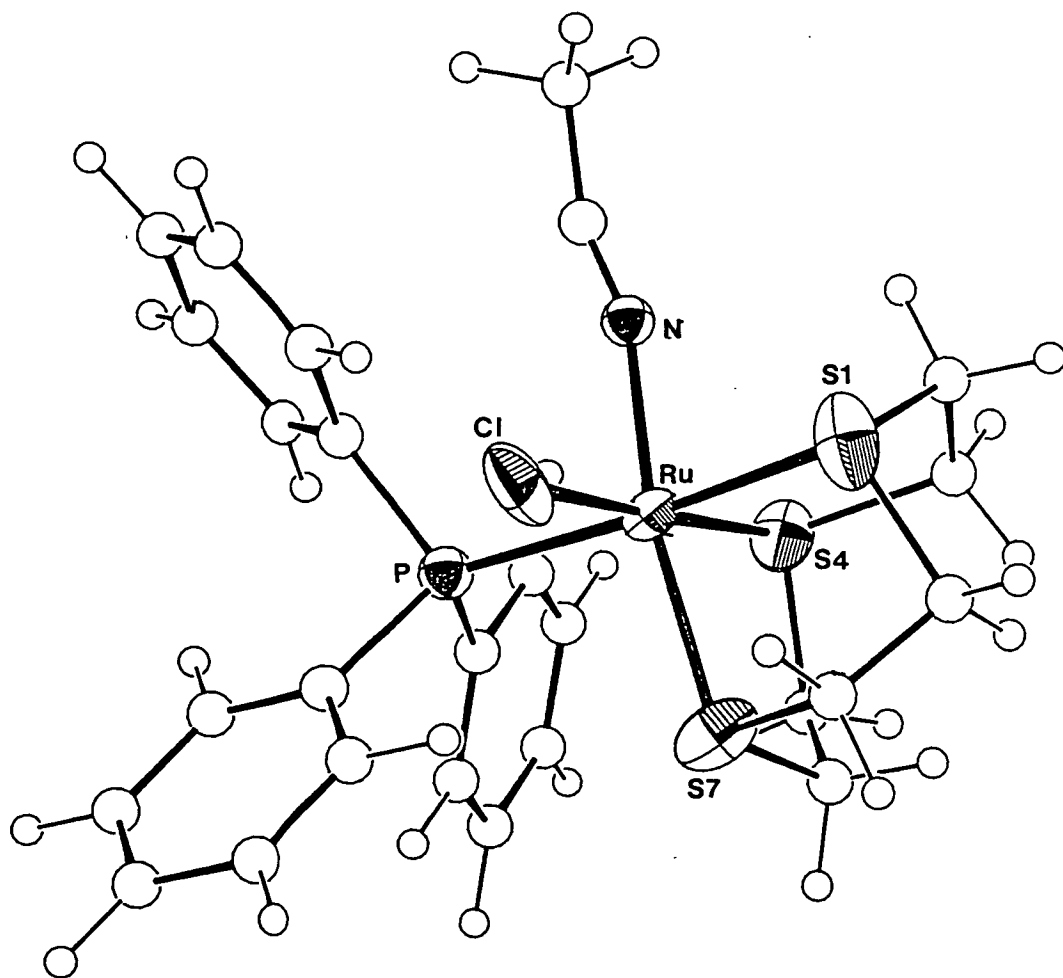


Table 2.8: Selected Bond Lengths (Å) with Standard Deviations

for  $[\text{RuCl}(\text{MeCN})(\text{PPh}_3)([\text{9}] \text{aneS3})]^+$ 

Ru(1) - S(1)	2.348(16)	P(1) -C(31)	1.81( 3)
Ru(1) - P(1)	2.360(14)	S(4) - C(3)	1.87( 4)
Ru(1) - S(4)	2.248(14)	S(4) - C(5)	1.87( 4)
Ru(1) - S(7)	2.332(15)	S(7) - C(6)	1.87( 4)
Ru(1) - N(1)	2.01( 4)	S(7) - C(8)	1.87( 5)
Ru(1) -Cl(1)	2.439(13)	C(2) - C(3)	1.50( 5)
S(1) - C(2)	1.87( 4)	C(5) - C(6)	1.50( 5)
S(1) - C(9)	1.87( 4)	C(8) - C(9)	1.50( 6)
P(1) -C(11)	1.81( 3)	N(1) -C(1N)	1.14( 6)
P(1) -C(21)	1.83( 3)	C(1N) -C(2N)	1.42( 7)

Table 2.9: Selected Angles (°) with Standard Deviations for

 $[\text{RuCl}(\text{MeCN})(\text{PPh}_3)([\text{9}] \text{aneS3})]^+$ 

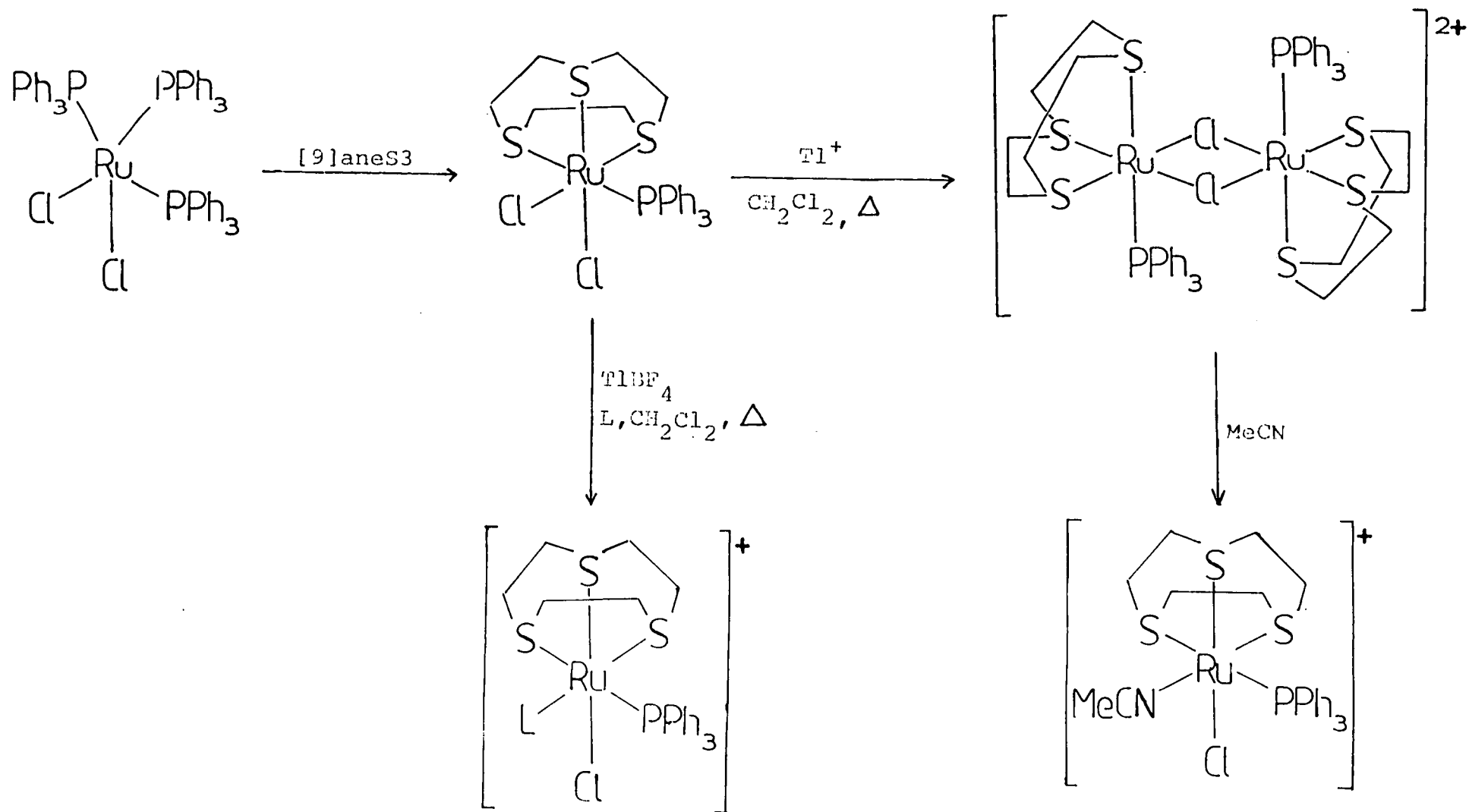
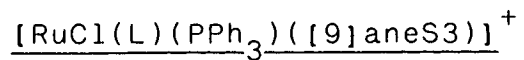
S(1) -Ru(1) - P(1)	174.9( 5)	C(11) - P(1) -C(31)	101.3(13)
S(1) -Ru(1) - S(4)	88.6( 5)	C(21) - P(1) -C(31)	104.6(13)
S(1) -Ru(1) - S(7)	87.9( 5)	Ru(1) - S(4) - C(3)	107.7(13)
S(1) -Ru(1) - N(1)	84.2(11)	Ru(1) - S(4) - C(5)	108.6(13)
S(1) -Ru(1) -Cl(1)	85.5( 5)	C(3) - S(4) - C(5)	103.6(17)
P(1) -Ru(1) - S(4)	95.6( 5)	Ru(1) - S(7) - C(6)	104.6(13)
P(1) -Ru(1) - S(7)	95.1( 5)	Ru(1) - S(7) - C(8)	97.9(15)
P(1) -Ru(1) - N(1)	93.0(11)	C(6) - S(7) - C(8)	103.7(19)
P(1) -Ru(1) -Cl(1)	90.4( 5)	S(1) - C(2) - C(3)	113.5(27)
S(4) -Ru(1) - S(7)	87.2( 5)	S(4) - C(3) - C(2)	108.5(26)
S(4) -Ru(1) - N(1)	89.2(11)	S(4) - C(5) - C(6)	107.9(25)
S(4) -Ru(1) -Cl(1)	174.1( 5)	S(7) - C(6) - C(5)	116.3(26)
S(7) -Ru(1) - N(1)	171.5(11)	S(7) - C(8) - C(9)	118.1(31)
S(7) -Ru(1) -Cl(1)	91.9( 5)	S(1) - C(9) - C(8)	102.9(28)
N(1) -Ru(1) -Cl(1)	90.8(11)	Ru(1) - N(1) -C(1N)	161(4)
Ru(1) - S(1) - C(2)	98.0(14)	N(1) -C(1N) -C(2N)	158(5)
Ru(1) - S(1) - C(9)	107.8(14)	P(1) -C(11) -C(12)	124.1(20)
C(2) - S(1) - C(9)	105.3(19)	P(1) -C(11) -C(16)	115.4(19)
Ru(1) - P(1) -C(11)	120.3(10)	P(1) -C(21) -C(22)	114.9(18)
Ru(1) - P(1) -C(21)	113.4(10)	P(1) -C(21) -C(26)	125.0(19)
Ru(1) - P(1) -C(31)	113.7(10)	P(1) -C(31) -C(32)	122.8(20)
C(11) - P(1) -C(21)	101.6(13)	P(1) -C(31) -C(36)	117.0(19)

Table 2.10: Selected Torsion Angles (°) with Standard Deviations for [RuCl(MeCN)(PPh<sub>3</sub>)([9]aneS3)]<sup>+</sup>

C(9) - S(1) - C(2) - C(3)	59.8(32)
C(2) - S(1) - C(9) - C(8)	-135.9(28)
C(3) - S(4) - C(5) - C(6)	75.4(27)
C(8) - S(7) - C(6) - C(5)	-129.3(29)
C(6) - S(7) - C(8) - C(9)	55.4(36)
S(1) - C(2) - C(3) - S(4)	51.2(32)
S(4) - C(5) - C(6) - S(7)	42.7(33)
S(7) - C(8) - C(9) - S(1)	56.9(35)

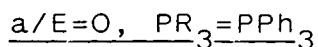
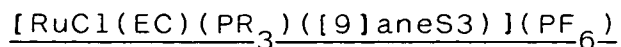


Scheme 2.8: Synthetic Routes to the Chiral complexes



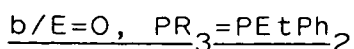
L = PhCN, Py, PMe<sub>2</sub>Ph, P(OMe)<sub>2</sub>Ph

### 2.2.5 Chiral Chlorocarbonyl and Chlorothiocarbonyl Complexes:



Although  $[\text{RuCl}(\text{CO})(\text{PPh}_3)([\text{9}] \text{aneS3})]^+$  may be synthesised from  $\text{RuCl}_2(\text{PPh}_3)([\text{9}] \text{aneS3})$  as outlined in section 2.2.4, the yield is low due to the formation of the binuclear species [54]. A more convenient and high yield synthesis can be achieved by the direct reaction of  $\text{RuCl}_2(\text{CO})(\text{PPh}_3)_2(\text{DMF})$  with  $[\text{9}] \text{aneS3}$  in refluxing EtOH. After 10 minutes a pale yellow solution forms and on addition of an excess of  $\text{NH}_4\text{PF}_6$  a very pale yellow precipitate is deposited.

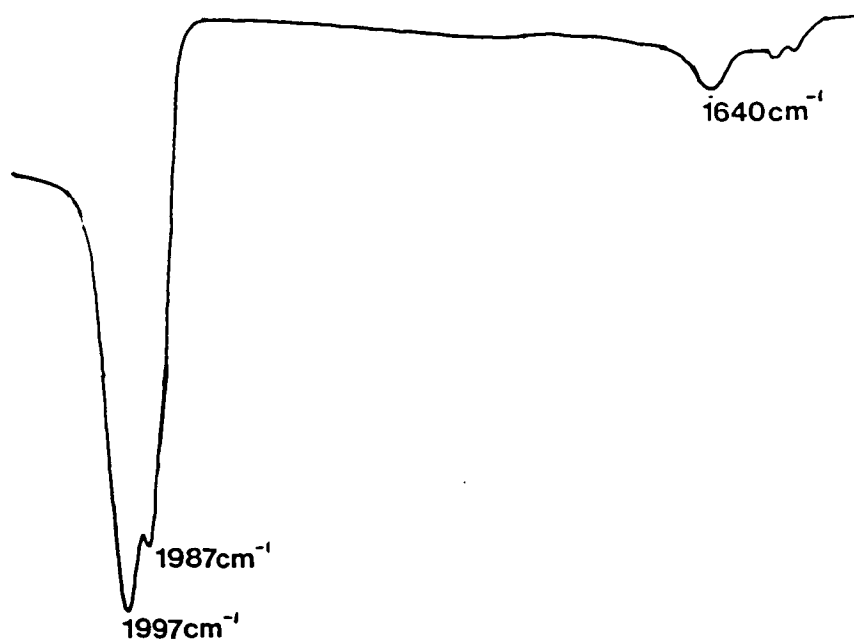
The IR spectrum of the complex exhibited a strong band at  $2010\text{cm}^{-1}$  which was assigned as a  $\nu_{\text{CO}}$  stretching vibration, while the  $^{31}\text{P}$ -( $^1\text{H}$ ) n.m.r. spectrum consisted of a resonance at 30.83 p.p.m. as well as the usual multiplet for  $(\text{PF}_6)^-$ . The  $^1\text{H}$  n.m.r. spectrum confirmed that the macrocycle was co-ordinated, with the  $[\text{9}] \text{aneS3}:\text{PPh}_3$  ratio found to be 1:1. The formulation of the complex as  $(\text{RuCl}(\text{CO})(\text{PPh}_3)([\text{9}] \text{aneS3})](\text{PF}_6^-)$  [55] was confirmed by FAB mass spectral data and elemental analysis.



Reaction of  $\text{RuCl}_2(\text{CO})(\text{PEtPh}_2)(\text{DMF})$  with one molar equivalent of  $[\text{9}] \text{aneS3}$  in refluxing EtOH for 10 minutes affords a light

yellow solution. On addition of an excess of  $\text{NH}_4\text{PF}_6$  a light yellow precipitate formed. The  $^{31}\text{P}$ -( $^1\text{H}$ ) n.m.r. spectrum of this material indicated that it was a mixture of two products as resonances for co-ordinated  $\text{PEtPh}_2$  were observed at 31.46 and 21.24p.p.m.. The IR spectrum of the mixture exhibited a strong band at 1997, a shoulder at 1987 as well as a band at  $1640\text{cm}^{-1}$  (see Figure 2.9).

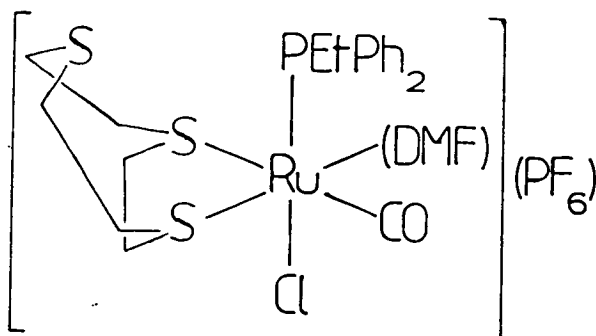
Figure 2.9: IR Spectrum (in the Region  $1500\text{-}2100\text{cm}^{-1}$ ) of the Product Mixture on Reacting  $\text{RuCl}_2(\text{CO})(\text{DMF})(\text{PEtPh}_2)_2$  with [9]aneS3



If a longer reaction time is used only the resonance at 31.46p.p.m. and the band at  $1997\text{cm}^{-1}$  ( $\nu_{\text{CO}}$ ) are observed in the  $^{31}\text{P}$ -( $^1\text{H}$ ) n.m.r. and the IR spectra respectively. This

species, from elemental analysis and FAB mass spectral data proved to be the title complex  $[\text{RuCl}(\text{CO})(\text{PEtPh}_2)(\text{[9]aneS3})](\text{PF}_6)$  (56).

The other species isolated on a short reaction time, is a DMF co-ordinated intermediate ( $1640\text{-DMF}$ ,  $1987\text{cm}^{-1} - \nu_{\text{CO}}$ ). Attempts to isolate this species by the use of a Sephadex LH20 column ( $\text{CH}_2\text{Cl}_2$  eluent) proved unsuccessful as it was found to convert to [56]. However from the available data the species seems likely to be  $[\text{RuCl}(\text{CO})(\text{DMF})(\text{PEtPh}_2)(\text{[9]aneS3})](\text{PF}_6)$  [57].



[57]

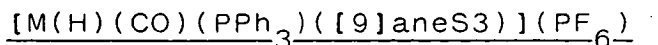
The relative difficulty in displacing DMF to give [56] compared to the analogous complex [55] is paralleled in the starting materials where DMF is totally replaced by MeOH on recrystallising  $\text{RuCl}_2(\text{CO})(\text{PPh}_3)_2(\text{DMF})$  from MeOH but only partially so for  $\text{RuCl}_2(\text{CO})(\text{PEtPh}_2)_3(\text{DMF})$  (64).

c/E=S, PR<sub>3</sub>=PPh<sub>3</sub>

Reacting  $[\text{RuCl}_2(\text{CS})(\text{PPh}_3)]_2$  with one molar equivalent of

[9]aneS3 in refluxing EtOH for 1 hour afforded a bright yellow precipitate (which proved to be  $\text{RuCl}_2(\text{PPh}_3)([\text{9]aneS3})$ ) and a yellow solution. On filtration and addition of an excess of  $\text{NH}_4\text{PF}_6$  a light yellow solid precipitated out of solution. The IR spectrum of the material exhibited a band at  $1295\text{cm}^{-1}$  for co-ordinated CS while only one resonance at 32.08 p.p.m., for co-ordinated  $\text{PPh}_3$ , was observed in the  $^{31}\text{P}$ -( $^1\text{H}$ ) n.m.r. spectrum. The  $^1\text{H}$  n.m.r. spectrum exhibited resonances for co-ordinated [9]aneS3 and  $\text{PPh}_3$  in the ratio of 1:1 and elemental analysis and FAB mass spectral data confirmed the complex to be  $[\text{RuCl}(\text{CS})(\text{PPh}_3)([\text{9]aneS3})](\text{PF}_6)$ .

#### 2.2.6 Chiral Hydridocarbonyl complexes:



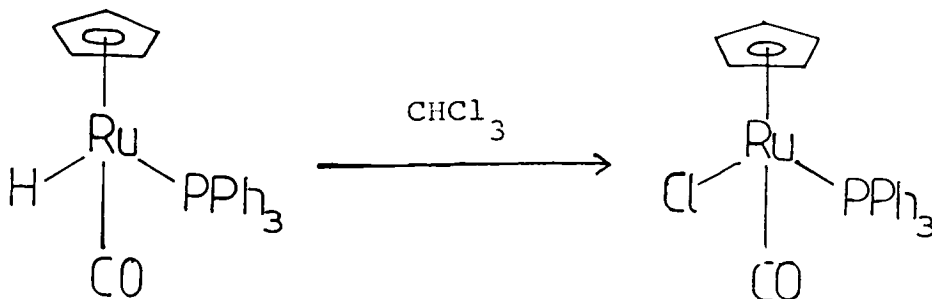
Having successfully synthesised chlorocarbonyl complexes attention turned to the synthesis of hydridocarbonyl complexes and for this purpose the bis-hydridocarbonyl complexes  $\text{M}(\text{H})_2(\text{CO})(\text{PPh}_3)_3$  (M=Ru, Os) proved to be useful starting materials.

##### a/M=Ru

Reaction of  $\text{Ru}(\text{H})_2(\text{CO})(\text{PPh}_3)_3$  with one molar equivalent of [9]aneS3 for 15 hours in refluxing  $\text{CH}_2\text{Cl}_2$  under an atmosphere of nitrogen afforded a light yellow solution. On removal of the solvent, addition of a small volume of EtOH and an excess of  $\text{NH}_4\text{PF}_6$  a pale yellow precipitate formed. Apart from

resonances associated with  $(PF_6)^-$ , only one other at 30.83 p.p.m., due to co-ordinated  $PPh_3$ , was observed in the  $^{31}P-(^1H)$  n.m.r. spectrum. This species however was not the desired hydridocarbonyl complex but the already known  $[RuCl(CO)(PPh_3)(\eta^5-C_5H_5)](PF_6)$ . The IR spectrum only exhibited the characteristic stretch for the chlorocarbonyl complex at  $2010cm^{-1}$  while elemental analysis confirmed that this was the only product of the reaction. The chloride source must have been the solvent itself as it had been pretreated to remove any HCl present, such abstraction processes have been observed before <sup>(60)</sup> (see Figure 2.10).

Figure 2.10: Synthesis of  $RuCl(CO)(PPh_3)(C_5H_5)$  from  $RuH(CO)(PPh_3)(C_5H_5)$  via Chloride Abstraction from  $CHCl_3$



To avoid the possibility of chloride abstraction a non-chlorinated solvent, acetone, was used. Thus over a period of 2 hours a suspension of  $\text{Ru}(\text{H})_2(\text{CO})(\text{PPh}_3)_3$ , in the presence of one molar equivalent of [9]aneS3, an excess of  $\text{NH}_4\text{PF}_6$  and under an atmosphere of  $\text{N}_2$ , dissolved in refluxing acetone to give a colourless solution. At this point an equal volume of EtOH was added and the solution was held at reflux for a further 2 hours. On reducing the volume of the still colourless solution a white microcrystalline solid formed.

The IR spectrum of this material indicated the presence of  $(\text{PF}_6)^-$  and  $\text{PPh}_3$  while in the region about  $2000\text{cm}^{-1}$  two stretches were observed. The first at  $1982\text{cm}^{-1}$  is very strong and thus assigned as a  $\nu_{\text{CO}}$  stretching vibration while the weaker at  $1910\text{cm}^{-1}$  is attributed to  $\nu_{\text{RuH}}$  (see Figure 2.11).

In order to characterise the product by n.m.r. spectroscopy a sealed tube had to be used due to the sensitivity of the product to oxygen (see later). The  $^1\text{H}$  n.m.r. spectrum exhibited a doublet centred at  $-9.29$  p.p.m. confirming that the product did indeed contain a hydride, this being coupled to only one phosphine ( $J_{\text{PH}}$   $20.8\text{Hz}$ ). Analysis of the rest of the spectrum confirmed that [9]aneS3 was co-ordinated and that the [9]aneS3:PPh ratio was 1:1. As expected the  $^{31}\text{P}$ -( $^1\text{H}$ ) n.m.r. spectrum consisted of only one resonance, at  $48.19$  p.p.m., for co-ordinated  $\text{PPh}_3$ . On selectively coupling the hydride this resonance became a doublet as shown in Figure 2.12.

Figure 2.11: IR Spectrum of  $[\text{RuH}(\text{CO})(\text{PPh}_3)([\text{9]aneS3})](\text{PF}_6)$  in the Region  $1800\text{-}2100\text{cm}^{-1}$

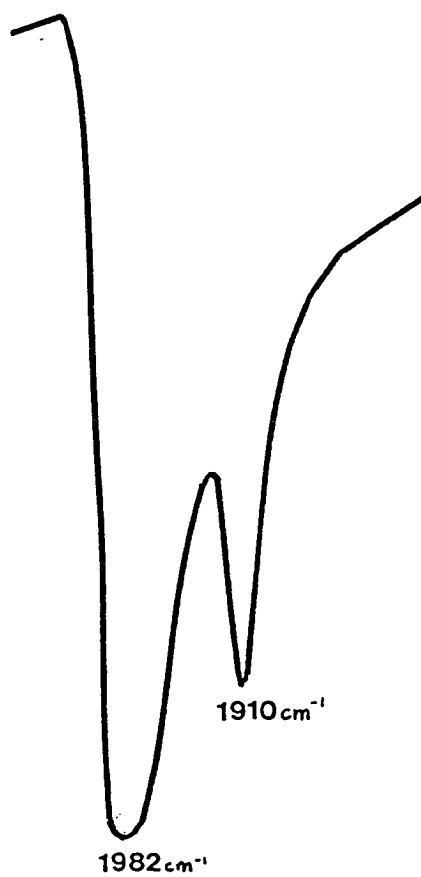
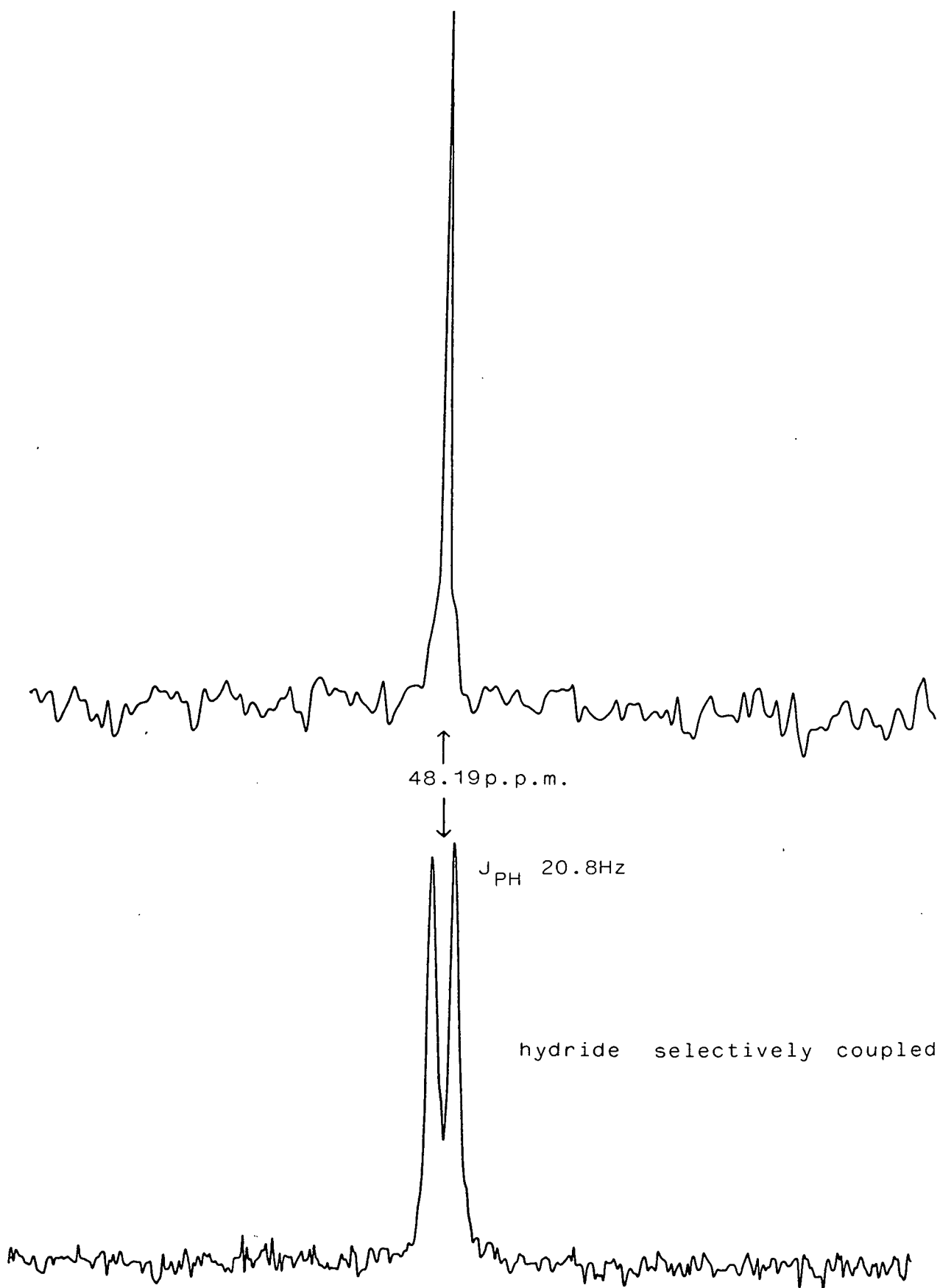




Figure 2.12:  $^{31}\text{P}$ -( $^1\text{H}$ )nmr of  $[\text{RuH}(\text{CO})(\text{PPh}_3)([9]\text{aneS3})](\text{PF}_6)$



This, plus elemental analysis and FAB mass spectral data confirmed that the isolated product was the desired hydridocarbonyl complex  $[\text{RuH}(\text{CO})(\text{PPh}_3)(\text{[9]laneS3})](\text{PF}_6)$  [58].

As mentioned previously the complex is not stable in oxygenated solvents. In acetone a greenish tinge to the initially colourless solution is observed within minutes. This colouration deepens, then further reaction occurs to yield a light yellow solution after a few hours from which a very pale yellow solid can be isolated [59]. Contrasting behaviour is exhibited if [58] is dissolved in non-degassed  $\text{CH}_2\text{Cl}_2$  where after a few minutes a blue/green tinge is observed. This deepens over a period of 2 hours and a very light blue/green solid [60] can be isolated. If however the solution is left over a couple of days it turns yellow and a light yellow solid can be isolated [61].

The  $^{31}\text{P}$ -( $^1\text{H}$ ) n.m.r. spectra of [59] and [60] are identical, with resonances observed at 38.10 and 30.56 p.p.m. for co-ordinated  $\text{PPh}_3$  (though the species they are associated with remains unknown). The IR spectrum of both materials exhibits a relatively "weaker"  $\nu_{\text{CO}}$  stretching vibration at  $2000\text{cm}^{-1}$  while the UV spectrum contains a common shoulder at  $27,680\text{cm}^{-1}$  (see Figure 2.13a and b).

The colour difference between the two materials, [59] and [60], is due to an absorption at  $15960\text{cm}^{-1}$  (see Figure 2.13b) and reflects the presence of another species.

Figure 2.13: UV/Vis/NIR Spectra of  $[\text{RuH}(\text{CO})(\text{PPh}_3)(\text{[9]aneS3})](\text{PF}_6)$  after 2 hours in Non-degassed Acetone (a) and Methylenechloride (b)

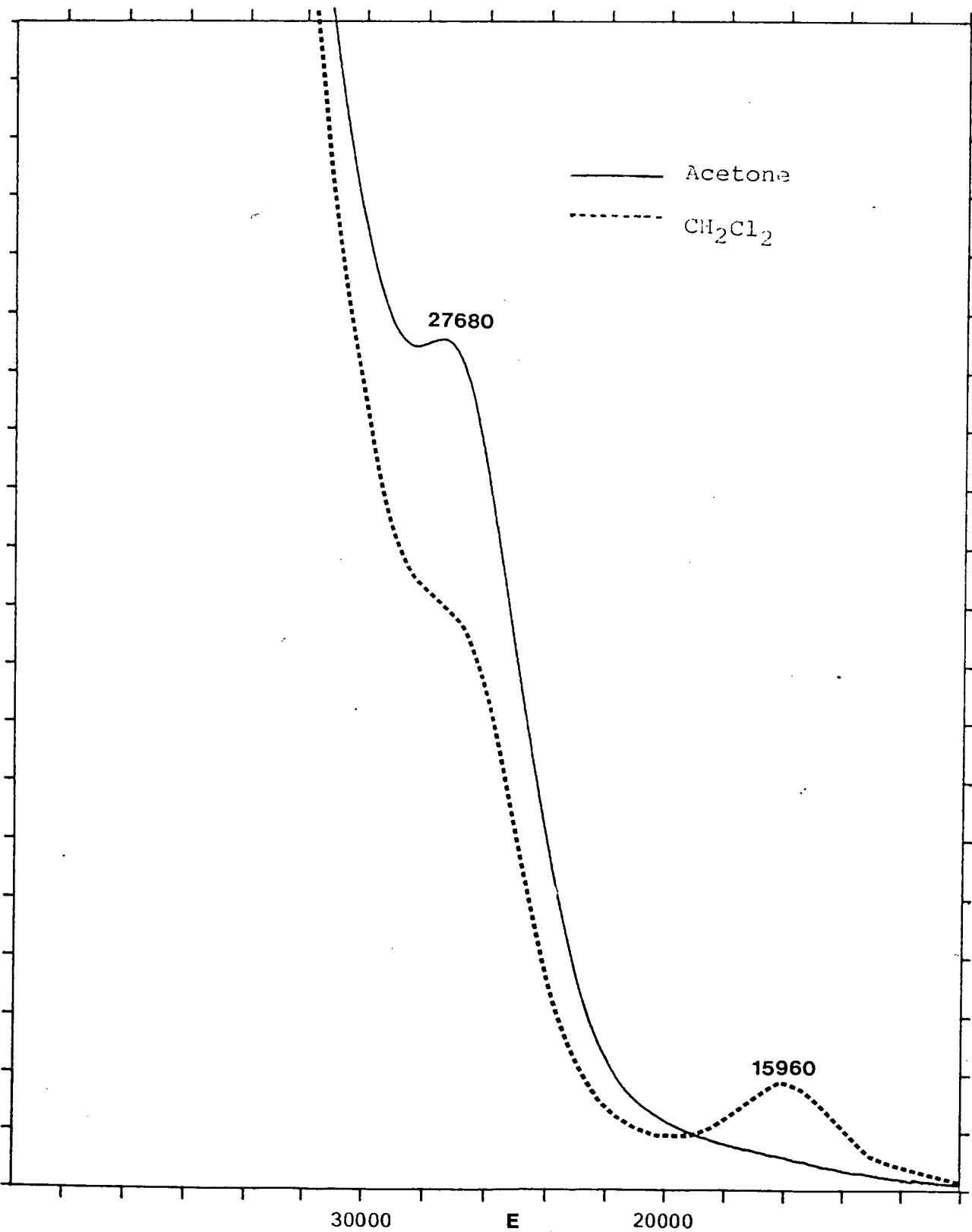
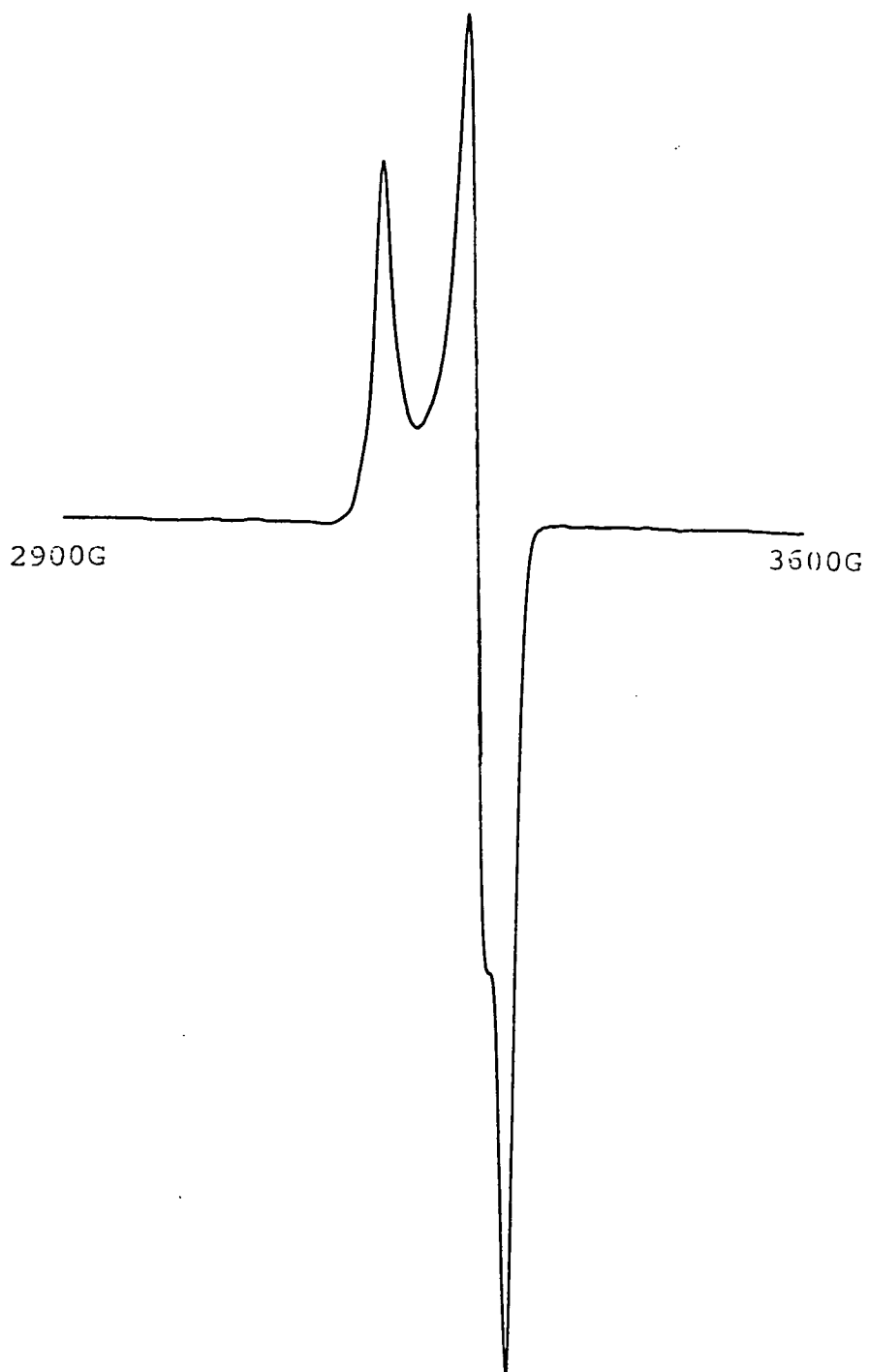


Figure 2.14: E.S.R. Spectrum of  $[\text{RuH}(\text{CO})(\text{PPh}_3)(\text{19laneS3})](\text{PF}_6)$  after 2 hours in Non-degassed Methylenechloride at 77K



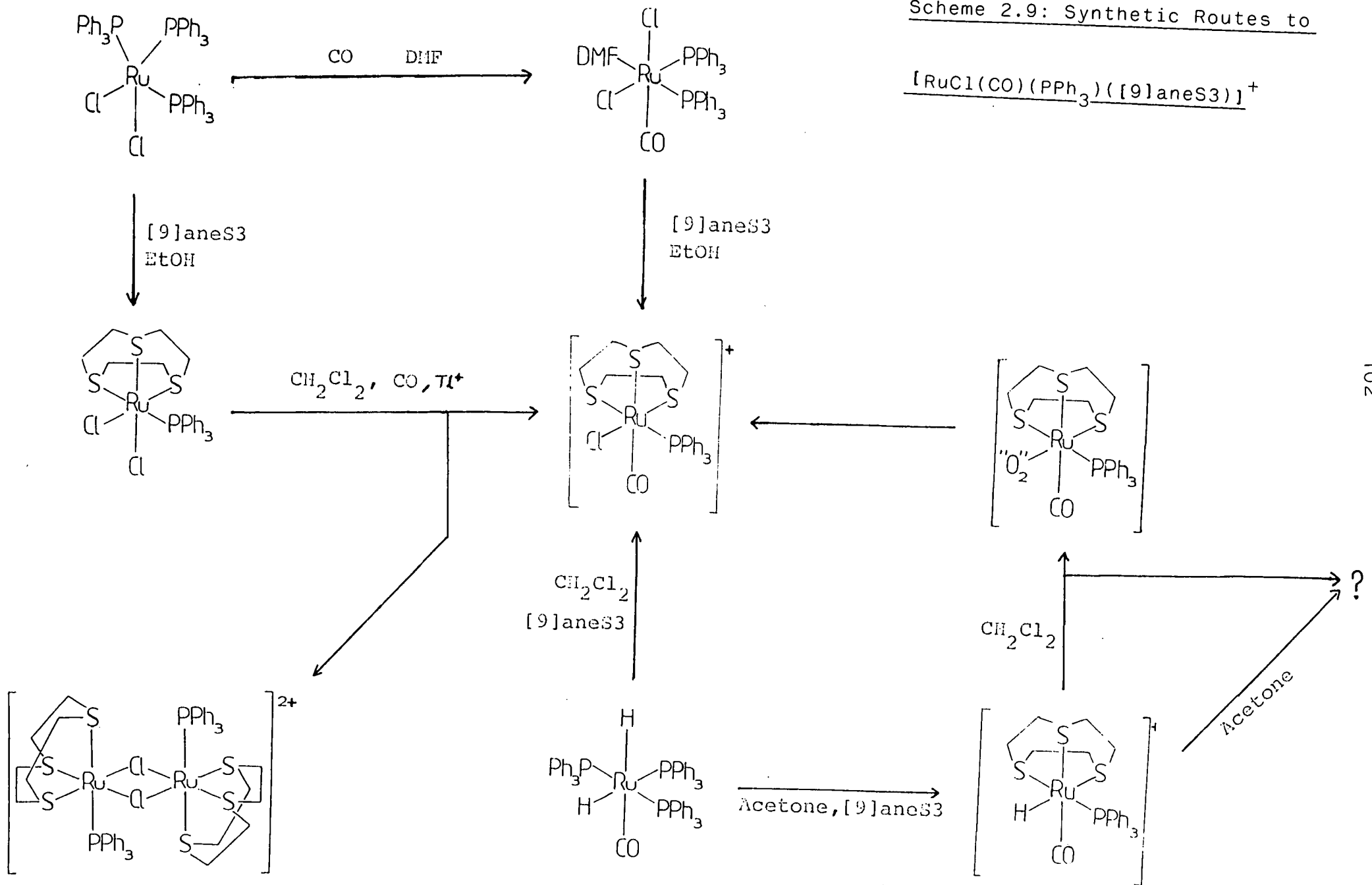
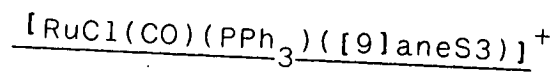
This was found to be e.s.r. active as a weak signal is observed in the e.s.r. spectrum (see Figure 2.14). This signal, however, decays over time in accordance with the observed colour change from blue/green to yellow, [61].

The  $^{31}\text{P}$ -( $^1\text{H}$ ) n.m.r. spectrum of [61] exhibits a signal at 30.83 p.p.m. in addition to those previously observed for [59] and [60] and this can be assigned as  $[\text{RuCl}(\text{CO})(\text{PPh}_3)([9]\text{aneS3})]^+$ . This implies that the e.s.r. active species must contain the  $[\text{Ru}(\text{CO})(\text{PPh}_3)([9]\text{aneS3})]$  fragment and it is tentatively suggested that a reactive  $\text{RuO}_2$  species might have been formed. A summary of the synthetic routes to  $[\text{RuCl}(\text{CO})(\text{PPh}_3)([9]\text{aneS3})]^+$  is given in scheme 2.9.

b/M = Os

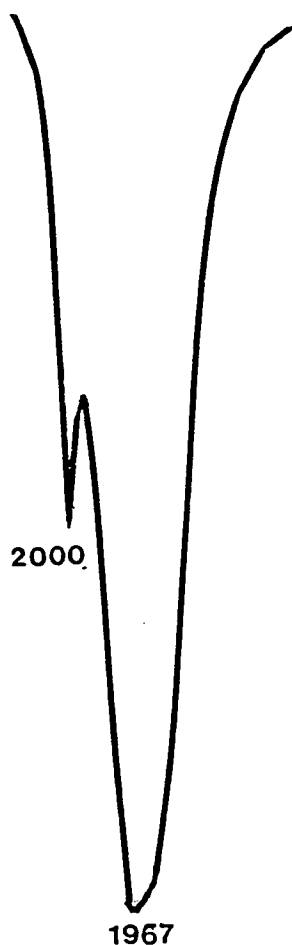
Unlike its Ru analogue, no reaction occurs in refluxing acetone between  $\text{Os}(\text{H})_2(\text{CO})(\text{PPh}_3)_3$  and [9]aneS3 in the presence of an excess of  $\text{NH}_4\text{PF}_6$ . If however methoxyethanol is used instead of acetone, the initial suspension of  $\text{Os}(\text{H})_2(\text{CO})(\text{PPh}_3)_3$  dissolves to yield a very light brown solution after 2 hours at reflux. On partial removal of the methoxyethanol and addition of an excess of  $\text{Et}_2\text{O}$  a very pale brown precipitate was formed. On recrystallisation from a  $\text{CH}_3\text{NO}_2/\text{Et}_2\text{O}$  solvent system a white product could be isolated.

Scheme 2.9: Synthetic Routes to



The IR spectrum of the complex as well as indicating the presence of  $(PF_6)^-$  and  $PPh_3$  also exhibited a very strong band at 1967 and a weaker one at  $2000\text{cm}^{-1}$  these being assigned as  $\nu_{CO}$  and  $\nu_{RuH}$  stretching vibrations respectively (see Figure 2.15). This compares with  $[RuH(CO)(PPh_3)([9]aneS3)](PF_6)$  where the comparable stretching vibrations occur at 1982 and  $1910\text{cm}^{-1}$ .

Figure 2.15: IR Spectrum of  $[OsH(CO)(PPh_3)([9]aneS3)](PF_6)$  in the region  $1800-2100\text{cm}^{-1}$



The Os(II) complex, unlike  $[RuH(CO)(PPh_3)([9]aneS3)](PF_6)$ , is relatively stable in oxygenated solvents as only a faint colouration, of the initially colourless solution, is

observed after a couple of weeks. The  $^1\text{H}$  n.m.r. spectrum revealed the expected doublet at  $-10.20$  p.p.m. ( $J_{\text{PH}} 18.0\text{Hz}$ ) for a hydride coupled to one  $\text{PPh}_3$  ligand. Analysis of the rest of the spectrum confirmed the presence of co-ordinated [9]aneS3 and the [9]aneS3: $\text{PPh}_3$  ratio was found to be 1:1. The  $^{31}\text{P}$ -( $^1\text{H}$ ) n.m.r. spectrum consisted of a singlet at  $13.19$  p.p.m. for co-ordinated  $\text{PPh}_3$  (as well as resonances for  $(\text{PF}_6)^-$ ) which became a doublet on selectively coupling the hydride.

The formulation of the white material as  $[\text{OsH}(\text{CO})(\text{PPh}_3)([\text{9]aneS3})](\text{PF}_6)$  [62] was confirmed by elemental analysis and FAB mass spectral data.

Clear colourless crystals suitable for a single crystal X-Ray structural analysis could be grown by the slow diffusion of  $\text{Et}_2\text{O}$  into a  $\text{CH}_2\text{Cl}_2$  solution of [62]. Details of the structural solution, which converged to give a final R factor of 5.27%, are given in the experimental section. An ortep plot of the structure is given in Figure 2.18 while selected bond lengths, bond angles and torsion angles are given in Tables 2.11-13.

As expected the Os(II) centre is in an octahedral environment, bound to a hydride (OS-H bond length was fixed at  $1.69\text{\AA}$ ), a  $\text{CO}(\text{Os-C-O } 177.1^\circ)$ , a phosphine and all three sulphur atoms of the macrocycle. These Os-S bond lengths, in conjunction with other structurally characterised complexes (see Table 2.14), allow a rough series of Os-S bond lengths to be obtained as a function of the trans ligand L i.e.

arene and  $\text{SR}_2 < \text{PPh}_3 < \text{CO} < \text{H}^-$

( $2.338-2.402\text{\AA}$ ).



Figure 2.16: Ortep Plot of  $[\text{OsH}(\text{CO})(\text{PPh}_3)(\text{[9]aneS3})]^+$

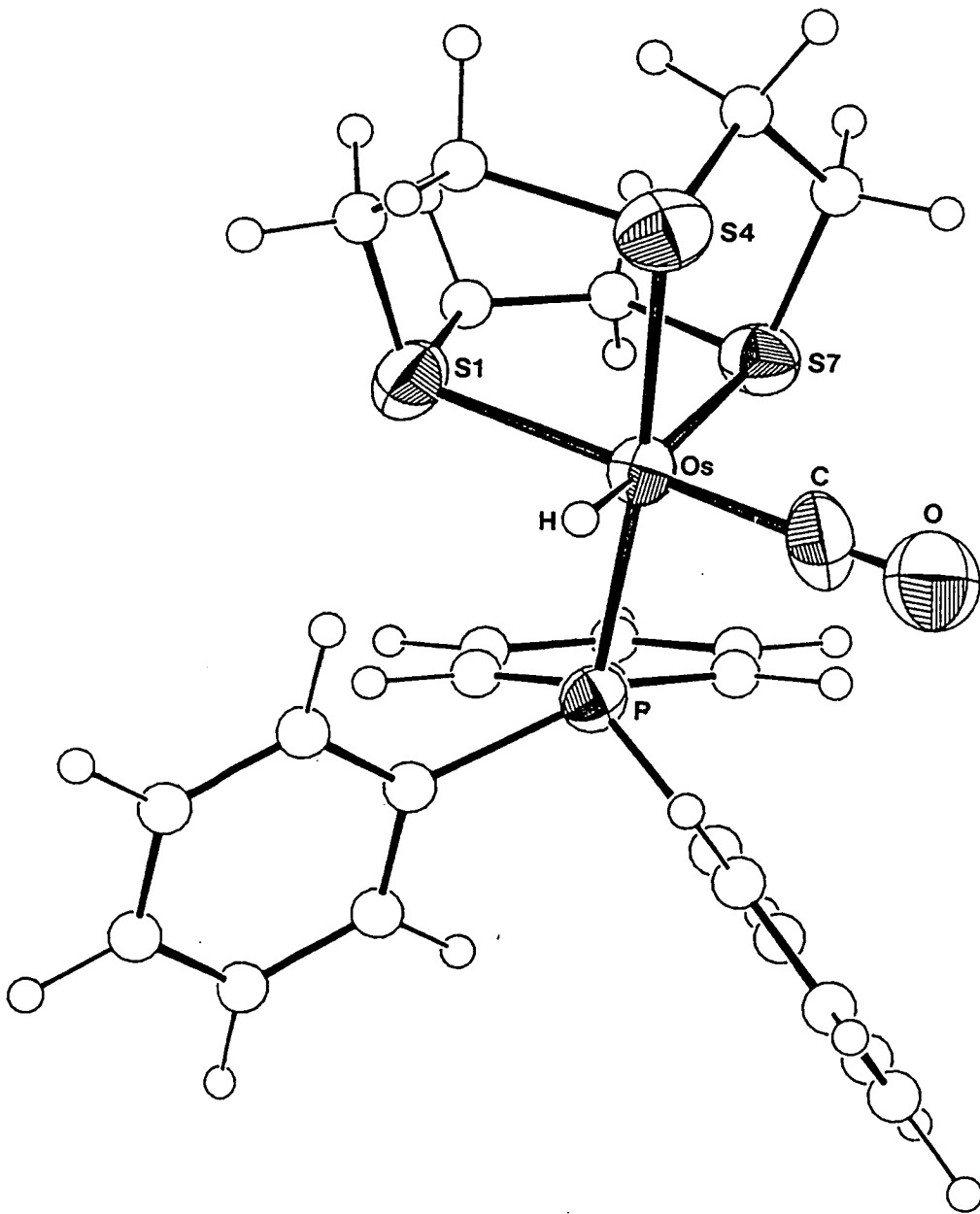


Table 2.11: Selected Bond Lengths (Å) with Standard Deviations  
for  $[\text{OsH}(\text{CO})(\text{PPh}_3)([\text{9}] \text{aneS3})]^+$

Os - H	1.60( 9)	C(3) - S(4)	1.824(13)
Os - C	1.868(11)	S(4) - C(5)	1.823(14)
Os - S(1)	2.377( 3)	C(5) - C(6)	1.490(18)
Os - S(4)	2.369( 3)	C(6) - S(7)	1.815(12)
Os - S(7)	2.402( 3)	S(7) - C(8)	1.794(13)
Os - P	2.3344(24)	C(8) - C(9)	1.393(19)
C - O	1.149(14)	P -C(11)	1.814( 7)
S(1) - C(2)	1.776(14)	P -C(21)	1.825( 6)
S(1) - C(9)	1.803(14)	P -C(31)	1.823( 7)
C(2) - C(3)	1.434(19)		

Table 2.12: Selected Angles (°) with Standard Deviations for  
 $[\text{OsH}(\text{CO})(\text{PPh}_3)([\text{9}] \text{aneS3})]^+$

H - Os - C	76.1(31)	Os - S(4) - C(5)	106.3( 4)
H - Os - S(1)	99.4(31)	C(3) - S(4) - C(5)	101.3( 6)
H - Os - S(4)	81.4(31)	S(4) - C(5) - C(6)	114.4( 9)
H - Os - S(7)	166.3(31)	C(5) - C(6) - S(7)	116.1( 9)
H - Os - P	94.6(31)	Os - S(7) - C(6)	103.3( 4)
C - Os - S(1)	175.1( 3)	Os - S(7) - C(8)	105.7( 4)
C - Os - S(4)	91.5( 3)	C(6) - S(7) - C(8)	101.4( 6)
C - Os - S(7)	98.1( 3)	S(7) - C(8) - C(9)	120.6(10)
C - Os - P	92.4( 3)	S(1) - C(9) - C(8)	121.9(10)
S(1) - Os - S(4)	85.85( 9)	Os - P -C(11)	116.82(23)
S(1) - Os - S(7)	85.97( 9)	Os - P -C(21)	112.31(22)
S(1) - Os - P	89.90( 9)	Os - P -C(31)	117.50(23)
S(4) - Os - S(7)	86.45( 9)	C(11) - P -C(21)	105.3( 3)
S(4) - Os - P	173.65( 9)	C(11) - P -C(31)	98.5( 3)
S(7) - Os - P	97.97( 9)	C(21) - P -C(31)	104.6( 3)
Os - C - O	177.1(10)	P -C(11) -C(12)	116.5( 5)
Os - S(1) - C(2)	105.8( 4)	P -C(11) -C(16)	123.4( 5)
Os - S(1) - C(9)	105.5( 5)	P -C(21) -C(22)	120.4( 5)
C(2) - S(1) - C(9)	100.8( 6)	P -C(21) -C(26)	119.2( 5)
S(1) - C(2) - C(3)	119.1(10)	P -C(31) -C(32)	118.2( 5)
C(2) - C(3) - S(4)	119.0(10)	P -C(31) -C(36)	121.7( 5)
Os - S(4) - C(3)	102.4( 4)		

Table 2.13: Selected Torsion Angles (°) with Standard

Deviations for  $[\text{OsH}(\text{CO})(\text{PPh}_3)(\text{9}]\text{aneS3}]\text{ }^+$ 

H	-	Os	-	S(1)	-	C(2)	65.9(32)	S(7)	-	Os	-	P	-C(21)	-18.38(24)	
H	-	Os	-	S(1)	-	C(9)	172.2(32)	S(7)	-	Os	-	P	-C(31)	-139.8( 3)	
C	-	Os	-	S(1)	-	C(2)	43.4(40)	Os	-	S(1)	-	C(2)	-	C(3)	0.6(11)
C	-	Os	-	S(1)	-	C(9)	149.6(39)	C(9)	-	S(1)	-	C(2)	-	C(3)	-109.1(11)
S(4)	-	Os	-	S(1)	-	C(2)	-14.7( 5)	Os	-	S(1)	-	C(9)	-	C(8)	-4.1(13)
S(4)	-	Os	-	S(1)	-	C(9)	91.6( 5)	C(2)	-	S(1)	-	C(9)	-	C(8)	105.8(12)
S(7)	-	Os	-	S(1)	-	C(2)	-101.4( 5)	S(1)	-	C(2)	-	C(3)	-	S(4)	20.9(15)
S(7)	-	Os	-	S(1)	-	C(9)	4.9( 5)	C(2)	-	C(3)	-	S(4)	-	Os	-30.5(11)
P	-	Os	-	S(1)	-	C(2)	160.6( 5)	C(2)	-	C(3)	-	S(4)	-	C(5)	79.2(11)
P	-	Os	-	S(1)	-	C(9)	-93.1( 5)	Os	-	S(4)	-	C(5)	-	C(6)	-25.4(10)
H	-	Os	-	S(4)	-	C(3)	-77.8(31)	C(3)	-	S(4)	-	C(5)	-	C(6)	-132.1(10)
H	-	Os	-	S(4)	-	C(5)	176.3(32)	S(4)	-	C(5)	-	C(6)	-	S(7)	42.6(12)
C	-	Os	-	S(4)	-	C(3)	-153.5( 5)	C(5)	-	C(6)	-	S(7)	-	Os	-36.5(10)
C	-	Os	-	S(4)	-	C(5)	100.6( 6)	C(5)	-	C(6)	-	S(7)	-	C(8)	72.9(10)
S(1)	-	Os	-	S(4)	-	C(3)	22.3( 4)	Os	-	S(7)	-	C(8)	-	C(9)	4.3(12)
S(1)	-	Os	-	S(4)	-	C(5)	-83.6( 5)	C(6)	-	S(7)	-	C(8)	-	C(9)	-103.1(11)
S(7)	-	Os	-	S(4)	-	C(3)	108.5( 4)	S(7)	-	C(8)	-	C(9)	-	S(1)	-0.2(16)
S(7)	-	Os	-	S(4)	-	C(5)	2.6( 5)	Os	-	P	-C(11)	-C(12)	50.8( 5)		
P	-	Os	-	S(4)	-	C(3)	-25.8(10)	Os	-	P	-C(11)	-C(16)	-132.7( 5)		
P	-	Os	-	S(4)	-	C(5)	-131.7( 9)	C(21)	-	P	-C(11)	-C(12)	176.2( 5)		
C	-	Os	-	S(7)	-	C(6)	-76.0( 5)	C(21)	-	P	-C(11)	-C(16)	-7.3( 6)		
C	-	Os	-	S(7)	-	C(8)	177.9( 5)	C(31)	-	P	-C(11)	-C(12)	-76.0( 5)		
S(1)	-	Os	-	S(7)	-	C(6)	101.1( 4)	C(31)	-	P	-C(11)	-C(16)	100.5( 6)		
S(1)	-	Os	-	S(7)	-	C(8)	-5.0( 4)	Os	-	P	-C(21)	-C(22)	74.3( 5)		
S(4)	-	Os	-	S(7)	-	C(6)	15.0( 4)	Os	-	P	-C(21)	-C(26)	-98.9( 5)		
S(4)	-	Os	-	S(7)	-	C(8)	-91.1( 4)	C(11)	-	P	-C(21)	-C(22)	-53.9( 6)		
P	-	Os	-	S(7)	-	C(6)	-169.6( 4)	C(11)	-	P	-C(21)	-C(26)	133.0( 5)		
P	-	Os	-	S(7)	-	C(8)	84.3( 4)	C(31)	-	P	-C(21)	-C(22)	-157.2( 5)		
H	-	Os	-	P	-C(11)	-71.3(31)	C(31)	-	P	-C(21)	-C(26)	29.6( 6)			
H	-	Os	-	P	-C(21)	166.9(31)	Os	-	P	-C(31)	-C(32)	175.5( 4)			
H	-	Os	-	P	-C(31)	45.5(31)	Os	-	P	-C(31)	-C(36)	-6.8( 6)			
C	-	Os	-	P	-C(11)	4.9( 4)	C(11)	-	P	-C(31)	-C(32)	-58.2( 6)			
C	-	Os	-	P	-C(21)	-116.9( 4)	C(11)	-	P	-C(31)	-C(36)	119.5( 6)			
C	-	Os	-	P	-C(31)	121.7( 4)	C(21)	-	P	-C(31)	-C(32)	50.2( 6)			
S(1)	-	Os	-	P	-C(11)	-170.7( 3)	C(21)	-	P	-C(31)	-C(36)	-132.1( 5)			
S(1)	-	Os	-	P	-C(21)	67.54(24)	C(13)	-	C(12)	-C(11)	-	P	176.6( 5)		
S(1)	-	Os	-	P	-C(31)	-53.9( 3)	C(15)	-	C(16)	-C(11)	-	P	-176.4( 5)		
S(4)	-	Os	-	P	-C(11)	-122.7( 8)	C(23)	-	C(22)	-C(21)	-	P	-173.1( 5)		
S(4)	-	Os	-	P	-C(21)	115.5( 8)	C(25)	-	C(26)	-C(21)	-	P	173.2( 5)		
S(4)	-	Os	-	P	-C(31)	-6.0( 9)	C(33)	-	C(32)	-C(31)	-	P	177.8( 5)		
S(7)	-	Os	-	P	-C(11)	103.4( 3)	C(35)	-	C(36)	-C(31)	-	P	-177.7( 5)		

Table 2.14: Selected Structural Parameters for [9]aneS3  
Complexes of Os(II)

	[OsH(CO)(PPh <sub>3</sub> )([9]aneS3)] <sup>+</sup>	[Os(4-MeC <sub>6</sub> H <sub>4</sub> <sup>i</sup> Pr)([9]aneS3)] <sup>+</sup>	[Os([9]aneS3) <sub>2</sub> ] <sup>2+</sup>
Os - S trans to H	2.402(3)Å		
Os - S trans to CO	2.377(3)Å		
Os - S trans to PPh <sub>3</sub>	2.369(3)Å		
Os - S (av.)		2.338	2.341
Σ S - Os - S	248.27	262.78	263.31

As the Os-S bond trans to CO (and  $\text{PPh}_3$ ) is lengthened compared to a trans  $\text{SR}_2$  group it is again suggested that this is direct evidence for the macrocycle acting as a  $\Pi$ -acceptor (cf section 2.2.1.d).

### 2.2.7 $[\text{Os}([\text{9}] \text{aneS3})_2](\text{PF}_6)_2$

The complex  $[\text{Os}([\text{9}] \text{aneS3})_2](\text{PF}_6)_2$ , synthesised by the prolonged reaction of  $\{\text{OsCl}_2(4\text{-MeC}_6\text{H}_4\text{Pr})\}_2$  with an excess of  $[\text{9}] \text{aneS3}$  in refluxing MeOH, has been previously reported (35). However, the low yield prohibited a full characterisation. Attempts to increase the yield by using higher boiling solvents such as ethylene glycol and DMSO induced decomposition and thus no useful product was isolated (36). If however the reaction is carried out in EtOH a light brown solution forms over a period of 48 hours and on addition of an excess of  $\text{NH}_4\text{PF}_6$  a light brown precipitate formed. Repeated recrystallisation from a minimum volume of hot water yielded a white material which analysed for  $[\text{Os}([\text{9}] \text{aneS3})_2](\text{PF}_6)_2$ .

Suitable crystals of  $[\text{Os}([\text{9}] \text{aneS3})_2](\text{PF}_6)_2$  for a single crystal X-Ray structural analysis were grown by the slow diffusion of  $\text{Et}_2\text{O}$  into a  $\text{CH}_3\text{NO}_2$  solution of the complex. Details of the structural solution, which converged to give a final R factor of 4.01%, are given in the experimental section. An ortep plot of the structure is given in Figure 2.17 while selected bond lengths, bond angles and torsion angles are given in Tables 2.15-17.

Figure 2.17: Ortep Plot of  $[\text{Os}(\text{[9]aneS3})_2]^{2+}$

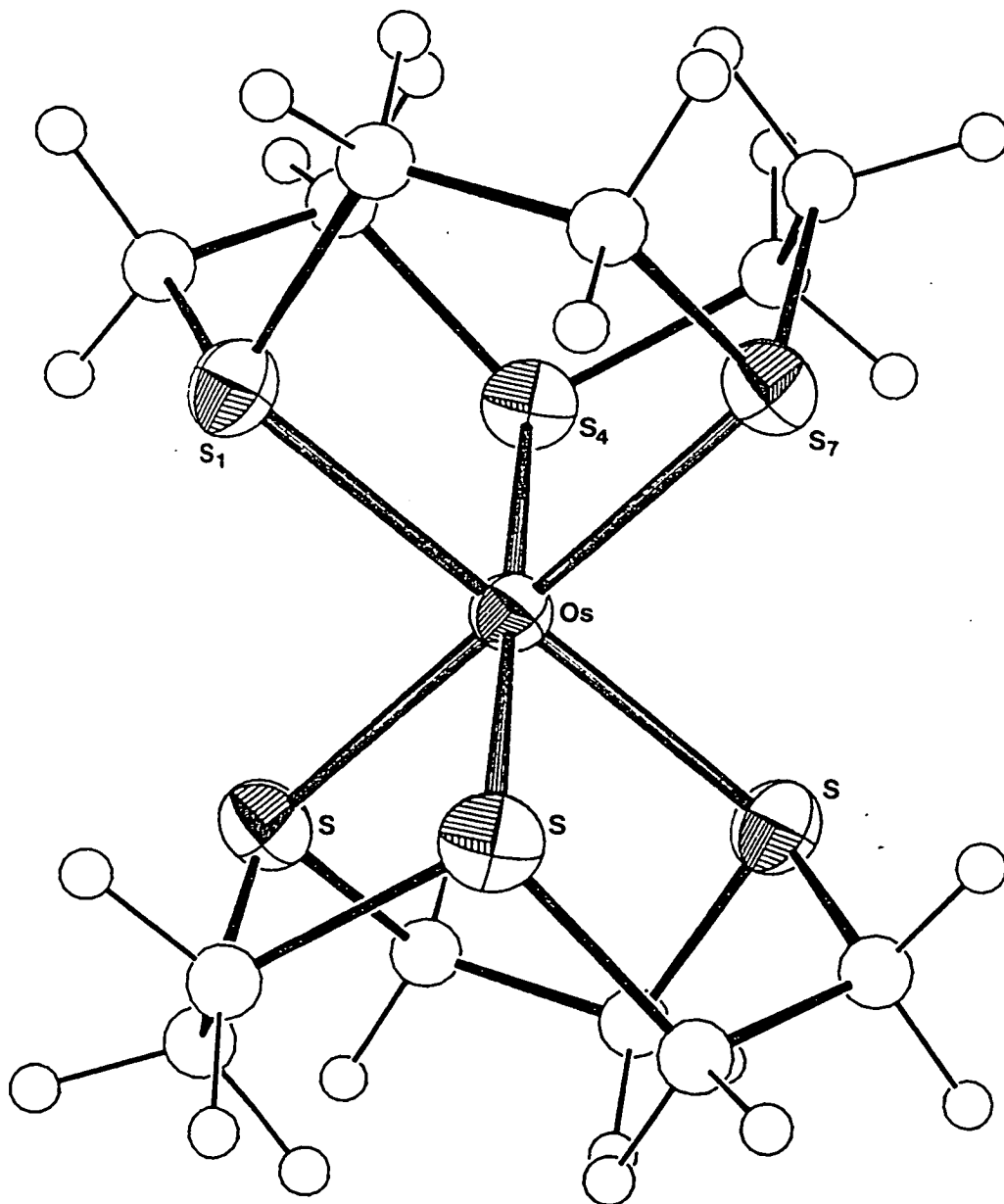


Table 2.15: Selected Bond Lengths (Å) with Standard Deviations  
for [Os([9]aneS3)<sub>2</sub>]<sup>2+</sup>

Os - S(1)	2.3313(18)	C(3) - S(4)	1.848( 8)
Os - S(4)	2.3380(19)	S(4) - C(5)	1.816( 8)
Os - S(7)	2.3408(20)	C(5) - C(6)	1.502(11)
S(1) - C(2)	1.819( 9)	C(6) - S(7)	1.823( 8)
S(1) - C(9)	1.843( 8)	S(7) - C(8)	1.825( 8)
C(2) - C(3)	1.509(11)	C(8) - C(9)	1.532(11)

Table 2.16: Selected Angles (°) with Standard Deviations for  
[Os([9]aneS3)<sub>2</sub>]<sup>2+</sup>

S(1) - Os - S(4)	87.92( 6)	Os - S(4) - C(5)	102.1( 3)
S(1) - Os - S(7)	87.87( 7)	C(3) - S(4) - C(5)	101.9( 4)
S(4) - Os - S(7)	87.52( 7)	S(4) - C(5) - C(6)	112.9( 5)
Os - S(1) - C(2)	103.3( 3)	C(5) - C(6) - S(7)	112.1( 5)
Os - S(1) - C(9)	106.12(25)	Os - S(7) - C(6)	105.0( 3)
C(2) - S(1) - C(9)	100.7( 4)	Os - S(7) - C(8)	102.4( 3)
S(1) - C(2) - C(3)	113.6( 6)	C(6) - S(7) - C(8)	101.7( 4)
C(2) - C(3) - S(4)	112.9( 5)	S(7) - C(8) - C(9)	113.6( 5)
Os - S(4) - C(3)	105.13(25)	S(1) - C(9) - C(8)	111.4( 5)

Table 2.17: Selected Torsion Angles ( $^{\circ}$ ) with Standard Deviations for  $[\text{Os}(\text{[9]aneS3})_2]^{2+}$

S(4) - Os - S(1) - C(2)	-18.6( 3)
S(4) - Os - S(1) - C(9)	86.9( 3)
S(7) - Os - S(1) - C(2)	-106.2( 3)
S(7) - Os - S(1) - C(9)	-0.7( 3)
S(1) - Os - S(4) - C(3)	-1.4( 3)
S(1) - Os - S(4) - C(5)	-107.5( 3)
S(7) - Os - S(4) - C(3)	86.5( 3)
S(7) - Os - S(4) - C(5)	-19.5( 3)
S(1) - Os - S(7) - C(6)	85.9( 3)
S(1) - Os - S(7) - C(8)	-20.0( 3)
S(4) - Os - S(7) - C(6)	-2.1( 3)
S(4) - Os - S(7) - C(8)	-108.0( 3)
Os - S(1) - C(2) - C(3)	41.7( 6)
C(9) - S(1) - C(2) - C(3)	-67.9( 6)
Os - S(1) - C(9) - C(8)	26.8( 6)
C(2) - S(1) - C(9) - C(8)	134.1( 6)
S(1) - C(2) - C(3) - S(4)	-46.6( 7)
C(2) - C(3) - S(4) - Os	27.0( 6)
C(2) - C(3) - S(4) - C(5)	133.1( 6)
Os - S(4) - C(5) - C(6)	44.8( 6)
C(3) - S(4) - C(5) - C(6)	-63.7( 6)
S(4) - C(5) - C(6) - S(7)	-50.9( 7)
C(5) - C(6) - S(7) - Os	29.8( 6)
C(5) - C(6) - S(7) - C(8)	136.2( 6)
Os - S(7) - C(8) - C(9)	43.7( 6)
C(6) - S(7) - C(8) - C(9)	-64.7( 6)
S(7) - C(8) - C(9) - S(1)	-47.8( 7)



As with its Ru analogue, structural analysis reveals a centrosymmetric cation with the osmium atom sited on an inversion centre. Both macrocycles are fully co-ordinated (Os-S: 2.3312(18), 2.3389(19) and 2.3426(20) Å) to give near octahedral geometry (S-Os-S: 87.92, 87.87 and 87.52°) about the metal centre.

### 2.3 Conclusions

This investigation has shown that half sandwich complexes of [9]aneS3 with Ru(II) and Os(II) centres, incorporating a range of other ligands, may be synthesised. Further work to see if these, or analogous complexes, may prove to be catalytically useful is required though the reactivity of  $[\text{Ru}(\text{H})(\text{CO})(\text{PPh}_3)([\text{9]aneS3})](\text{PF}_6)$  seems promising.

In addition to synthesising these complexes some information on the trans influence of various ligands on the M-S bond lengths has also been obtained. This gives direct evidence for the sulphur macrocycle acting as a  $\pi$ -acceptor via the sulphurs low-lying empty d orbitals. To investigate the electronic properties of the macrocycle further an in-depth study via spectroelectrochemical techniques has been carried out and is described in Chapter 3.

## 2.4 Experimental

### Physical Measurements

Microanalyses were carried out by the University of Edinburgh, Chemistry Department analytical service. IR spectra were recorded (in the region  $4000-200\text{cm}^{-1}$ ) on a Perkin-Elmer 598 Spectrometer using KBr discs.  $^1\text{H}$  n.m.r. spectra were recorded on Bruker WP80SY and WP200SY Spectrometers.  $^{31}\text{P}$  n.m.r. were recorded on Bruker WP80SY and WP200SY and Joel FX60Q and FX90Q spectrometers. X-band electron spin resonance (e.s.r.) spectra were recorded using a Bruker ER-200D spectrometer employing 100KHz field modulation. Fast atom bombardment (FAB) spectra were obtained in 3-NOBA or glycerol/DMF matrices on a Kratos MS50TC spectrometer. UV/Vis/NIR spectra were recorded on a Perkin-Elmer  $\lambda 9$  spectrophotometer.

### Single Crystal Structure Determinations

The following computer programs were used in the solution and refinement of the crystal structures; SHELX76 <sup>(65)</sup>, SHELX86 <sup>(66)</sup>, CALC <sup>(67)</sup>, DIFABS <sup>(68)</sup>. The scattering factor curves for elements not inlaid in SHELX76, (Ru, Os), were taken from reference <sup>(69)</sup>. The graphics program ORTEP <sup>(70)</sup> was used to obtain plots of the molecules.

Materials

$\text{RuCl}_3 \cdot 3\text{H}_2\text{O}$  and  $(\text{NH}_4)_2[\text{OsCl}_6]$  (Johnson Matthey plc), [9]aneS3 (Aldrich) and Sephadex LH20 (Pharmacia). The following materials were prepared by literature methods;  $\text{RuCl}_2(\text{PMe}_2\text{Ph})_4$ ,  $\text{RuCl}_2(\text{PEtPh}_2)_3$ ,  $\text{RuBr}_2(\text{PEtPh}_2)_3$  (71),  $\text{RuCl}_3(\text{PMe}_2\text{Ph})_3$ ,  $\text{RuCl}_3(\text{PEt}_2\text{Ph})_3$  (72),  $\text{RuCl}_2(\text{PPh}_3)_3$ ,  $\text{RuBr}_2(\text{PPh}_3)_3$  (73),  $\text{RuCl}_3(\text{AsPh}_3)_2(\text{MeOH})$  (74),  $\text{RuCl}_3(\text{NO})(\text{PPh}_3)_2$ ,  $\text{Ru}(\text{H})_2(\text{CO})(\text{PEtPh}_3)_3$ ,  $\text{Os}(\text{H})_2(\text{CO})(\text{PPh}_3)_3$  (75),  $[\text{RuCl}_2(\text{CS})(\text{PPh}_3)_2]_2$  (76),  $\text{RuCl}_2(\text{CO})(\text{PPh}_3)_2(\text{DMF})$  (77),  $\text{RuCl}_2(\text{CO})(\text{PEtPh}_2)_2(\text{DMF})$  (64) and  $\{\text{OsCl}_2(4\text{-MeC}_6\text{H}_4^i\text{Pr})\}_2$  (78).

Dichloromethane was allowed to stand for one week over KOH pellets and dried by distillation over  $\text{P}_2\text{O}_5$ . All other solvents were used as supplied without further purification.  $^1\text{H}$  and  $^{31}\text{P}$  n.m.r. spectra for the new complexes are given in Table 2.18.

 $[\text{RuCl}(\text{PMe}_2\text{Ph})_2((9)\text{aneS3})](\text{PF}_6)$ 

(1)  $\text{RuCl}_3(\text{PMe}_2\text{Ph})_3$  (153.1mg,  $2.46 \times 10^{-4}$  mmol) and [9]aneS3 ( $2.46 \times 10^{-4}$  mmol) were heated under reflux in dichloromethane (8ml) for 4 hours to afford a yellow solution. On removing the solvent under reduced pressure the residue was redissolved in a small volume of hot ethanol (8ml). Addition of excess  $\text{NH}_4\text{PF}_6$  in water precipitated a light yellow powder which was collected, washed with ethanol (1ml) and diethylether (15ml) and dried in vacuo. Yield 117.7mg, 78% Mol.Wt. 738.1 Found C 35.9, H 4.77 Calc for  $\text{RuP}_3\text{F}_6\text{ClS}_3\text{C}_{22}\text{H}_{36}$  C 35.8, H 4.64% FAB

mass spectrum: found  $M^+ = 594, 427$ .

<u>Calculated for</u>	<u><math>M^+</math></u>
$^{102}\text{Ru}^{35}\text{Cl}(\text{PMe}_2\text{Ph})_2([\text{9}]\text{aneS3})$	593
$^{102}\text{Ru}^{35}\text{Cl}(\text{PMe}_2\text{Ph})(\text{SC}_2\text{H}_4\text{SC}_2\text{H}_4\text{S})$	427

$[\text{RuCl}(\text{PEt}_2\text{Ph})_2([\text{9}]\text{aneS3})](\text{PF}_6)$

Method as for (1) above using  $\text{RuCl}_3(\text{PEt}_2\text{Ph})_3$  (104.7mg,  $1.48 \times 10^{-4}$  mmol) and  $[\text{9}]\text{aneS3}$  ( $1.48 \times 10^{-4}$  mmol). The product was isolated as a light yellow powder. Yield 94.3mg 80% Mol.Wt. 794.2. Found C 39.1, H 5.24 Calc for  $\text{RuP}_3\text{F}_6\text{ClS}_3\text{C}_{26}\text{H}_{42}$  C 39.3, H 5.33%. FAB mass spectrum: found  $M^+ = 649, 586, 455$ .

<u>Calculated for</u>	<u><math>M^+</math></u>
$^{102}\text{Ru}^{35}\text{Cl}(\text{PEt}_2\text{Ph})_2([\text{9}]\text{aneS3})$	649
$^{102}\text{Ru}(\text{PEt}_2\text{Ph})_2([\text{9}]\text{aneS3})$	586
$^{102}\text{Ru}^{35}\text{Cl}(\text{PEt}_2\text{Ph})(\text{SC}_2\text{H}_4\text{SC}_2\text{H}_4\text{S})$	455

Single Crystal Structure Determination of

$[\text{RuCl}(\text{PEtPh}_2)_2([\text{9}]\text{aneS3})](\text{PF}_6) \cdot \frac{1}{2}(\text{CH}_2\text{Cl}_2)$

Crystals were obtained by the slow diffusion of  $\text{Et}_2\text{O}$  into a  $\text{CH}_2\text{Cl}_2$  solution of the complex.

Crystal Data

$(\text{C}_{34}\text{H}_{42}\text{ClP}_2\text{S}_3\text{Ru})(\text{PF}_6) \cdot \frac{1}{2}(\text{CH}_2\text{Cl}_2)$ ,  $M = 932.81$  monoclinic

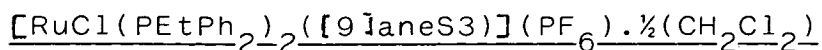
$a = 18.553(4)$ ,  $b = 10.796(5)$ ,  $c = 21.891(5)$  Å,  $\alpha = 90$ ,  $\beta = 114.147(9)$ ,  $\gamma = 90^\circ$ ,  $v = 4001.1 \text{ \AA}^{-3}$  (from setting angles for 15 reflections with  $\theta = 10-15^\circ$   $\lambda = 0.71069$  Å), space group  $P2_1/c$ ,  $Z = 4$ ,  $D_{\text{calc}} = 1.548 \text{ g cm}^{-3}$  Bright yellow plates. Crystal dimensions  $0.40 \times 0.144 \times 0.016$  mm,  $(\text{Mo-K}\alpha) = 8.40 \text{ cm}^{-1}$ .

### Data Collection and Processing

Stoe STADI-2 two circle diffractometer, Mo-K $\alpha$  x-radiation  $\omega$  scans with width  $(1.0 + 0.5(\sin \mu / \tan \theta))^\circ$ ; 5771 reflections measured,  $(2.5 \leq \theta \leq 25^\circ)$ ,  $h0 \rightarrow 22$ ,  $k0 \rightarrow 11$ ,  $l-26 \rightarrow 26$ , giving 2130 with  $F \geq 6 \sigma(F)$ .

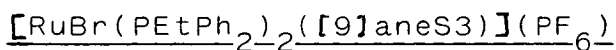
### Structure Analysis and Refinement

Patterson Synthesis (Ru) followed by iterative cycles of least squares refinement and difference Fourier synthesis revealed the positions of all non-H atoms. Full matrix least squares with C(phenyl) and H-atoms in calculated positions and anisotropic thermal parameters for Ru, Cl, S, P, F atoms. Final R,  $R_w$  and S are 0.0584, 0.0503 and  $S = 1.099$  for 234 parameters and the final  $\Delta F$  synthesis showed max. peak and min trough of 0.52 and  $-0.48 \text{ e \AA}^{-3}$ . The weighting scheme  $W = 1.6208 / (\sigma^2 F + 0.000182 F^2)$  gave satisfactory agreement analysis.



(2)  $\text{RuCl}_2(\text{PEtPh}_2)_3$  (152.9mg  $1.88 \times 10^{-4}$  mmol) and **[9]anes3** ( $1.88 \times 10^{-4}$  mmol) were heated under reflux in ethanol (8ml) for 20 minutes to yield a yellow solution. Addition of excess  $\text{NH}_4\text{PF}_6$  in water precipitated a light yellow powder. This product was recrystallised from a dichloromethane/diethylether solvent system and air dried. Yield 144.3mg 86% Mol.Wt. 932.8 Found C 44.0, H 4.68 calc for  $\text{RuP}_3\text{F}_3\text{S}_3\text{C}_{34}\text{H}_{42} \cdot \frac{1}{2}(\text{CH}_2\text{Cl}_2)$  C 44.5, H 4.64%. FAB mass spectrum: found  $M^+ = 744, 681, 503$ .

<u>Calculated for</u>	<u><math>M^+</math></u>
$^{102}\text{Ru}^{35}\text{Cl}(\text{PEtPh}_2)_2([\text{9]aneS3})$	745
$^{102}\text{Ru}(\text{PEtPh}_2)_2(\text{SC}_2\text{H}_4\text{SC}_2\text{H}_4\text{S})$	682
$^{102}\text{Ru}^{35}\text{Cl}(\text{PEtPh}_2)(\text{SC}_2\text{H}_4\text{SC}_2\text{H}_4\text{S})$	503



Method as for (2) above using  $\text{RuBr}_2(\text{PEtPh}_2)_3$  (122.7mg,  $1.34 \times 10^{-4}$  mmol) and **[9]anes3** ( $1.34 \times 10^{-4}$  mmol). The product, isolated as a light yellow powder, was washed with ethanol (1ml) and diethylether (15ml) and dried in vacuo. Yield 104.3mg 82% mol.Wt. 934.8. Found C 43.4, H 4.59 Calc for  $\text{RuP}_3\text{F}_6\text{BrS}_3\text{C}_{34}\text{H}_{42}$  C 43.7, H 4.3%. FAB mass spectrum: found  $M^+ = 790, 683, 547$ .

<u>Calculated for</u>	<u><math>M^+</math></u>
$^{102}\text{Ru}^{79}\text{Br}(\text{PEtPh}_2)_2([\text{9]aneS3})$	789

$^{102}\text{Ru}(\text{PEtPh}_2)_2(\text{SC}_2\text{H}_4\text{SC}_2\text{H}_4\text{S})$	682
$^{102}\text{Ru}^{79}\text{Br}(\text{PEtPh}_2)(\text{SC}_2\text{H}_4\text{SC}_2\text{H}_4\text{S})$	547

$\text{RuCl}_2(\text{PPh}_3)(\text{[9]aneS3})$

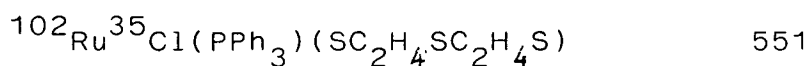
(3a)  $\text{RuCl}_2(\text{PPh}_3)_3$  (140.5mg  $1.47 \times 10^{-4}$  mmol) and [9]aneS3 ( $1.47 \times 10^{-4}$  mmol) were heated under reflux in ethanol (8ml) for 20 minutes to yield a bright yellow precipitate. This was collected and washed with ethanol (10ml) and diethylether (15ml) and dried in vacuo. Yield 77.2mg 86%.

(3b)  $\text{RuCl}_2(\text{PPh}_3)_3$  (135.6mg  $1.41 \times 10^{-4}$  mmol) and [9]aneS3 ( $1.41 \times 10^{-4}$  mmol) were heated under reflux in dichloromethane (8ml) for 1 hour to yield a bright yellow solution. On removing the solvent under reduced pressure the bright yellow residue was washed with ethanol (10ml) and diethylether (15ml) and dried in vacuo. Yield 77.6mg 89%.

(3c) Method as for (3b) above using  $\text{RuCl}_3(\text{NO})(\text{PPh}_3)_2$  (120.1mg  $1.44 \times 10^{-4}$  mmol) and [9]aneS3 ( $1.44 \times 10^{-4}$  mmol) and refluxing for 4 hours. Yield 79.9mg 88%.

Mol.Wt 614.6. Found C 46.6, H 4.66 Calc for  $\text{RuP}_3\text{Cl}_2\text{S}_3\text{C}_{24}\text{H}_{27}$  C 46.9, H 4.43%. FAB mass spectrum: found  $M^+ = 615, 579, 551$ .

<u>Calculated for</u>	<u><math>M^+</math></u>
$^{102}\text{Ru}^{35}\text{Cl}_2(\text{PPh}_3)(\text{[9]aneS3})$	614
$^{102}\text{Ru}^{35}\text{Cl}(\text{PPh}_3)(\text{[9]aneS3})$	579



$\text{RuBr}_2(\text{PPh}_3)([\text{9}]\text{aneS3})$

Methods as for (3a) above using  $\text{RuBr}_2(\text{PPh}_3)_3$  (156.2mg  $1.49 \times 10^{-4}$  mmol) and  $[\text{9}]$ aneS3 ( $1.49 \times 10^{-4}$  mmol) to yield a yellow precipitate. Yield 92.7mg 88% Mol.Wt. 703.5 Found C 41.2, H 3.99 Calc for  $\text{RuPBr}_2\text{S}_3\text{C}_{24}\text{H}_{27}$  C 41.0, H 3.87%. FAB mass spectrum: found  $\text{M}^+ = 703,596$ .

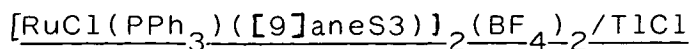
<u>Calculated for</u>	<u><math>\text{M}^+</math></u>
$^{102}\text{Ru}^{79}\text{Br}_2(\text{PPh}_3)([\text{9}]\text{aneS3})$	702
$^{102}\text{Ru}^{79}\text{Br}(\text{PPh}_3)(\text{SC}_2\text{H}_4\text{SC}_2\text{H}_4\text{S})$	595

$\text{RuCl}_2(\text{AsPh}_3)([\text{9}]\text{aneS3})$

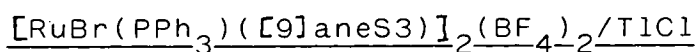
(4)  $\text{RuCl}_3(\text{AsPh}_3)_2(\text{MeOH})$  (128.0mg 1.39mmol) and  $[\text{9}]$ aneS3 were heated under reflux in ethanol (8ml) for 15 hours to afford a bright yellow precipitate. This was collected and washed with ethanol (10ml) and diethylether (15ml) and dried in vacuo. Yield 77.1mg 85% Mol.Wt. 658.6 Found C 43.7, H 4.55 Calc for  $\text{RuAsClS}_3\text{C}_{24}\text{H}_{27}$  C 43.8 H 4.13% FAB mass spectrum: Found  $\text{M}^+ = 658,623,595$ .

<u>Calculated for</u>	<u><math>\text{M}^+</math></u>
$^{102}\text{Ru}^{35}\text{Cl}_2(\text{AsPh}_3)([\text{9}]\text{aneS3})$	658
$^{102}\text{Ru}^{35}\text{Cl}(\text{AsPh}_3)([\text{9}]\text{aneS3})$	623
$^{102}\text{Ru}^{35}\text{Cl}(\text{AsPh}_3)(\text{SC}_2\text{H}_4\text{SC}_2\text{H}_4\text{S})$	595

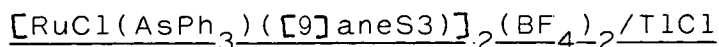




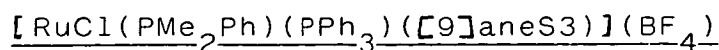
(5)  $\text{RuCl}_2(\text{PPh}_3)([\text{9}]\text{aneS3})$  (81.4mg  $1.32 \times 10^{-4}$  mmol) and  $\text{Tl}(\text{BF}_4)$  ( $1.32 \times 10^{-4}$  mmol) were heated under reflux in degassed dichloromethane (8ml) for 15 hours to afford an orange precipitate. This was collected and washed with ethanol (10ml) and diethylether (15ml) and dried in vacuo.



Method as for (5) above using  $\text{RuCl}_2(\text{AsPh}_3)([\text{9}]\text{aneS3})$  (85.2mg  $1.21 \times 10^{-4}$  mmol) and  $\text{Tl}(\text{BF}_4)$  ( $1.21 \times 10^{-4}$  mmol) to afford a pink precipitate.



Method as for (5) above using  $\text{RuCl}_2(\text{AsPh}_3)([\text{9}]\text{aneS3})$  (82.9mg  $1.36 \times 10^{-4}$  mmol) and  $\text{Tl}(\text{BF}_4)$  ( $1.36 \times 10^{-4}$  mmol) to afford an orange precipitate.



(6)  $\text{RuCl}_2(\text{PPh}_3)([\text{9}]\text{aneS3})$  (91.4mg  $1.49 \times 10^{-4}$  mmol),  $\text{Tl}(\text{BF}_4)$  ( $1.49 \times 10^{-4}$  mmol) and  $\text{PMe}_2\text{Ph}$  ( $1.49 \times 10^{-4}$  mmol) were heated under reflux in degassed dichloromethane (8ml) for 15 hours under  $\text{N}_2$  to afford a white precipitate ( $\text{TlCl}$ ) and a light yellow solution. Upon filtration through celite, partial removal of the solvent and addition of an excess of diethylether a light

yellow precipitate formed. This was collected, recrystallised from a dichloromethane/diethylether solvent system and air dried. Yield 102.2mg 65% Mol.Wt. 804.1. Found C 47.6, H 4.48 Calc for  $\text{RuBP}_2\text{F}_4\text{ClS}_3\text{C}_{32}\text{H}_{38}$  C 47.8, H 4.76%. FAB mass spectrum: found  $M^+ = 718, 702, 684, 655, 427$ .

<u>Calculated for</u>	<u><math>M^+</math></u>
$^{102}\text{Ru}^{35}\text{Cl}(\text{PMe}_2\text{Ph})(\text{PPh}_3)([\text{9}] \text{aneS3})$	717
$^{102}\text{Ru}^{35}\text{Cl}(\text{PMePh})(\text{PPh}_3)([\text{9}] \text{aneS3})$	702
$^{102}\text{Ru}(\text{PMe}_2\text{Ph})(\text{PPh}_3)([\text{9}] \text{aneS3})$	682
$^{102}\text{Ru}^{35}\text{Cl}(\text{PMe}_2\text{Ph})(\text{PPh}_3)(\text{SC}_2\text{H}_4\text{SC}_2\text{H}_4\text{S})$	655
$^{102}\text{RuCl}(\text{PMe}_2\text{Ph})(\text{SC}_2\text{H}_4\text{SC}_2\text{H}_4\text{S})$	427

$[\text{RuBr}(\text{PMe}_2\text{Ph})(\text{PPh}_3)([\text{9}] \text{aneS3})](\text{BF}_4)$

Method as for (6) above using  $\text{RuCl}_2(\text{AsPh}_3)([\text{9}] \text{aneS3})$  (94.2mg  $1.43 \times 10^{-4}$  mmol),  $\text{Tl}(\text{BF}_4)$  ( $1.43 \times 10^{-4}$  mmol) and  $\text{PMe}_2\text{Ph}$  ( $1.43 \times 10^{-4}$  mmol) to afford a light yellow powder. Yield 94.5mg 83.2% Mol.Wt 848.6 Found C 45.4, H 4.46 Calc for  $\text{RuBP}_2\text{F}_4\text{BrS}_3\text{C}_{32}\text{H}_{38}$  C 45.3, H 4.51%. FAB mass spectrum: Found  $M^+ = 762, 655, 471$ .

<u>Calculated for</u>	<u><math>M^+</math></u>
$^{102}\text{Ru}^{79}\text{Br}(\text{PMe}_2\text{Ph})(\text{PPh}_3)([\text{9}] \text{aneS3})$	761
$^{102}\text{Ru}(\text{PMe}_2\text{Ph})(\text{PPh}_3)(\text{SC}_2\text{H}_4\text{SC}_2\text{H}_4\text{S})$	655
$^{102}\text{Ru}^{79}\text{Br}(\text{PMe}_2\text{Ph})\text{SC}_2\text{H}_4\text{SC}_2\text{H}_4\text{S}$	471

[RuCl(PMe<sub>2</sub>Ph)(AsPh<sub>3</sub>)([9]aneS<sub>3</sub>)](BF<sub>4</sub>)

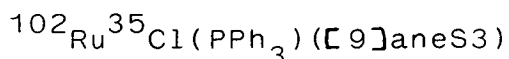
Method as for (6) above using RuBr<sub>2</sub>(PPh<sub>3</sub>)([9]aneS<sub>3</sub>) (91,0mg 1.29x10<sup>-4</sup>mmol), Tl(BF<sub>4</sub>) (1.29x10<sup>-4</sup>mmol) and PMe<sub>2</sub>Ph (1.29x10<sup>-4</sup>mmol) to afford a light yellow powder. Yield 95.6mg 82% Mol.Wt 848.1. Found C 45.5, H 4.80 Calc for RuBAsPF<sub>4</sub>ClS<sub>3</sub>C<sub>32</sub>H<sub>38</sub> C 45.3, H 4.52%. FAB mass spectrum: Found M<sup>+</sup> = 761, 746, 726, 699, 427.

<u>Calculated for</u>	<u>M<sup>+</sup></u>
<sup>102</sup> Ru <sup>35</sup> Cl(PMe <sub>2</sub> Ph)(AsPh <sub>3</sub> )([9]aneS <sub>3</sub> )	761
<sup>102</sup> Ru <sup>35</sup> Cl(PMePh)(AsPh <sub>3</sub> )([9]aneS <sub>3</sub> )	746
<sup>102</sup> Ru(PMe <sub>2</sub> Ph)(AsPh <sub>3</sub> )([9]aneS <sub>3</sub> )	726
<sup>102</sup> Ru(PMe <sub>2</sub> Ph)(AsPh <sub>3</sub> )(SC <sub>2</sub> H <sub>4</sub> SC <sub>2</sub> H <sub>4</sub> S)	698
<sup>102</sup> Ru <sup>35</sup> Cl(PMe <sub>2</sub> Ph)(SC <sub>2</sub> H <sub>4</sub> SC <sub>2</sub> H <sub>4</sub> S)	427

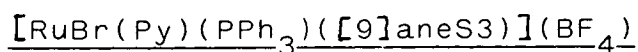
[RuCl(Py)(PPh<sub>3</sub>)([9]aneS<sub>3</sub>)](BF<sub>4</sub>)

Method as for (6) above using RuCl<sub>2</sub>(PPh<sub>3</sub>)([9]aneS<sub>3</sub>) (91.4mg 1.49x10<sup>-4</sup>mmol), Tl(BF<sub>4</sub>) (1.49x10<sup>-4</sup>mmol) and Py (1.49x10<sup>-4</sup>mmol) to afford a light yellow powder. Yield 96.2mg 87% Mol.Wt. 745.1 Found C 46.4, H 4.40, N 1.96 Calc for RuBNPF<sub>4</sub>ClS<sub>3</sub>C<sub>29</sub>H<sub>32</sub> C 46.7, H 4.33, N 1.96%. I.R.  $\nu_{(C=C)}$ (Py) 1602cm<sup>-1</sup>. FAB mass spectrum: found M<sup>+</sup> = 657, 578, 550.

<u>Calculated for</u>	<u>M<sup>+</sup></u>
<sup>102</sup> Ru <sup>35</sup> Cl(Py)(PPh <sub>3</sub> )([9]aneS <sub>3</sub> )	658
<sup>102</sup> Ru <sup>35</sup> Cl(PPh <sub>3</sub> )([9]aneS <sub>3</sub> )	579

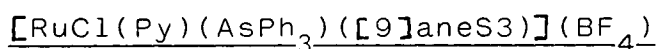


551



Method as for (6) above using  $\text{RuBr}_2(\text{PPh}_3)([\text{9}]\text{aneS3})$  (95.6mg  $1.36 \times 10^{-4}$  mmol),  $\text{Tl}(\text{BF}_4)$  ( $1.36 \times 10^{-4}$  mmol) and Py ( $1.36 \times 10^{-4}$  mmol) to afford a light yellow powder. Yield 88.1mg 82% Mol.Wt. 789.5. Found C 44.3, H 4.21, N 1.70 Calc for  $\text{RuBNPF}_4\text{BrS}_3\text{C}_{29}\text{H}_{32}$  C 44.1, H 4.09, N 1.77%. I.R.  $\nu_{(\text{C}=\text{C})}(\text{Py})$   $1608\text{cm}^{-1}$ . FAB mass spectrum: found  $M^+ = 702, 595$ .

<u>Calculated for</u>	<u><math>M^+</math></u>
$^{102}\text{Ru}^{79}\text{Br}(\text{Py})(\text{PPh}_4)([\text{9}]\text{aneS3})$	702
$^{102}\text{Ru}^{79}\text{Br}(\text{PPh}_3)(\text{SC}_2\text{H}_4\text{SC}_2\text{H}_4\text{S})$	595



Method as for (6) above using  $\text{RuCl}_2(\text{AsPh}_3)([\text{9}]\text{aneS3})$  (95.6mg  $1.45 \times 10^{-4}$  mmol),  $\text{Tl}(\text{BF}_4)$  ( $1.45 \times 10^{-4}$  mmol) and Py ( $1.45 \times 10^{-4}$  mmol) to afford a light yellow powder. Yield 92.0mg 79% Mol.Wt. 789.0. Found C 43.8, H 4.12, N 1.84 Calc for  $\text{RuBNAsF}_4\text{ClS}_3\text{C}_{29}\text{H}_{32}$  C 44.1, H 4.09, N 1.78%. I.R.  $\nu_{(\text{C}=\text{C})}(\text{Py})$   $1604\text{cm}^{-1}$ . FAB mass spectrum: found  $M^+ = 703, 594$ .

<u>Calculated for</u>	<u><math>M^+</math></u>
$^{102}\text{Ru}^{35}\text{Cl}(\text{Py})(\text{AsPh}_3)([\text{9}]\text{aneS3})$	702
$^{102}\text{Ru}^{35}\text{Cl}(\text{AsPh}_3)(\text{SC}_2\text{H}_4\text{SC}_2\text{H}_4\text{S})$	595

[RuCl(PhCN)(PPh<sub>3</sub>)([9]aneS3)](BF<sub>4</sub>)

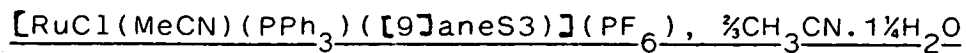
Method as for (6) above using RuCl<sub>2</sub>(PPh<sub>3</sub>)([9]aneS3) (91.2mg 1.48x10<sup>-4</sup>mmol), Tl(BF<sub>4</sub>) (1.48x10<sup>-4</sup>mmol) and PhCN (1.48x10<sup>-4</sup>mmol) to afford a light yellow powder. Yield 90.8mg 80% Mol.Wt. 769.1. Found C 47.9, H 4.10, N 1.84 Calc for RuBNPF<sub>4</sub>ClS<sub>3</sub>C<sub>31</sub>H<sub>32</sub> C 48.4, H 4.19, N 1.82%. I.R.  $\nu_{(\text{CN})}$  2240cm<sup>-1</sup>. FAB mass spectrum: found M<sup>+</sup> = 682,578,550.

<u>Calculated for</u>	<u>M<sup>+</sup></u>
<sup>102</sup> Ru <sup>35</sup> Cl(PhCN)(PPh <sub>4</sub> )([9]aneS3)	682
<sup>102</sup> Ru <sup>35</sup> Cl(PPh <sub>3</sub> )([9]aneS3)	579
<sup>102</sup> Ru <sup>35</sup> Cl(PPh <sub>3</sub> )(SC <sub>2</sub> H <sub>4</sub> SC <sub>2</sub> H <sub>4</sub> S)	551

[RuCl(P(OMe)<sub>2</sub>Ph)(PPh<sub>3</sub>)([9]aneS3)](BF<sub>4</sub>)

Method as for (6) above using RuCl<sub>2</sub>(PPh<sub>3</sub>)([9]aneS3) (91.3mg 1.49x10<sup>-4</sup>mmol), Tl(BF<sub>4</sub>) (1.49x10<sup>-4</sup>mmol) and P(OMe)<sub>2</sub>Ph (1.49x10<sup>-4</sup>mmol) to afford a yellow powder. Yield 103.4mg 83% Mol.Wt. 836.1. Found C 45.5, H 4.53 Calc for RuClBOP<sub>2</sub>F<sub>4</sub>S<sub>3</sub>C<sub>32</sub>H<sub>38</sub> C 46.0, H 4.58%. FAB mass spectrum: found M<sup>+</sup> = 750,714,687,459.

<u>Calculated for</u>	<u>M<sup>+</sup></u>
<sup>102</sup> Ru <sup>35</sup> Cl(P(OMe) <sub>2</sub> Ph)(PPh <sub>3</sub> )([9]aneS3)	749
<sup>102</sup> Ru(P(OMe) <sub>2</sub> Ph)PPh <sub>3</sub> ([9]aneS3)	714
<sup>102</sup> Ru(P(OMe) <sub>2</sub> Ph)(PPh <sub>3</sub> )(SC <sub>2</sub> H <sub>4</sub> SC <sub>2</sub> H <sub>4</sub> S)	686
<sup>102</sup> Ru <sup>35</sup> Cl(P(OMe) <sub>2</sub> Ph)(SC <sub>2</sub> H <sub>4</sub> SC <sub>2</sub> H <sub>4</sub> S)	459

Single Crystal Structure Determination of

Crystals were obtained by the slow diffusion of  $\text{Et}_2\text{O}$  into a MeCN solution of the complex.

Crystal Data

( $\text{C}_{26}\text{H}_{30}\text{ClNPS}_3\text{Ru}$ ).  $\text{PF}_6 \cdot \frac{2}{3}\text{CH}_3\text{CN} \cdot \frac{1}{4}\text{H}_2\text{O}$   $M = 815.08$ , Orthorhombic,  $a = 8.534(3)$ ,  $b = 16.786(7)$ ,  $c = 27.107(13)$ ,  $\alpha = \beta = \gamma = 90^\circ$ ,  $V = 3885 \text{ \AA}^3$  (from setting angles for 12 reflections with  $2\theta = 24-42^\circ$   $\lambda = 1.54184 \text{ \AA}$ ), space group  $P2_12_12_1$ ,  $z = 4$ ,  $D_{\text{calc}} = 1.359 \text{ g cm}^{-3}$ ,  $(\text{CuK}\alpha) = 67.06 \text{ cm}^{-1}$ .

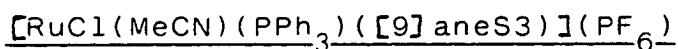
Data Collection and Processing

Stoe STADI-4 four circle diffractometer,  $\text{CuK}\alpha$  X-radiation,  $\omega$  scans with width  $(1.32 + 0.34 \tan \theta)^\circ$ , 3473 reflections measured,  $(1.5 \leq \theta \leq 59.17)$ ,  $h = -9 \rightarrow 3$ ,  $k = 0 \rightarrow 18$ ,  $l = 0 \rightarrow 29$ , giving 1089 with  $F \geq 4 \sigma(F)$ . Initial correction for absorption was by  $\psi$  scans (min 0.0918 and max 0.2884 transition factors).

Structure Analysis and Refinement

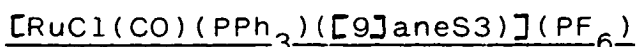
Patterson synthesis (Ru) followed by iterative cycles of least squares refinement and difference Fourier synthesis revealed the positions of all non-H atoms. At isotropic convergence corrections (min 0.791, max 1.544) for absorption

was made using DIFABS. Full matrix least squares with H-atoms and phenyl carbons in calculated positions and anisotropic thermal parameters for Ru, S, Cl, P and ordered F. Final R, Rw and S values were 0.0924, 0.1117 and 1.070 for 213 parameters and the final  $\Delta F$  synthesis showed max peak and min trough of 1.03 and  $-1.08\text{\AA}^{-3}$ . The weighting scheme  $w = 0.9308 / (\sigma^2(F) + 0.007352F^2)$  gave satisfactory agreement analysis.



Method as for (6) above using  $\text{RuCl}_2(\text{PPh}_3)([\text{9}] \text{aneS3})$  (85.7mg  $1.39 \times 10^{-4}$  mmol),  $\text{Tl}(\text{PF}_6)$  ( $1.39 \times 10^{-4}$  mmol) and MeCN ( $1.39 \times 10^{-4}$  mmol) to afford a yellow powder which was recrystallised from a  $\text{CH}_2\text{Cl}_2$ /diethylether solvent system and dried in vacuo. Yield 89.5mg 81% Mol.Wt. 765.2. Found C 40.7, H 4.23, N 1.95 Calc for  $\text{RuBNPF}_4\text{S}_3\text{C}_{26}\text{H}_{30}$  C 40.8, H 3.96, N 1.83%. I.R.  $\nu_{(\text{CN})}$   $2041\text{cm}^{-1}$ . FAB mass spectrum: found  $M^+ = 621, 580$ .

<u>Calculated for</u>	<u><math>M^+</math></u>
$^{102}\text{Ru}^{35}\text{Cl}(\text{MeCN})(\text{PPh}_3)([\text{9}] \text{aneS3})$	620
$^{102}\text{Ru}^{35}\text{Cl}(\text{PPh}_3)([\text{9}] \text{aneS3})$	579



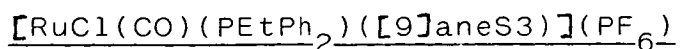
(7a)  $\text{RuCl}_2(\text{CO})(\text{PPh}_4)(\text{DMF})$  (106.6mg  $1.34 \times 10^{-4}$  mmol) and  $[\text{9}] \text{aneS3}$  ( $1.34 \times 10^{-4}$  mmol) were heated under reflux in ethanol for 10

minutes to afford a pale yellow solution. Addition of excess  $\text{NH}_4\text{PF}_6$  in water precipitated a pale yellow powder which was collected, washed with ethanol (1ml) and diethylether (15ml) and dried in vacuo. Yield 82.4mg 82%.

(7b)  $\text{Ru}(\text{H})_2(\text{CO})(\text{PPh}_3)_3$  (107.4mg  $1.17 \times 10^{-4}$  mmol) and [9]aneS3 ( $1.17 \times 10^{-4}$  mmol) were heated under refluxed in degassed dichloromethane (8ml) for 15 hours under  $\text{N}_2$  to afford a pale yellow solution. On removing the solvent under reduced pressure the residue was redissolved in a small volume of hot ethanol (8ml). Addition of excess  $\text{NH}_4\text{PF}_6$  in water precipitated a pale yellow powder which was washed with ethanol (1ml) and diethylether (15ml) and dried in vacuo. Yield 72.8mg 83%.

Mol.Wt. 752.1. found C 39.6, H 3.50 Calc for  $\text{RuOP}_2\text{F}_6\text{ClS}_3\text{C}_{25}\text{H}_{27}$  C 39.9, H 3.62%. I.R.  $\nu_{(\text{CO})}$   $2010\text{cm}^{-1}$ . FAB mass spectrum: found  $M^+$  = 607, 573, 551, 516.

<u>Calculated for</u>	<u><math>M^+</math></u>
$^{102}\text{Ru}^{35}\text{Cl}(\text{CO})(\text{PPh}_3)([\text{9}] \text{aneS3})$	607
$^{102}\text{Ru}(\text{CO})(\text{PPh}_3)([\text{9}] \text{aneS3})$	572
$^{102}\text{Ru}^{35}\text{Cl}(\text{PPh}_3)(\text{SC}_2\text{H}_4\text{SC}_2\text{H}_4\text{S})$	551
$^{102}\text{Ru}(\text{PPh}_3)(\text{SC}_2\text{H}_4\text{SC}_2\text{H}_4\text{S})$	516

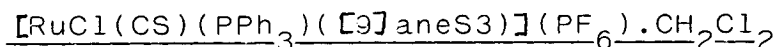


Method as for (7a) above using  $\text{RuCl}_2(\text{CO})(\text{PEtPh}_2)_2(\text{DMF})$



(151.9mg  $2.17 \times 10^{-4}$  mmol) and refluxing for 30 minutes to afford a pale yellow precipitate. Yield 125.2mg 87% Mol.Wt. 704.1. Found C 35.9, H 3.99 Calc for  $\text{RuOP}_2\text{F}_6\text{S}_3\text{C}_{25}\text{H}_{28}$  C 35.8, H 3.87%. FAB mass spectrum: found  $M^+ = 560, 504, 469$

<u>Calculated for</u>	<u><math>M^+</math></u>
$^{102}\text{Ru}^{35}\text{Cl}(\text{CO})(\text{PEtPh}_2)([\text{9}] \text{aneS4})$	559
$^{102}\text{Ru}^{35}\text{Cl}(\text{PEtPh}_2)(\text{SC}_2\text{H}_4\text{SC}_2\text{H}_4\text{S})$	503
$^{102}\text{Ru}(\text{PEtPh}_2)(\text{SC}_2\text{H}_4\text{SC}_2\text{H}_4\text{S})$	468



(8)  $[\text{RuCl}_2(\text{CS})(\text{PPh}_3)_2]_2$  (132.4mg  $8.9 \times 10^{-5}$  mmol) and  $[\text{9}] \text{aneS3}$  ( $1.78 \times 10^{-4}$  mmol) were heated under reflux in ethanol (8ml) for 4 hours to afford a yellow precipitate  $\text{RuCl}_2(\text{PPh}_3)([\text{9}] \text{aneS3})$  (Yield 32.6mg 30%) and an orange/yellow solution. On filtration and addition of excess  $\text{NH}_4\text{PF}_6$  in water to the filtrate a light orange/yellow precipitate formed. This was collected, recrystallised from a dichloromethane/diethylether solvent system and air dried. Yield 67.1mg 49% Mol.Wt. 853.1. Found C 36.2, H 3.19 Calc for  $\text{RuP}_2\text{F}_6\text{ClS}_4\text{C}_{25}\text{H}_{27}$  C 36.6, H 3.42%. I.R.  $\nu_{(\text{CS})} 1295\text{cm}^{-1}$ . FAB mass spectrum: found  $M^+ = 623$

<u>Calculated for</u>	<u><math>M^+</math></u>
$^{102}\text{Ru}^{35}\text{Cl}(\text{CS})(\text{PPh}_3)([\text{9}] \text{aneS3})$	623

[RuH(CO)(PPh<sub>3</sub>)([9]aneS3)](PF<sub>6</sub>)

(9) Ru(H)<sub>2</sub>(CO)(PPh<sub>3</sub>)<sub>3</sub> (113.0mg 1.23x10<sup>-4</sup>mmol), [9]aneS3 (1.23x10<sup>-4</sup>mmol) and excess NH<sub>4</sub>PF<sub>6</sub> were heated under reflux in degassed acetone (8ml) for 2 hours under N<sub>2</sub> to afford a colourless solution. Degassed ethanol (8ml) was then added and the solution was held at reflux for a further 2 hours. On partial removal of the solvent a white powder formed which was collected and recrystallised from a degassed dichloromethane/hexane solvent system and air dried. yield 69.8mg 79% Mol.Wt. 769.2. Found C 40.7, H 3.85 Calc. for RuOP<sub>2</sub>F<sub>6</sub>S<sub>3</sub>C<sub>25</sub>H<sub>28</sub>.½(CH<sub>2</sub>Cl<sub>2</sub>) C 40.3, H 3.85%. I.R.ν(CO) 1982, ν(Ru-H) 1910cm<sup>-1</sup>. FAB mass spectrum: found M<sup>+</sup> = 573,515

<u>Calculated for</u>	<u>M<sup>+</sup></u>
<sup>102</sup> RuH(CO)(PPh <sub>4</sub> )([9]aneS3)	573
<sup>102</sup> Ru(PPh <sub>3</sub> )(SC <sub>2</sub> H <sub>4</sub> SC <sub>2</sub> H <sub>4</sub> S)	516

Single Crystal Structure Determination of[OsH(CO)(PPh<sub>3</sub>)([9]aneS3)](PF<sub>6</sub>).½(CH<sub>2</sub>Cl<sub>2</sub>)

Crystals were obtained by the slow diffusion of Et<sub>2</sub>O into a CH<sub>2</sub>Cl<sub>2</sub> solution of the complex.

Crystal Data

(C<sub>25</sub>H<sub>28</sub>S<sub>3</sub>OPOs) (PF<sub>6</sub>).½(CH<sub>2</sub>Cl<sub>2</sub>), M = 849.29, monoclinic, a = 15.955(6), b = 21.929(9), c = 8.895(7)Å, α = 90, β = 96.69(8),

$\gamma = 90^\circ$ ,  $v = 3091.0 \text{ \AA}^{-3}$  (from setting angles for 13 reflections with  $2\theta = 14-24^\circ$ ,  $\lambda = 0.71069 \text{ \AA}$ ) space group  $P2_1/n$ ,  $Z = 4$ ,  $D_{\text{calc}} = 1.825 \text{ g cm}^{-3}$ . Colourless lath. Crystal dimensions  $1.00 \times 0.40 \times 0.12 \text{ mm}$ ,  $(\text{Mok}_\alpha) = 45.70 \text{ cm}^{-1}$ .

### Data Collection and Processing

Stoe STADI-2 two circle diffractometer,  $\text{Mo-k}_\alpha$  X-radiation,  $\omega$  scans with width  $(1.50 + 0.75(\sin \theta / \tan \theta))^\circ$ ; 5871 reflections measured, ( $2.5 \leq \theta \leq 25^\circ$ ,  $h = -18 \rightarrow 18$ ,  $k = 0 \rightarrow 26$ ,  $f = 0 \rightarrow 10$ ), giving 3760 with  $F \geq 6 \sigma(F)$ .

### Structure Analysis and Refinement

Patterson synthesis (Os) followed by iterative cycles of least squares refinement and difference Fourier synthesis revealed the positions of all non-H atoms. At isotropic convergence corrections for absorption was made using DIFABS. Full matrix least squares with H-atoms (except for the hydride which was constrained to be  $1.60 \text{ \AA}$  from the Os) and phenyl carbons in calculated positions and anisotropic thermal parameters for Os, O, S, P, F, C (carbonyl). Final R,  $R_w$  and S are 0.0527, 0.0430 and 1.161 for 210 parameters and the final  $\Delta F$  synthesis showed max. peak and min trough of 1.33 and  $-1.14 \text{ e \AA}^{-3}$ . The weighting scheme  $W = 3.7853 / (\sigma^2(F) + 0.000242F^2)$  gave satisfactory agreement analysis.

[OsH(CO)(PPh<sub>3</sub>)([9]aneS3)](PF<sub>6</sub>)

(10) Os(H)<sub>2</sub>(CO)(PPh<sub>3</sub>)<sub>3</sub> (129.5mg 1.29x10<sup>-4</sup>mmol), [9]aneS3 (1.29x10<sup>-4</sup>mmol) and excess NH<sub>4</sub>PF<sub>6</sub> were heated under reflux in degassed methoxyethanol (8ml) for 2 hours under N<sub>2</sub> to afford a pale brown solution. On partial removal of the solvent and addition of excess diethylether a light brown precipitate formed. This was collected and recrystallised from a CH<sub>3</sub>NO<sub>2</sub>/diethylether solvent system to afford a white product which was dried in vacuo. Yield 82.0mg 79% Mol.Wt. 806.8. Found C 37.0, H 3.51 Calc for OsOP<sub>2</sub>F<sub>6</sub>S<sub>3</sub>C<sub>25</sub>H<sub>28</sub> C 37.2, H 3.50%. I.R.  $\nu_{(\text{CO})}$  1967,  $\nu_{(\text{Os-H})}$  2000cm<sup>-1</sup>. FAB mass spectrum: found M<sup>+</sup> = 664,607

<u>Calculated for</u>	<u>M<sup>+</sup></u>
<sup>192</sup> OsH(CO)(PPh <sub>3</sub> )([9]aneS <sub>3</sub> )	663
<sup>192</sup> Os(PPh <sub>3</sub> )(SC <sub>2</sub> H <sub>4</sub> SC <sub>2</sub> H <sub>4</sub> S)	606

Single Crystal Structure Determination of[Os([9]aneS<sub>3</sub>)<sub>2</sub>](PF<sub>6</sub>)<sub>2</sub>·2(CH<sub>3</sub>NO<sub>2</sub>)

Crystals were obtained by the slow diffusion of Et<sub>2</sub>O into a CH<sub>3</sub>NO<sub>2</sub> solution of the complex.

Crystal Data

(C<sub>12</sub>H<sub>24</sub>S<sub>6</sub>Os)<sub>2</sub>(PF<sub>6</sub>)<sub>2</sub>·2(CH<sub>3</sub>NO<sub>2</sub>), M = 962.75, monoclinic a = 9.6621(5), b = 15.1573(8), c = 10.636Å, α = 90°, β =

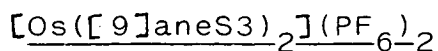
100.524(5),  $\gamma = 90^\circ$ ,  $V = 1539.1 \text{ \AA}^3$  (from setting angles for 48 reflections with  $2\Theta = 30\text{--}32^\circ$ ,  $\lambda = 0.71069 \text{ \AA}$ ), space group  $P2_{1/a}$ ,  $Z = 2$   $D_{\text{calc}} = 2.087 \text{ g cm}^{-3}$ , Colourless plates. Crystal dimensions  $0.42 \times 0.42 \times 0.12 \text{ mm}$ ,  $(\text{Mo-K}\alpha) = 47.63 \text{ cm}^{-1}$ .

### Data Collection and Processing

Stoe STADI-4 four circle diffractometer,  $\text{Mo-K}\alpha$  radiation,  $\omega$  scans with width  $(0.90 + 0.35 \tan \Theta)$ , 2118 reflections measured,  $(2.5 \leq \Theta \leq 22.5^\circ, h -10 \rightarrow 10, k 0 \rightarrow 16, l 0 \rightarrow 11)$ , giving 1715 with  $F \geq 6 \sigma(F)$ . Initial correction for absorption was by  $\psi$  scans (min 0.1042, max 0.3410 transition factors).

### Structure Analysis and Refinement

Patterson synthesis (Os) followed by iterative cycles of least squares refinement and difference. Fourier synthesis revealed the positions of all non-H atoms. At isotropic convergence correction (min 0.877, max 1.212) for absorption was made using DIFABS. Full matrix least squares with H-atoms in calculated positions and anisotropic thermal parameters for Os, S, P, F. Final R,  $R_w$  and S are 0.0401, 0.0582 and 1.221 for 191 parameters and the final F synthesis showed max. peak and min trough of 1.04 and  $-0.61 \text{ e \AA}^{-3}$ . The weighting scheme  $w^{-1} = \sigma^2 F + 0.00193 F^2$  gave satisfactory agreement analysis.



(11)  $[\text{OsCl}_2(4\text{-MeC}_6\text{H}_4^i\text{Pr})]_2$  (63.6mg  $8.0 \times 10^{-5}$  mmol) and  $[\text{9}] \text{aneS3}$  ( $1.6 \times 10^{-4}$  mmol) were refluxed in ethanol for 48 hours to yield a dark brown solution. On addition of excess  $\text{NH}_4\text{PF}_6$  in water precipitated a brown powder. This was collected and recrystallised from a minimum volume of hot water and dried in vacuo. Yield 71.5mg 53% Mol.Wt. 840.8. Found C 17.2, H 2.86  
 Calc for  $\text{OsP}_2\text{F}_{12}\text{S}_3\text{C}_{12}\text{H}_{24}$  C 17.1, H 2.88%. I.R.  $\nu_{(\text{Os-S})}$   $319\text{cm}^{-1}$ . FAB mass spectrum: found  $M^+ = 697, 551, 523$

<u>Calculated for</u>	<u><math>M^+</math></u>
$^{192}\text{Os}([\text{9}] \text{aneS3})_2(\text{PF}_6)$	695
$^{192}\text{Os}([\text{9}] \text{aneS3})_2$	550
$^{192}\text{Os}([\text{9}] \text{aneS3})(\text{SC}_2\text{H}_4\text{SC}_2\text{H}_4\text{S})$	522

Table 2.18:  $^{31}\text{P}$ -( $^1\text{H}$ ) and  $^1\text{H}$  n.m.r. Spectra of the new [9]aneS3

Complexes in  $d^6$ -acetone Unless Otherwise Stated

Complex	$^{31}\text{P}$ -( $^1\text{H}$ ) n.m.r. (p.p.m.)	$^1\text{H}$ n.m.r. (p.p.m.)
$\text{RuCl}_2(\text{PPh}_3)([9]\text{aneS3})$	22.96 (d, 2)	2.25-3.14 ([9]aneS3 - 12H); 7.38-7.69 (Ph - 15H) (d, 2)
$\text{RuCl}_2(\text{AsPh}_3)([9]\text{aneS3})$		2.28-3.12 ([9]aneS3 - 12H); 7.45-7.81 (Ph - 15H) (d, 2)
$\text{RuBr}_2(\text{PPh}_3)([9]\text{aneS3})$	22.08 (d, 2)	2.20-3.08 ([9]aneS3 - 12H); 7.29-7.74 (Ph - 15H) (d, 2)
$[\text{RuCl}(\text{PMe}_2\text{Ph})_2([9]\text{aneS3})](\text{PF}_6)$	4.84 (b, 2)	1.68-1.86 (Me - 12H); 2.18-3.16 ([9]aneS3 - 12H); 7.42-7.71 (Ph - 10H) (d, 2)
$[\text{RuCl}(\text{PEt}_2\text{Ph})_2([9]\text{aneS3})](\text{PF}_6)$	21.30 (d, 2)	0.68-1.27 (Me - 12H); 2.12-3.14 ([9]aneS3, $\text{CH}_2$ - 20H); 7.42-7.67 (Ph - 10H) (a, 2)
$[\text{RuCl}(\text{PEtPh}_2)_2([9]\text{aneS3})](\text{PF}_6)$	24.46 (d, 2)	0.42-0.78 (Me - 6H); 1.84-3.20 ([9]aneS3, $\text{CH}_2$ - 16H); 7.05-7.70 (Ph - 20H) (d, 2)
$[\text{RuBr}(\text{PEtPh}_2)_2([9]\text{aneS3})](\text{PF}_6)$	23.14 (d, 2)	0.48-0.64 (Me - 6H); 1.82-3.28([9]aneS3, $\text{CH}_2$ - 16H); 7.14-7.71 (Ph - 20H) (d, 3)
$[\text{RuCl}(\text{Py})(\text{PPh}_3)([9]\text{aneS3})](\text{BF}_4)$	34.41 (a, 1)	1.95-3.18 ([9]aneS3 - 12H); 7.20-7.90 and 8.85-9.95 (Ph, py - 20H) (a, 2)
$[\text{RuBr}(\text{Py})(\text{PPh}_3)([9]\text{aneS3})](\text{BF}_4)$	33.92 (a, 1)	1.67-3.56 ([9]aneS3 - 12H); 7.19-7.85 and 8.95 (Ph, py - 20H) (a, 3)
$[\text{RuCl}(\text{Py})(\text{AsPh}_3)([9]\text{aneS3})](\text{BF}_4)$		1.73-3.33 ([9]aneS3 - 12H); 7.23-9.00 (Ph, py - 20H) (a, 3)
$[\text{RuCl}(\text{PMe}_2\text{Ph})(\text{PPh}_3)([9]\text{aneS3})](\text{BF}_4)$	28.50 ( $\text{PPh}_3$ ), 1.99 ( $\text{PMe}_2\text{Ph}$ ) $J_{\text{pp}}^{\text{z}} = 36\text{Hz}$ (b, 2)	1.31 and 1.69 (Me - 6H, $J_{\text{HP}}^{\text{z}}=9\text{Hz}$ ); 1.80-3.20 ([9]aneS3 - 12H); 7.22-7.72 (Ph - 20H) (a, 2)

Complex	$^{31}\text{P}-\{^1\text{H}\}$ n.m.r. (p.p.m.)	$^1\text{H}$ n.m.r. (p.p.m.)
$[\text{RuBr}(\text{PMe}_2\text{Ph})(\text{PPh}_3)([\text{9}]\text{aneS3})](\text{BF}_4)$	27.76 ( $\text{PPh}_3$ ), -0.74 ( $\text{PMe}_2\text{Ph}$ ) $J_{\text{pp}}^2 = 35\text{Hz}$ (b, 2)	1.32 and 1.67 (Me - 6H, $J_{\text{HP}}^2=9\text{Hz}$ ); 1.84-3.16 ( $[\text{9}]$ aneS3 - 12H); 7.24-7.77 (Ph - 20H) (a, 2)
$[\text{RuCl}(\text{PMe}_2\text{Ph})(\text{AsPh}_3)([\text{9}]\text{aneS3})](\text{BF}_4)$	2.69 (a, 1)	1.60-3.25 ( $[\text{9}]$ aneS3, Me - 18H); 7.36-7.74 (Ph - 20H) (a, 3)
$[\text{RuCl}(\text{P}(\text{OMe})_2\text{Ph})(\text{PPh}_3)([\text{9}]\text{aneS3})](\text{BF}_4)$	32.0 ( $\text{PPh}_3$ ), 113.04 ( $\text{P}(\text{OMe})_2\text{Ph}$ ) $J_{\text{pp}}^2 = 44\text{Hz}$ (a, 1)	2.14-3.15 ( $[\text{9}]$ aneS3 - 12H); 3.23 and 3.69 (Me - 6H, $J_{\text{HP}}^2=11\text{Hz}$ ); 7.11-7.49 (Ph - 20H) (c, 3)
$[\text{RuCl}(\text{PhCN})(\text{PPh}_3)([\text{9}]\text{aneS3})](\text{BF}_4)$	32.72 (a, 1)	1.80-3.20 ( $[\text{9}]$ aneS3 - 12H); 7.34-8.00 (Ph - 20H) (a, 2)
$[\text{RuCl}(\text{MeCN})(\text{PPh}_3)([\text{9}]\text{aneS3})](\text{PF}_6)$	35.44 (c, 2)	1.59-3.10 ( $[\text{9}]$ aneS3 - 12H); 7.38-7.78 (Ph - 15H) (c, 3)
$[\text{RuCl}(\text{CO})(\text{PPh}_3)([\text{9}]\text{aneS3})](\text{PF}_6)$	30.83 (a, 1)	2.08-3.57 ( $[\text{9}]$ aneS3 - 12H); 7.38-7.81 (Ph - 15H) (e, 2)
$[\text{RuCl}(\text{CO})(\text{PEtPh}_2)([\text{9}]\text{aneS3})](\text{PF}_6)$	31.52 (d, 2)	0.78-1.32 (Me - 3H); 2.33-3.47 ( $[\text{9}]$ aneS3, $\text{CH}_2$ - 14H); 7.50-7.99 (Ph - 25H) (d, 2)
$[\text{RuCl}(\text{CS})(\text{PPh}_3)([\text{9}]\text{aneS3})](\text{PF}_6)$	32.08 (a, 1)	1.78-3.45 ( $[\text{9}]$ aneS3 - 12H); 7.34-7.98 (Ph - 15H) (a, 2)
$[\text{RuH}(\text{CO})(\text{PPh}_3)([\text{9}]\text{aneS3})](\text{PF}_6)$	48.19 (a, 1)	-9.30 (hydride $J_{\text{HP}}^2=20.9\text{Hz}$ ); 2.38-3.38 ( $[\text{9}]$ aneS3 - 12H); 7.47-7.80 (Ph - 15H) (a, 2)
$[\text{OsH}(\text{CO})(\text{PPh}_3)([\text{9}]\text{aneS3})](\text{PF}_6)$	13.19 (a, 1)	-10.20 (hydride $J_{\text{HP}}^2=18.0\text{Hz}$ ); 2.41-3.52 ( $[\text{9}]$ aneS3 - 12H); 7.48-7.78 (Ph - 15H) (a, 2)

a -  $(\text{CD}_3)_2\text{CO}$  b -  $\text{CDCl}_3$  c -  $\text{CD}_3\text{CN}$  d -  $\text{CD}_3\text{NO}_2$  e -  $\text{CH}_2\text{Cl}_2$

1 - Joel FXQ90 2 - Bruker WP80SY 3 - Bruker WP200SY



References

1. N.F. Curtis, J Chem. Soc., 1960, 4409.
2. N.F. Curtis and D A House, Chem. Ins., 1961, 42, 1708.
3. N.F. Curtis, Coord. Chem. Rev., 1968, 3, 3.
4. M.C. Thompson and D. H. Busch, Chem. Eng. News, 1962, Sept 17, 57.
5. M. C. Thompson and D. H. Busch, J. Am. Chem. Soc., 1964 86, 3651.
6. G. A. Melson and D. H. Busch, Proc. Chem. Soc., 1963, 233, 1963.
7. C. J. Pederson, J. Am. Chem. Soc., 1963, 233, 1963.
8. J. S. Bradshaw, J. Y. Hui, B. L. Haymore, J. J. Christensen and R. M. Izatt, J. Heterocyclic Chem., 1973, 10, 1 and 1974, 11, 45.
9. B. Dietrich, J-M. Lehn and J. P. Sauvage, Tetrahedron Lett., 1969, 2885 and 2889.
10. J-M. Lehn, J. Simon and J. Wagner, Nouv. J. Chem., 1977, 1, 77.
11. D. K. Cabbiness and D. W. Margerum, J. Am. Chem. Soc., 1969, 91, 6540.
12. L. Fabbrizzi, P. Paoletti and A. B. P. Lever, Inorg. Chem. 1976, 15, 1503.
13. F. P. Hinz and D. W. Margerum, Inorg. Chem., 1974, 13, 2941.
14. M. Kodama and E. Kimura, J. Chem. Soc., Dalton Trans., 1976, 116.

15. A. Anichini, L. Fabbrizzi, P. Paolette and R. M. Clay, J. Chem. Soc., Dalton Trans., 1978, 577.
16. D. K. Cabbiness and D. W. Margerum, J. Am. Chem. Soc., 1970, 92, 2151.
17. T. E. Jones, D. B. Rorabacher and L. A. Ochrymowycz, J. Am. Chem. Soc., 1975, 97, 7485.
18. D. Gerber, P. Chongsawangvirod, A. K. Leung and L. A. Ochrymowycz, J. Org. Chem., 1977, 42, 2644.
19. P. C. Ray, J. Chem. Soc., 1920, 1090.
20. W. N. Setzer, C. A. Ogle, G. S. Wilson, R. S. Glass, Inorg. Chem., 1983, 22, 266.
21. J. R. Hartman and S. R. Cooper, J. Am. Chem. Soc., 1986, 108, 1202.
22. D. Sellman and L. Zapf, Angew. Chem. Int. Ed. Engl., 1984, 23, 807.
23. P. J. Blower and S. R. Cooper, Inorg. Chem., 1987, 26, 2009.
24. J. Butler and R. M. Kellogg, J. Chem. Soc., Chem. Commun., 1980, 466.
25. J. Butler and R. M. Kellogg, J. Org. Chem., 1981, 46, 4481.
26. R. S. Glass, G. S. Wilson and W. N. Setzer, J. Am. Chem. Soc., 1980, 102, 5068.
27. W. N. Setzer, B. R. Coleman, G. S. Wilson and R. S. Glass, Tetrahedron, 1981, 37(3), 2743.
28. G. Borgen, J. Dale, F. A. L. Anet and J. Krane, J. Chem. Soc. Chem. Commun., 1974, 243.

29. L. Pauling, "The Nature of the Chemical Bond" (3rd Ed) Cornell Uni. Press. Ithaca, N. Y. 1965.
30. R. E. Desimone and M. D. Glick, J. Am. Chem. Soc., 1976, 98, 762.
31. J. A. R. Hartman, R. E. Wolf, B. M. Foxman, S. R. Cooper, J. Am. Chem. soc., 1983, 105, 131.
32. M. T. Ashby and D. L. Lichtenberger, Inorg. Chem., 1985, 24, 636.
33. D. Sellmann and L. Zapf, J. Organom. Chem., 1985, 289, 57.
34. K. Wieghardt, H-J. Kuppers and J. Weiss, Inorg. Chem., 1985, 24, 3067.
35. M. N. Bell, A. J. Blake, M. Schroder, H-J. Kuppers and K. Wieghardt, Angew. Chem. Int. Ed. Engl., 1987, 26, 250.
36. M. N. Bell, PhD Thesis, University of Edinburgh, 1987.
37. S. C. Rawle and S. R. Cooper, J. Chem. Soc., Chem. Commun. 1987, 308.
38. S. C. Rawle, T. J. Sewell and S. R. Cooper, Inorg. Chem., 1987, 26, 3769.
39. H-J. Kuppers, K. Wieghardt, B. Nuber, J. Weiss, E. Bill and A. X. Trautwein, Inorg. Chem., 1987, 26, 3762.
40. A. J. Blake, R. D. Crofts, G. Reid and M. Schroder J. Organom. Chem., 1989, 359, 371.
41. H-J. Kuppers, A. Neves, C. Pomp, D. Ventur, K. Wieghardt, B. Nuber and J. Weiss, Inorg. Chem., 1986, 25, 2400.
42. S. C. Rawle, R. Yagbasan, K. Prout and S. R. Cooper, J. Am. Chem. Soc., 1987, 109, 6181.
43. A. J. Blake, R. O. Gould, A. K. Holder, T. I. Hyde and M. Schroder, J. Chem. Soc., Dalton Trans., 1988, 1861.

44. A. J. Blake, A. J. Holder, M. Schroder, Unpublished work.
45. A. J. Blake, A. J. Holder, T. I. Hyde, Y. V. Roberts, A. J. Lavery and M. Schroder, J. Organom. Chem., 1987, 323, 261.
46. K. Wieghardt, H-J. Kuppers, E. Raabe and C. Kruger, Angew. Chem. Int. Ed. Engl., 1986, 25, 1101.
47. A. J. Blake, R. O. Gould, A. J. Holder, T. I. Hyde, A. J. Lavery, M. O. Odulate and M. Schroder, J. Chem. Soc. Chem. Commun., 1987, 118.
48. A. J. Blake, A. J. Holder, T. I. Hyde and M. Schroder, J. Chem. Soc. Chem. Commun., 1987, 987.
49. M. Schroder, Pure Appl. Chem., 1988, 60(4), 517.
50. A. J. Blake, A. J. Holder, Y. V. Roberts and M. Schroder, Acta Cryst., 1988, C44, 360.
51. H-J. Kuppers, K. Wieghardt, Y-H. Tsay, C. Kruger, B. Nuber and J. Weiss, Angew. Chem. Int. Ed. Engl., 1987, 26, 575.
52. A. J. Holder, PhD. Thesis, University of Edinburgh, 1987.
53. R. O. Gould, A. J. Lavery and M. Schroder, J. Chem. Soc., Chem. Commun., 1985, 1492.
54. J. Clarkson, R. Yagbasan, P. J. Blower, S. C. Rawle and S. R. Cooper, J. Chem. Soc. Chem. Commun., 1987, 950.
55. Y. Kojima, T. Yamashita, Y. Ishino, T. Hirashima and K. Hirotsu, Chem. Lett, 1983, 453.
56. H. W. Roesley, H. Hoffmann, P. G. Jones, W. Pinkert and G. M. Shelrdick, J. Chem. Soc., Dalton. Trans., 1983, 1215.
57. B. Noren and A. Oskarsson, Acta Chem. Scand. Ser A, 1984, 38, 479.

58. R. S. Ashworth, C. K. Prout, A. Domenicano and A. Vaciago, J. Chem. Soc. A, 1968, 93.
59. A. J. Blake, R. O. Gould, J. A. Greig, A. J. Holder, T. I. Hyde and M. Schroder, J. Chem. Soc. Chem. Commun., 1989, 877.
60. T. Blackmore, M. I. Bruce and F. G. A. Stone, J. Chem. Soc. A, 1971, 2376.
61. D. R. Robertson, T. A. Stephenson and T. Arthur, J. Organomet. Chem., 1978, 162, 121.
62. M. A. Bennett and A. K. Smith, J. Chem. Soc., Dalton Trans 1974, 233.
63. H. Werner and R. Werner, Chem. Ber., 1982, 115, 3766.
64. P. W. Armit, PhD Thesis, University of Edinburgh, 1977.
65. G. M. Sheldrick, SHELX76, Program for Crystal Structure Refinement, University of Cambridge, 1976.
66. G. M. Sheldrick, SHELX86, Program for Crystal Structure Determination, University of Gottingen, 1986.
67. R. O. Gould, P. Taylor, CALC, Interactive Molecular Geometry Program, University of Edinburgh.
68. N. Walker and D. Stuart, DIFABS, Acta. Cryst. A39, 158.
69. D. T. Cromer, J. L. Mann, Acta. Cryst., A24, 321, 1968.
70. P. D. Mallinson, K. W. Muir, ORTEP, J. Appl. Cryst., 1985, 18, 51.
71. P. W. Armit, A. Boyd and T. A. Stephenson, J. Chem. Soc., Dalton Trans., 1975, 1663.
72. J. Chatt, G. J. Leigh and D. M. P. Mingos, J. Chem. Soc., A 1969, 1674.

73. T. A. Stephenson and G. Wilkinson, J. Inorg. Nucl. Chem., 1966, 28, 945.
74. L. Ruiz-Ramirez, T. A. Stephenson and E. S. Switkes, J. Chem. Soc., Dalton Trans., 1973, 1770.
75. N. Ahmed, J. J. Levinson, S. D. Robinson and M. F. Uttley, Inorg. Synth., 15, 45.
76. T. A. Stephenson, E. S. Switkes and P. W. Armit, J. Chem. Soc., Dalton Trans., 1974, 1134.
77. B. R. James, L. D. Markham, B. C. Hui and G. L. Rempel, J. Chem. Soc., Dalton Trans., 1973, 2247.
78. J. A. Cabeza and P. M. Maillis, J. Chem. Soc., Dalton Trans., 1985, 573.

Chapter 3

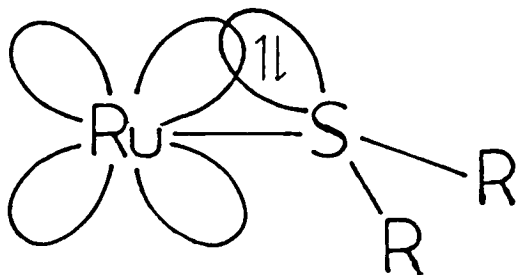
Spectroscopic and Electrochemical Studies of Complexes of

[9]aneS3

### 3.1 Introduction

To date no detailed study of the electronic structure of complexes containing [9]aneS3 has been carried out. It has previously been considered that [9]aneS3 acts only as a  $\sigma$ -donor through the lone pairs on the sulphurs' and a  $\Pi$ -acceptor via the sulphurs' accessible empty d-orbitals (1,2). This ignores the possibility of  $\Pi$ -donation from the lone-pair on the sulphurs not involved in the  $\sigma$ -bond (see Figure 3.1).

Figure 3.1: Possibility of  $\Pi S \rightarrow M$  CT Transitions in  $M(SR_2)$  Complexes via the Lone Pair not Involved in the  $\sigma$ -Bond



Although such an interaction with the metal centre is not favourable due to the constrained spacial orientation of the lone pair, it seems unlikely that such an interaction is completely precluded. Indeed  $\Pi S \rightarrow M$  charge transfer (CT) in complexes such as  $[Ru(NH_3)_5(SMe_2)]^{3+}$  have been observed, in



this case  $22100\text{cm}^{-1}$  ( $\epsilon = 300\text{cm}^{-1}\text{M}^{-1}$ ). (3) The minimal interaction is responsible for the low intensity of the CT transition.

In order to investigate the possibility of  $\pi$ -donation an electrochemical and spectroelectrochemical investigation of a number of the Ru complexes of [9]aneS3 discussed in Chapter 2 has been carried out. The inherent advantage in this study is the close relationship of one complex to another (i.e. a difference of only one ligand in many cases) thus making analysis of the absorption spectra easier.

In these systems there are four types of electronic transition to be considered:

#### 1/ d-d Transitions or Ligand-field Transitions

For centrosymmetric complexes although some transitions may be spin allowed (selection rule:  $\Delta S=0$ ), all transitions are orbitally forbidden (selection rule:  $\Delta l = 1$ ) and thus no d-d transitions should be observed. However, the orbital selection rule may be relaxed if there is no centre of symmetry, or via vibronic coupling. Spin allowed, formally orbitally forbidden absorption bands are then observed. In addition, spin and orbitally forbidden bands may also be observed due to spin-orbit coupling, especially with the heavy transition metals where the spin-orbit coupling constant is large.

Thus from theoretical considerations and the observed extinction coefficients ( $0 < \epsilon < \text{a few hundred cm}^{-1}\text{M}^{-1}$ ) assignment may be possible though it should be borne in mind that  $\epsilon$  is also dependant upon the overlap of the orbitals involved in the transition.

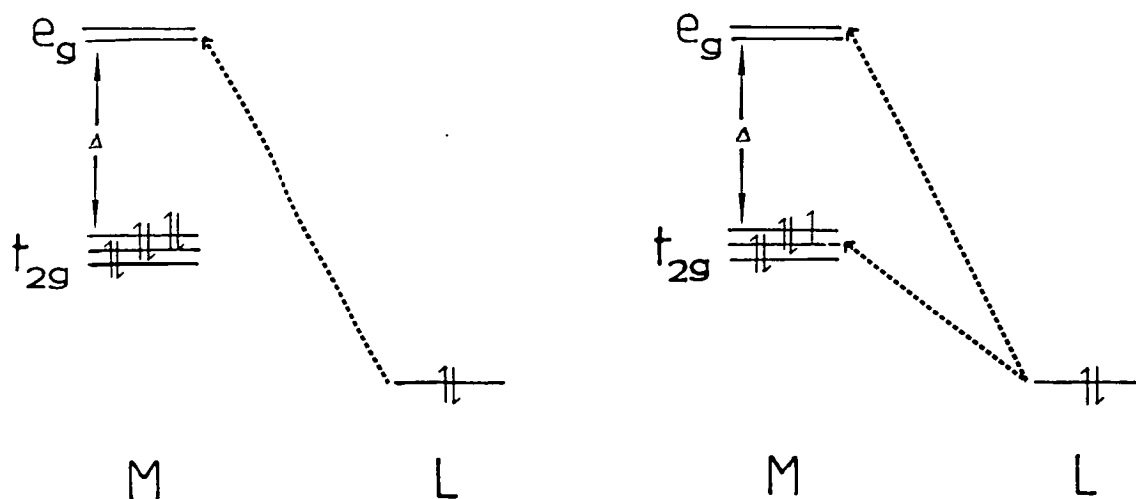
## 2/ Ligand to Metal Charge Transfer (LMCT)

These are transitions from the filled  $\pi$ -orbitals on the ligand to a vacant nd orbital of the metal. The value of  $\epsilon$  is dependant on the change in the electric dipole moment and the overlap of the orbitals involved in the transitions (for symmetry allowed transitions  $\epsilon$  has a value between  $10^2$  and  $10^4 \text{ cm}^{-1}\text{M}^{-1}$ ).

The bands observed are dependant on a number of factors which includes the  $d^n$  configuration. For instance, for low spin  $d^6$  octahedral complexes (e.g. Ru(II) complexes) the " $t_{2g}$ " set of orbitals will be full, and thus only high energy transitions to the " $e_g$ " orbitals may be observed (see Figure 3.2a). If a "hole" is now created in the " $t_{2g}$ " set (e.g. one electron oxidation of Ru(II) to Ru(III)) then both low and high energy LMCT transitions may be observed to the " $t_{2g}$ " and " $e_g$ " orbital sets respectively (see Figure 3.2b). These transitions will be separated by  $\Delta$ , which for 2nd row transition metals has a value of approximately  $20000\text{cm}^{-1}$ .

Figure 3.2:  $\pi L \rightarrow M$  CT Transitions in Low Spin  $d^6$  and  $d^5$ 

Octahedral complexes

Table 3.1: Variation of  $\pi L \rightarrow M$  CT Transition on Changing M, its Oxidation State and L

Variation of M	$\pi L \rightarrow M$ CT ( $\text{cm}^{-1}$ )	ref
$[\text{Ru}(\text{NH}_3)_5\text{Cl}]^{2+}$	30480	4
$[\text{Os}(\text{NH}_3)_5\text{Cl}]^{2+}$	37450	4
<u>Variation of Oxidation State</u>		
$t-[\text{Os}(\text{NH}_3)_4\text{Cl}_2]^+$	36900	4
$t-[\text{Os}(\text{NH}_3)_4\text{Cl}_2]^{2+}$	28010	5
<u>Variation of L<sup>-</sup></u>		
$[\text{Ru}(\text{NH}_3)_5\text{Cl}]^{2+}$	30480	4
$[\text{Ru}(\text{NH}_3)_5\text{Br}]^{2+}$	25120	4
$[\text{Ru}(\text{NH}_3)_5\text{I}]^{2+}$	18500	4

The energy of a band will also vary on altering the metal centre (increases on going from a  $4d^n$  to a  $5d^n$  centre), the oxidation state (decreases on increasing the oxidation state) and altering L (decreases on moving down a group e.g.  $Cl^- \rightarrow Br^-$ ) as exemplified by the examples given in Table 3.1.

### 3/ Metal to Ligand Charge Transfer (MLCT)

This involves transitions from the metal d-orbital manifold to low lying empty  $\pi$ -orbitals on the ligand. As with LMCT transitions the magnitude of  $\epsilon$  will depend on the change in the electric dipole moment and the degree of overlap between the orbitals involved in the transition (for symmetry allowed transitions  $\epsilon$  falls between  $10^2$  and  $10^4 \text{ cm}^{-1} \text{ M}^{-1}$ ).

For say a low spin  $d^7$  octahedral complex " $e_g$ "  $\rightarrow$  L and " $t_{2g}$ "  $\rightarrow$  L or only " $t_{2g}$ "  $\rightarrow$  L MLCT transitions may be observed depending on the relative energies of the " $e_g$ " and vacant ligand orbitals (see Figures 3.3a and b). Notice that " $e_g$ "  $\rightarrow$  L will be at low energy while " $t_{2g}$ "  $\rightarrow$  L MLCT transitions will be at high energy, the difference being approximately equal to  $\Delta$ .

The energy of the transitions will also vary on changing the metal centre (decreases on going from a  $4d^n$  to a  $5d^n$  centre) and the oxidation state of the metal (increases as the oxidation state increases) as shown in Table 3.2.

Figure 3.3:  $M \rightarrow \Pi_L$  CT Transition in a Low Spin  $d^7$  Octahedral Complex

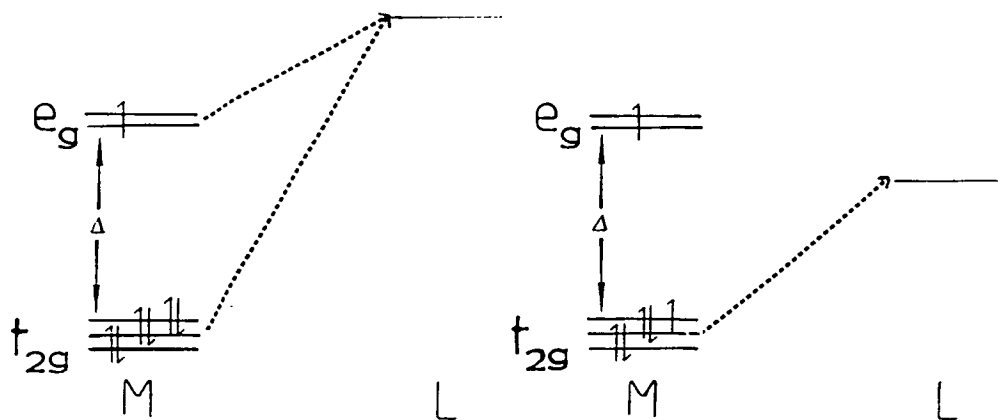


Table 3.2: Variation of  $M \rightarrow \Pi_L$  CT Transition on Changing M and its Oxidation State

<u>Variation of M</u>	$d \rightarrow \Pi_2$ ( $\text{cm}^{-1}$ )	$d \rightarrow \Pi_2$ ( $\text{cm}^{-1}$ )	<u>ref</u>
$[\text{Ru}(\text{bipy})_2(\text{en})]^{2+}$	20600	29100	6
$[\text{Os}(\text{bipy})_2(\text{en})]^{2+}$	17240	23150	7
	20790		
<u>Variation of Oxidation State</u>	$\text{Os} \rightarrow \text{Py}$ ( $\text{cm}^{-1}$ )	<u>ref</u>	
$\text{OsCl}_3(\text{Py})_3$	31600	8	
$[\text{OsCl}_3(\text{Py})_3]^-$	22000		

#### 4/ Intra-Ligand Transitions

Such transitions occur between orbitals based on the ligand itself with the magnitude of  $\epsilon$  again dependant on the change in electric dipole moment and the extent of orbital overlap.

The energy of the transition is relatively unaffected by changes in the rest of the ligation about the metal centre, even on changing the identity of the metal. It is however affected by a change in the oxidation state of the metal, and as this increases the energy of the intra-ligand transition decreases; i.e. the increase in the charge affects the energy levels of the ligand, L. For instance the lowest  $\Pi \rightarrow \Pi^*$  transition of bipy decreases from 33560<sup>(7)</sup> to 31730cm<sup>-1</sup><sup>(9)</sup> on oxidising  $(\text{Fe}(\text{bipy})_3)^{2+}$  to  $(\text{Fe}(\text{bipy})_3)^{3+}$ .

### 3.2 Results and Discussion

#### 3.2.1 UV/Vis/NIR Spectra in the (II) Oxidation State

The spectral data for the complexes studied in the (II) oxidation state is given in Table 3.3, and in the majority of cases consists of three bands in the region 10000-45450cm<sup>-1</sup>.

A typical example is  $\text{RuCl}_2(\text{PPh}_3)([9]\text{aneS3})$  where the bands are observed at 23042(830), 29657(1070) and 41530cm<sup>-1</sup> (44880cm<sup>-1</sup>M<sup>-1</sup>) as shown in Figure 3.4.

Table 3.3: Spectral Data for [9]aneS3 Complexes in the (II) Oxidation State at 238K in CH<sub>2</sub>Cl<sub>2</sub>

Complex	d - d		d - d	
	<u>E (cm<sup>-1</sup>)</u>	<u>ε (M<sup>-1</sup>cm<sup>-1</sup>)</u>	<u>E (cm<sup>-1</sup>)</u>	<u>ε (M<sup>-1</sup>cm<sup>-1</sup>)</u>
RuCl <sub>2</sub> (PPh <sub>3</sub> )([9]aneS3)	23042	830	29657	1070
RuBr <sub>2</sub> (PPh <sub>3</sub> )([9]aneS3)	22686	580	29206	680
RuCl <sub>2</sub> (AsPh <sub>3</sub> )([9]aneS3)	23787	640	28969	720
[RuCl(PEtPh <sub>2</sub> ) <sub>2</sub> ([9]aneS3)](PF <sub>6</sub> )	26767	400	31970	400
[RuBr(PEtPh <sub>2</sub> ) <sub>2</sub> ([9]aneS3)](PF <sub>6</sub> )	26124	380	31448	1190
[RuCl(PMe <sub>2</sub> Ph) <sub>2</sub> ([9]aneS3)](PF <sub>6</sub> )	27564	500	33513	1360
[RuCl(Py)(PPh <sub>3</sub> )([9]aneS3)](BF <sub>4</sub> )	25988	(650)	31889	(4200)
[RuCl(Py)(AsPh <sub>3</sub> )([9]aneS3)](BF <sub>4</sub> )	26206	(770)	31767	4370
[RuBr(Py)(PPh <sub>3</sub> )([9]aneS3)](BF <sub>4</sub> )	25537	530	31606	4170
[RuCl(PMe <sub>2</sub> Ph)(PPh <sub>3</sub> )([9]aneS3)](BF <sub>4</sub> )	26484	(330)	32510	1230
[RuCl(PMe <sub>2</sub> Ph)(AsPh <sub>3</sub> )([9]aneS3)](BF <sub>4</sub> )	27480	490	32638	1360
[RuBr(PMe <sub>2</sub> Ph)(PPh <sub>3</sub> )([9]aneS3)](BF <sub>4</sub> )	25746	390	31646	1590
[RuCl(PhCN)(PPh <sub>3</sub> )([9]aneS3)](BF <sub>4</sub> )	26568	(900)	33423	(6020)
[RuCl(P(OMe) <sub>2</sub> Ph)(PPh <sub>3</sub> )([9]aneS3)](BF <sub>4</sub> )	27965	430	34200	(1770)

( ) - shoulder

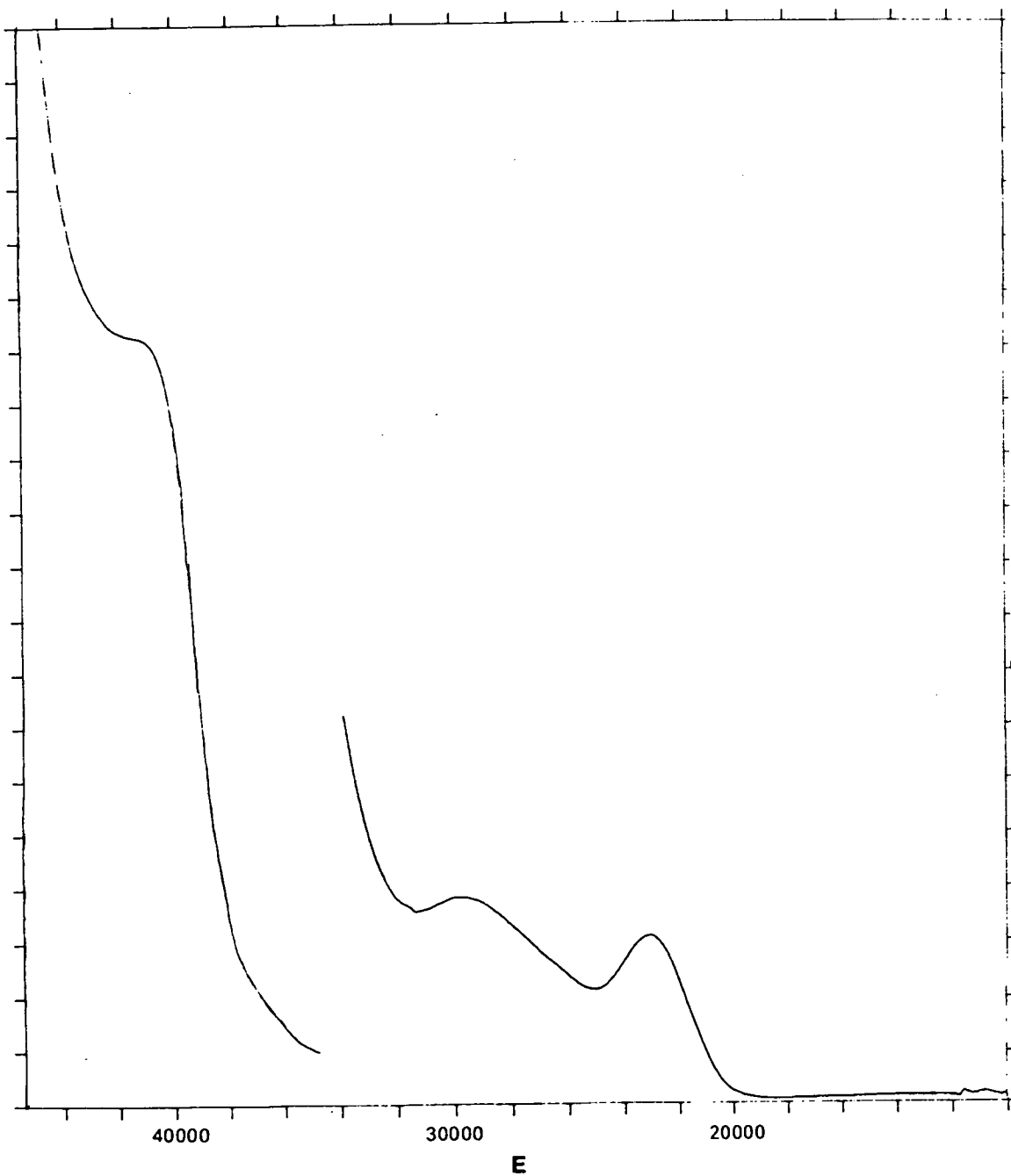
Table 3.3 (contd.)

Complex	$\pi S \rightarrow Ru$		E (cm <sup>-1</sup> )	$\epsilon$ (M <sup>-1</sup> cm <sup>-1</sup> )
	E (cm <sup>-1</sup> )	$\epsilon$ (M <sup>-1</sup> cm <sup>-1</sup> )		
RuCl <sub>2</sub> (PPh <sub>3</sub> )([9]aneS3)	41530	(44880)		
RuBr <sub>2</sub> (PPh <sub>3</sub> )([9]aneS3)	41120	(33630)		
RuCl <sub>2</sub> (AsPh <sub>3</sub> )([9]aneS3)	41737	28170		
[RuCl(PEtPh <sub>2</sub> ) <sub>2</sub> ([9]aneS3)](PF <sub>6</sub> )	40587	44360		
[RuBr(PEtPh <sub>2</sub> ) <sub>2</sub> ([9]aneS3)](PF <sub>6</sub> )	41325	46070		
[RuCl(PMe <sub>2</sub> Ph) <sub>2</sub> ([9]aneS3)](PF <sub>6</sub> )	42884	38160		
[RuCl(Py)(PPh <sub>3</sub> )([9]aneS3)](BF <sub>4</sub> )	41257	(30730)	43632	(34900)
[RuCl(Py)(AsPh <sub>3</sub> )([9]aneS3)](BF <sub>4</sub> )	41393	34720		
[RuBr(Py)(PPh <sub>3</sub> )([9]aneS3)](BF <sub>4</sub> )	40851	(27400)	42884	(34840)
[RuCl(PMe <sub>2</sub> Ph)(PPh <sub>3</sub> )([9]aneS3)](BF <sub>4</sub> )	42446	49910		
[RuCl(PMe <sub>2</sub> Ph)(AsPh <sub>3</sub> )([9]aneS3)](BF <sub>4</sub> )	42302	50240		
[RuBr(PMe <sub>2</sub> Ph)(PPh <sub>3</sub> )([9]aneS3)](BF <sub>4</sub> )	41949	51600		
[RuCl(PhCN)(PPh <sub>3</sub> )([9]aneS3)](BF <sub>4</sub> )	40717	(8200)		
[RuCl(P(OMe) <sub>2</sub> Ph)(PPh <sub>3</sub> )([9]aneS3)](BF <sub>4</sub> )	43481	39340		

( ) - shoulder



Figure 3.4: UV/Vis/NIR Spectrum of  $\text{RuCl}_2(\text{PPh}_3)([9]\text{aneS}_3)$  at 238K in  $\text{CH}_2\text{Cl}_2$



The first two transitions are assigned as d-d transitions. The reported values of the extinction coefficients,  $\epsilon$ , for these bands are much higher than expected as they are superimposed on the tail of a much more intense transition. The assignment is enforced by comparing the energies of these transitions for the bis chloride complex with a mono chloride complex such as  $[\text{RuCl}(\text{PMe}_2\text{Ph})(\text{PPh}_3)(\text{[9]aneS3})]^+$ . For the latter species the comparable bands are observed at 26484(330) and  $32510\text{cm}^{-1}$  ( $1230\text{cm}^{-1}\text{M}^{-1}$ ). This is consistent with substituting a  $\Pi$ -donor  $\text{Cl}^-$  ligand for a  $\Pi$ -acceptor  $\text{PMe}_2\text{Ph}$  ligand.

The third band varies little over the range of complexes ( $43481\text{--}40851\text{cm}^{-1}$ ) unlike the other two energy bands. Such behaviour precludes the band from being assigned as a d-d,  $\text{Ru}\rightarrow\text{L}$  CT or halide(X) $\rightarrow\text{Ru}$  CT transition. Thus the band is tentatively assigned as a  $\Pi\text{S}\rightarrow\text{Ru}^{\text{eg}}$  CT transition, though the possibility exists that this may be an intra-ligand transition within the macrocycle [9]aneS3 (no absorption is exhibited by the free ligand in the region  $10000\text{--}45450\text{cm}^{-1}$ ).

### 3.2.2 Electrochemical Experiments

Prior to any spectroelectrochemical experiments it was necessary to determine the nature of the electrochemical processes exhibited by the Ru(II) complexes. These electrochemical experiments were carried out at 238K in  $\text{CH}_2\text{Cl}_2$  using 0.5M  $(\text{TBA})(\text{BF}_4)$  as supporting electrolyte, Ag/AgCl as

the reference electrode and under an atmosphere of argon (see Appendix 1). The data from these experiments are given in Table 3.4.

Table 3.4: Electrode Potentials for some [9]aneS3 Complexes  $E_{1/2}$  (volts) at 238K in  $\text{CH}_2\text{Cl}_2$  0.5M (TBA)( $\text{BF}_4$ )

Complex	Oxidation $E_{1/2}(\text{V})$	Reduction $E_{1/2}(\text{V})$
$\text{RuCl}_2(\text{PPh}_3)([\text{9}] \text{aneS3})$	+0.86	
$\text{RuBr}_2(\text{PPh}_3)([\text{9}] \text{aneS3})$	+0.90	
$\text{RuCl}_2(\text{AsPh}_3)([\text{9}] \text{aneS3})$	+0.86	
$[\text{RuCl}(\text{PEtPh}_2)_2([\text{9}] \text{aneS3})](\text{PF}_6)$	+1.42	
$[\text{RuBr}(\text{PEtPh}_2)_2([\text{9}] \text{aneS3})](\text{PF}_6)$	+1.42	
$[\text{RuCl}(\text{PMe}_2\text{Ph})_2([\text{9}] \text{aneS3})](\text{PF}_6)$	+1.42	
$[\text{RuCl}(\text{Py})(\text{PPh}_3)([\text{9}] \text{aneS3})](\text{BF}_4)$	+1.39	
$[\text{RuCl}(\text{Py})(\text{AsPh}_3)([\text{9}] \text{aneS3})](\text{BF}_4)$	+1.39	
$[\text{RuBr}(\text{Py})(\text{PPh}_3)([\text{9}] \text{aneS3})](\text{BF}_4)$	+1.40	
$[\text{RuCl}(\text{PMe}_2\text{Ph})(\text{PPh}_3)([\text{9}] \text{aneS3})](\text{BF}_4)$	+1.45	
$[\text{RuCl}(\text{PMe}_2\text{Ph})(\text{AsPh}_3)([\text{9}] \text{aneS3})](\text{BF}_4)$	+1.45	
$[\text{RuBr}(\text{PMe}_2\text{Ph})(\text{PPh}_3)([\text{9}] \text{aneS3})](\text{BF}_4)$	+1.46	
$[\text{RuCl}(\text{PhCN})(\text{PPh}_3)([\text{9}] \text{aneS3})](\text{BF}_4)$	+1.48	
$[\text{RuCl}(\text{P}(\text{OMe})_2\text{Ph})(\text{PPh}_3)([\text{9}] \text{aneS3})](\text{BF}_4)$	+1.54	$[-1.63]^*$
$[\text{RuCl}(\text{CO})(\text{PPh}_3)([\text{9}] \text{aneS3})](\text{PF}_6)$	$[+2.05]^*$	$[-1.4]^*$
$[\text{RuCl}(\text{CS})(\text{PPh}_3)([\text{9}] \text{aneS3})](\text{PF}_6)$	$[2.06]^*$	$[-1.16]^*$

[ ] - irreversible \* -  $E_p^F$

Ag/AgCl reference electrode at which ferrocene is oxidised at 0.56V

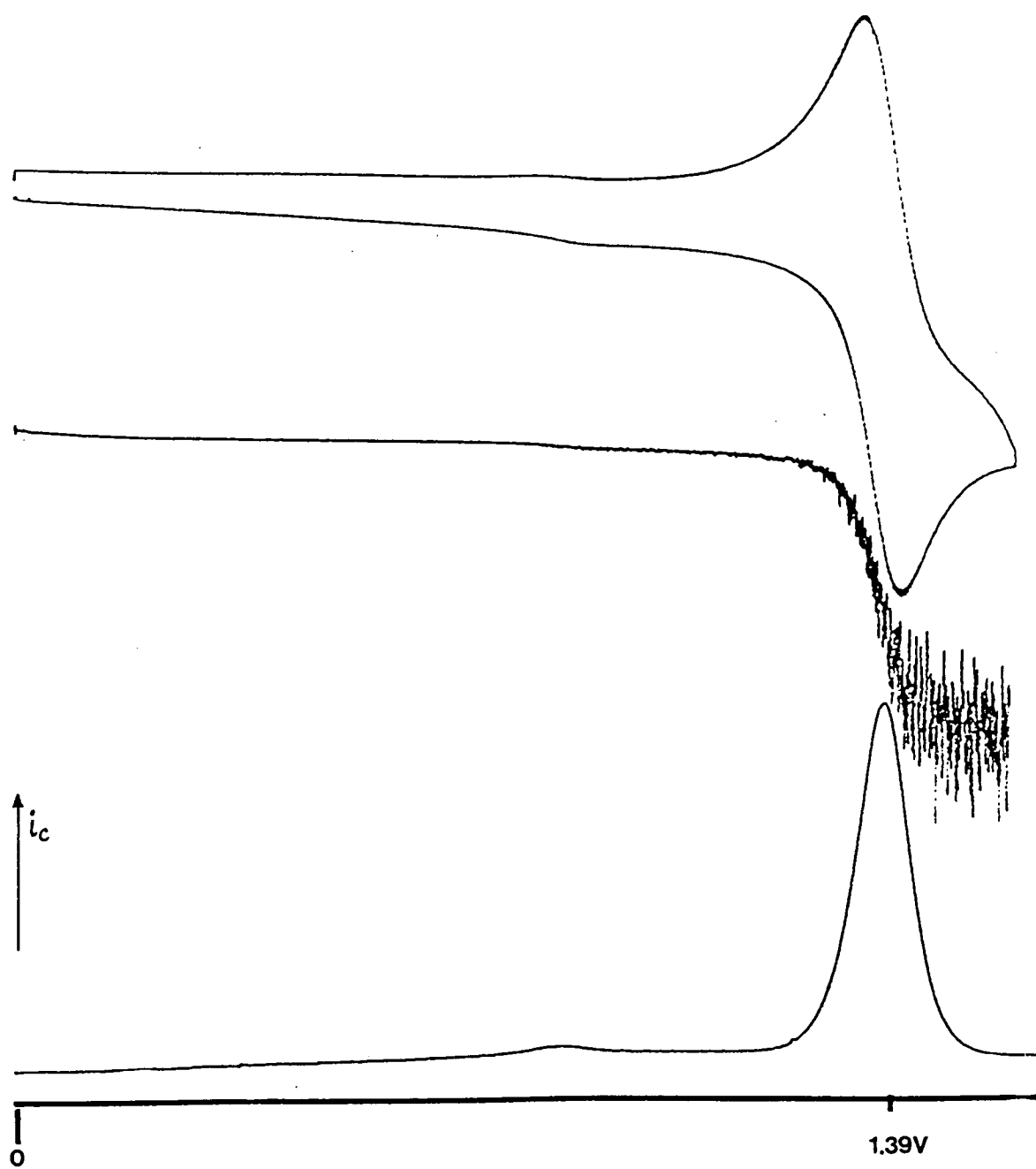
In the oxidative range the complexes, except for the CS and CO complexes, exhibit a one-electron transfer process (from coulometry) with  $i_c/i_a=1$ . A typical example of which is shown for  $[\text{RuCl}(\text{Py})(\text{PPh}_3)([\text{9}] \text{aneS3})]^+$  in Figure 3.5. The difference in anodic and cathodic peak potentials ( $\Delta E_p$ ) for these processes is 60–70mV, at a scan rate of  $100\text{mVs}^{-1}$ , which is greater than the ideal value of 48mV at 238K. It is also found that  $\Delta E_p$  increases slightly on lowering the scan rate (see Table 3.5 for a typical example). Both these observations indicate that there is some structural reorganisation about the metal centre on oxidation (under the same conditions ferrocene behaves ideally). It is thus thought these quasi-reversible processes are all metal-based Ru(II)→Ru(III) couples.

Table 3.5: Variation of  $\Delta E_p$  with Scan Rate for  $[\text{RuCl}(\text{Py})(\text{PPh}_3)([\text{9}] \text{aneS3})]^+$  at 238K in  $\text{CH}_2\text{Cl}_2/0.5\text{M}(\text{TBA})(\text{BF}_4)$

<u>Scan Rate (<math>\text{mVs}^{-1}</math>)</u>	<u><math>\Delta E_p</math> (mV)</u>
200	58
100	60
50	63

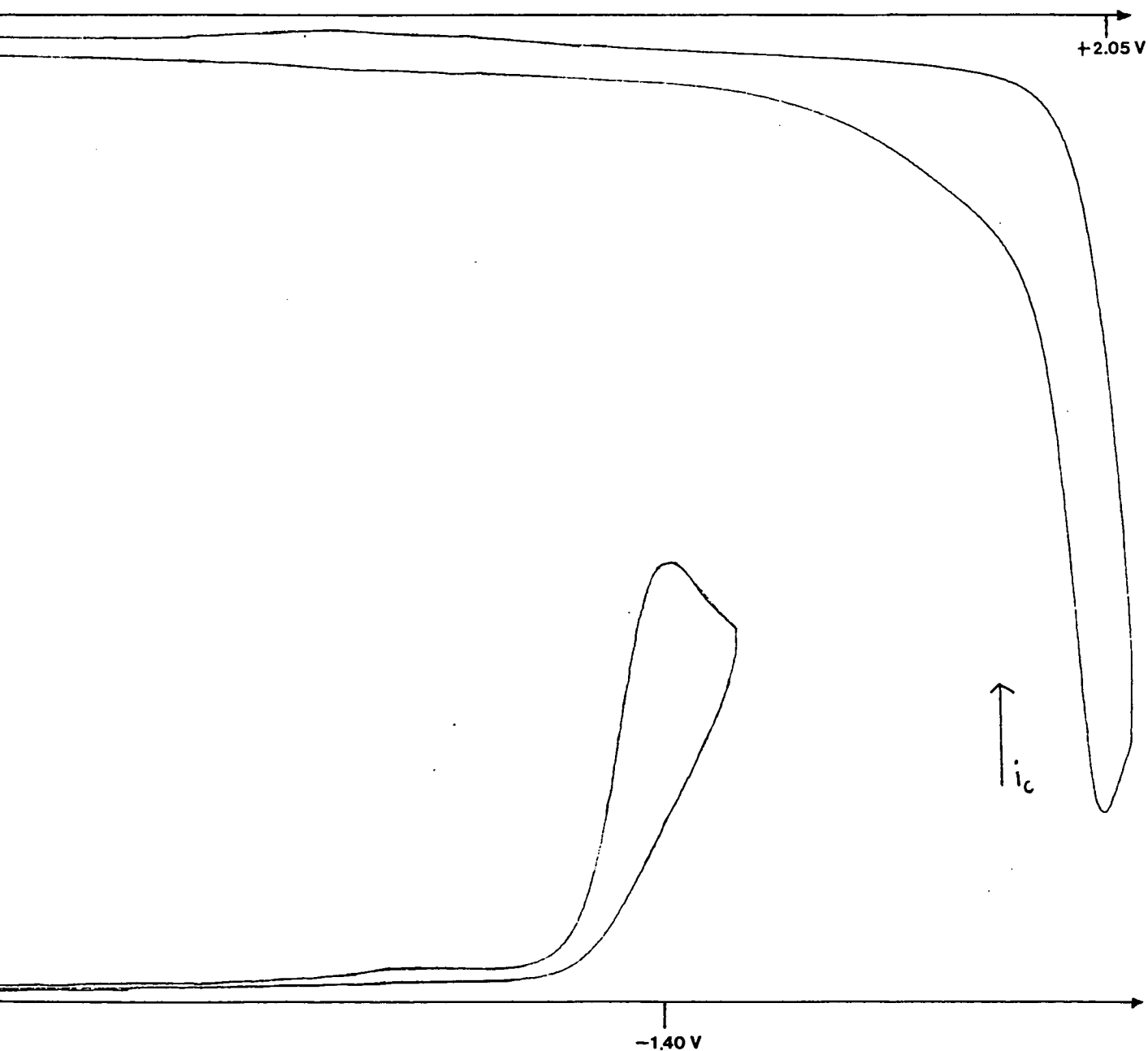
The oxidative behaviour of the CS and CO complexes differs from that discussed above. Although an oxidative process at high positive potentials ( $E_p^f$  ca +2V) is observed, it is

Figure 3.5: Electrochemical Response of  $[\text{RuCl}(\text{Py})(\text{PPh}_3)(\text{[9]aneS3})]^+$  at 238K in  $\text{CH}_2\text{Cl}_2/0.5\text{M}(\text{TBA})(\text{BF}_4)$



irreversible (see Figure 3.6) and the possibility of ligand rather than metal based oxidation cannot be ruled out.

Figure 3.6: Electrochemical Response of  $[\text{RuCl}(\text{CO})(\text{PPh}_3)(\text{9}]\text{aneS3})]^+$  at 238K in  $\text{CH}_2\text{Cl}_2/0.5\text{M}(\text{TBA})(\text{BF}_4)$



The relative values of the oxidation potentials reflects the energy of the HOMO of the complex, and thus the nature of the electronic interaction of the ligand set with the d orbitals of the Ru centre. This is exemplified by considering the series of complexes  $[\text{RuCl}(\text{L})(\text{PPh}_3)([\text{9}]\text{aneS3})]^{n+}$ , where the two extremes are +0.86V for  $\text{L}=\text{Cl}^-$  ( $n=0$ ) and ca +2V( $E_p^f$ ) for  $\text{L}=\text{CO}/\text{CS}$  ( $n=1$ ). For the chloride complex, Ru(III) is stabilised with respect to Ru(II), due to the presence of a negatively charged ligand which is also capable of donating electron density to the metal centre via its filled  $\Pi$ -orbitals. For the CO/CS complexes, Ru(II) is stabilised with respect to Ru(III) due to the metal centre donating electron density to the  $\Pi^*$  orbitals of the CO or CS ligands, thus making oxidation processes unfavourable.

In the reductive range the CO and CS complexes also exhibit an irreversible reduction,  $E_p^f$  ca -1.3V (see Figure 3.6). A similar process is also exhibited by  $[\text{RuCl}(\text{P}(\text{OMe})_2\text{Ph})(\text{PPh}_3)([\text{9}]\text{aneS3})]^+$ ,  $E_p^f$  -1.63V, on the solvent front. Presumably the other complexes will exhibit similar processes, though at potentials beyond the reduction of the solvent itself. It is not known whether this is a metal or ligand based process.

### 3.2.3 UV/Vis/NIR Spectra in the (III) Oxidation State

The electrochemical investigations discussed in section 3.2.2 indicated that a stable Ru(III) centre could be generated for

most of the complexes studied. Thus, spectroelectrochemical studies using an O.T.T.L.E. (Optically Transparent Thin Layer Electrode - see Appendix 1) cell on the Ru(II) complexes were initiated in order to probe their electronic structures further.

All the experiments were carried out at 238K in  $\text{CH}_2\text{Cl}_2$  using 0.5M (TBA)( $\text{BF}_4$ ) as supporting electrolyte. A typical experiment showing the conversion of Ru(II)  $\rightarrow$  Ru(III) is shown in Figure 3.7 where the generating potential used was approximately 0.2V more positive than that of the Ru(II)/(III) couple. In each case the (II) oxidation state was regenerated after recording the Ru(III) spectrum, by reverting the applied potential to 0V. A successful experiment was judged to have occurred if the spectrum of the parent complex could be regenerated completely.

The spectra of the complexes in the (III) oxidation state are given in Figures 3.8-3.21, while the peak positions and molar extinction coefficients,  $\epsilon$ , are given in Tables 3.6-3.10. As mentioned in the introduction, assignment of the various bands, although never easy, is helped if comparative absorption spectroscopy can be used i.e. the spectra of several closely related complexes are compared and contrasted.



Figure 3.7: Spectroelectrochemical Oxidation of  
 $[\text{RuCl}(\text{Py})(\text{AsPh}_3)([9]\text{aneS}_3)]\text{BF}_4$

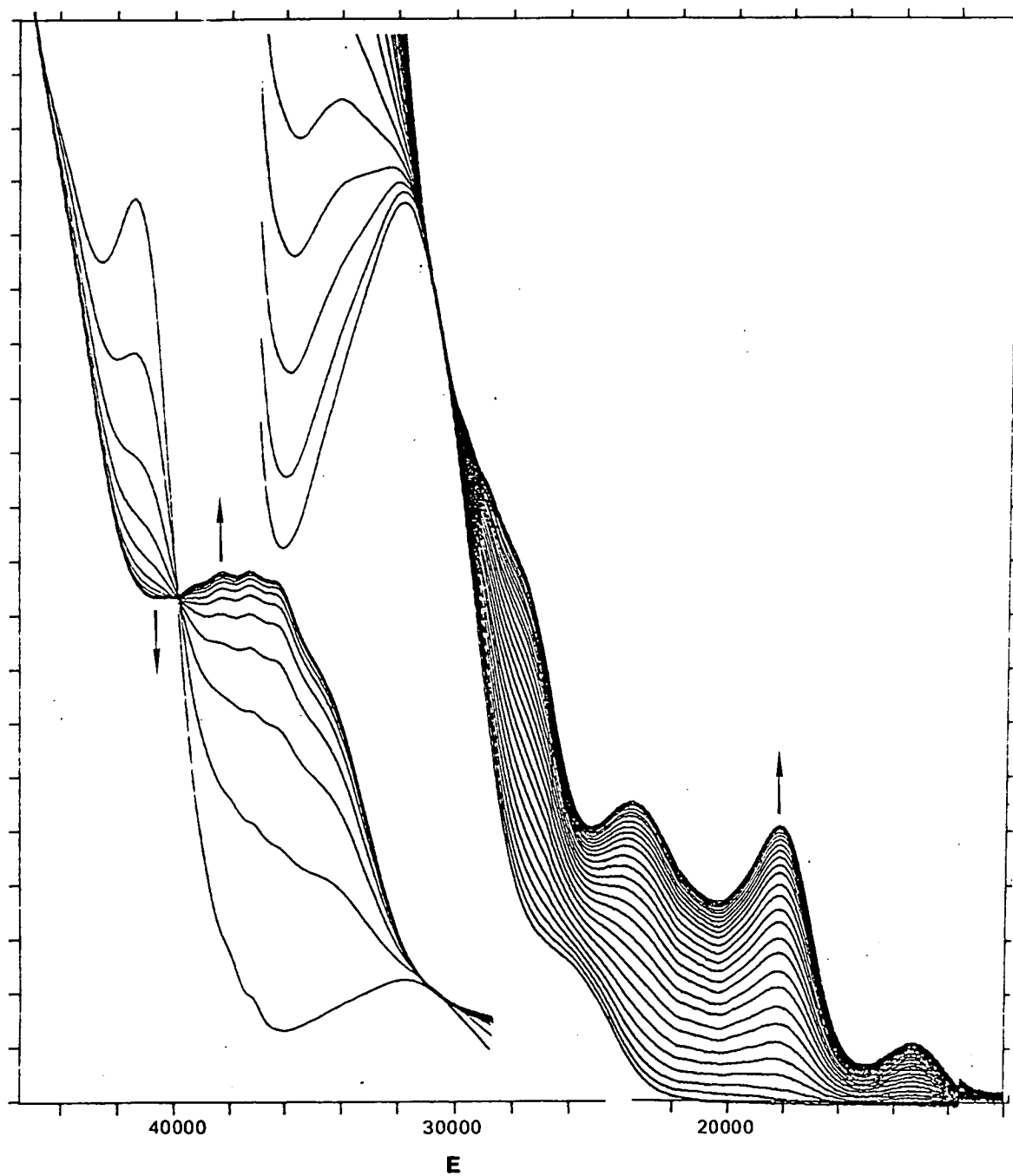


Figure 3.8: UV/Vis/NIR Spectrum of  $[\text{RuCl}_2(\text{PPh}_3)(\text{[9]aneS3})]^+$  at 238K in  $\text{CH}_2\text{Cl}_2$

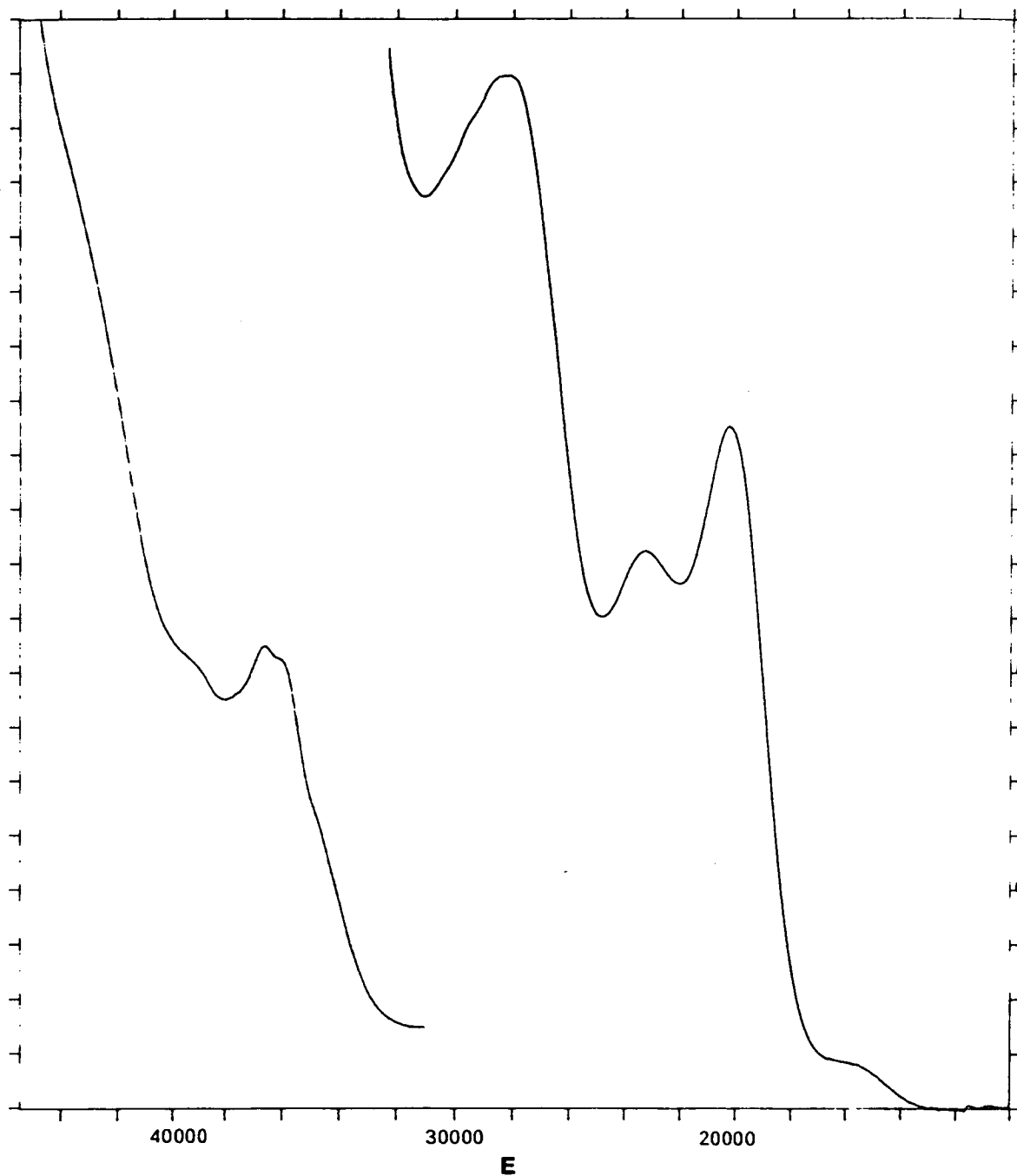


Figure 3.9: UV/Vis/NIR Spectrum of  $[\text{RuBr}_2(\text{PPh}_3)([9]\text{aneS3})^+$  at 238K in  $\text{CH}_2\text{Cl}_2$

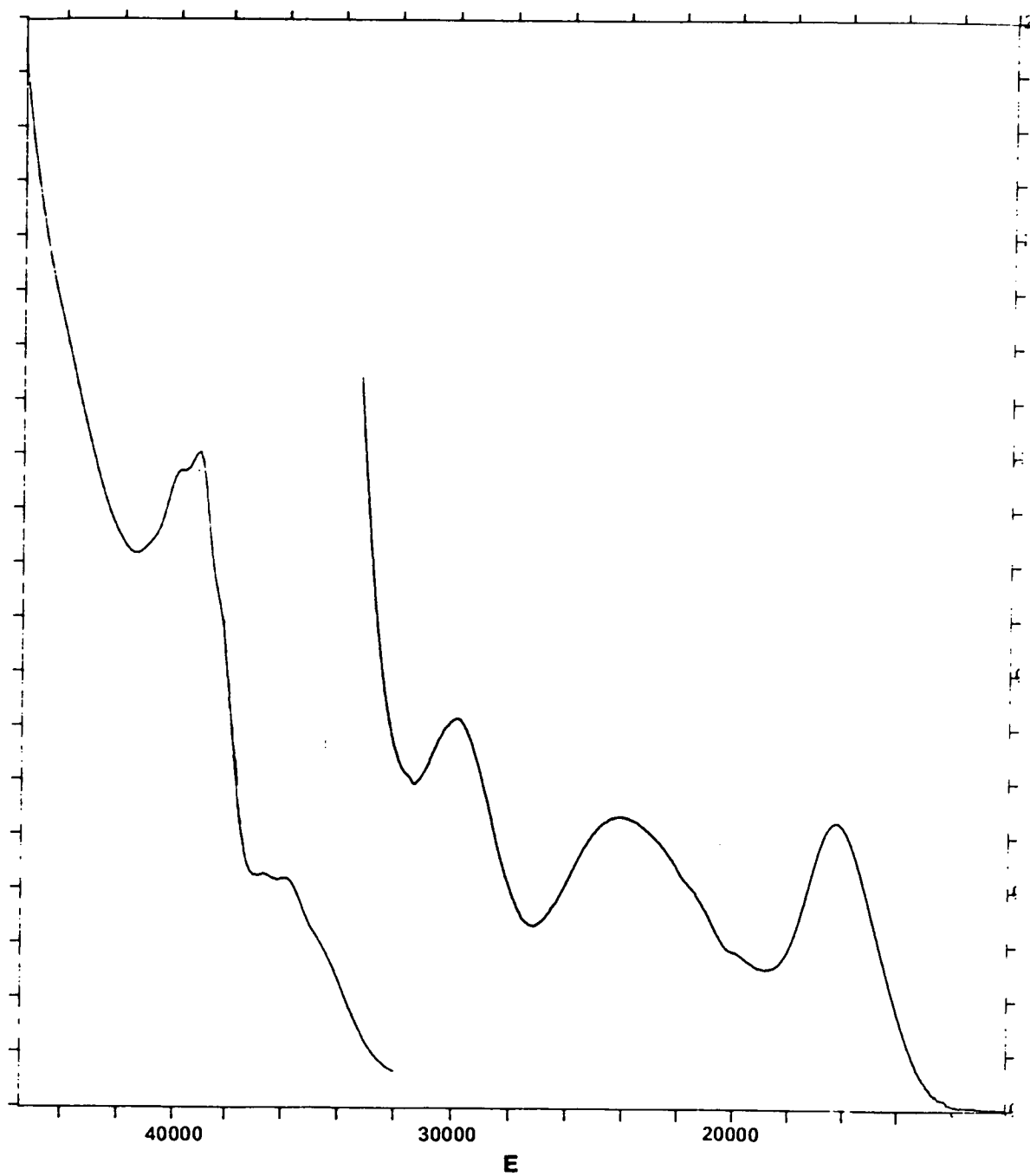


Figure 3.10: UV/Vis/NIR Spectrum of  $[\text{RuCl}_2(\text{AsPh}_3)(\text{9}]\text{aneS3}]^+$   
at 238K in  $\text{CH}_2\text{Cl}_2$

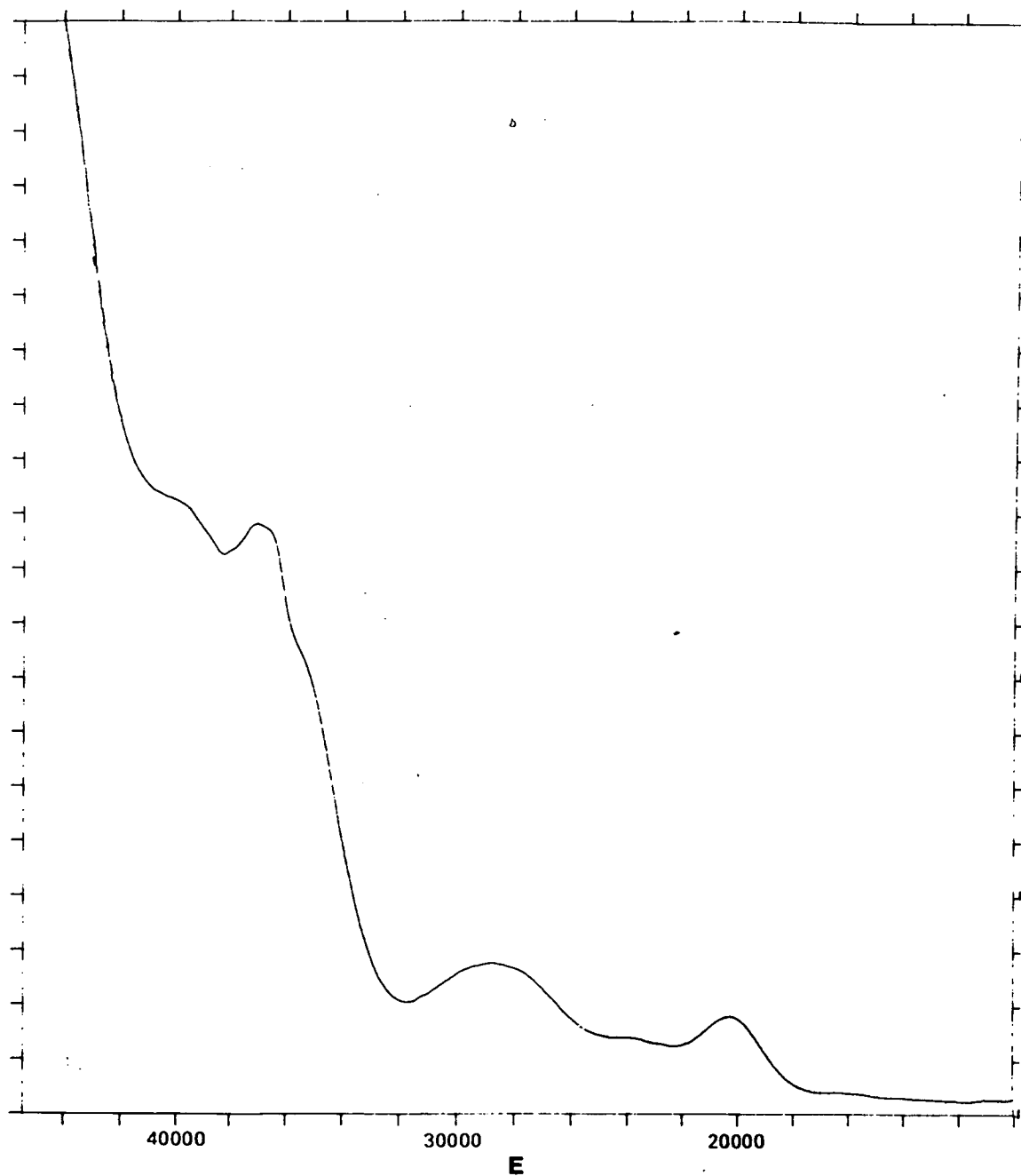


Table 3.6: Spectral Data for  $[\text{RuX}_2(\text{EPh}_3)([9]\text{aneS3})]^+$  ( $\text{X}=\text{Cl}^-$ ,  
 $\text{E}=\text{P, As}; \text{X}=\text{Br}^-$ ,  $\text{E}=\text{P}$ ) at 238K in  $\text{CH}_2\text{Cl}_2$  /0.5M (TBA)( $\text{BF}_4$ )

$\text{RuCl}_2(\text{PPh}_3)([9]\text{aneS3})$		$\text{RuCl}_2(\text{AsPh}_3)([9]\text{aneS3})$		Assignment	$\text{RuBr}_2(\text{PPh}_3)([9]\text{aneS3})$		Assignment
$\underline{\text{E}} \text{ (cm}^{-1}\text{)}$	$\underline{\epsilon} \text{ (M}^{-1}\text{cm}^{-1}\text{)}$	$\underline{\text{E}} \text{ (cm}^{-1}\text{)}$	$\underline{\epsilon} \text{ (M}^{-1}\text{cm}^{-1}\text{)}$		$\underline{\text{E}} \text{ (cm}^{-1}\text{)}$	$\underline{\epsilon} \text{ (M}^{-1}\text{cm}^{-1}\text{)}$	
16207	(240)	16255	220	$\pi\text{S} \rightarrow \text{Ru}$	16202	2200	$\pi\text{S} \rightarrow \text{Ru} / \pi\text{Br} \rightarrow \text{Ru}$
20325	3260	30314	2340	$\pi\text{Cl}^- \rightarrow \text{Ru}$	23992	2250	$\pi\text{S} \rightarrow \text{Ru} / \pi\text{Br} \rightarrow \text{Ru}$
23342	2660	24438	(1780)	$\pi\text{S} \rightarrow \text{Ru}$	29869	2990	intraligand-[9]aneS3
28217	4927	28836	3840	intraligand-[9]aneS3 / $\pi\text{Cl}^- \rightarrow \text{Ru}$	34868	(13780)	intraligand-[9]aneS3
34868	(17340)	35563	(12960)	intraligand-[9]aneS3	35971	16934	
36181	(25720)	37093	16170		36604	16577	
36658	26790				38403	(31680)	$\pi\text{Br} \rightarrow \text{Ru}$
39559	(26030)	40130	(16950)		39187	37780	
43786	(56360)				39435	(36720)	

( ) - shoulder

Figure 3.11: UV/Vis/NIR Spectrum of  $[\text{RuCl}(\text{PEtPh}_2)_2(\text{[9]aneS3})]^{2+}$  at 238K in  $\text{CH}_2\text{Cl}_2$

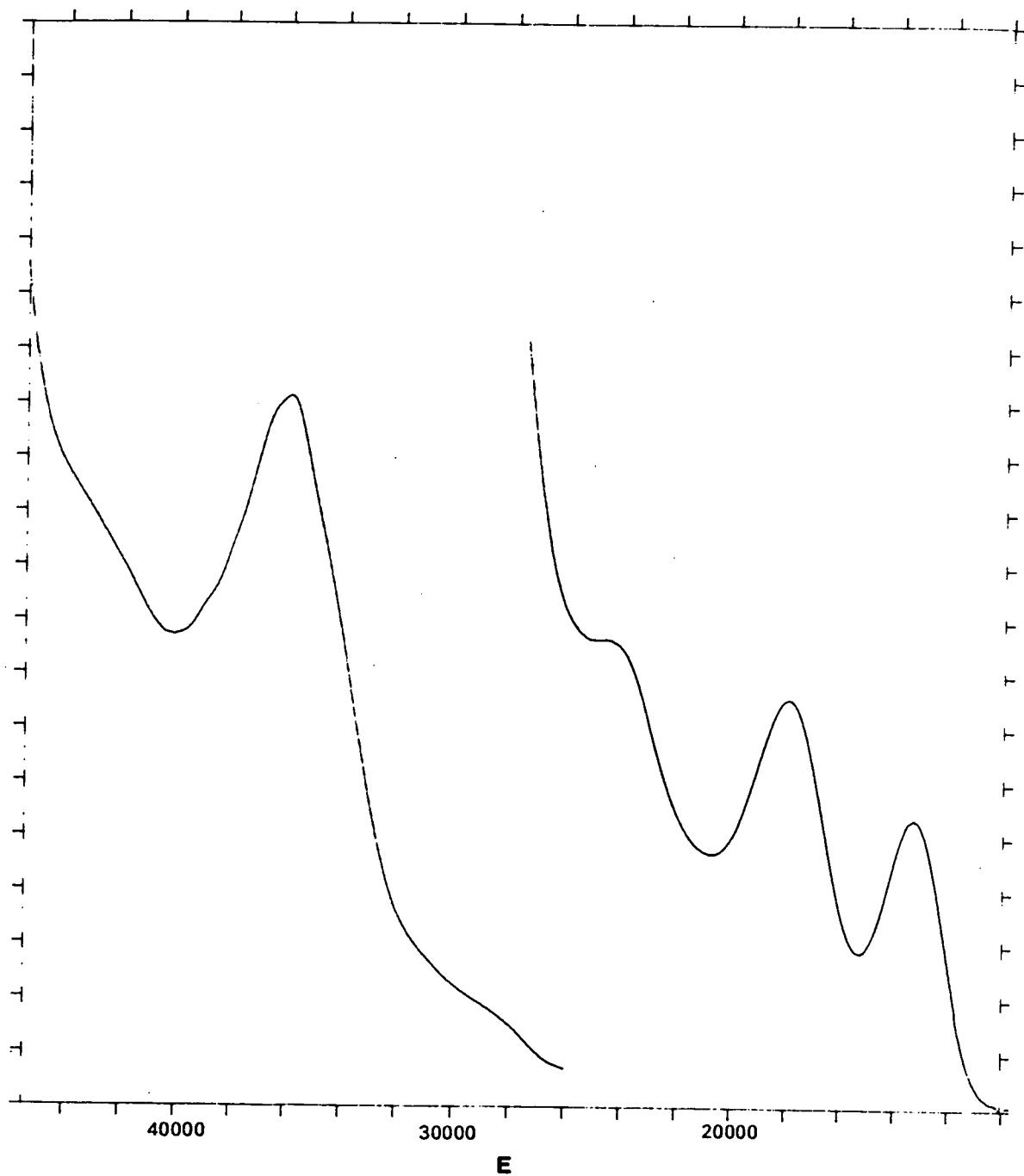


Figure 3.12: UV/Vis/NIR Spectrum of  $[\text{RuBr}(\text{PEtPh}_2)_2([\text{9}] \text{aneS3})]^{2+}$  at 238K in  $\text{CH}_2\text{Cl}_2$

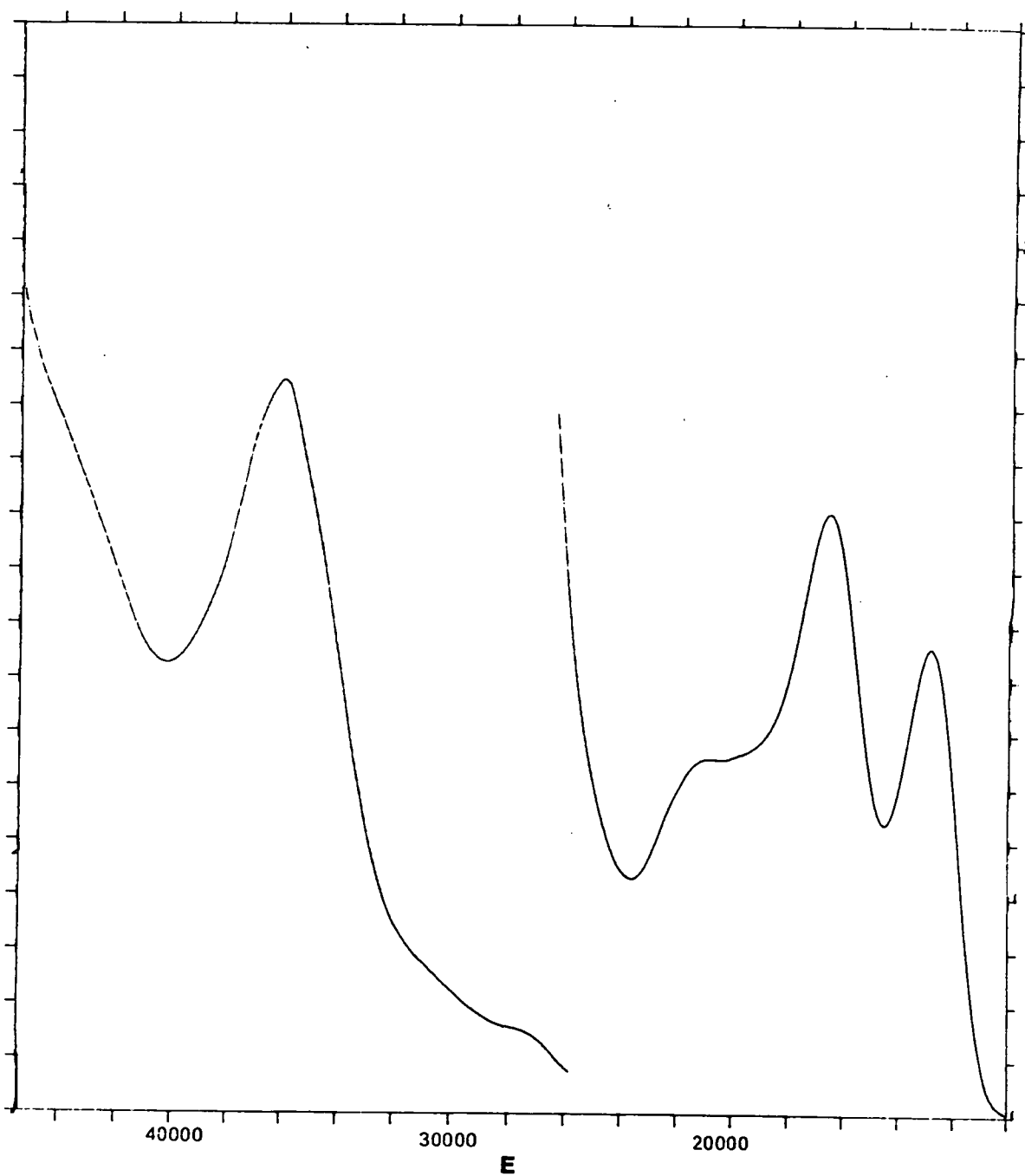


Figure 3.13: UV/Vis/NIR Spectrum of

$[\text{RuCl}(\text{PMe}_2\text{Ph}_2)_2(\text{[9]aneS3})]^{2+}$  at 238K in  $\text{CH}_2\text{Cl}_2$

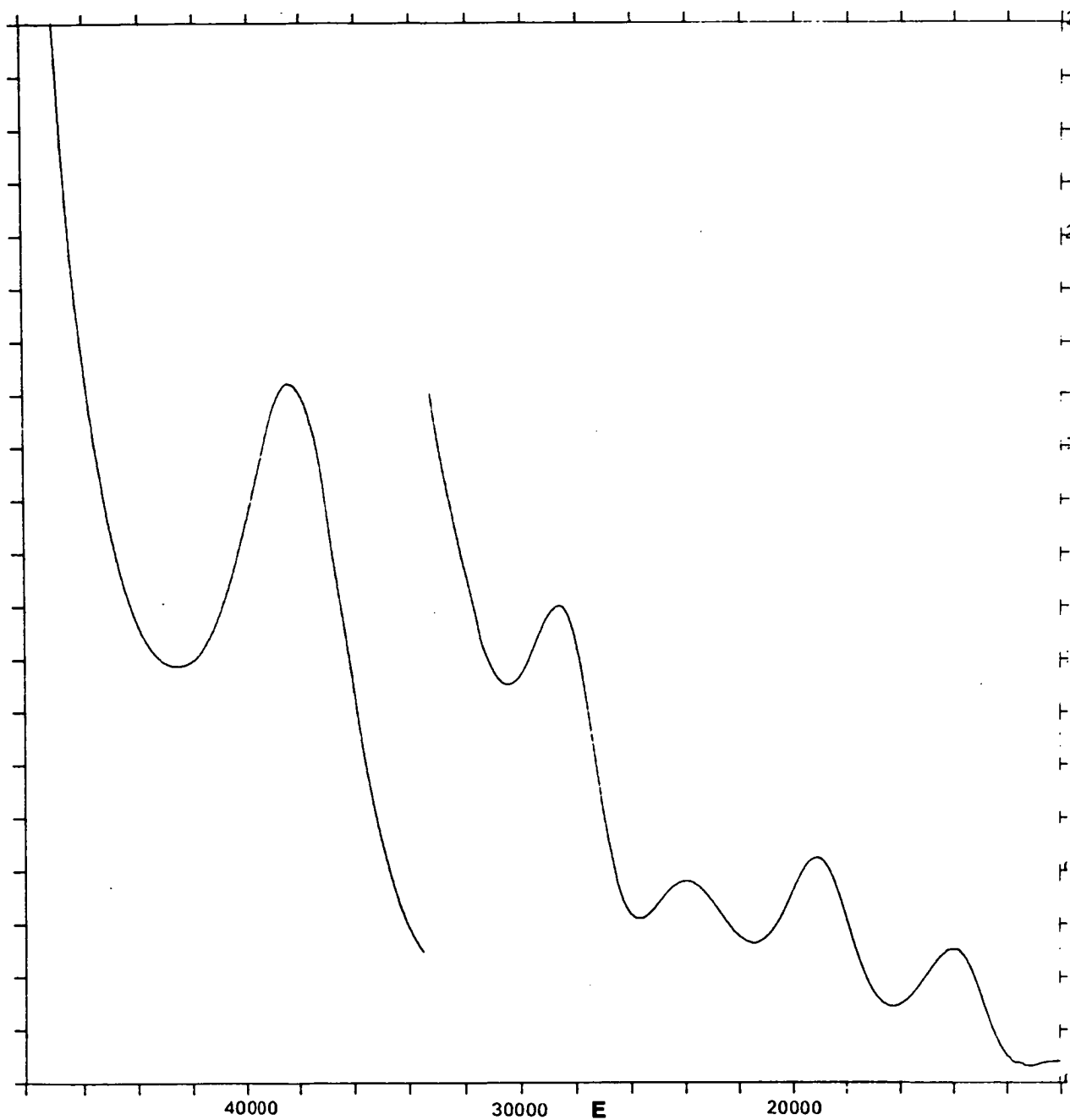




Table 3.7: Spectral Data for  $[\text{RuX}(\text{PR}_3)_2([\text{9}] \text{aneS3})]^{2+}$  ( $\text{X}=\text{Cl}^-$ ,  $\text{PR}_3=\text{PEtPh}_2$ ,  $\text{PMe}_2\text{Ph}$ ;  $\text{X}=\text{Br}^-$ ,  $\text{PR}_3=\text{PEtPh}_2$ ) at 238K in  $\text{CH}_2\text{Cl}_2/0.5\text{M}$  (TBA)( $\text{BF}_4$ )

$[\text{RuCl}(\text{PMe}_2\text{Ph})_2([\text{9}] \text{aneS3})](\text{PF}_6)$		$[\text{RuCl}(\text{PEtPh}_2)_2([\text{9}] \text{aneS3})](\text{PF}_6)$		$[\text{RuBr}(\text{PEtPh}_2)_2([\text{9}] \text{aneS3})](\text{PF}_6)$		Assignment
$E$ ( $\text{cm}^{-1}$ )	$\epsilon$ ( $\text{M}^{-1}\text{cm}^{-1}$ )	$E$ ( $\text{cm}^{-1}$ )	$\epsilon$ ( $\text{M}^{-1}\text{cm}^{-1}$ )	$E$ ( $\text{cm}^{-1}$ )	$\epsilon$ ( $\text{M}^{-1}\text{cm}^{-1}$ )	
14005	860	13144	960	12847	1530	$\pi\text{S} \rightarrow \text{Ru}$
19098	1500	17818	(1361)	16545	1930	
23901	1340	24606	(1450)	22482	(950)	$\pi\text{Cl}^-/\pi\text{Br}^- \rightarrow \text{Ru}$
28507	3270	28936	(4430)	27996	(3610)	intraligand-[9]aneS3
38403	28850	35921	30850	36024	32980	intraligand-[9]aneS3

( ) - shoulder

Figure 3.14: UV/Vis/NIR Spectrum of  
 $[\text{RuCl}(\text{Py})(\text{PPh}_3)(\text{[9]aneS3})]^{2+}$  at 238k in  $\text{CH}_2\text{Cl}_2$

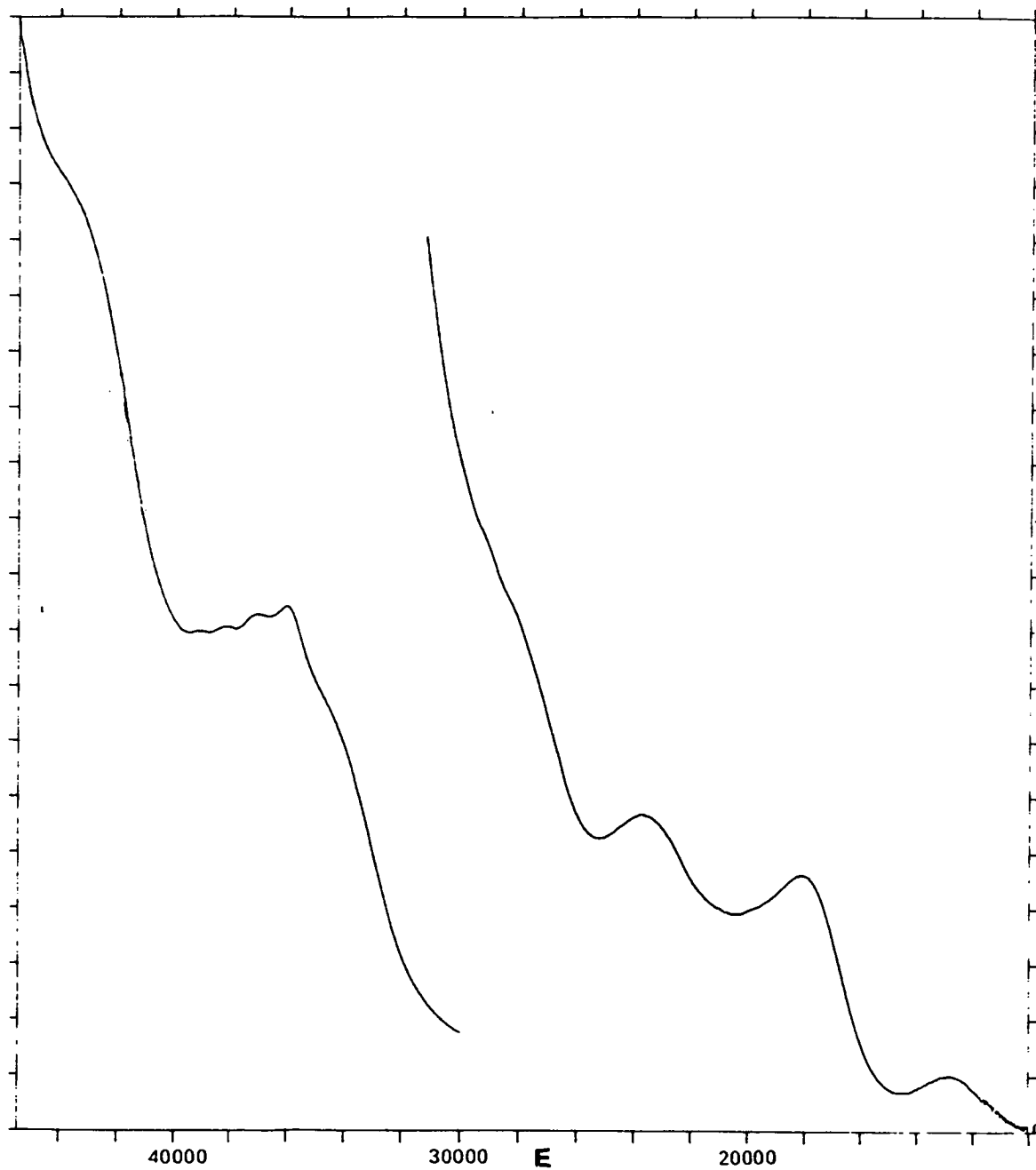


Figure 3.15: UV/Vis/NIR Spectrum of  $[\text{RuBr}(\text{Py})(\text{PPh}_3)([9]\text{aneS3})]^{2+}$  at 238K in  $\text{CH}_2\text{Cl}_2$

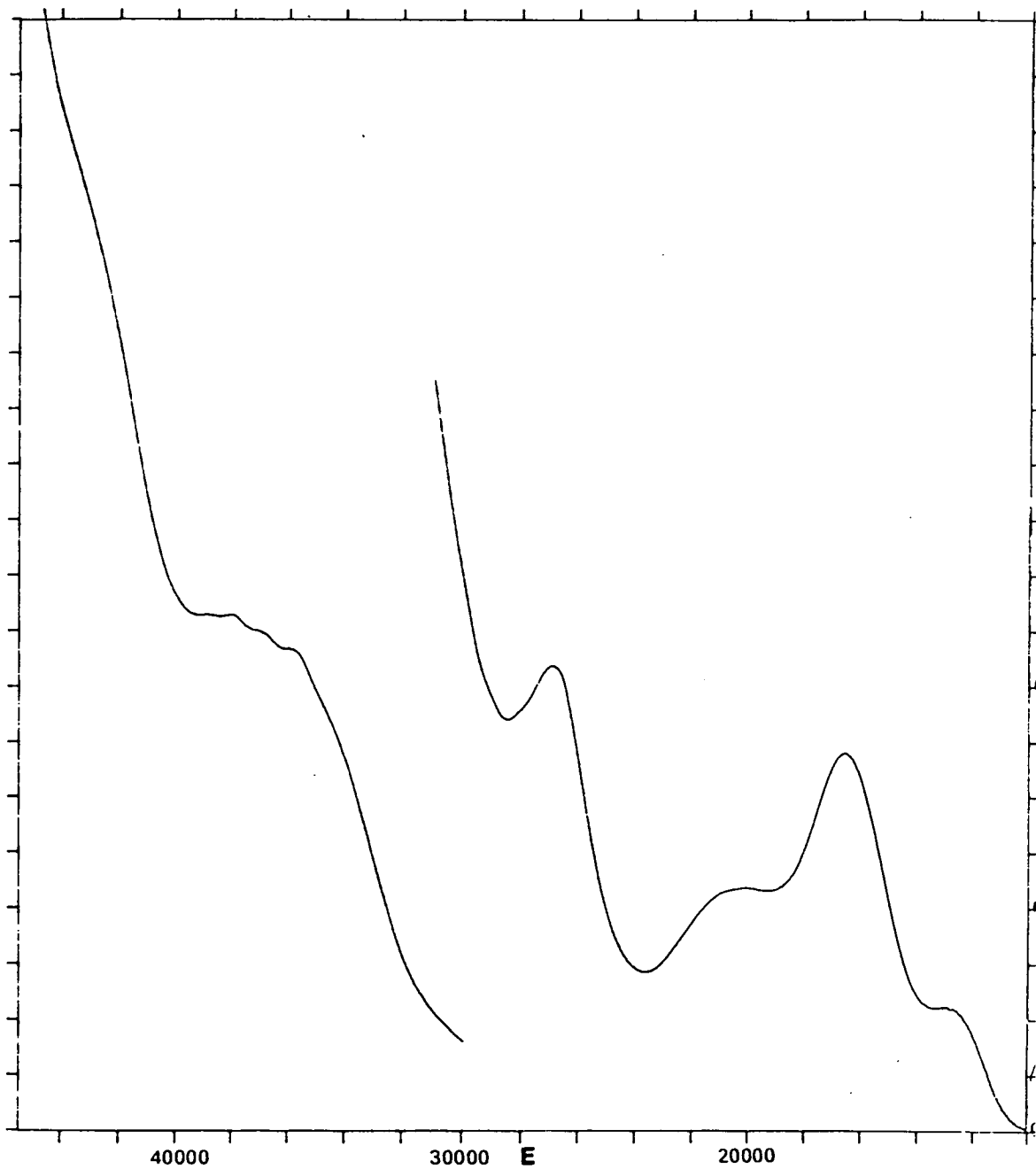


Figure 3.16: UV/Vis/NIR Spectrum of  $[\text{RuCl}(\text{Py})(\text{AsPH}_3)(\text{[9]aneS3})]^{2+}$  at 238K in  $\text{CH}_2\text{Cl}_2$

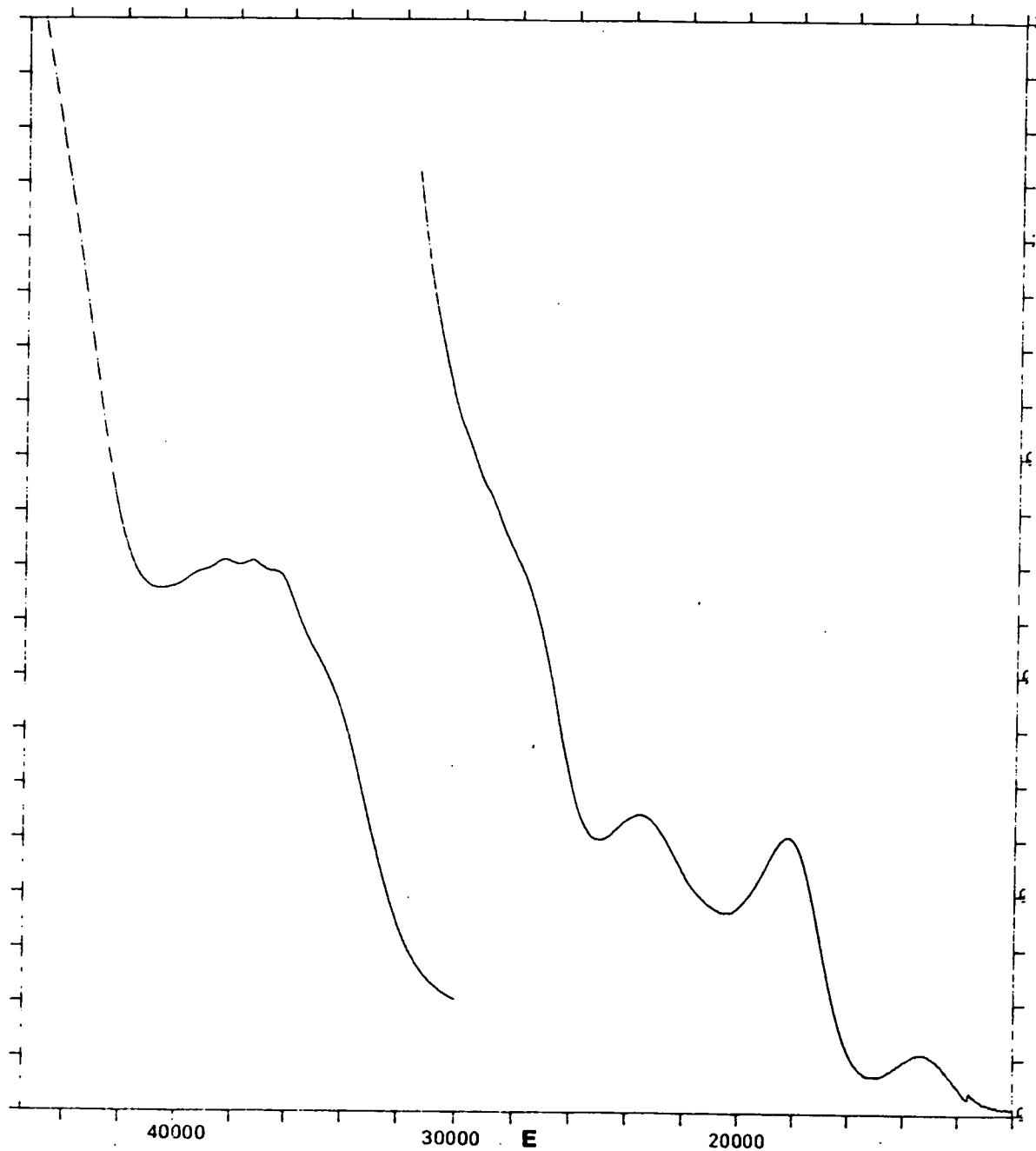


Table 3.8: Spectral Data for  $[\text{RuX}(\text{Py})(\text{EPh}_3)([\text{9}] \text{aneS3})]^{2+}$   
 ( $\text{X}=\text{Cl}^-$ ,  $\text{E}=\text{P}$ ,  $\text{As}$ ;  $\text{X}=\text{Br}^-$ ,  $\text{E}=\text{P}$ ) at 238K in  $\text{CH}_2\text{Cl}_2/0.5\text{M}(\text{TBA})(\text{BF}_4)$

$[\text{RuCl}(\text{Py})(\text{AsPh}_3)([\text{9}] \text{aneS3})](\text{BF}_4)$		$[\text{RuCl}(\text{Py})(\text{PPh}_3)([\text{9}] \text{aneS3})](\text{BF}_4)$		$[\text{RuBr}(\text{Py})(\text{PPh}_3)([\text{9}] \text{aneS3})](\text{BF}_4)$		Assignment
$\underline{\text{E}} \text{ (cm}^{-1}\text{)}$	$\underline{\epsilon} \text{ (M}^{-1}\text{cm}^{-1}\text{)}$	$\underline{\text{E}} \text{ (cm}^{-1}\text{)}$	$\underline{\epsilon} \text{ (M}^{-1}\text{cm}^{-1}\text{)}$	$\underline{\text{E}} \text{ (cm}^{-1}\text{)}$	$\underline{\epsilon} \text{ (M}^{-1}\text{cm}^{-1}\text{)}$	
13448	230	12900	235	12911	580	$\pi\text{S} \rightarrow \text{Ru}$
18208	1230	18116	1120	16567	1780	
23585	1320	23697	1380	20161	1140	$\pi\text{Cl}^-/\pi\text{Br}^- \rightarrow \text{Ru}$
		29172	(2960)	26911	2190	
35014	(17530)	34674	(15910)	34770	(14900)	intraligand-[9]aneS3
36550	(20250)	36024	19140	36076	(16760)	
37313	20600	36984	18810	37148	(17760)	
38403	20750	38170	18380	38053	18340	
39784	(19900)	39125	17980	38942	18317	
		44016	(35414)	43178	(32630)	

( ) - shoulder

Figure 3.17: UV/Vis/NIR Spectrum of

$[\text{RuCl}(\text{PMe}_2\text{Ph})(\text{PPh}_3)(\text{[9]aneS3})]^{2+}$  at 238K in  $\text{CH}_2\text{Cl}_2$

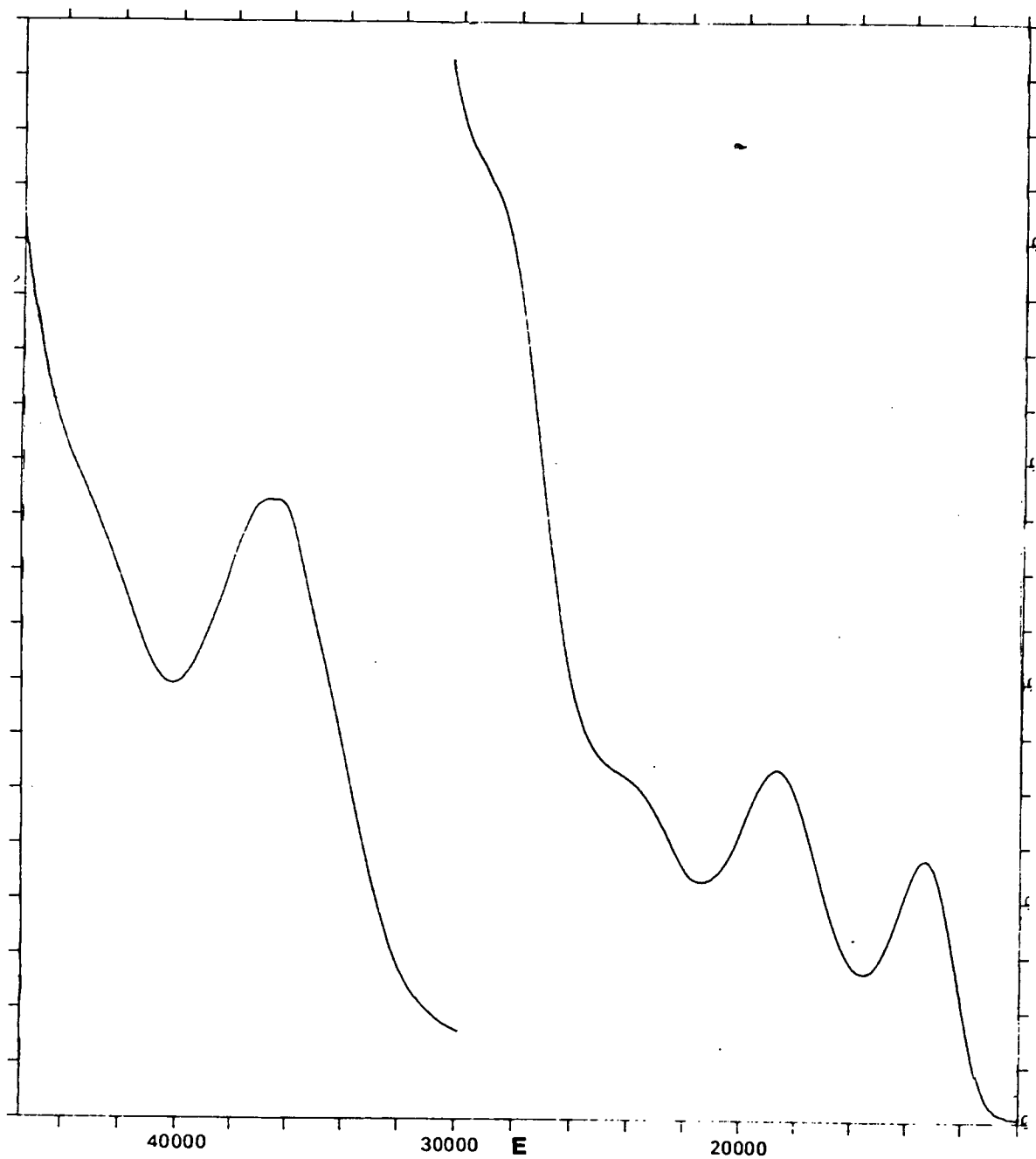


Figure 3.18: UV/Vis/NIR Spectrum of  $[\text{RuBr}(\text{PMe}_2\text{Ph})(\text{PPh}_3)([9]\text{aneS3})]^{2+}$  at 238K in  $\text{CH}_2\text{Cl}_2$

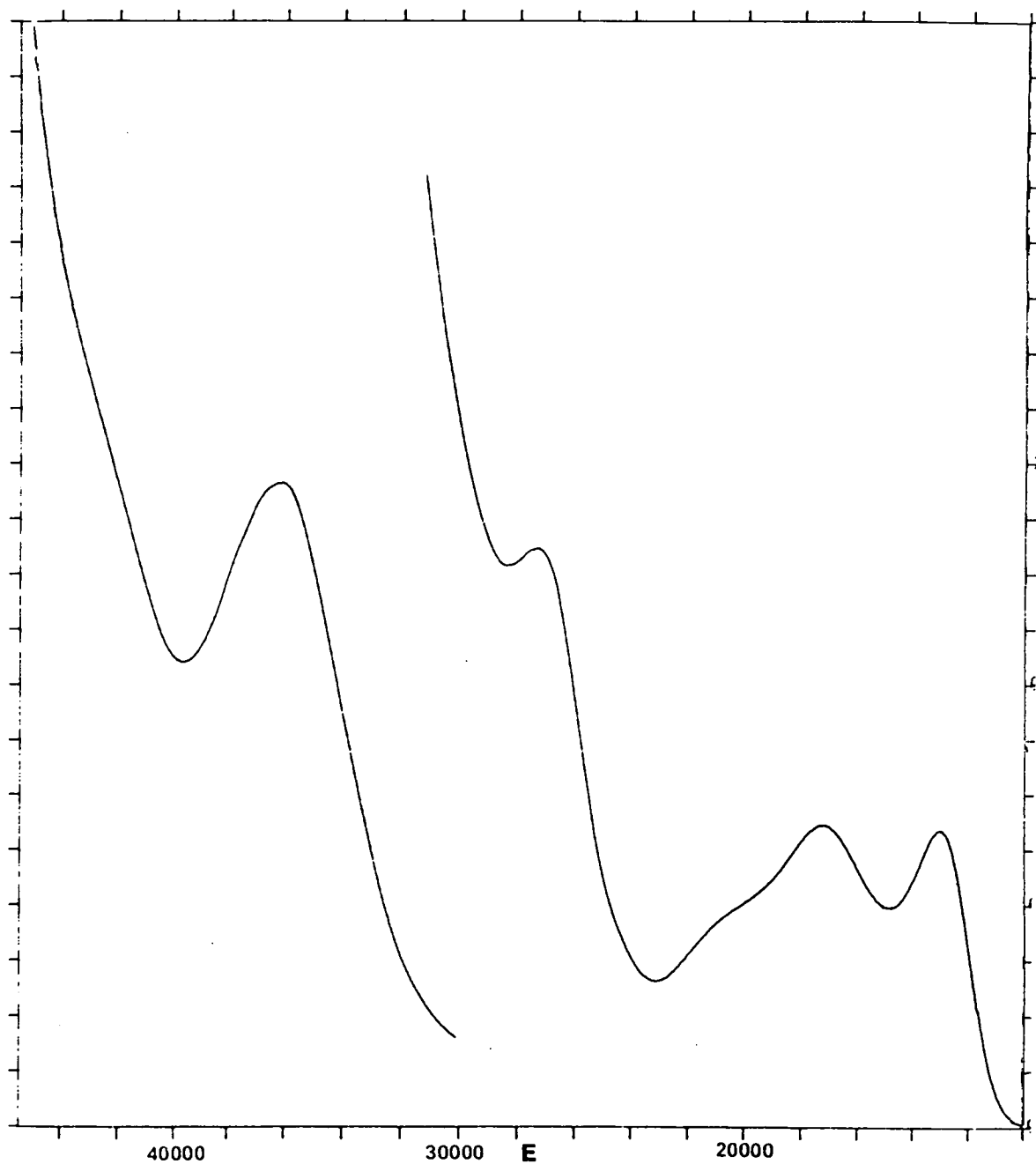


Figure 3.19: UV/Vis/NIR Spectrum of  $[\text{RuCl}(\text{PMe}_2\text{Ph})(\text{AsPh}_3)([9]\text{aneS}_3)]^{2+}$  at 238K in  $\text{CH}_2\text{Cl}_2$

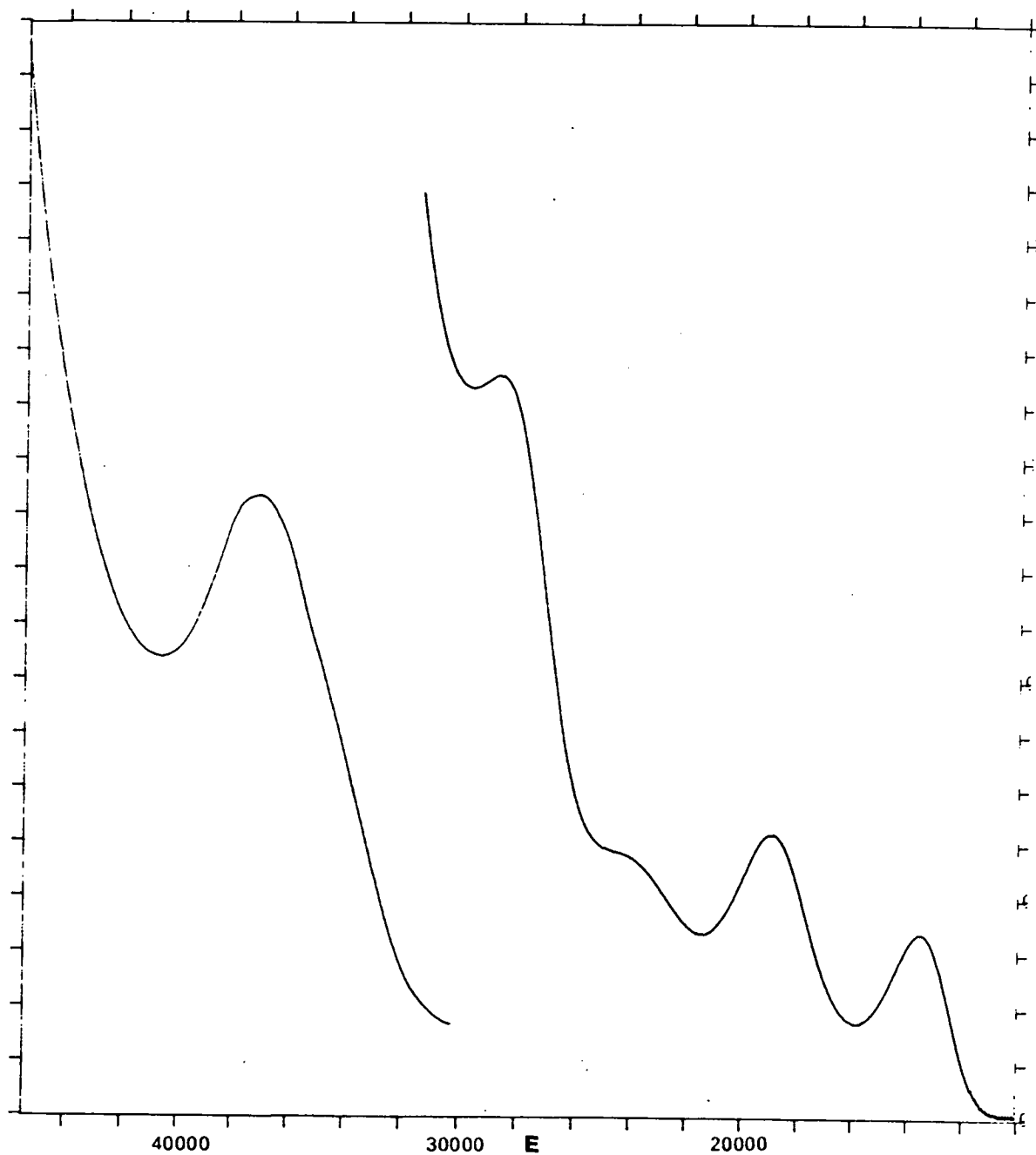




Table 3.9: Spectral Data for  $[\text{RuX}(\text{PMe}_2\text{Ph})(\text{EPh}_3)([\text{9}]\text{aneS3})]^{2+}$   
(X=Cl<sup>-</sup>, E=P, As; X=Br<sup>-</sup>, E=P) at 238K in CH<sub>2</sub>Cl<sub>2</sub>/0.5M (TBA)(BF<sub>4</sub>)

$[\text{RuCl}(\text{PMe}_2\text{Ph})(\text{AsPh}_3)([\text{9}]\text{aneS3})](\text{BF}_4)$		$[\text{RuCl}(\text{PMe}_2\text{Ph})(\text{PPh}_3)([\text{9}]\text{aneS3})](\text{BF}_4)$		$[\text{RuBr}(\text{PMe}_2\text{Ph})(\text{PPh}_3)([\text{9}]\text{aneS3})](\text{BF}_4)$		Assignment
<u>E (cm<sup>-1</sup>)</u>	<u>ε (M<sup>-1</sup>cm<sup>-1</sup>)</u>	<u>E (cm<sup>-1</sup>)</u>	<u>ε (M<sup>-1</sup>cm<sup>-1</sup>)</u>	<u>E (cm<sup>-1</sup>)</u>	<u>ε (M<sup>-1</sup>cm<sup>-1</sup>)</u>	
13448	1030	13405	870	12893	1580	πS → Ru
18896	1580	18755	1150	17205	1620	
24486	(1500)	24343	1150	20000	(1200)	πCl <sup>-</sup> /πBr <sup>-</sup> → Ru
28507	4140	29070	(3080)	27144	3100	intaligand-[9]aneS3
37148	30670	36765	28170	36232	30110	intraligand-[9]aneS3

( ) - shoulder

Figure 3.20: UV/vis/NIR Spectrum of  $[\text{RuCl}(\text{P}(\text{OMe})_2\text{Ph})(\text{PPh}_3)(\text{[9]aneS3})]^{2+}$  at 238K in  $\text{CH}_2\text{Cl}_2$

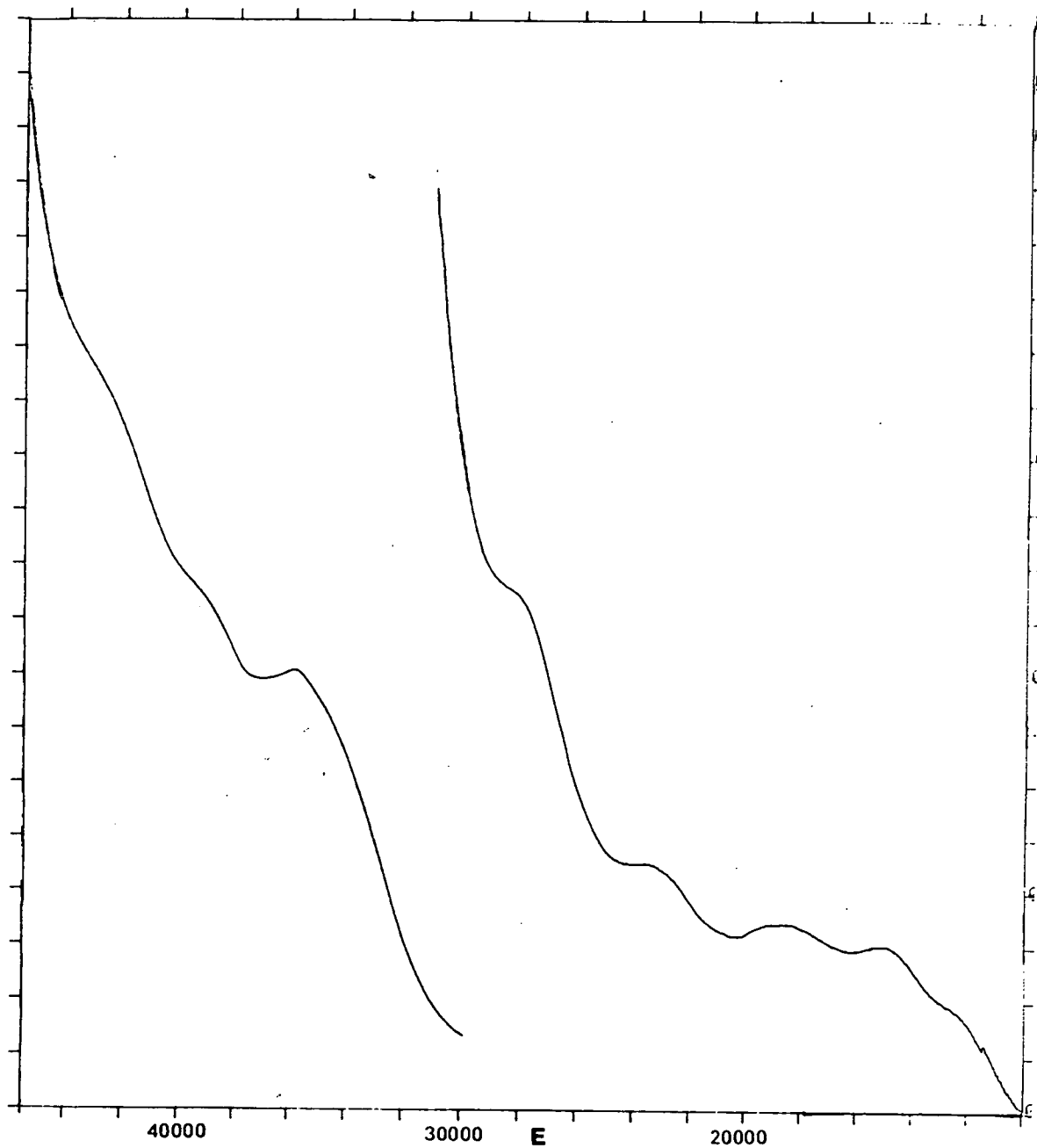


Figure 3.21: UV/Vis/NIR Spectrum of  $[\text{RuCl}(\text{PhCN})(\text{PPh}_3)(\text{[9]aneS3})]^{2+}$  at 238K in  $\text{CH}_2\text{Cl}_2$

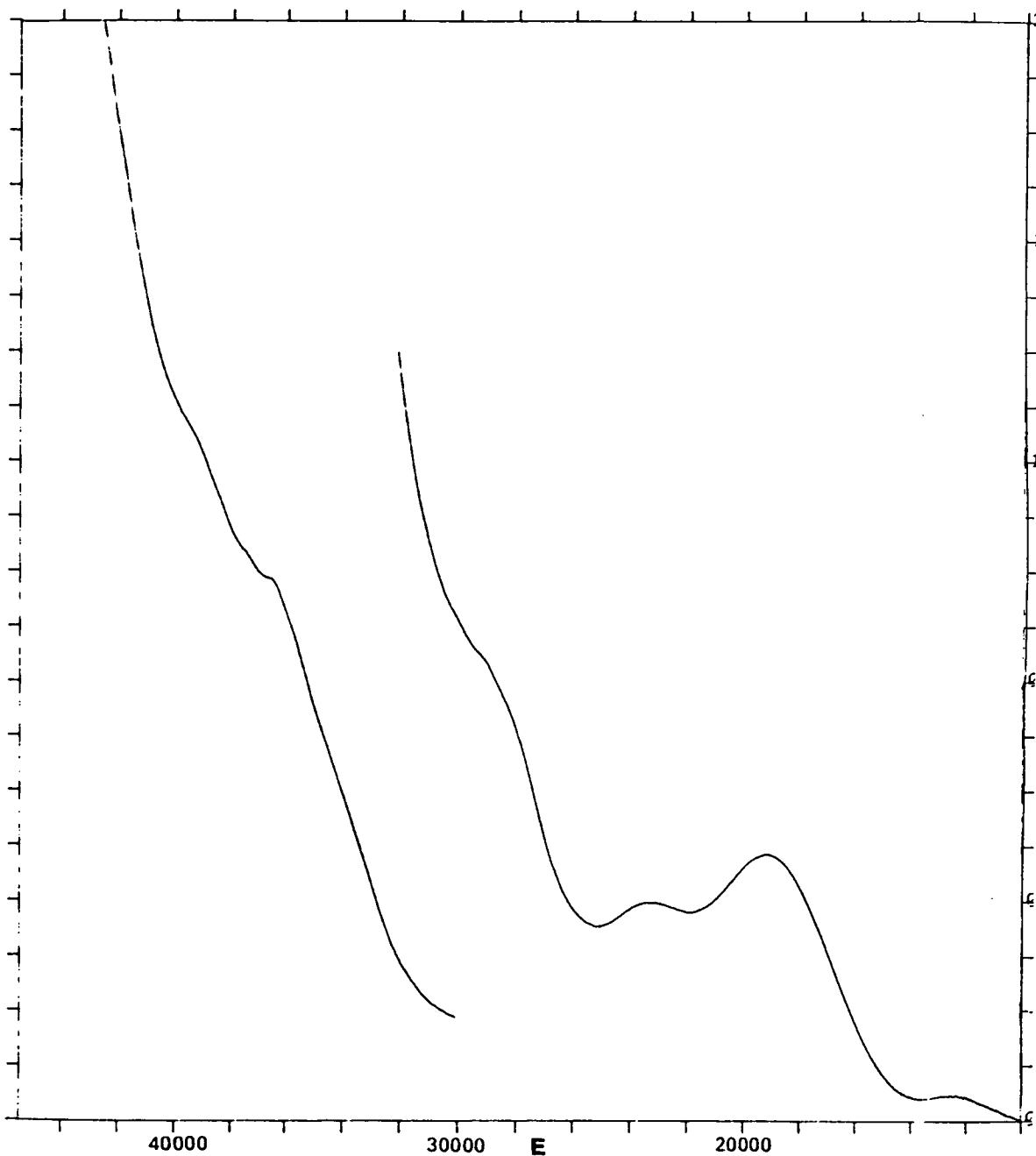
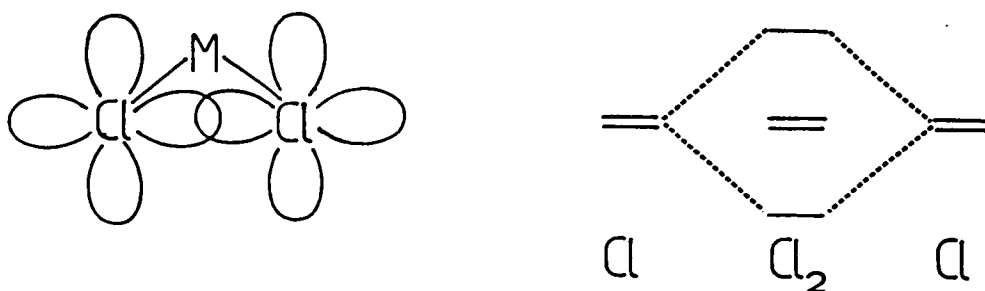


Table 3.10: Spectral Data for  $[\text{RuCl}(\text{L})(\text{PPh}_3)([\text{9}] \text{aneS3})]^{2+}$   
 (L=P(OMe)<sub>2</sub>Ph, PhCN) at 238K in CH<sub>2</sub>Cl<sub>2</sub>/0.5(TBA)(BF<sub>4</sub>)

$[\text{RuCl}(\text{PhCN})(\text{PPh}_3)([\text{9}] \text{aneS3})](\text{BF}_4)$		$[\text{RuCl}(\text{P}(\text{OMe})_2\text{Ph})(\text{PPh}_3)([\text{9}] \text{aneS3})](\text{BF}_4)$		Assignment
$\underline{E} \text{ (cm}^{-1}\text{)}$	$\underline{\epsilon} \text{ (M}^{-1}\text{cm}^{-1}\text{)}$	$\underline{E} \text{ (cm}^{-1}\text{)}$	$\underline{\epsilon} \text{ (M}^{-1}\text{cm}^{-1}\text{)}$	
12549	170	12840	(620)	$\pi\text{S} \rightarrow \text{Ru}$
19128	1770	15309	920	"
		18882	1030	"
23299	1450	23855	(1320)	$\pi\text{Cl}^- \rightarrow \text{Ru}$
29241	(3090)	28313	(2660)	intraligand-[9]aneS3
		35869	18620	intraligand-[9]aneS3
( ) - shoulder		39683	(22710)	
		43103	(31970)	

For the purposes of this study the bis-halide complexes will be considered first e.g.  $[\text{RuCl}_2(\text{PPh}_3)(\text{[9]aneS3})]^+$ . Due to the interaction of the in-plane  $\Pi$  orbitals of the cis-halides in these complexes to give a bonding and an anti-bonding orbital (see Figure 3.22) we might expect to see more than one low energy  $\text{X}^- \rightarrow \text{Ru(III)}$  CT to the vacancy in the " $t_{2g}$ " set of orbitals of the now  $d^5$  centre. In cis  $[\text{Ru}(\text{NH}_3)_4\text{Cl}_2]^+$  these transitions are observed at 28400(1640) and 32250 $\text{cm}^{-1}$  (1380 $\text{cm}^{-1}\text{M}^{-1}$ ) (4). Thus the energy difference between the two highest  $\text{Cl}^-$  transitions is approximately 4000 $\text{cm}^{-1}$ . For the bromide analogue the bands are found at 22600 (1670) and 27000 $\text{cm}^{-1}$  (1370 $\text{cm}^{-1}\text{M}^{-1}$ ) (4), i.e. the equivalent bromide to Ru(III) transitions are lower by approximately 5000 $\text{cm}^{-1}$ .

Figure 3.22: Halide  $\Pi$ -orbital Interaction in cis-dihalide Complexes



On comparison of the spectra of  $[\text{RuCl}_2(\text{PPh}_3)([9]\text{aneS}_3)]^+$  and  $[\text{RuBr}_2(\text{PPh}_3)([9]\text{aneS}_3)]^+$  in the region  $10000\text{--}30000\text{cm}^{-1}$  (see Figure 3.23) the lowest energy  $\text{X}^- \rightarrow \text{Ru(III)}$  CT transition is immediately obvious, occurring at  $20325(3260)$  and  $16202\text{cm}^{-1}$  ( $2200\text{cm}^{-1}\text{M}^{-1}$ ) for the chloride and bromide complex respectively. The difference of approximately  $4000\text{cm}^{-1}$  between the  $\text{X}^- \rightarrow \text{Ru(III)}$  transitions for the chloride and bromide complexes agrees well with that for the ammine species.

On a closer examination of the two spectra (see Figure 3.23) it is apparent that the bands centred at  $28217$  (chloride) and  $23992\text{cm}^{-1}$  (bromide) are asymmetric and hence more than one transition is occurring under the band envelope. In each case there may be a contribution from the 2nd  $\text{X}^- \rightarrow \text{Ru(III)}$  CT transition. The energy difference between the chloride and bromide transitions is again approximately  $4000\text{cm}^{-1}$  while the difference between the assigned 1st and 2nd  $\text{X}^- \rightarrow \text{Ru(III)}$  CT transition is approximately  $8000\text{cm}^{-1}$ . These figures are in acceptable agreement with those observed for the ammine complexes, considering the large differences in the ligand sets.

Figure 3.23: UV/Vis/NIR Spectra of  $[\text{RuX}_2(\text{PPh}_3)([9]\text{aneS3})]^+$   
( $\text{X}=\text{Cl}^-$ ,  $\text{Br}^-$ ) in the Region  $10000\text{--}30000\text{cm}^{-1}$

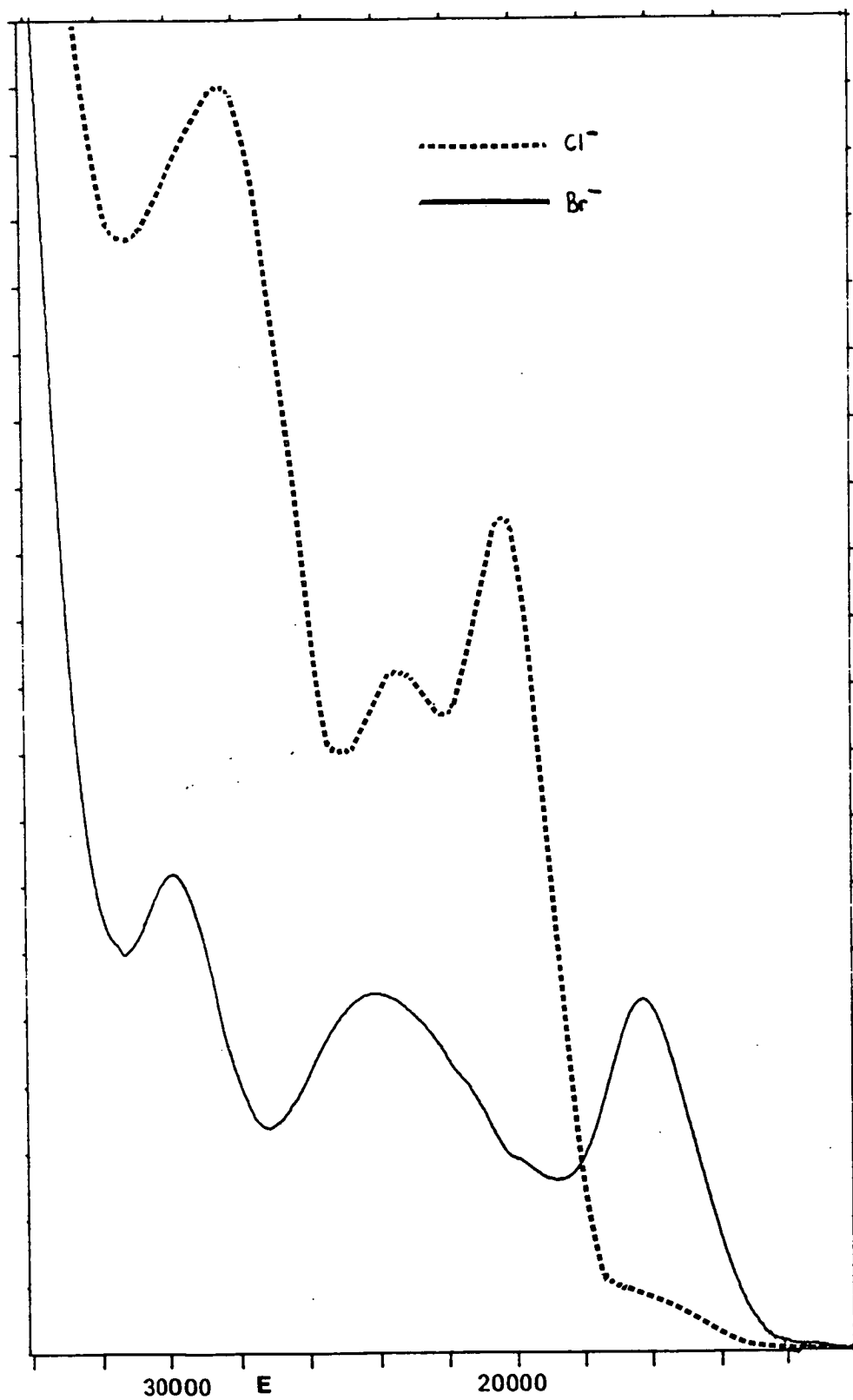
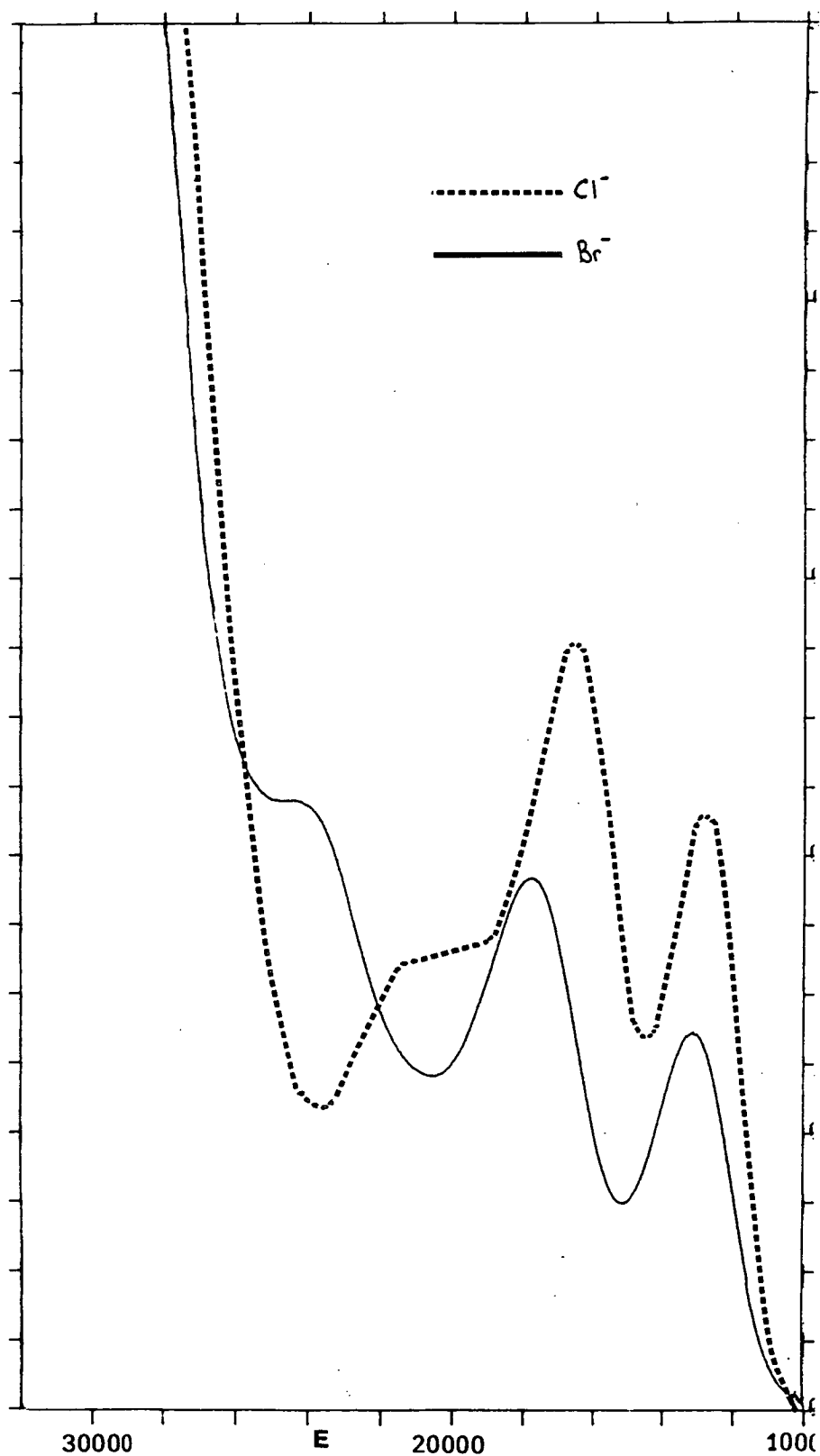


Figure 3.24: UV/Vis/NIR Spectra of  $[\text{RuX}(\text{PEtPh}_2)_2([\text{9]aneS3})]^{2+}$   
( $\text{X}=\text{Cl}^-$ ,  $\text{Br}^-$ ) in the Region  $10000\text{-}30000\text{cm}^{-1}$





For the mono-halo complexes  $[\text{RuX}(\text{NH}_3)_5]^{2+}$  ( $\text{X}^- = \text{Cl}^-, \text{Br}^-$ ), as the  $\Pi$ -orbitals are equivalent only one low energy transition is expected, and this is observed at 30500(1930) and 25100 $\text{cm}^{-1}$  (1920 $\text{cm}^{-1}\text{M}^{-1}$ ) for the chloride and bromide complexes respectively (4). These values are approximately half way between the two transitions observed for the bis-halo complexes  $[\text{RuX}_2(\text{NH}_3)_4]^+$  described previously. On comparing the spectra for  $[\text{RuX}(\text{PEtPh}_2)_2([\text{9]aneS3})]^{2+}$  ( $\text{X}^- = \text{Cl}^-, \text{Br}^-$ ; see Figure 3.24) the bands at 24606(1450) and 22482 $\text{cm}^{-1}$  (950 $\text{cm}^{-1}\text{M}^{-1}$ ) can be assigned as the  $\text{Cl}^- \rightarrow \text{Ru(III)}$  and  $\text{Br}^- \rightarrow \text{Ru(III)}$  CT transitions respectively. Although the  $\text{Cl}^- \rightarrow \text{Ru(III)}$  transition occurs at its predicted energy, as do all the other mono chloro complexes studies (i.e. approximately half way between the two transitions observed for  $[\text{RuCl}_2(\text{PPh}_3)([\text{9]aneS3})]^+$ ) the  $\text{Br}^- \rightarrow \text{Ru(III)}$  transition is at higher energy. This may be due to steric considerations as the other mono bromo complexes,  $[\text{RuBr}(\text{L})(\text{PPh}_3)([\text{9]aneS3})]^{2+}$  ( $\text{L} = \text{Py}, \text{PMe}_2\text{Ph}$ ), exhibit  $\text{Br}^- \rightarrow \text{Ru(III)}$  CT transitions at 20161 (1140) and 20000 $\text{cm}^{-1}$  (1200 $\text{cm}^{-1}\text{M}^{-1}$ ) respectively which is approximately 4000 $\text{cm}^{-1}$  lower in energy than the chloride transitions (as predicted).

The increase in energy of the lowest  $\text{X}^- \rightarrow \text{Ru(III)}$  transitions on going from bis to mono halide containing complexes is the result of the loss of the in-plane interaction of the halide  $\Pi$ -orbitals in the bis complexes coupled with the substitution of a  $\Pi$ -donor for a  $\Pi$ -acceptor. The net effect of the two factors yields the observed result.

Returning to Figure 3.23, for the chloro species  $[\text{RuCl}_2(\text{PPh}_3)([9]\text{aneS3})]$  the bands at 16207 (240) and 23342 ( $2660\text{cm}^{-1}\text{M}^{-1}$ ) must be  $\Pi_{\text{L}} \rightarrow \text{Ru(III)}$  CT transitions. The observed transitions are not d-d transitions since these increase in energy on increasing the oxidation state while  $\text{L} \rightarrow \text{Ru(III)}$  CT transitions would come at much higher energy. Only the sulphurs of the macrocycle contain a suitable orbital, namely the "non-interacting" lone pair, and thus the two transitions are assigned as  $\Pi_{\text{S}} \rightarrow \text{Ru(III)}$  CTs. Analogous transitions for the bromo complex which would be expected to occur at similar energies are obscured by the two  $\Pi_{\text{BR}^-} \rightarrow \text{Ru(III)}$  CTs which are found at similar energies.

The energy of the  $\Pi_{\text{S}} \rightarrow \text{Ru(III)}$  CTs should decrease on replacing a halide ( $\Pi$ -donor) for a phosphine ( $\Pi$ -acceptor) and this is found to be the case. Thus for the complexes  $[\text{RuX}(\text{PEtPh}_2)_2([9]\text{aneS3})]^{2+}$  ( $\text{X}^- = \text{Cl}^-, \text{Br}^-$  - see Figure 3.24) the  $\Pi_{\text{S}} \rightarrow \text{Ru(III)}$  transitions are observed at 13144 (960) and 17818 (1361) for the chloride and at 12847 (1530) and  $16545\text{cm}^{-1}$  ( $1930\text{cm}^{-1}\text{M}^{-1}$ ) for the bromide complex.

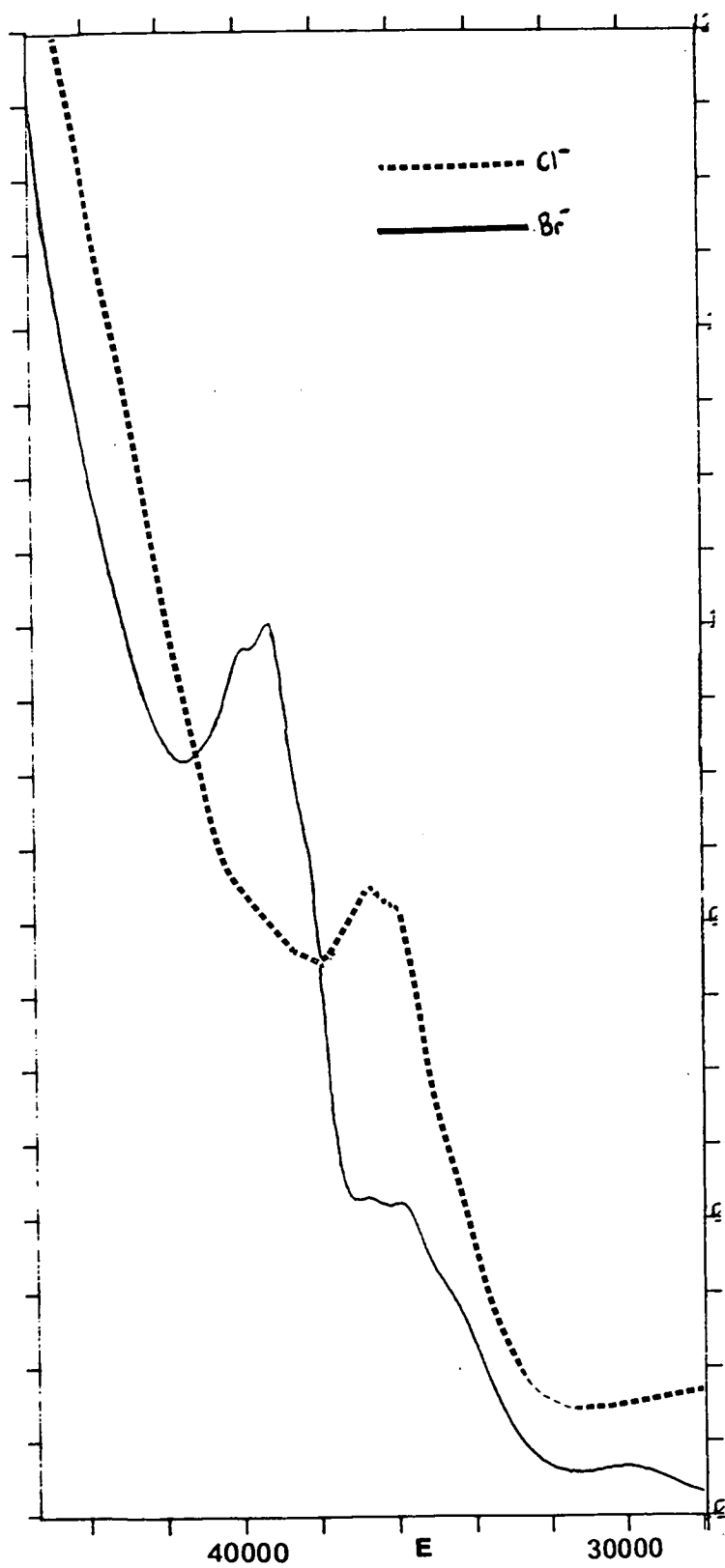
For the mono halo complexes two  $\Pi_{\text{S}} \rightarrow \text{Ru(III)}$  transitions are observed ( $12549\text{--}14005$  and  $16545\text{--}19098\text{cm}^{-1}$ ) except for  $[\text{RuCl}(\text{P}(\text{OMe})_2\text{Ph})(\text{PPh}_3)([9]\text{aneS3})]^{2+}$  where a third is observed at  $15309\text{cm}^{-1}$ . This at first seems surprising; however, these transitions will depend on the electronic effect of the ligands trans to the macrocycle as this may alter the energy and spacial orientation of the  $\Pi_{\text{S}}$ -orbitals. The electronic

difference between MeCN and  $\text{PPh}_3$  is not so great with Ru-S trans to MeCN being 2.332(15) while that trans to  $\text{PPh}_3$  is 2.348(16) Å in  $[\text{RuCl}(\text{MeCN})(\text{PPh}_3)([9]\text{aneS3})]^+$  (see Chapter 2). Thus superimposition of transitions is likely, so yielding only two  $\text{HS} \rightarrow \text{Ru(III)}$  CTs in most cases.

The other band observed under  $30000\text{cm}^{-1}$  is found in all of the spectra, occurring between 27144 and  $29869\text{cm}^{-1}$ . This band, due to its relative invariance, especially on comparing the spectra of bis and mono halide species, and its low energy, which precludes a CT to the "eg" orbitals, is thus assigned as an intra-ligand transition within the sulphur macrocycle. A similar assignment is given to the band at approximately  $37,000\text{cm}^{-1}$  which is also observed in all of the spectra. It is interesting to note the structure exhibited by this band in some cases, particularly for the bis halides and pyridine complexes. The resolution is not sufficient, however, to attempt further analysis.

Finally, comparison of the spectra of  $[\text{RuCl}_2(\text{PPh}_3)([9]\text{aneS3})]^+$  and its bromide analogue above 30000 (see Figure 3.25) shows a unique and structured band for the latter at approximately  $39000\text{cm}^{-1}$  and is assigned as a  $\text{Br}^- \rightarrow \text{Ru(III)} \text{ "eg"}$  CT transition. The comparable transition for the chloro complex would be expected at higher energy as would the  $\text{PX} \rightarrow \text{Ru(III)}$  "eg" CTs of the mono-halides, for reasons outline previously, and are thus not observed in the spectral window available.

Figure 3.25: UV/Vis/NIR Spectra of  $[\text{RuX}_2(\text{PPh}_3)([9]\text{aneS}_3)]^+$   
( $\text{X}=\text{Cl}^-$ ,  $\text{Br}^-$ ) in the Region  $30000\text{-}45000\text{cm}^{-1}$



### 3.3 Conclusions

It has been shown that the sulphur lone pairs of the ligand [9]aneS3 do interact with the Ru(III) centre in the complexes studied. The energy of the  $\pi S \rightarrow Ru(III)$  CT is dependant on the ligation trans to the macrocycle as this not only effects the trans Ru-S bond length but also the spacial orientation and energy of the lone pair. The latter effect should show up in the extinction coefficient values; however, Gaussian analysis of the spectra was not available at the time these experiments were carried out.

This work has thus provided a greater understanding of the interaction of the ligand [9]aneS3 with a metal centre, in this case Ru(II) and Ru(III), and indeed this should apply to other sulphur macrocycles such as [18]aneS6. Interpretation of the UV/Vis/NIR spectra of other complexes of [9]aneS3 should be easier in future and previous assignments may have to be changed. For example the spectrum of  $[Fe([9]aneS3)_2]^{3+}$  (1) was assigned to the transitions given in Table 3.11 without the benefit of comparative spectra. In the light of this work the transitions at  $15770(700)$  and  $21830\text{cm}^{-1}(520\text{cm}^{-1}\text{M}^{-1})$  should be reassigned as  $\pi S \rightarrow Fe(III)$ , the high  $\epsilon$  values precluding them from being d-d transitions. There are two bands due to the two different Ru-S bond lengths consistent with the reported tetragonal elongation in the complex.

Table 3.11: Spectral Data for  $[\text{Fe}(\text{[9]aneS3})_2]^{3+}$

E (cm <sup>-1</sup> )	$\epsilon$ (M <sup>-1</sup> cm <sup>-1</sup> )	Assignment
15770	700	${}^1\text{T}_{1g} \rightarrow {}^1\text{T}_{1g}$
17040	shoulder	${}^1\text{T}_{2g} \rightarrow {}^4\text{T}_{2g}$
20080	shoulder	${}^4\text{T}_{1g} \rightarrow {}^2\text{A}_{2g}, {}^2\text{T}_{1g}$
21830	520	${}^4\text{T}_{1g} \rightarrow {}^2\text{E}_g$
29410	7600	MLCT

The band at  $29410\text{cm}^{-1}$  is assigned as the same [9]aneS3 intra-ligand transition band observed in the complexes of this study, which should not change in energy on variation of the metal centre. The value of the extinction coefficient,  $\epsilon$ , of  $7600\text{cm}^{-1}$  is also consistent with this assignment, being approximately double that observed for the comparable transition in the present study.

### 3.4 Experimental

Investigative electrochemistry was performed using a PAR 170 potentiostat and programmer, 0.5M (TBA)(BF<sub>4</sub>)/CH<sub>2</sub>Cl<sub>2</sub> solutions with Pt working and auxiliary electrodes and an Ag/AgCl reference electrode (against which ferrocene is oxidised at

$E_{1/2}=0.56\text{V}$ ). Scan rates were from  $50$  to  $200\text{mVs}^{-1}$  (C.V.),  $20\text{mVs}^{-1}$  (S.L.S.V.) and  $10\text{mVs}^{-1}$  (a.c.v.) with  $\omega=205\text{Hz}$  (see Appendix 1). The jacketed electrochemical cell was thermostated to the required temperature using a Haake FX6Q refrigeration unit.

Electrosyntheses were carried out in a standard three compartment cell with a Pt basket working and a Pt gauze counter electrode. Temperature control, monitored by a thermocouple/digital thermometer, was achieved by the use of a MeOH/dry ice slush bath.

The chilled O.T.T.L.E. cell used is described in Appendix 1 and was placed in the beam of a Perkin-Elmer  $\lambda 9$  spectrophotometer. The progress of the electrosynthesis, performed by the use of a Metrohm Polarecord E506 potentiostat, was monitored spectroscopically to the limiting absorption curve. Standard practice was to regenerate the original species by reverse electrolysis to ensure that no significant degradation had occurred.

### Reagents

Methylenechloride was allowed to stand for one week over KOH pellets and dried by distillation over  $\text{P}_2\text{O}_5$ .

References

1. H-H. Kuppers, K. Wieghardt, B. Nuber, J. Weiss, E. Bill and A. X. Trautwein, Inorg. Chem., 1987, 26, 3762.
2. J. R. Hartman, E. J. Hintsa and S. R. Cooper, J. Am. Chem. Soc., 1986, 108, 1208.
3. C. A. Stein and H. Taube, Inorg. Chem., 1979, 18, 168.
4. L. G. Vanquickenborne and E. Verdonck, Inorg. Chem., 1974 13, 762.
5. J. D. Buhr, J. R. Winkler and H. Taube, Inorg. Chem., 1980, 19, 2416.
6. G. M. Brown, T. R. Weaver, F. R. Keene and T. J. Mayer, Inorg. Chem., 1976, 190.
7. G. M. Bryant, J. E. Ferguson and H. K. J. Powell, Aus. J. Chem., 1971, 24, 257.
8. K. Taylor, University of Edinburgh, Unpublished work.
9. G. M. Bryand and J. E. Fergusson, Aus. J. Chem., 1971, 24, 275.



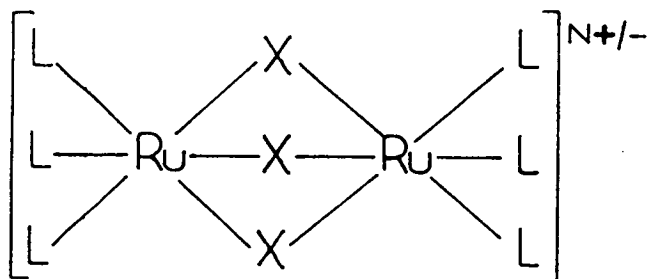
Chapter 4

Synthesis and Characterisation of  $[\text{Ru}_2\text{Cl}_8(\text{Py})]^{n-}$   
in Differing Oxidation States

#### 4.1 Introduction

Since the early 1960's a large number of triply bridged ruthenium binuclear complexes of the general formula  $[L_{(3-x)}Y_xRuX_3RuZ_yL_{(3-y)}]^{n+/-}$  have been synthesised. The first to be isolated were the symmetric complexes  $[L_3RuCl_3RuL_3]^+$  (L=PMe<sub>2</sub>Ph, PEt<sub>2</sub>Ph, PMePh<sub>2</sub> and PEtPh<sub>2</sub>) (1) with the proposed confacial bioctahedral geometry (see Figure 4.1) being confirmed by an X-Ray diffraction study carried out by Raspin on  $[(PEt_2Ph)_3RuCl_3Ru(PEt_2Ph)_3]^+$  (2).

Figure 4.1 Confacial Bioctahedral Geometry Adopted by the Family of Complexes  $[L_3RuCl_3RuL_3]^{n+/-}$



Although the bridging group X in  $[L_{(3-x)}Y_xRuX_3RuZyL_{(3-y)}]^{n+/-}$  is usually  $Cl^-$  other ligands can be incorporated such as  $Br^-$ ,  $I^-$ ,  $H^-$ ,  $OH^-$ ,  $SEt^-$ , and  $(CH_2)^{2-}$ . The terminal ligand set L, Y and Z can contain neutral soft ligands such as  $ER_3$  ( $E=P,As$ ), CO and CS, harder ones such as  $H_2$  and  $NH_3$  but also negatively charged ligands e.g.  $Cl^-$  and  $Br^-$ . A few examples of this diversity are given in Figure 4.2.

Our interest in these complexes concerns the nature of the metal-metal interaction particularly when the formal oxidation state of the two ruthenium centres is different (termed mixed valency) i.e.  $Ru(II)Ru(III)$  or  $Ru(III)Ru(IV)$ . A few mixed-valence complexes can be synthesised directly (see Figure 4.3) but the majority are isolated as  $Ru(II)Ru(II)$  or  $Ru(III)Ru(III)$  binuclear species. Fortunately the complexes are redox-active and generally exhibit two one-electron processes (see Table 4.1). Although as indicated in Table 4.1, not all of these processes are reversible, even at low temperatures, it was generally found that one stable mixed-valence state could be electrochemically generated and studied via O.T.T.L.E. (Optically Transparent Thin Layer Electrode) experiments, e.s.r. spectroscopy and magnetic susceptibility measurements.

A classification of the differing types of metal-metal interaction was put forward by Robin and Day<sup>(18)</sup>. They divided the types of interaction into four classes, ranging from fully localised, isolated valence, Class 1 systems to

Figure 4.2 Some Examples of Triple Bridged Ruthenium Binuclear Complexes

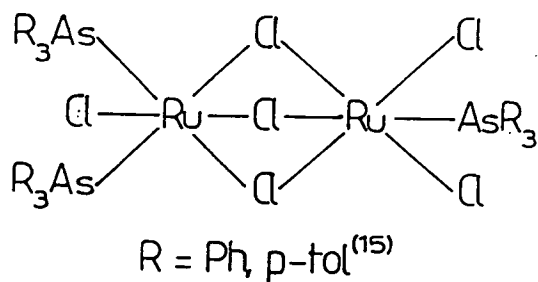
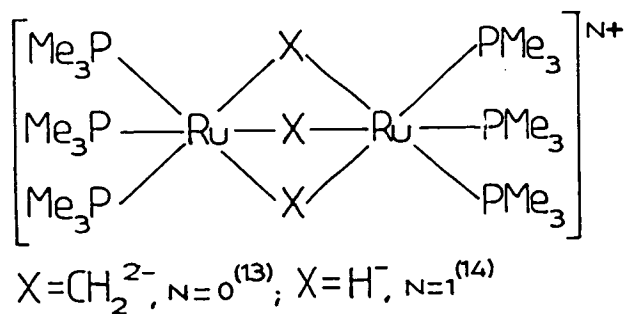
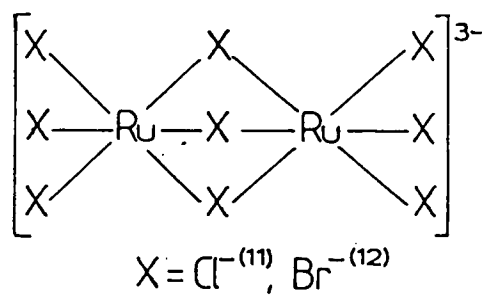
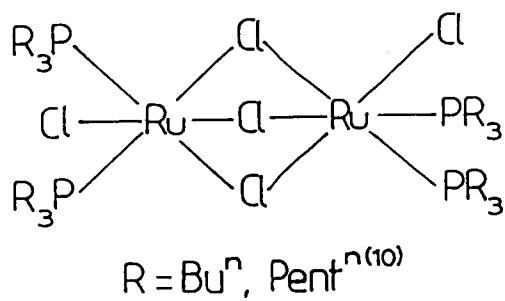
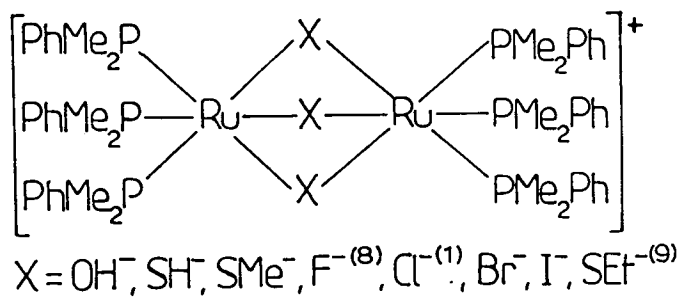
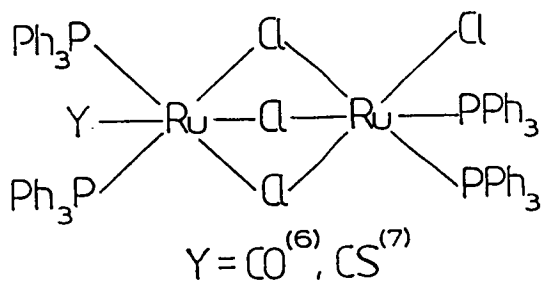
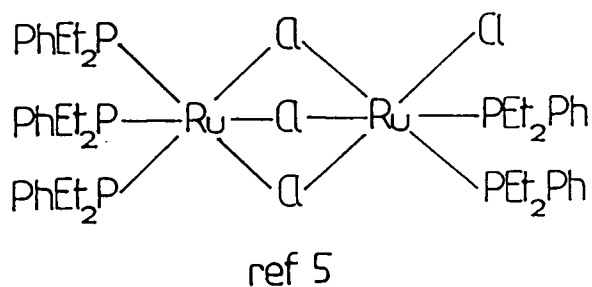
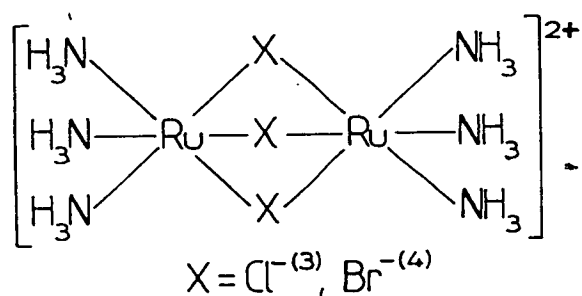




Table 4.1 Electrode Potentials for some Triple Chloride Bridged Ruthenium Binuclear Complexes  $E_{1/2}$  (volts) at 20°C in CH<sub>2</sub>Cl<sub>2</sub>/0.5M (TBA)(BF<sub>4</sub>)<sup>(9)</sup>

Compound	(II)(II)/(II)(III)	(II)(III)/(III)(III)	(III)(III)/(III)(IV)	(III)(IV)/(IV)(IV)
$[(PMe_2Ph)_3RuCl_3Ru(PMe_2Ph)_3]^+$	+1.33	+1.87		
$(PEtPh_2)_3RuCl_3RuCl(PEtPh_2)_2$	+0.58	(+1.53)		
$(PPh_3)_2(CS)RuCl_3RuCl(PPh_3)_2$	+1.18			
$[(PPh_3)_2(CS)RuCl_3Ru(CS)(PPh_3)]^+$	[+1.50]			
$(AsPh_3)_2ClRuCl_3RuCl(AsPh_3)_2$	+0.14	+0.90		
$(As(p-tol)_3)_2ClRuCl_3RuCl(As(p-tol)_3)_2$	+0.10	+0.83		
$(As(p-tol)_3)_3RuCl_3RuCl_2(As(p-tol)_3)$	-0.22	+1.25		
$(PPh_3)_2(CS)RuCl_3RuCl_2(PPh_3)$	+0.02			
$(AsPh_3)_2ClRuCl_3RuCl_2(AsPh_3)$	-0.44	+0.62		
$[Cl_3RuCl_3RuCl_3]^{-3}$ <sup>(17)</sup>		[-0.57]	0.92	1.58

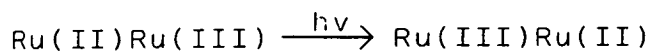
( ) - partially reversible, [ ] - irreversible

ref 9 versus Ag/AgI reference at which ferrocene is oxidised at 0.60V

ref 17 versus Ag/AgCl reference at which ferrocene is oxidised at 0.55V

average valence Class IIIB behaviour. A description of the general characteristics of these classifications is outlined in Table 4.2.

For a symmetrical complex such as  $[(\text{PMe}_2\text{Ph})_3\text{RuCl}_3\text{Ru}(\text{PMe}_2\text{Ph})_3]^{2+}$  a simple energy configurational diagram can be drawn as shown in Figure 4.4a. Using this simple static model it can be shown that if the optical transition energy ( $E_{op}$ ) for electron transfer e.g.



is assumed to obey the Franck-Condon principle then  $E_{op} = 4E^{th}$  (19) where  $E^{th}$  is the thermal activation barrier to electron transfer. However in order to account for a number of experimental observations other factors have to be incorporated into this simple static model. Firstly the system is not static. The degree of interaction between the two metal sites is dependant on the magnitude of the resonance energy ( $H_{res}$ ).

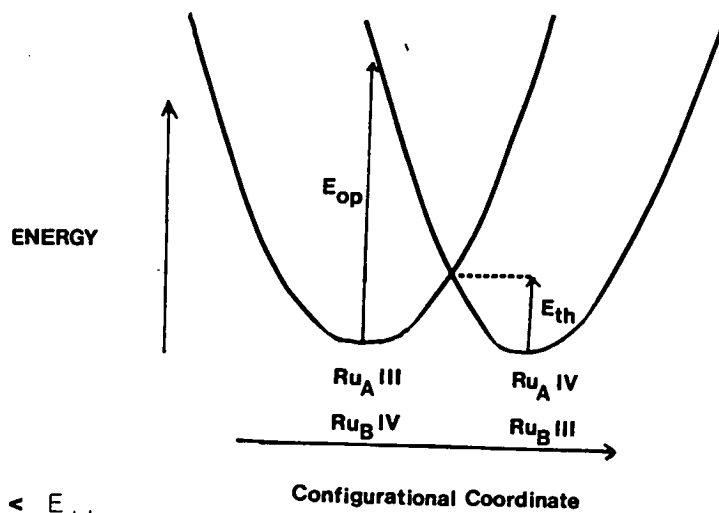
Table 4.2    Characteristics of the Four Classes of Mixed  
Valence Compounds

<u>Class I</u>	<u>Class II</u>	<u>Class IIIA</u>	<u>Class IIIB</u>
1. Metal ions in ligand fields of very different symmetry and/or strength, i.e. tetrahedral vs octahedral	1. Metal ions in ligand fields of nearly identical symmetry relative distortion < 50pm	1. metal ions indistinguishable but grouped into polynuclear clusters	1. All metal ions indistinguishable
2. $\alpha = 0$ ; valences very firmly trapped	2. $\alpha > 0$ ; valences distinguishable, but with slight delocalisation	2. $\alpha$ maximal locally	2. $\alpha$ maximal; complete delocalisation over the cationic sublattice
3. Insulator; resistivity of $10^{10} \Omega \text{ cm}$ or greater	3. Semiconductor; resistivity in the $10-10^7 \Omega \text{ cm}$	3. probably insulating	3. Metallic conductivity; resistivity in $10^{-2}-10^{-6} \text{ cm}$
4. No mixed-valence transitions in the Vis/NIR region	4. One or more mixed-valence transitions in the Vis/NIR region	4. One or more mixed-valence transitions in the Vis/NIR region	4. Absorption edge in the infrared, opaque with metallic reflectivity in the visible region
5. Clearly shows spectra of constituent ions IR, UV, Mossbauer	5. Shows spectra of constituent ions at very nearly normal frequencies	5. Spectra of constituent ions not discernable	5. Spectra of constituent ions not discernable
6. Magnetically dilute paramagnetic or diamagnetic to very low temperatures	6. Magnetically dilute, with both ferromagnetic and antiferromagnetic interactions at low temperatures	6. Magnetically dilute	6. Either ferromagnetic with a high Curie temperature or diamagnetic, depending on the presence or absence of local moments

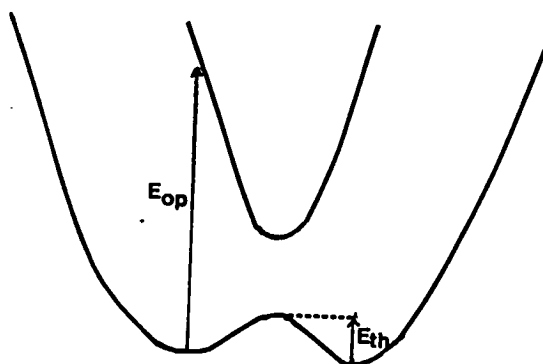


Figure 4.4 Energy Configurational Co-ordinate Diagram for  
Valence Interchange in Symmetric Complexes

a) Static Case



b)  $H_{res} < E_{th}$



c)  $H_{res} > E_{th}$

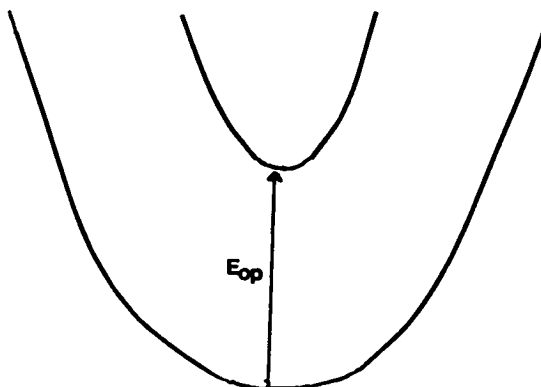
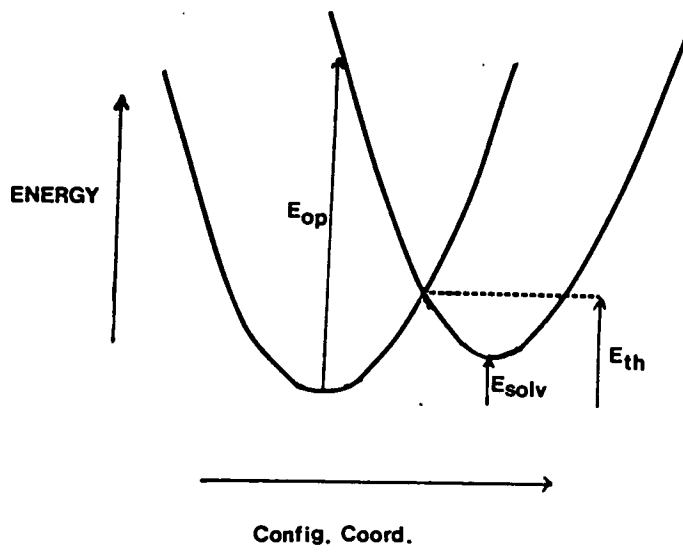
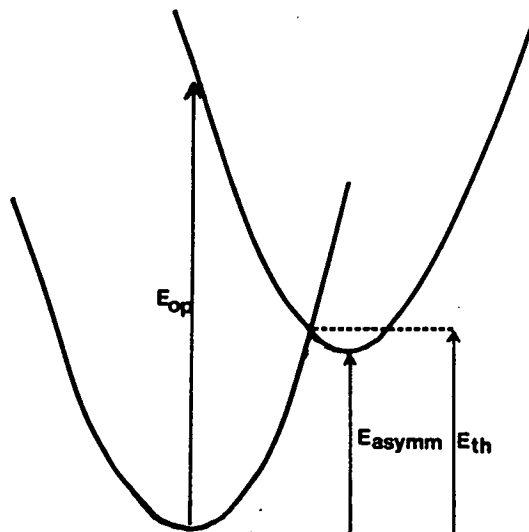


Figure 4.5 Energy Configurational Co-ordinate Diagram for  
Valence Interchange Taking into Consideration  
Polarised Solvent and Terminal Ligand Asymmetry

a) Polarised Solvent



b) Terminal Ligand Asymmetry



If  $H_{res}$  is small compared to  $E_{th}$ , Class II, weakly interacting behaviour will be observed, if large then delocalised Class IIIA behaviour will result (see Figure 4.4b and c).

In solution the solvent molecules in the vicinity of the complexes will be orientated according to its polarity. The polarity of the complex will change as the odd electron is optically pumped from one site to the other. The orientated solvent molecules will resist the change and this leads to an increase in energy of the excited state's potential energy surface (see Figure 4.5a). A similar effect results for asymmetric terminal ligation due to the intrinsic energy difference between the two sets of metal-based orbitals (see Figure 4.5b).

In practice the net effect of these factors must be experimentally determined. Within the sub-family of triply bridged ruthenium binuclear complexes

$[L_{(3-x)}Cl_xRuCl_3RuCl_yL_{(3-y)}]^{n+/-}$  Class IIIA, II and I behaviour have been observed and are discussed in the following sections.

#### 4.1.2 Class IIIA Behaviour

This type of interaction involves the delocalisation of the "odd" electron over both metal centres to give an average valency of Ru(2.5)Ru(2.5) or Ru(3.5)Ru(3.5). The low energy optical transitions exhibited by these species are observed in the visible/NIR region with solvent independent behaviour

exhibited by  $V_{\max}$ .

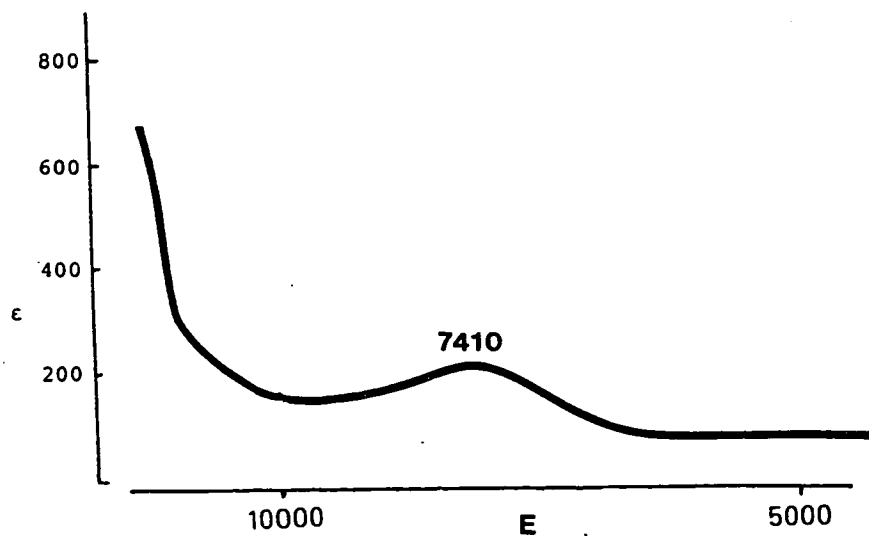
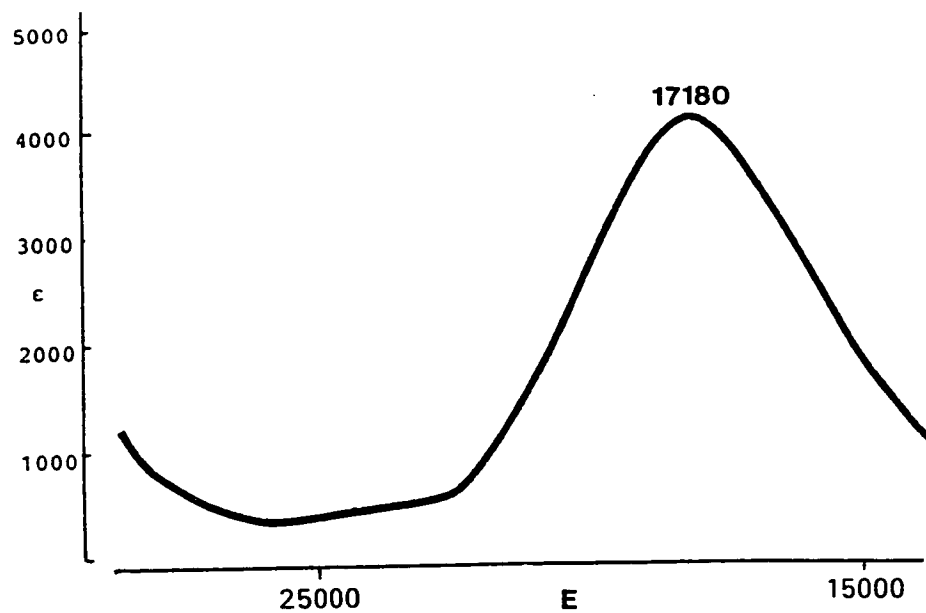
Only symmetric complexes such as

$[(9)\text{aneN3}]\text{RuCl}_3\text{Ru}((9)\text{aneN3})]^{2+}$  (20),

$[\text{As}(\text{tol})_3]_2\text{ClRuCl}_3\text{RuCl}(\text{As}(\text{tol})_3)_2$  (21),  $[\text{Y}_3\text{RuCl}_3\text{RuY}_3]^{2+}$

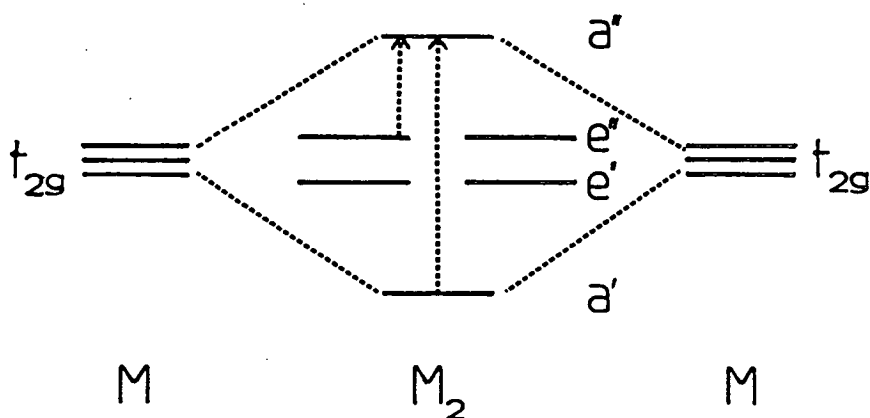
( $\text{Y}=\text{PEt}_2\text{Ph}$  (21),  $\text{NH}_3$  (17, 22) ) and  $[(\text{PE}_3)_3\text{RuCl}_3\text{Ru}(\text{PE}_3)_3]^{2+}$  ( $\text{PE}_3=\text{PPr}_3, \text{PR}_3, \text{PR}_2\text{Ph}, \text{PRPh}_2$ ;  $\text{R} = \text{Me}, \text{OMe}, \text{Et}$ ) (23) have been found to exhibit class IIIA behaviour. A spectroscopic study of these mixed valence compounds reveals two transitions in the visible/NIR region. For instance these occur at 17180 and 7410  $\text{cm}^{-1}$  for  $[(\text{NH}_3)_3\text{RuCl}_3\text{Ru}(\text{NH}_3)_3]^{2+}$  in MeCN (17) (see Figure 4.6).

Figure 4.6 Visible/NIR Spectrum of  $[(\text{NH}_3)_3\text{RuCl}_3\text{Ru}(\text{NH}_3)_3]^{2+}$  in MeCN



In these complexes the d-orbitals (the  $t_{2g}$  set in octahedral geometry) on the two Ru centres interact directly to give molecular orbitals of symmetry  $a'$ ,  $e''$ ,  $e''$  and  $a''$ <sup>(24)</sup> as shown in Figure 4.7.

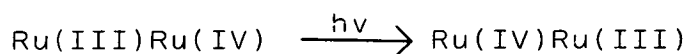
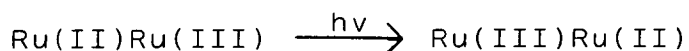
Figure 4.7    Schematic Representation of Metal Bonding  
Orbitals in Symmetric Triple Bridged Binuclear  
Ruthenium Complexes



Only two transitions (shown by arrows in Figure 4.7) are orbitally allowed, namely the  $e' \longrightarrow a''$  and  $a' \longrightarrow a''$  transitions, thus explaining the two experimentally observed absorption bands. The extent of the interaction depends on the terminal ligation as this will affect not only the energies and orientations of the " $t_{2g}$ " orbitals<sup>(24)</sup> but also the ability of the two metal centres to interact due to the steric bulk of these ligands. The latter consideration seems to be the dominant factor in these complexes<sup>(23)</sup>.

#### 4.1.3. Class II Behaviour.

The most important feature of class II type binuclear complexes is known as intervalence charge transfer transitions (IVCT's) or metal-metal charge transfer transitions (MMCT's) i.e.



An IVCT is defined by Allen and Hush<sup>(25)</sup> as the transfer of an optically excited electron from one nearly localised site to an adjacent one, the donor and acceptor having more than one accessible oxidation state. The transition manifests itself as a broad band ( $\Delta\nu_{1/2} = 4-5000\text{cm}^{-1}$ ) in the visible/NIR region of the spectrum. Three methods are generally employed to confirm the assignment:-

1/ Calculation of a Theoretical  $\Delta V_{1/2}$ 

$$\Delta V_{1/2} \text{ (theo)} = (E_{\text{op}} \times 2310)^{1/2}$$

$\Delta V_{1/2}$  (theo) must equal  $\Delta V_{1/2}$  (exp) to within +/-10%

2/ Variation of  $E_{\text{op}}$  with solvent

$$E_{\text{op}} \propto \left( \frac{1}{n^2} - \frac{1}{D} \right) \quad n = \text{refractive index of the solvent}$$

$D$  = static dielectric constant of the solvent

## 3/ Calculation of the Degree of Electron Delocalisation

$$\alpha^2 = \frac{(4.2 \times 10^{-4}) \times \epsilon_{\text{max}} \cdot \Delta V_{1/2}}{E_{\text{op}} \times R^2}$$

$\epsilon_{\text{max}}$  = extinction coefficient at  $E_{\text{op}}$

$E_{\text{op}}$  = band maximum in  $\text{cm}^{-1}$

$\Delta V_{1/2}$  = band halfwidth in  $\text{cm}^{-1}$

$R$  = metal-metal distance in nm

Where  $0 < \alpha^2 < 0.5$

The symmetric complexes  $[\text{Ru}_2\text{X}_9]^{2-}$  ( $X = \text{Cl}^-, \text{Br}^-$ ), the only known examples of Ru(III)Ru(IV) mixed valence complexes, might have been expected to show Class IIIA behaviour in common with the Ru(II)Ru(III) analogues.



However this proved not to be the case as they were found to be weakly interacting<sup>(17)</sup>, that is the Ru(III)Ru(IV) system exhibits Class II type behaviour. This apparent discrepancy has been ascribed to d-orbital contraction and increased electrostatic repulsion between the two metal centres on going from Ru(II)Ru(III) to Ru(III)Ru(IV). The combination of the two effects should lead to an elongation of the metal-metal vector and this is indeed observed in the analogous Tungsten complex where the W-W bond length increases by 12.2pm on oxidising  $[\text{Cl}_3\text{WCl}_3\text{WCl}_3]^{3-}$  to  $[\text{Cl}_3\text{WCl}_3\text{WCl}_3]^{2-}$ <sup>(26)</sup>.

In general, however, Class II behaviour is exhibited by asymmetric complexes such as  $[(\text{PEt}_2\text{Ph})_3\text{RuCl}_3\text{RuCl}(\text{PEt}_2\text{Ph})_3]^+$ <sup>(21)</sup> i.e.  $|y-x| > 0$  due to the energy and orbital symmetry mismatch of the two sets of metal based " $t_{2g}$ " orbitals. As would be predicted from the earlier treatment the energy of the optical transition increases as the asymmetry increases, some examples being shown in Table 4.3. A study of the solvent dependency of  $V_{\text{max}}$  has not been attempted for any of these asymmetric complexes.

#### 4.1.4 Class I Behaviour.

Asymmetric mixed valence complexes containing strongly  $\Pi$ -back donating ligands such as CO and CS will have an increased energy mismatch between the two metal centres compared to the ones considered in the previous section.

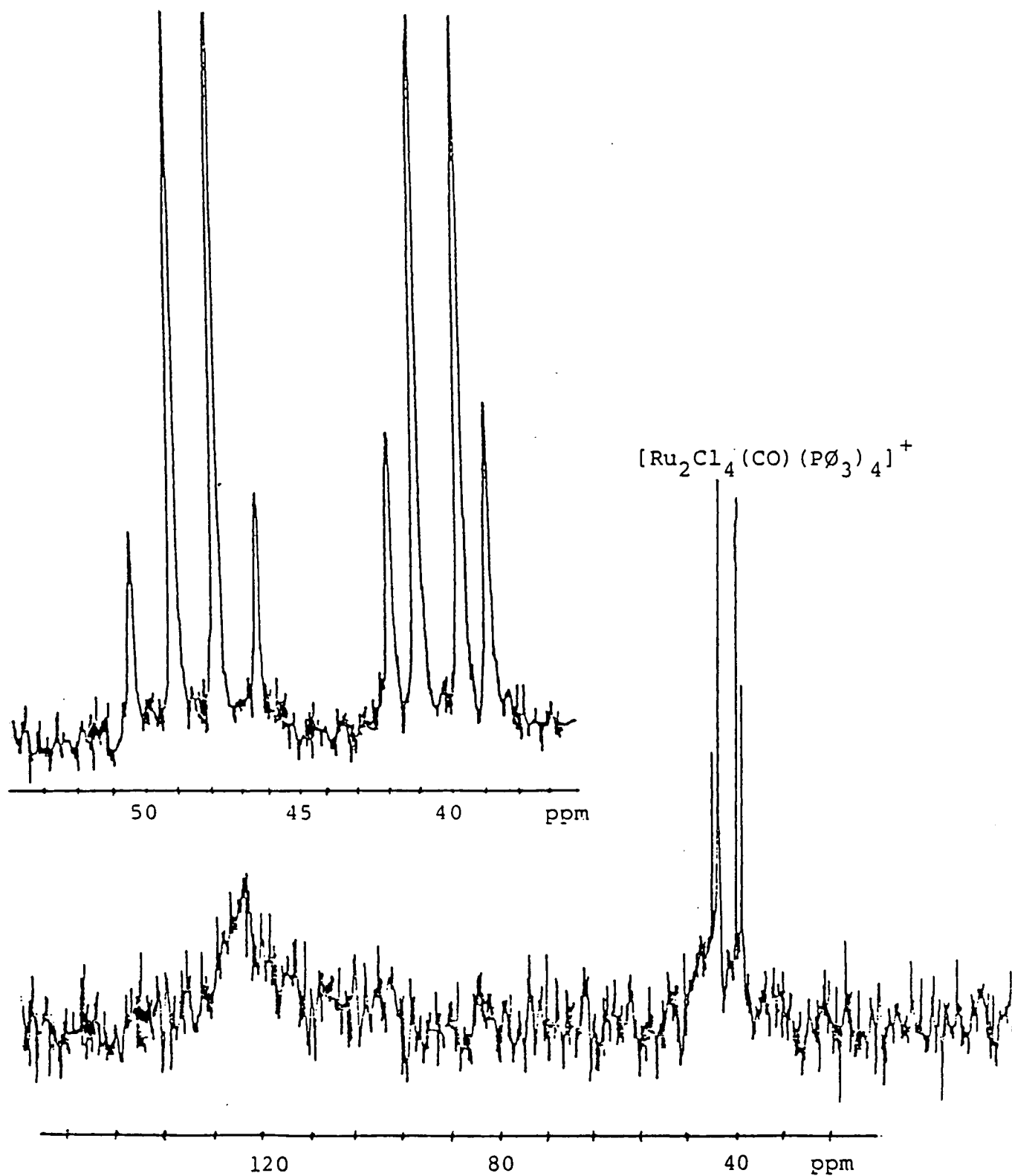
Table 4.3    Increase in Eop with Increasing Terminal Ligation  
Asymmetry

<u>Compound</u>	<u>Eop(cm<sup>-1</sup>)</u>
$[(\text{PEt}_2\text{Ph})_3\text{RuCl}_3\text{RuCl}(\text{PEt}_2\text{Ph})_2]^+$	9,700
$(\text{PEt}_2\text{Ph})_3\text{RuCl}_3\text{RuCl}_2(\text{PEt}_2\text{Ph})$	13,500
$[(\text{As}(p\text{-tol})_3)_2\text{ClRuCl}_3\text{RuCl}_2(\text{As}(p\text{-tol})_3)]^-$	7,800
$(\text{As}(p\text{-tol})_3)_3\text{RuCl}_3\text{RuCl}_2(\text{As}(p\text{-tol})_3)$	12,200

Thus the IVCT bands for the electrogenerated species  $[(\text{PPh}_3)_2\text{YRuCl}_3\text{RuCl}(\text{PPh}_3)_2]^+$  (Y=CO, CS) now occur at  $14800\text{cm}^{-1}$  ( $\epsilon = 100$ ) for both complexes (21). Further evidence for their "isolated" valency is provided by the  $^{31}\text{P}$ - $(^1\text{H})$ nmr spectra of the mixed valence species. These show that although the AB pattern for the terminal  $\text{Cl}^-$  end (the oxidised Ru(III) centre) is paramagnetically broadened and contact shifted, the CO/CS end (the Ru(II) centre) remains almost unchanged from the parent spectrum (see Figure 4.8 Y=CO). Class II and IIIA systems do not exhibit  $^{31}\text{P}$ - $(^1\text{H})$  nmr spectra for the mixed oxidation state species.

Thus for the sub-group of complexes  $[\text{L}_{(3-x)}\text{Cl}_x\text{RuCl}_3\text{RuCl}_y\text{L}_{(3-y)}]^{n+/-}$  which have been the most extensively studied the nature of the metal-metal interaction is dependant on the oxidation state (i.e. Ru(II)Ru(III) or

Figure 4.8  $^{31}\text{P}$ -( $^1\text{H}$ ) N.m.r. Spectra of  
 $(\text{PPh}_3)_2(\text{CO})\text{RuCl}_3\text{RuCl}(\text{PPh}_3)_2$   
Before and After Oxidation



Ru(III)Ru(IV)) and also on the asymmetry and nature of the terminal ligation.

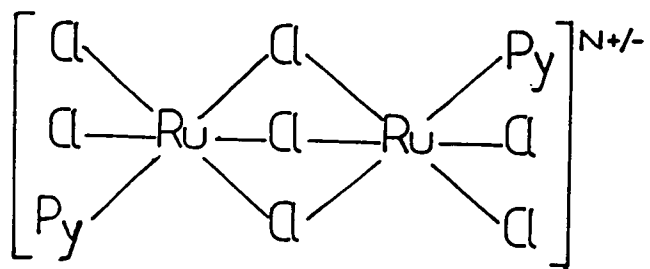
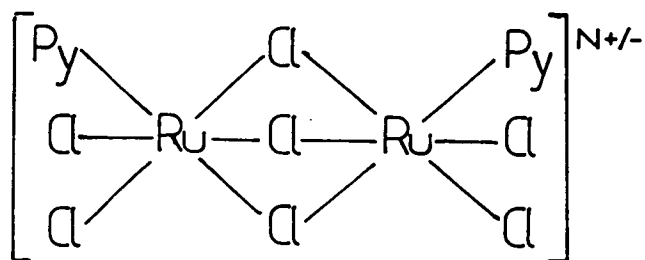
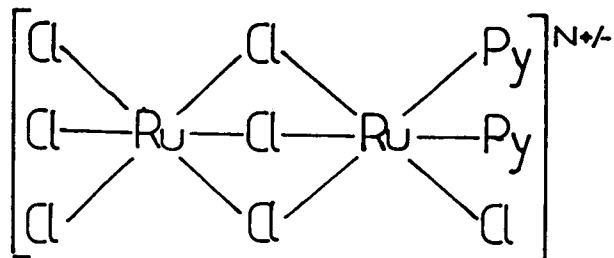
#### 4.2 Results and Discussion

Although a number of complexes of the sub-group of complexes  $[L_{(3-x)}Cl_xRuCl_3RuCl_yL_{(3-y)}]^{n+/-}$  have been synthesised and studied two members remain unknown, these being  $[Cl_3RuCl_3RuCl_2L]^{n-}$  and any of the isomers of  $[Ru_2Cl_7L_2]^{n-}$  (see Figure 4.9).

As was indicated in Table 4.1 the complex  $[Ru_2Cl_9]^{3-}$  exhibits an irreversible reduction process which becomes quasi-reversible on lowering the temperature (17).

Electrochemical studies have confirmed this to be an EC process, that is electron transfer (E) followed by a chemical reaction (C) which in this case involves the loss of a terminal chloride ligand. Previous work carried out on the osmium monomer  $OsCl_3(PMe_2Ph)_3$  revealed that such an EC process can be used to replace a chloride by other ligands to give  $OsCl_2L(PMe_2Ph)_3$  ( $L=MeCN, PhCN, DMF$  (15),  $CO, C_2H_2$  and  $N_2$  (17)). Thus a scheme was envisaged in which the desired complexes  $[Ru_2Cl_8L]^{n-}$  and  $[Ru_2Cl_7L_2]^{n-}$  could be generated via the controlled potential reduction of  $[Ru_2Cl_9]^{3-}$  in the presence of L (see Scheme 4.1).

Figure 4.9 Possible Isomeric Structures of  $[\text{Ru}_2\text{Cl}_7\text{L}_2]^{n+/-}$





Preliminary electrochemical studies showed that redox-active daughter products are formed on reducing  $[\text{Ru}_2\text{Cl}_9]^{3-}$  in the presence of  $\text{PPh}_3$  and these were tentatively assigned to the formation of  $[\text{Ru}_2\text{Cl}_8(\text{PPh}_3)]^{n-}$  and isomers of  $[\text{Ru}_2\text{Cl}_7(\text{PPh}_3)_2]^{n-}$  (27). Neither species could be isolated or characterised as bulk electrogenerations did not yield clean solutions.

#### 4.2.1 Electroreduction of $[\text{Ru}_2\text{Cl}_9]^{3-}$ in the presence of Py.

Due to the encouraging results from the earlier electrochemical studies a series of controlled potential electrogenerations on  $[\text{Ru}_2\text{Cl}_9]^{3-}$  was undertaken using Py as the replacement ligand, L. This ligand was chosen due to its small size, unhindered donor site and the stable complexes which usually result on using Py in redox induced substitution reactions (28).

On applying a potential slightly more negative than that of the (III)(III)/(II)(III) couple of  $[\text{Ru}_2\text{Cl}_9]^{3-}$  in  $\text{CH}_2\text{Cl}_2/0.5\text{M}$  (TBA)( $\text{BF}_4$ ), to which a slight excess of Py had been added, a smooth uptake of current was observed and the solution turned from brown to blue in colour. The potential was then reversed to OV and a current was observed to flow in the opposite direction with a concomitant colour change from blue to brown. Both these processes involved the uptake or loss of one electron per binuclear complex and the final brown product solution, unlike the blue solution, was found to be stable when exposed to oxygen.

The a.c. and stirred linear sweep responses of the brown product solution for a typical experiment are shown in Figure 4.10. The processes marked by an \* at  $-0.20(\text{red})$ ,  $+1.26(\text{ox})$  and  $+2.01\text{V}(\text{ox})$  vs Ag/AgCl were tentatively assigned to the formation of  $[\text{Ru}_2\text{Cl}_8(\text{Py})]^{2-}$  (the corresponding processes for  $[\text{Ru}_2\text{Cl}_9]^{3-}$  occur at  $-0.57$ ,  $+0.92$  and  $+1.58\text{V}$  respectively). The other observed processes may correspond to the redox steps of isomers of  $[\text{Ru}_2\text{Cl}_7(\text{Py})_2]^{n-}$  and/or monomeric species.

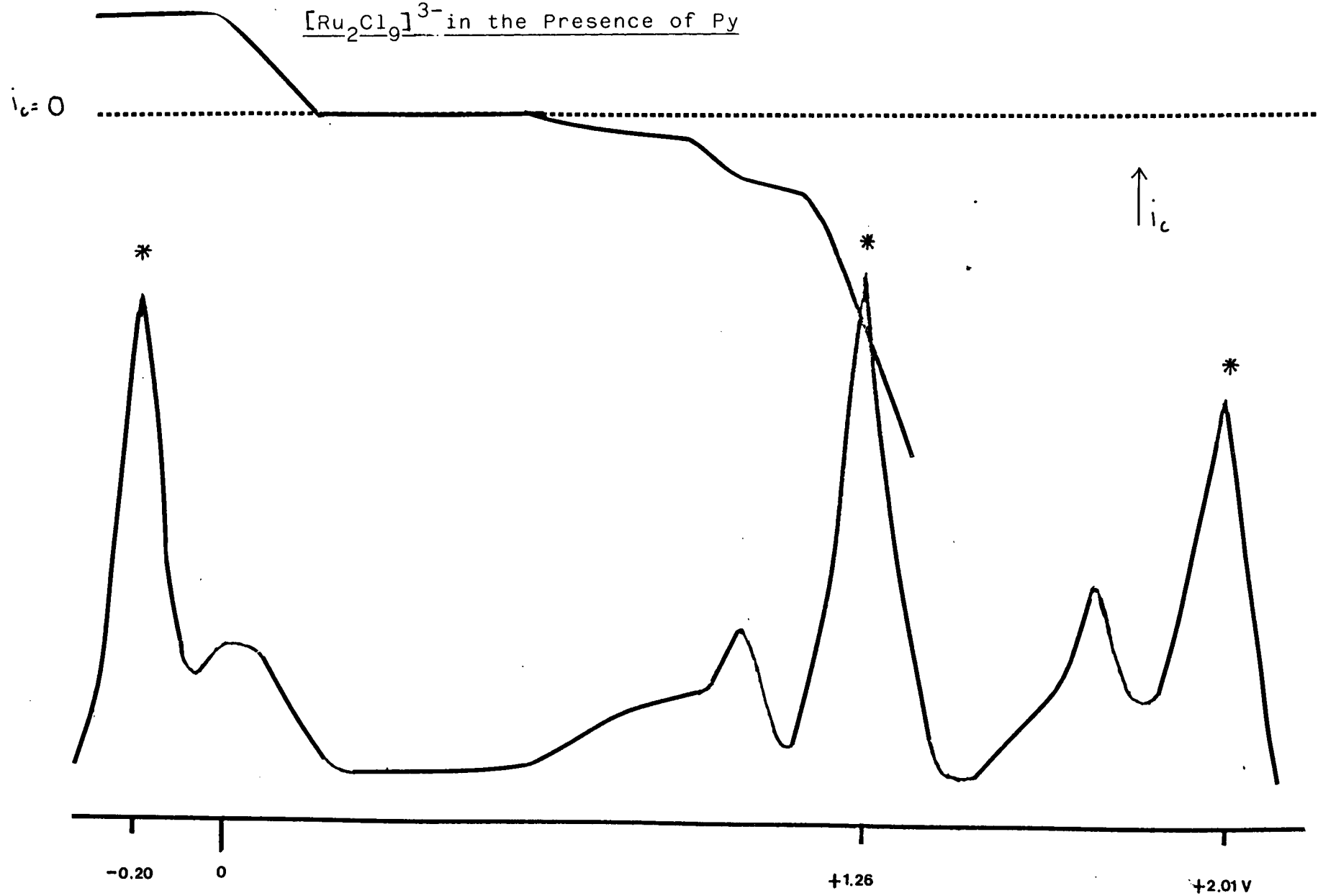
The ratio of  $[\text{Ru}_2\text{Cl}_8(\text{Py})]^{2-}$  to the other products, as measured by peak heights from an a.c. voltammogram (see Figure 4.10), was found to be largely dependant on the temperature at which the electrogeneration is performed and to a lesser extent on the initial  $[\text{Ru}_2\text{Cl}_9]^{3-}/\text{Py}$  ratio used. At low temperatures (ca 238K)  $[\text{Ru}_2\text{Cl}_8(\text{Py})]^{2-}$  is the major product (see Figure 4.10) even with initial  $[\text{Ru}_2\text{Cl}_9]^{3-}/\text{Py}$  concentrations of 1:6. As the temperature is raised the ratio of  $[\text{Ru}_2\text{Cl}_8(\text{Py})]^{2-}$  to the other products formed decreases even for only a slight Py excess (1:2) which reflects the instability of the proposed intermediate  $[\text{Ru}_2\text{Cl}_8]^{3-}$ .

#### 4.2.2 Purification of the Electrogenerated $[\text{Ru}_2\text{Cl}_8(\text{Py})]^{2-}$

By carrying out the electrogeneration at low temperatures a high yield of  $[\text{Ru}_2\text{Cl}_8(\text{Py})]^{2-}$  could be obtained. In order to study the complex further a pure sample of  $[\text{Ru}_2\text{Cl}_8(\text{Py})]^{2-}$  was required. This is by no means a trivial problem as it involves separating  $[\text{Ru}_2\text{Cl}_8(\text{Py})]^{2-}$  from the other products and



Figure 4.10: AC and Stirred Linear Sweep Responses of the Product Solution from a Typical Electroreduction/oxidation of  $[\text{Ru}_2\text{Cl}_9]^{3-}$  in the Presence of Py



also from the vast excess of inert electrolyte,  $(TBA)(BF_4)$ , present.

On removal of the solvent,  $CH_2Cl_2$ , a light brown solid was obtained and from this a large proportion (95%) of the inert electrolyte,  $(TBA)(BF_4)$ , could be removed by solvent extraction using chlorobenzene. This only involved a slight loss of the electrogenerated products as indicated by a faint colouration of the chlorobenzene. However it was not possible to remove all of the electrolyte by extraction so chromatographic methods were attempted.

Initial studies used a silica gel column, but despite passing the product mixture down the column several times using a 2:1 (v/v) chloroform/acetone eluant mix no further separation of the mixture of products or significant loss of the remaining electrolyte was achieved. A more polar eluant such as MeOH was found to degrade the product mixture as monitored by U.V. spectroscopy. The same lack of separation was also obtained using a Sephadex LH20 column (which is designed to separate on the basis of molecular weight).

These results suggested that the electrolyte is closely associated with the products and is probably responsible for the very poor separation. In an attempt to overcome this a different electrolyte,  $(TPA)(ClO_4)$ , was used in conjunction with the (TPA) salt of  $[Ru_2Cl_9]^{3-}$  in the initial electrogeneration solution. The advantage of using

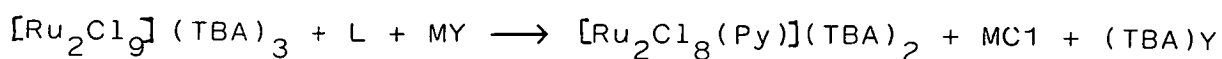
(TPA)(ClO<sub>4</sub>) was its low solubility in chloroform thus yielding an easy route for its removal providing the product is itself soluble. However the use of (TPA)(ClO<sub>4</sub>) presented another problem in that it began to fall out of solution at 260K. Electrogeneration at this temperature meant that control of the product distribution was lost. However enough of the desired product  $[\text{Ru}_2\text{Cl}_8(\text{Py})]^{2-}$  was generated, shown by an a.c. study, to make it worth while working up the resulting solution.

Adding a small volume of chloroform to the light brown solid obtained from the electrogeneration (in CH<sub>2</sub>Cl<sub>2</sub> and 0.5M (TPA)(ClO<sub>4</sub>)) followed by filtration resulted in most of the (TPA)(ClO<sub>4</sub>) being removed. From the solid, obtained on removal of the chloroform, six bands could be obtained by the use of thin layer chromatography using CH<sub>2</sub>Cl<sub>2</sub> as the eluent. Each of these bands was carefully scraped off, with the silica removed by addition of CH<sub>2</sub>Cl<sub>2</sub> followed by filtration. A.C. voltametric studies of these bands in CH<sub>2</sub>Cl<sub>2</sub>/0.5M(TPA)(ClO<sub>4</sub>) revealed that although each band consisted of mainly one product there still remained traces of others. None of the bands examined contained  $[\text{Ru}_2\text{Cl}_8(\text{Py})]^{2-}$  indicating degradation during the chromatographic technique.

#### 4.2.3 Chemical Synthesis of $[\text{Ru}_2\text{Cl}_8(\text{Py})]^{2-}$

Although the investigation of separation techniques has not been rigourously pursued it rapidly became obvious that the

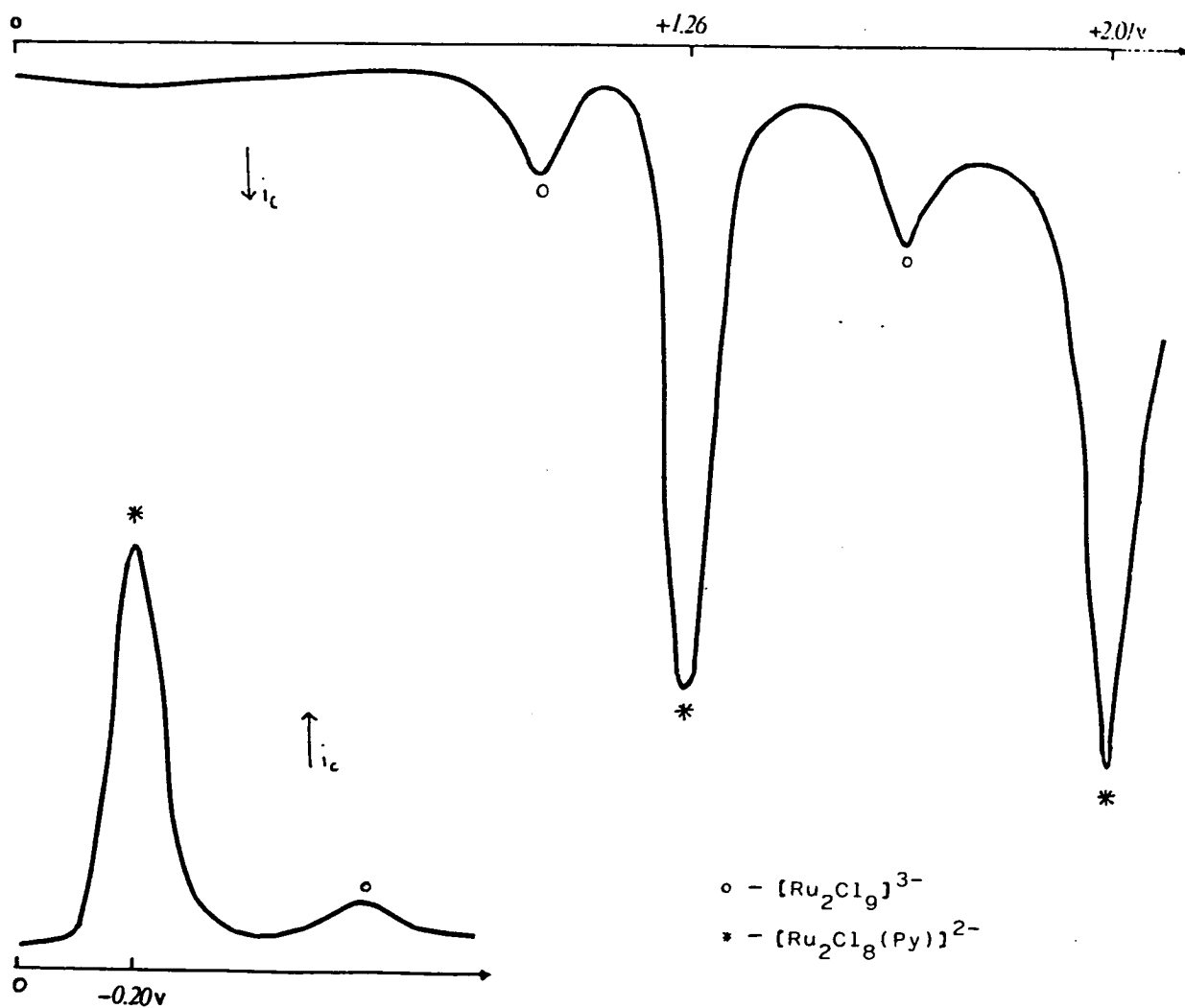
removal of the inert electrolyte and the minor impurities was not proving to be an easy task and so a new approach was required. The envisaged method involved the chemical abstraction of  $\text{Cl}^-$  from  $[\text{Ru}_2\text{Cl}_9]^{3-}$  by  $\text{M}^+$  i.e.



If  $\text{MY} = \text{Tl}(\text{BF}_4)$  as was used in Chapter 2 then one of the products would be  $(\text{TBA})(\text{BF}_4)$  which from previous experience is difficult to separate from  $[\text{Ru}_2\text{Cl}_8(\text{Py})]^{2-}$ . To circumvent this problem the silver salt  $\text{Ag}(\text{ClO}_4)$  was used although this required carrying out the reaction in the dark to avoid decomposition of the Ag salt.

A 1:1:1 molar ratio of  $[\text{Ru}_2\text{Cl}_9]^{3-}$ ,  $\text{Ag}(\text{ClO}_4)$  and Py in  $\text{CH}_2\text{Cl}_2$  was refluxed in the dark under an atmosphere of nitrogen and after 5 hours a precipitate was observed to have formed. A small amount of the brown solution was removed and injected into an electrochemical cell containing  $\text{CH}_2\text{Cl}_2/0.5\text{M} (\text{TBA})(\text{BF}_4)$  and an A.C. voltammogram was run. The electrochemical response was very similar to that observed for the electrosynthetic preparation but was much cleaner as  $[\text{Ru}_2\text{Cl}_8(\text{Py})]^{2-}$  was the only product (see Figure 4.11). By occasional monitoring of the chemical reaction mixture in this manner the steady conversion of  $[\text{Ru}_2\text{Cl}_9]^{3-}$  to  $[\text{Ru}_2\text{Cl}_8(\text{Py})]^{2-}$  could be monitored. At about 80% conversion, it became apparent that the reaction was no longer proceeding, possibly due to the partial decomposition of the Ag salt. This was confirmed when the reaction resumed on addition of a further small amount of  $\text{Ag}(\text{ClO}_4)$ .

Figure 4.11: AC Response of the Reaction Solution During the Chemical Synthesis of  $[\text{Ru}_2\text{Cl}_8(\text{Py})](\text{TBA})_2$



On working up the final reaction solution a dark brown solid was obtained. The infrared spectra revealed strong absorptions at 310 and  $340\text{cm}^{-1}$  assigned as Ru-Cl (terminal) stretching modes (cf  $[\text{Ru}_2\text{Cl}_9]^{3-}$  : 310 and  $344\text{cm}^{-1}$ ) and a weaker one at  $1600\text{cm}^{-1}$  assigned as  $\nu_{\text{C}=\text{C}}$  of Py. The material analysed well for  $[\text{Ru}_2\text{Cl}_8(\text{Py})](\text{TBA})_2$  (expected C 42.3, H 7.39, N 4.00; found C 42.5, H 7.42, N 3.84) and the FAB mass spectrum exhibited ion peaks which corresponded to  $[\text{Ru}_2\text{Cl}_8(\text{Py})](\text{TBA})$  (805 a.m.u.) and  $\text{Ru}_2\text{Cl}_8(\text{Py})$  (563 a.m.u.).

In addition the UV/VIS/NIR spectrum of the material (see Figure 4.12) consists of a band at 22,700 ( $\epsilon=8320$ ) and shoulders at 26,000 and  $33,300\text{cm}^{-1}$  which are assigned to  $\text{Cl} \rightarrow \text{Ru}(\text{III})$  charge transfers.

By virtue of having a pure sample of  $[\text{Ru}_2\text{Cl}_8(\text{Py})]^{2-}$  a full electrochemical study could now be carried out (see Figure 4.13). This revealed that the complex exhibited two reductive and two oxidative processes (in  $\text{CH}_2\text{Cl}_2/0.5\text{M}(\text{TBA})(\text{BF}_4)$  at 238K). Although the 2nd reductive process at  $-1.23\text{V}$  is totally irreversible even at 238K the first at  $-0.20\text{V}$  (a  $1e$  process) is fully reversible with  $i_a/i_c=1$  and  $\Delta E_p=48\text{mV}$  ( $\Delta E_p(\text{ideal})=47\text{mV}$ ) at  $100\text{mVs}^{-1}$ . The reversible nature of this process implies that substituting a terminal  $\text{Cl}^-$  by Py has stabilised the (III)(III)/(III)(II) couple which in the parent complex was only quasi-reversible at this temperature (238K). The substitution however destabilises the (III)(IV)/(IV)(IV) couple ( $+2.01\text{V}$ ) and it is thus only found to be

quasi-reversible. For the first oxidation at +1.26V,  $i_a/i_c=1$  and  $\Delta E_p=60\text{mV}$  at  $100\text{mVs}^{-1}$ . The larger  $\Delta E_p$  value of 60mV compared to the ideal value of 47mV (at 238K) possibly reflects the structural change involved on increasing the Ru-Ru vector (cf  $[\text{W}_2\text{Cl}_9]^{3/2-}$  mentioned earlier (26)).

As the first reduction and the first oxidation processes are reversible a study of two-mixed valence states on the same nuclear centres is possible. Such a study has not previously been attempted.

#### 4.2.4 Spectroelectrochemical synthesis of $[\text{Ru}_2\text{Cl}_8(\text{Py})]^{3-}$

The reduced species  $[\text{Ru}_2\text{Cl}_8(\text{Py})]^{3-}$  was formed in an O.T.T.L.E. cell at 238K by applying an electrogenerating potential of -0.4V vs Ag/AgCl in  $\text{CH}_2\text{Cl}_2/0.5\text{M}$  (TBA)( $\text{BF}_4$ ). The smooth conversion of  $[\text{Ru}_2\text{Cl}_8(\text{Py})]^{2-}$  to  $[\text{Ru}_2\text{Cl}_8(\text{Py})]^{3-}$  was exemplified by the isosbestic points observed at approximately 19500, 24500 and  $28500\text{cm}^{-1}$  (see Figure 4.14)

Figure 4.12: UV/Vis/NIR Spectrum of  $[\text{Ru}_2\text{Cl}_8(\text{Py})](\text{TBA})_2$  in  $\text{CH}_2\text{Cl}_2$

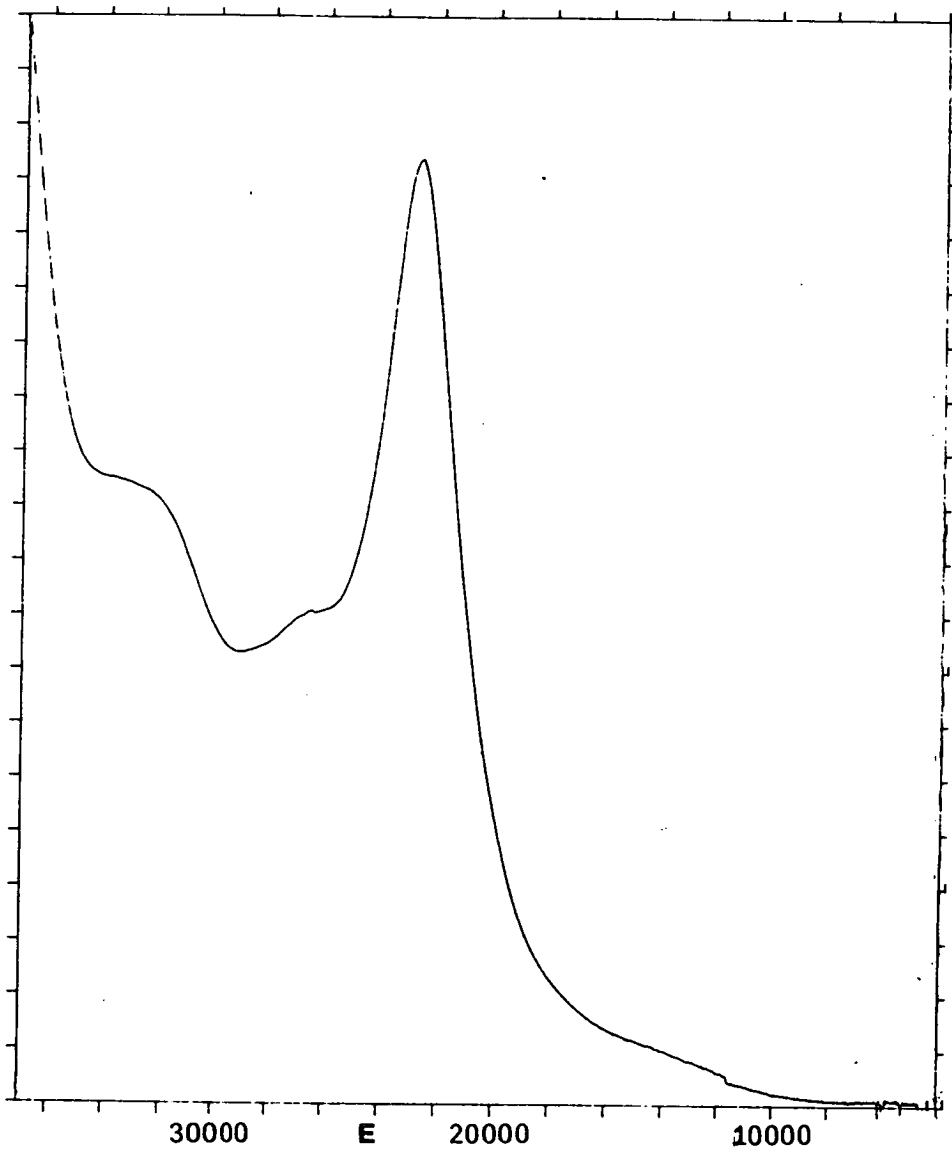




Figure 4.13 CV and AC Responses of  $[\text{Ru}_2\text{Cl}_8(\text{Py})](\text{TBA})_2$   
in  $\text{CH}_2\text{Cl}_2/0.5\text{M}(\text{TBA})(\text{BF}_4)$  at 238K

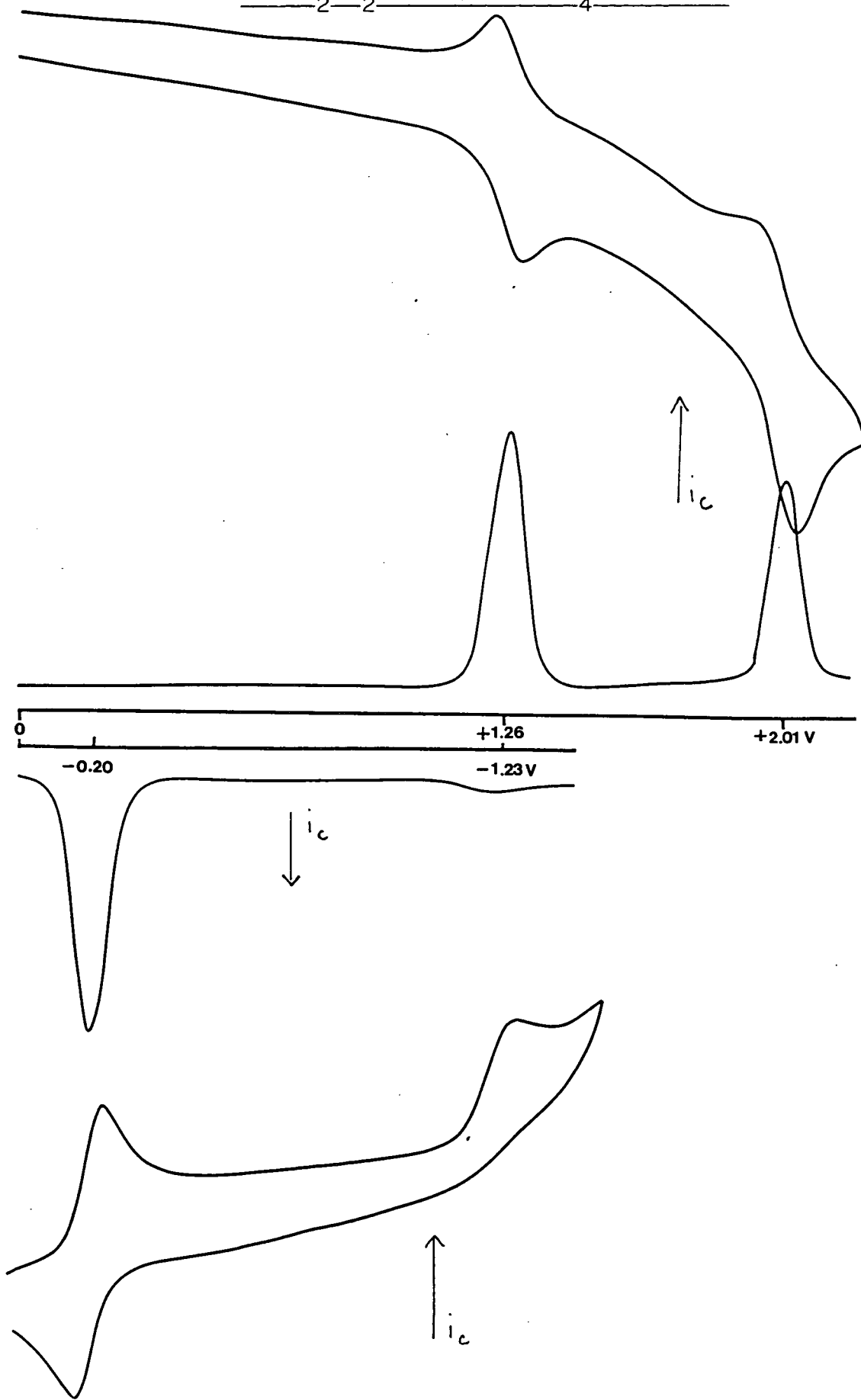
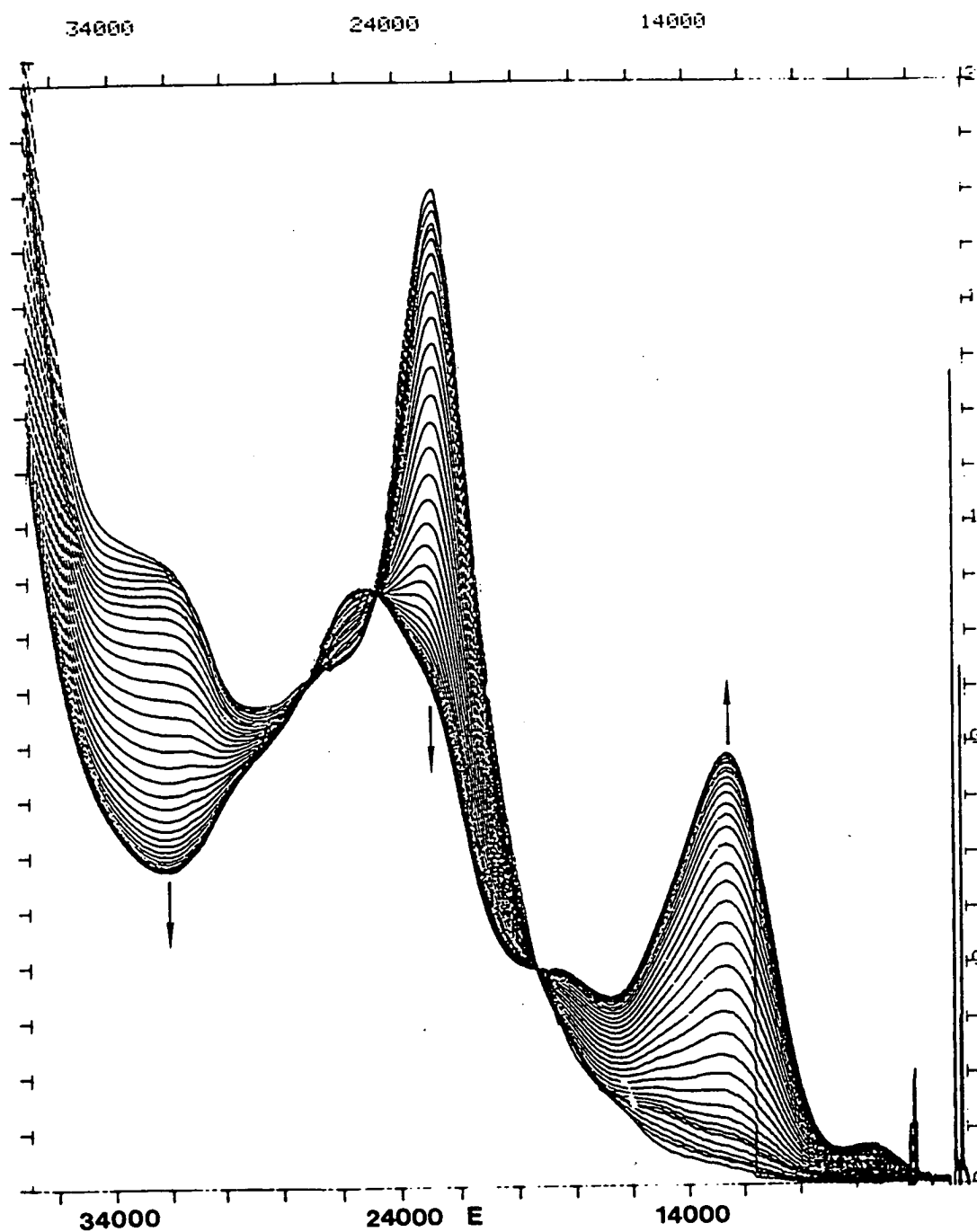


Figure 4.14 UV/Vis/NIR Spectra of  $[\text{Ru}_2\text{Cl}_8(\text{Py})]^{2-/3-}$  in  $\text{CH}_2\text{Cl}_2$  at 238K



On reversing the applied potential to OV the absorption spectra of  $[\text{Ru}_2\text{Cl}_8(\text{Py})]^{2-}$  was obtained in full i.e. no significant degradation of  $[\text{Ru}_2\text{Cl}_8(\text{Py})]^{2-}$  occurs during the redox process.

The complex  $[\text{Ru}_2\text{Cl}_8(\text{py})]^{3-}$  is blue in colour which is very reminiscent of the other ruthenium (II)(III) binuclear complexes with  $\sigma$ -donor terminal ligation. Such complexes as mentioned in Section 4.1.2. exhibit two absorption bands in the NIR/VIS/NIR region, the higher energy absorption being far more intense (see Table 4.4).

$[\text{Ru}_2\text{Cl}_8(\text{Py})]^{3-}$  is of a lower symmetry than these complexes and thus more than two transitions might be expected. This seems to be the case as although two bands are found at 7600(290) and  $12,600\text{cm}^{-1}$ (3440) a definite high energy shoulder is observed on the latter (see Figure 4.14).

Such metal based transitions should exhibit solvent invariant spectra (i.e.  $\nu_{\text{max}}$  independent of solvent) as no reorganisation of the solvent sheath is required for these transitions. This is observed experimentally as can be seen from Table 4.5.

Table 4.4    Molecular Orbital Transitions Observed for Some  
Blue Ruthenium (II)(III) Binuclear Complexes

Compound	e"-----a"		a'-----a"	
	$V_{\max}$ (cm <sup>-1</sup> )	$\epsilon$ (M <sup>-1</sup> cm <sup>-1</sup> )	$V_{\max}$ (cm <sup>-1</sup> )	$\epsilon$ (M <sup>-1</sup> cm <sup>-1</sup> )
$[(\text{NH}_3)_3\text{RuCl}_3\text{Ru}(\text{NH}_3)_3]^{2+}$	7,410	230	17,180	4,300
$[(\text{H}_2\text{O})_3\text{RuCl}_3\text{Ru}(\text{H}_2\text{O})_3]^{2+}$	unresolved		16,500	1,150
$[[9]\text{aneN}_3\text{RuCl}_3\text{Ru}([9]\text{aneN}_3)]^{2+}$	not reported		16,450	6,600

Table 4.5  $V_{\max}$  for the  $e'' \rightarrow a''$  and  $a' \rightarrow a''$  Transitions on  
Variation of Solvent at 248K

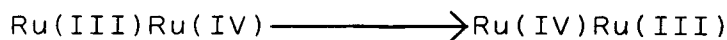
<u>Solvent</u>	<u><math>V_{\max}(\text{cm}^{-1})</math></u>	
	$e'' \rightarrow a''$	$a' \rightarrow a''$
$\text{CH}_2\text{Cl}_2$	7,600	12,600
Acetone	7,600	12,550
MeCN	7,550	12,650

These observations suggest that there is a strong metal-metal interaction in the mixed valence complex  $[\text{Ru}_2\text{Cl}_8(\text{Py})]^{3-}$ . Thus although the complex is asymmetric the resultant energy difference between the metal based " $t_{2g}$ " orbitals on the two Ru centres is insufficient to preclude extensive metal-metal interactions.

#### 4.2.5 Spectroelectrochemical Synthesis of $[\text{Ru}_2\text{Cl}_8(\text{Py})]^-$

Smooth conversion to  $[\text{Ru}_2\text{Cl}_8(\text{Py})]^-$  was observed on holding the electrogenerating potential at +1.4V(vs Ag/AgCl in  $\text{CH}_2\text{Cl}_2/0.5\text{M}(\text{TBA})(\text{BF}_4)$  at 238K in an O.T.T.L.E. cell with isosbestic points occurring at approx 20500, 28000, 30500, 32000, 39000, and 42500 $\text{cm}^{-1}$  (see Figure 4.15) Again on reversing the applied potential to 0V the absorption spectra of  $[\text{Ru}_2\text{Cl}_8(\text{Py})]^{2-}$  was obtained in full i.e. no significant degradation had occurred.

It can be seen that for  $[\text{Ru}_2\text{Cl}_8(\text{Py})]^-$  only one low energy band at 10250 $\text{cm}^{-1}$  (2220) is observed and it is assigned as an IVCT band i.e.



which can be compared to the analogous transition at 10300 $\text{cm}^{-1}$  for  $[\text{Ru}_2\text{Cl}_9]^{2-}$  (17)

However in order to confirm the IVCT assignment a solvent dependancy study was carried out and the values of  $\alpha^2$  and  $\nu_{\frac{1}{2}}(\text{theo})$  were calculated.

Experimental values for the bands solvent dependancy are given in Table 4.6 and plotted in Figure 4.16. As can be seen although  $E_{\text{op}}$  varies considerably the plot of  $E_{\text{op}}$  vs  $(\frac{1}{n^2} - \frac{1}{n_D^2})$  is not linear.

Figure 4.15 UV/Vis/NIR Spectra of  $[\text{Ru}_2\text{Cl}_8(\text{Py})]^{2-}$  in  $\text{CH}_2\text{Cl}_2$  at 238K

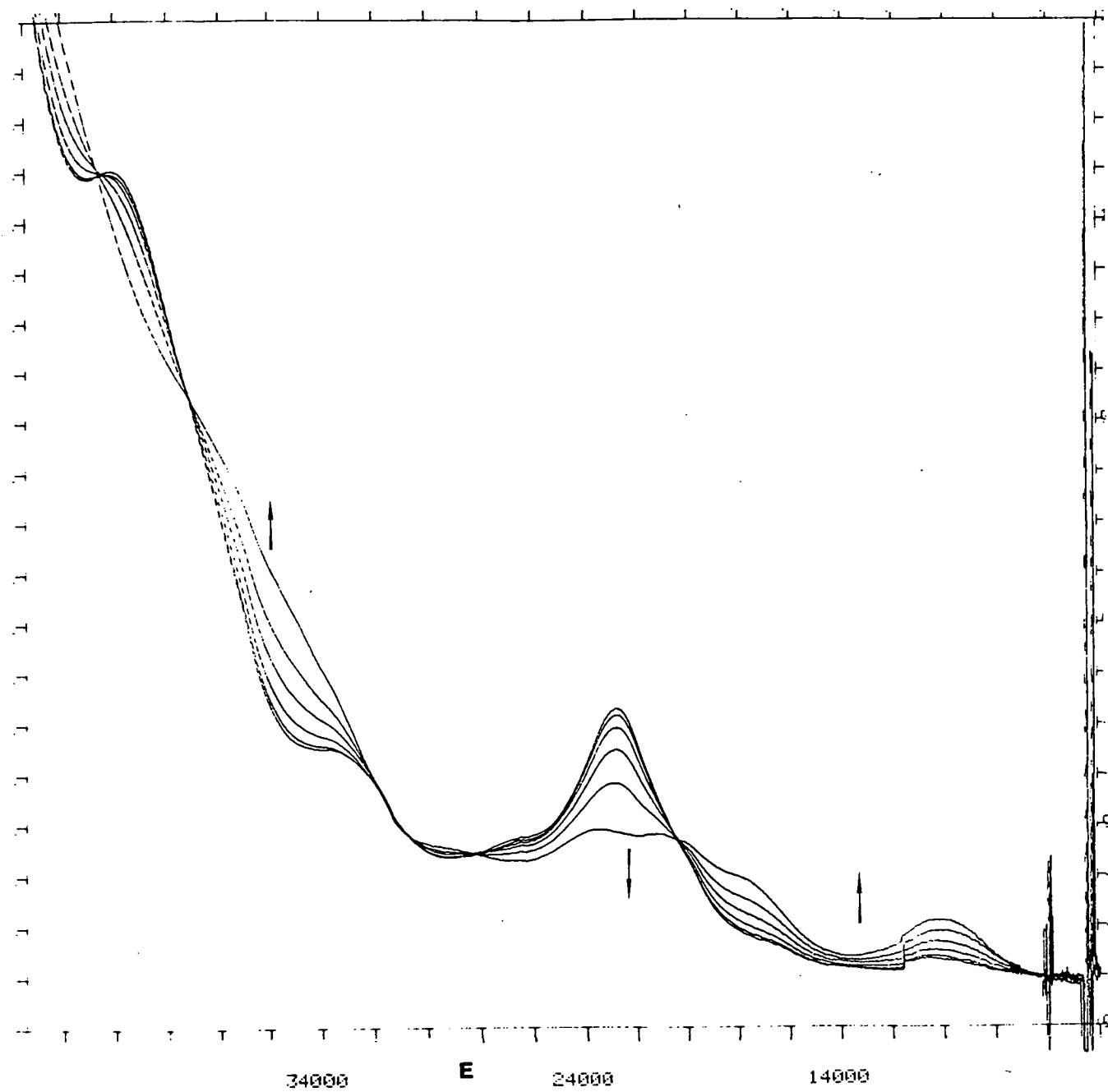
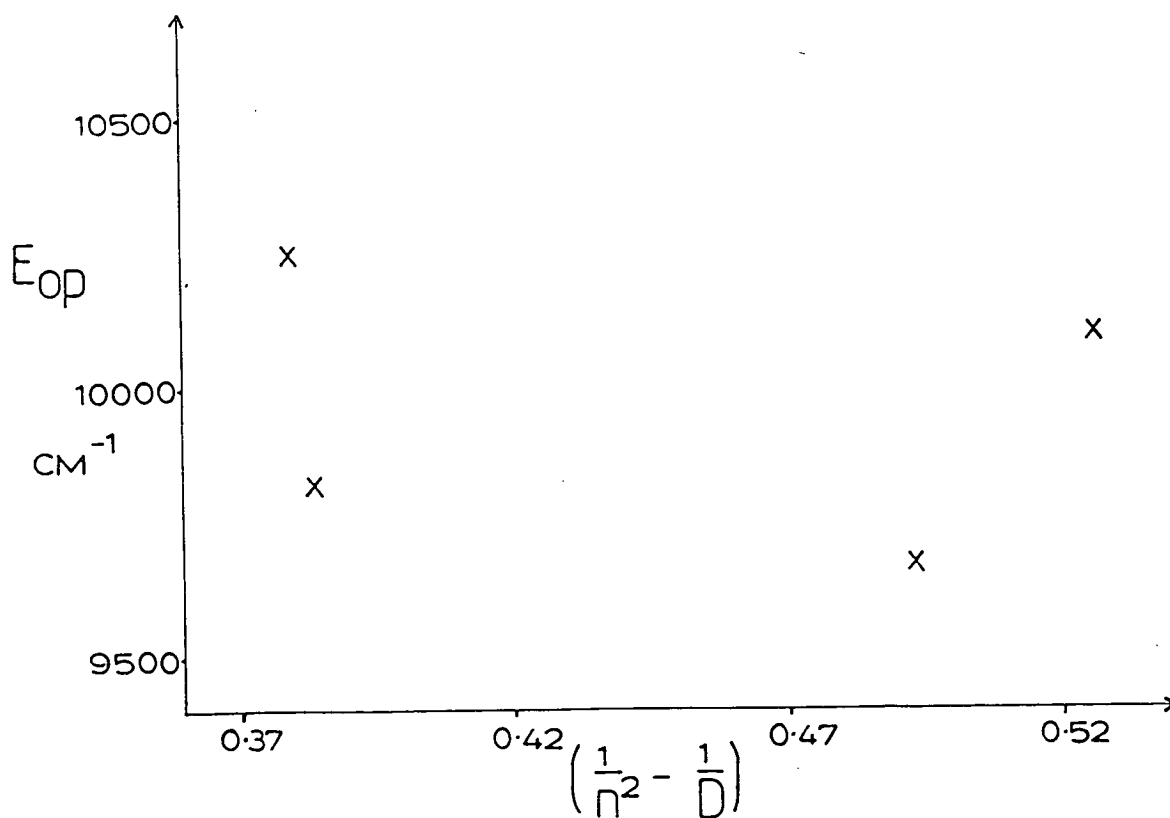


Table 4.6 Experimental Values of  $E_{op}$  for  $[\text{Ru}_2\text{Cl}_8(\text{Py})]^-$  in Various Solvents

<u>Solvent</u>	<u><math>E_{op}</math> (<math>\text{cm}^{-1}</math>)</u>
$\text{CH}_2\text{Cl}_2$	10,250
Acetone	9,675
MeCN	10,100
Nitrobenzene	9,825

Figure 4.16 Plot of  $E_{op}$  vs  $(1/n^2 - 1/D)$  for  $[\text{Ru}_2\text{Cl}_8(\text{Py})]^-$  in Various Solvents





This implies that the value of  $E_{op}$  is affected not only by  $n$  and  $D$  but also by the direct interaction of  $[\text{Ru}_2\text{Cl}_8(\text{Py})]^-$  with the solvent (previously observed by other workers for LMCT and MLCT transitions <sup>(29)</sup>), and/or the electrolyte.

Such interaction is probably responsible for the observed degradation of  $[\text{Ru}_2\text{Cl}_8(\text{Py})]^-$  in solvents other than  $\text{CH}_2\text{Cl}_2$  and thus extinction coefficients cannot be quoted. This is in contrast to  $[\text{Ru}_2\text{Cl}_8(\text{Py})]^{3-}$  which was not observed to be degraded by solvent.

However the variation of  $E_{op}$  in conjunction with the calculated values of  $\alpha^2 = 0.04$  ( $r$  assumed to equal  $3.11\text{nm}$ ) and  $\Delta V_{1/2}(\text{theo}) = 4870\text{cm}^{-1}$  ( $\Delta V_{1/2}(\text{exp}) = 4400\text{cm}^{-1}$ ) confirms that the interaction between the two metal centres is Class II in nature.

#### 4.3 Conclusions

This study has shown that  $[\text{Ru}_2\text{Cl}_8(\text{Py})]^{2-}$  can be synthesised chemically and by the originally conceived electrochemical method. Further investigation into chromatographic purification of the latter's product mixture may show that isomers of  $[\text{Ru}_2\text{Cl}_7(\text{Py})_2]^{n-}$  were also formed.

The substitution of  $\text{Cl}^-$  by  $L$ , in this case  $\text{Py}$ , to give  $[\text{Ru}_2\text{Cl}_8(\text{Py})]^{2-}$  yielded, as was hoped a complex which exhibited two stable mixed oxidation state species. Subsequent

investigations have shown that differing metal-metal interactions were involved for the two mixed-valence systems. It is thought that this is the first example of such behaviour and is certainly the first asymmetric complex of the family  $[L_{(3-x)}Cl_xRuCl_3RuCl_yL_{(3-y)}]^{n+/-}$  to exhibit strong metal-metal interactions in the (III)(II) state.

#### 4.4 Experimental

Physical measurements were performed as described in Chapters 2 and 3. The O.T.T.L.E. experiments carried out in acetonitrile, acetone and nitrobenzene employed 0.1M solutions of (TBA)(BF<sub>4</sub>).

#### Reagents

Methylenechloride was allowed to stand for one week over KOH pellets and dried by distillation over P<sub>2</sub>O<sub>5</sub>. All other solvents were used as supplied. [Ru<sub>2</sub>Cl<sub>9</sub>](TBA)<sub>3</sub> was prepared by the method of Coombe.<sup>(17)</sup>

#### [Ru<sub>2</sub>Cl<sub>8</sub>(Py)](TBA)<sub>2</sub>

[Ru<sub>2</sub>Cl<sub>9</sub>](TBA)<sub>3</sub> (136mg, 1.09x10<sup>-4</sup>mmol), Ag(ClO<sub>4</sub>) (1.09x10<sup>-4</sup>mmol) and Py (1.10x10<sup>-4</sup>mmol) were refluxed in degassed CH<sub>2</sub>Cl<sub>2</sub> (8ml) in a darkened room. By injecting a small sample of the reaction solution into an electrochemical cell, the reaction could be monitored by a.c. voltammetry. After 24 hours this analysis indicated that the reaction had ceased at about 80% conversion. However, on addition of Ag(ClO<sub>4</sub>) (0.24mmol), conversion resumed and the solution was held at reflux for a further 24 hours. The brown solution was filtered through celite, then, after partial removal of the solvent, was passed down a Sephadex LH20 column (CH<sub>2</sub>Cl<sub>2</sub> eluent). The central fraction of the band formed was isolated

isolated and on addition of an excess of diethylether a brown precipitate formed. This was collected, washed with diethylether (10ml) and dried in vacuo. Yield 60.2mg 53%.

Mol.Wt. 1049.8. Found C 42.5, H 7.42, N 3.84 Calc for  $\text{Ru}_2\text{Cl}_8\text{N}_3\text{C}_{37}\text{H}_{77}$  C 42.3, H 7.39, N 4.00%. I.R.  $\nu_{(\text{RuCl})}$  310 and 340,  $\nu_{(\text{C}=\text{C})}$  (Py)  $1600\text{cm}^{-1}$ . UV/Vis/NIR 22700 ( $\epsilon = 8320\text{M}^{-1}\text{cm}^{-1}$ ) 26000 and  $33300\text{cm}^{-1}$ . FAB mass spectrum: Found  $\text{M}^+ = 805, 563$

<u>Calculated for</u>	<u><math>\text{M}^+</math></u>
$^{102}\text{Ru}_2\ ^{35}\text{Cl}_8\text{NC}_5\text{H}_5$ (TBA)	805
$^{102}\text{Ru}_2\ ^{35}\text{Cl}_8\text{NC}_5\text{H}_5$	563

References

1. J. Chatt and R. G. Hayter, J. Chem. Soc., 1961, 896.
2. K.A. Raspin, J. Chem. Soc. A., 1969, 3, 461.
3. E.E. Mercer and L. W. Gray, J. Am. Chem. Soc., 1972, 94, 6427.
4. J.K. Beattie, P. Del Favera, T. W. Hambley and N. S. Hush, Inorg. Chem., 1988, 27, 2000.
5. N. W. Alcock and K. A. Raspin, J. Chem. Soc. A., 1968, 2108.
6. P. W. Armit, W. J. Sime and T. A. Stephenson, J. Chem. Soc. Dalton Trans., 1976, 2121.
7. P. W. Armit, T. A. Stephenson and E. S. Switkes, J. Chem. Soc. Dalton Trans., 1974, 1134.
8. T. V. Ashworth, N. J. Nolte and E. Singleton J. Chem. Soc. Chem. Commun., 1977, 936.
9. A. J. Lindsay, PhD Thesis, University of Edinburgh 1982.
10. J. K. Nicholson, Angew. Chem. Int. Ed. Engl., 1967, 6, 264
11. J. Darriet, Rev. Chim. Miner., 1981, 18, 27.
12. J. E. Ferguson, and A. M. Greenaway, Aust. J. Chem., 1978, 31, 497.
13. M. B. Hursthouse, R. A. Jones, K. M. A. Malik and G. Wilkinson, J. Am. Chem. Soc., 1979, 4128.
14. R. A. Jones, G. Wilkinson, I. J. Colquhoun, W. McFarlane, A. M. R. Galas and M. B. Hursthouse, J. Chem. Soc. Dalton Trans., 1980, 2480.
15. R. A. Contreras-Zarate, PhD Thesis, University of Edinburgh, 1981.

16. T. Arthur, PhD Thesis, University of Edinburgh, 1980.
17. V. T. Coombe, PhD Thesis, University of Edinburgh, 1985.
18. M. B. Robin and P. Day, Advan. Inorg. Chem. Radiochem., 1967, 10, 247.
19. N. S. Hush, Prog. in. Inorg. Chem., 8, 391.
20. K. Wieghart, W. Herrmann and M. Koppen, Z. Naturforsch B., 1984, 39, 1335.
21. G. A. Heath, A. J. Lindsay, T. A. Stephenson and D. K. Vattis, J. Organomet. Chem., 1982, 233, 353.
22. N. S. Hush, J. K. Beattie and V. M. Ellis, Inorg. Chem., 1984, 23, 3339.
23. R. Sorbie, University of Edinburgh, unpublished work.
24. R. H. Summerville and R. Hoffmann, J. Am. Chem. Soc., 1979 101, 3821.
25. G. C. Allen and N. S. Hush, Prog. Inorg. Chem., 8, 357.
26. F. A. Cotton and L. R. Favello, Inorg. Chem., 1983, 22, 2621.
27. A. Cunningham, University of Edinburgh, 4 year project, 1985.
28. K. Taylor, University of Edinburgh, unpublished work.
29. J. C. Curtis, B. P. Sullivan and T. J. Meyer, Inorg. Chem. 1983, 22, 224.

**Chapter 5**

**Heterotrimetallic Complexes of Ru(II)**

### 5.1 Introduction

In an attempt to synthesise a fluoro-bridged binuclear species Easton and Stephenson <sup>(1)</sup> treated  $\text{RuCl}_2(\text{PEtPh}_2)_3$  with  $\text{Ag}_2\text{CO}_3$  and aqueous HF in MeOH. However, instead of yielding the desired fluoride species the reaction product proved to be the novel heterotrimetallic complex  $\text{Ru}_2\text{Cl}_5(\text{PEtPh}_2)_4 \cdot \text{Ag}(\text{PEtPh}_2)$  (63). Subsequently, this species could be prepared by a rational synthetic route by treatment of  $\text{AgCl}$  or  $\text{AgCl}(\text{PEtPh}_2)_2$  with  $\text{RuCl}_2(\text{PEtPh}_2)_3$ ,  $\text{Ru}_2\text{Cl}_4(\text{PEtPh}_2)_5$  or  $[\text{Ru}_2\text{Cl}_3(\text{PEtPh}_2)_6] \text{Cl}$  in MeOH. The postulated pathways to (63) are shown in Scheme 5.1.

Variable Temperature  $^{31}\text{P}$ -( $^1\text{H}$ ) n.m.r. spectra of (63) are shown in Figures 5.1 and 5.2. At 183K the spectrum (see Figure 5.2) is consistent with the single crystal X-ray structure which revealed that the  $[\text{Ag}(\text{PEtPh}_2)]^+$  moiety is bound to one terminal and asymmetrically to two bridging chlorides of the  $[(\text{PEtPh}_2)_2\text{ClRuCl}_3\text{RuCl}(\text{PEtPh}_2)_2]^-$  unit (i.e. there is no plane of symmetry). Thus, two AB signals are observed for the Ru-bound  $\text{PEtPh}_2$  ligands, one centred at 50.0p.p.m. ( $J_{\text{AB}} = 42\text{Hz}$ ,  $V_{\text{AB}} = 58\text{Hz}$ ) and the other at 48.4p.p.m. ( $J_{\text{AB}} = 36\text{Hz}$ ,  $V_{\text{AB}} = 284\text{Hz}$ ) as well as two characteristic doublets centred at 10 p.p.m. for the Ag bound  $\text{PEtPh}_2$  ligand ( $J_{109_{\text{Ag}}^{31}\text{P}} = 771\text{Hz}$ ,  $J_{107_{\text{Ag}}^{31}\text{P}}$ )).



Scheme 5.1: Postulated Pathways for the Synthesis of

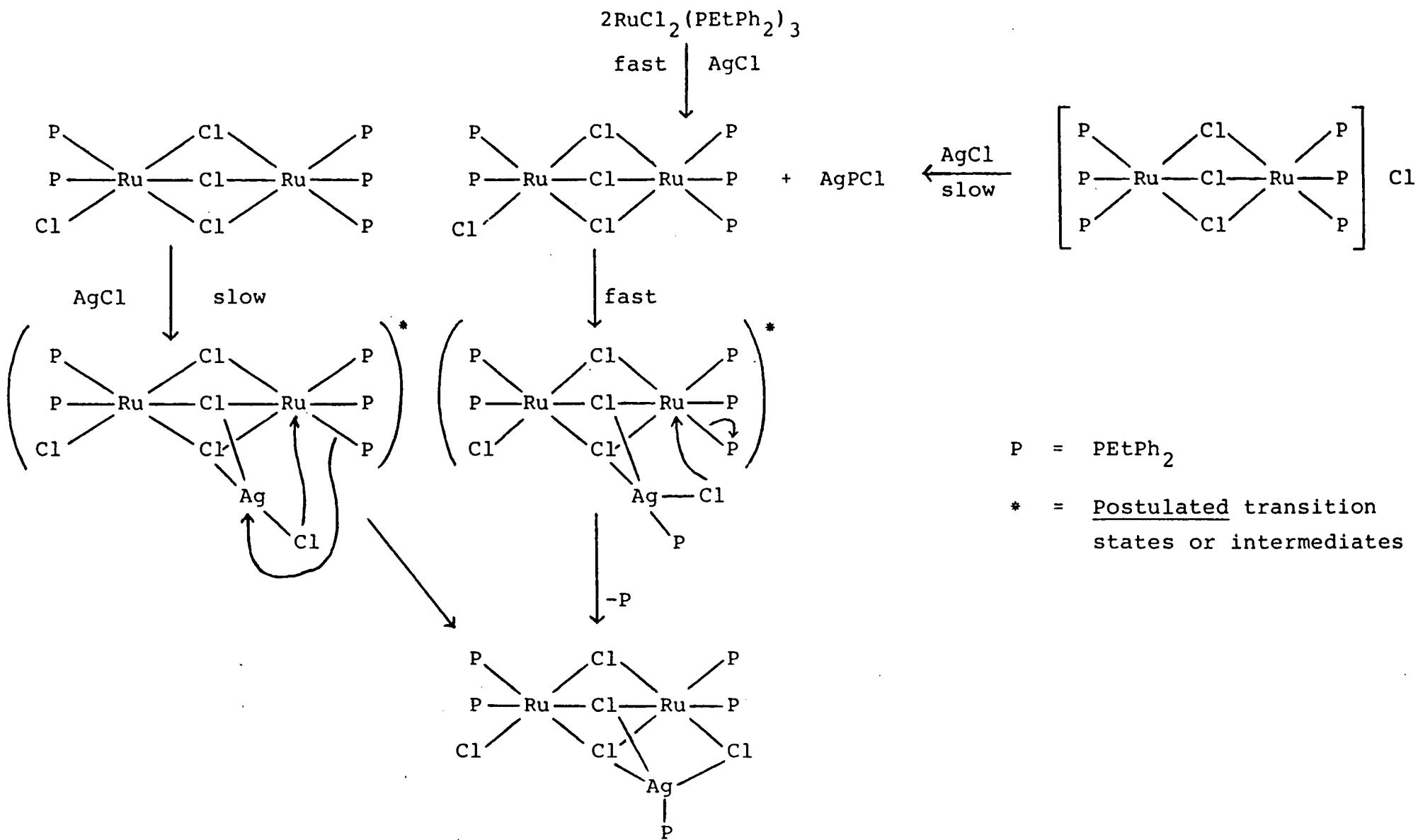
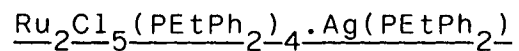


Figure 5.1:  $^{31}\text{P}$ -( $^1\text{H}$ )n.m.r. Spectrum of  
 $\text{Ru}_2\text{Cl}_5(\text{PEtPh}_2)_4 \cdot \text{Ag}(\text{PEtPh}_2)_2$  at 183K in  $\text{CD}_2\text{Cl}_2$

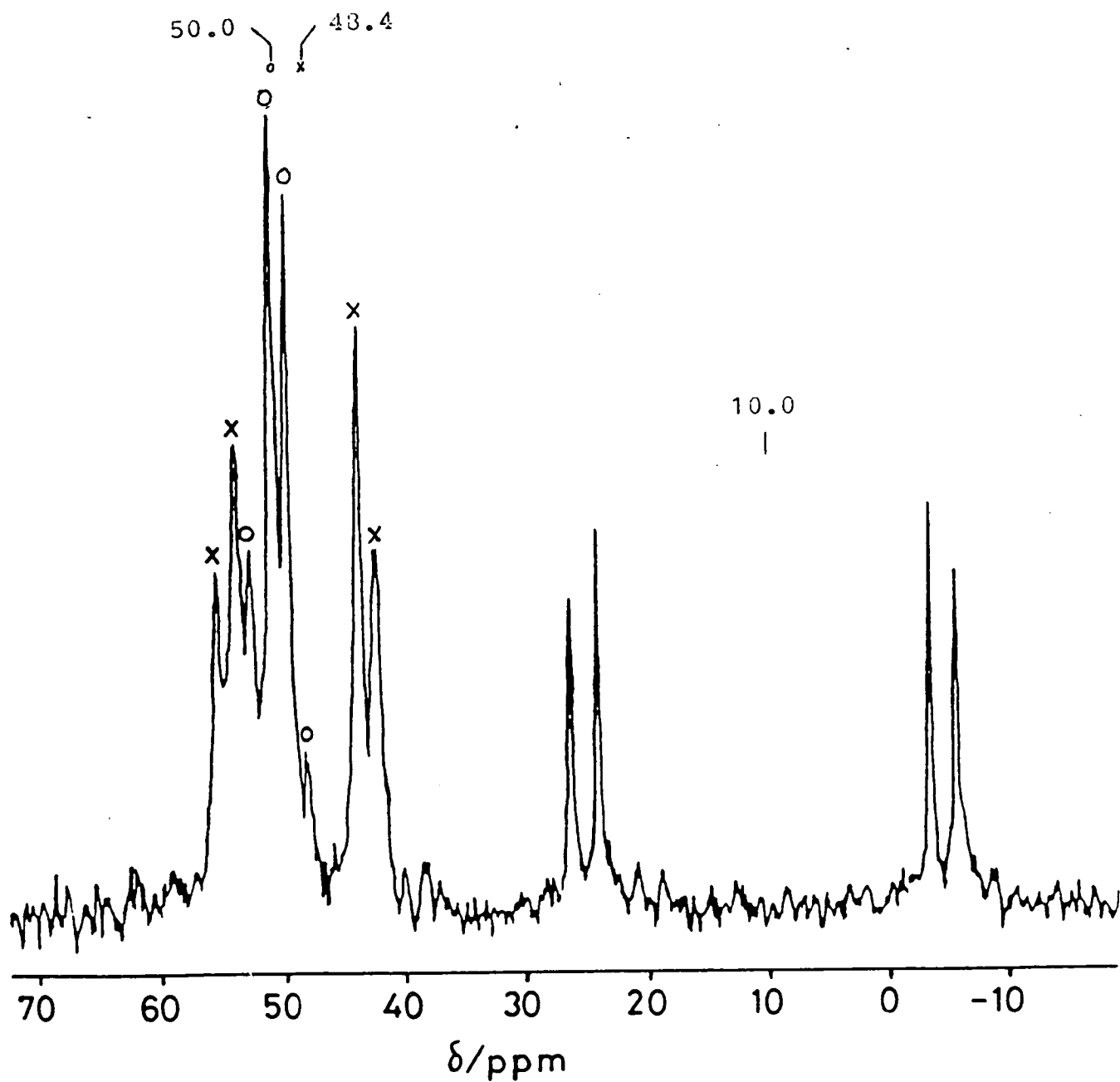
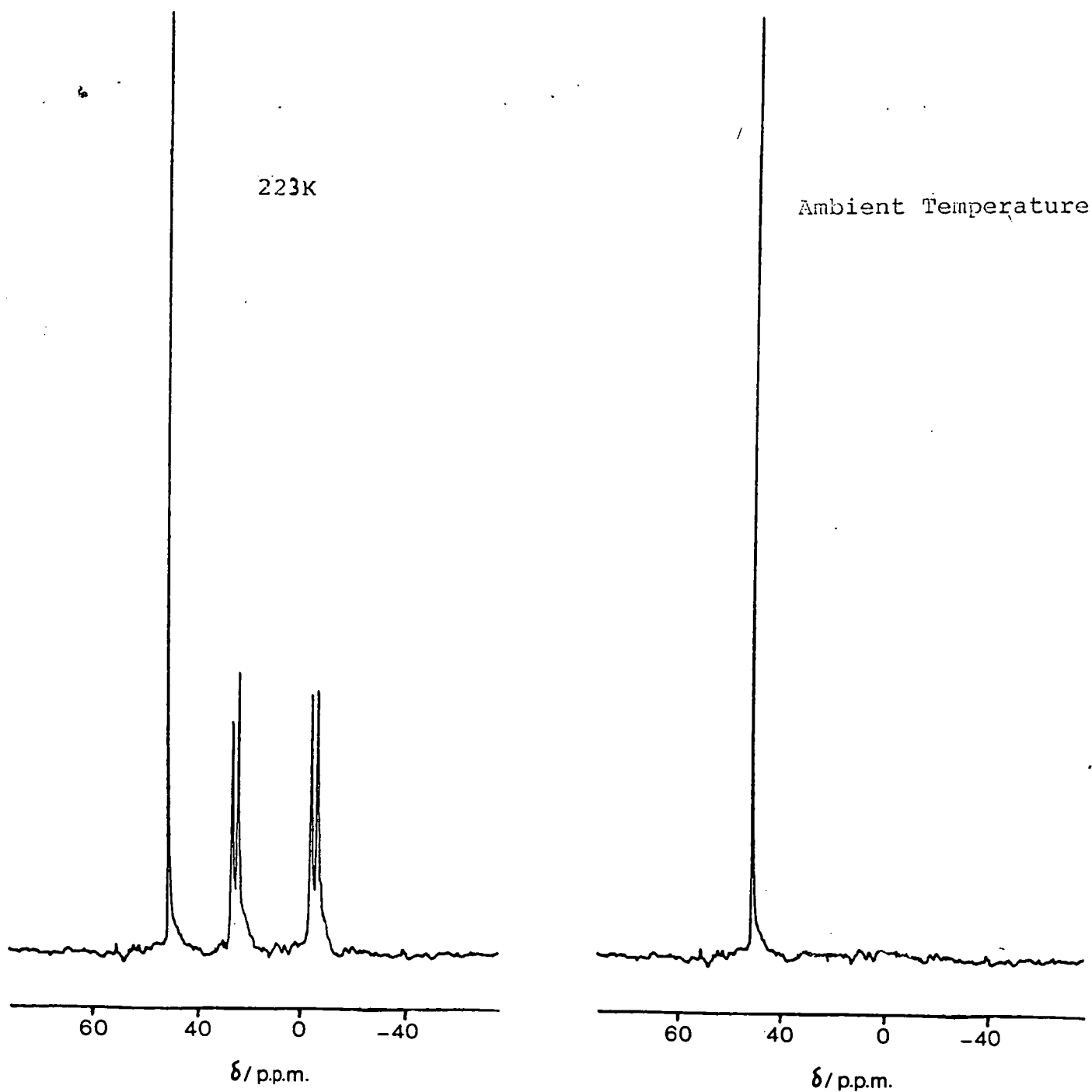


Figure 5.2:  $^{31}\text{P}$ -( $^1\text{H}$ ) n.m.r. Spectrum of  $\text{Ru}_2\text{Cl}_5(\text{PEtPh}_2)_4 \cdot \text{Ag}(\text{PEtPh}_2)$  at 223K and Ambient Temperature in  $\text{CD}_2\text{Cl}_2$



On warming, two separate fluxional processes are observed. The first results in the coalescence of the two AB signals to give a singlet at 48.9p.p.m. (see Figure 5.2a). This was attributed to the  $[\text{Ag}(\text{PEtPh}_2)]^+$  moiety switching between the two equivalent sites offered by the  $[(\text{PEtPh}_2)_2\text{ClRuCl}_3\text{RuCl}(\text{PEtPh}_2)_2]^-$  unit (i.e. an intramolecular exchange), the X-ray structure having revealed the proximity of the other terminal chloride ( $\text{Ag}\cdots\text{Cl} = 3.457(6)\text{\AA}$ ). The second fluxional process is a specific intermolecular tertiary phosphine exchange which results in the collapse of the signal associated with the Ag centre (see Figure 5.2b). This process is consistent with the kinetic lability of simple Ag(I) tertiary phosphine compounds<sup>(2)</sup>.

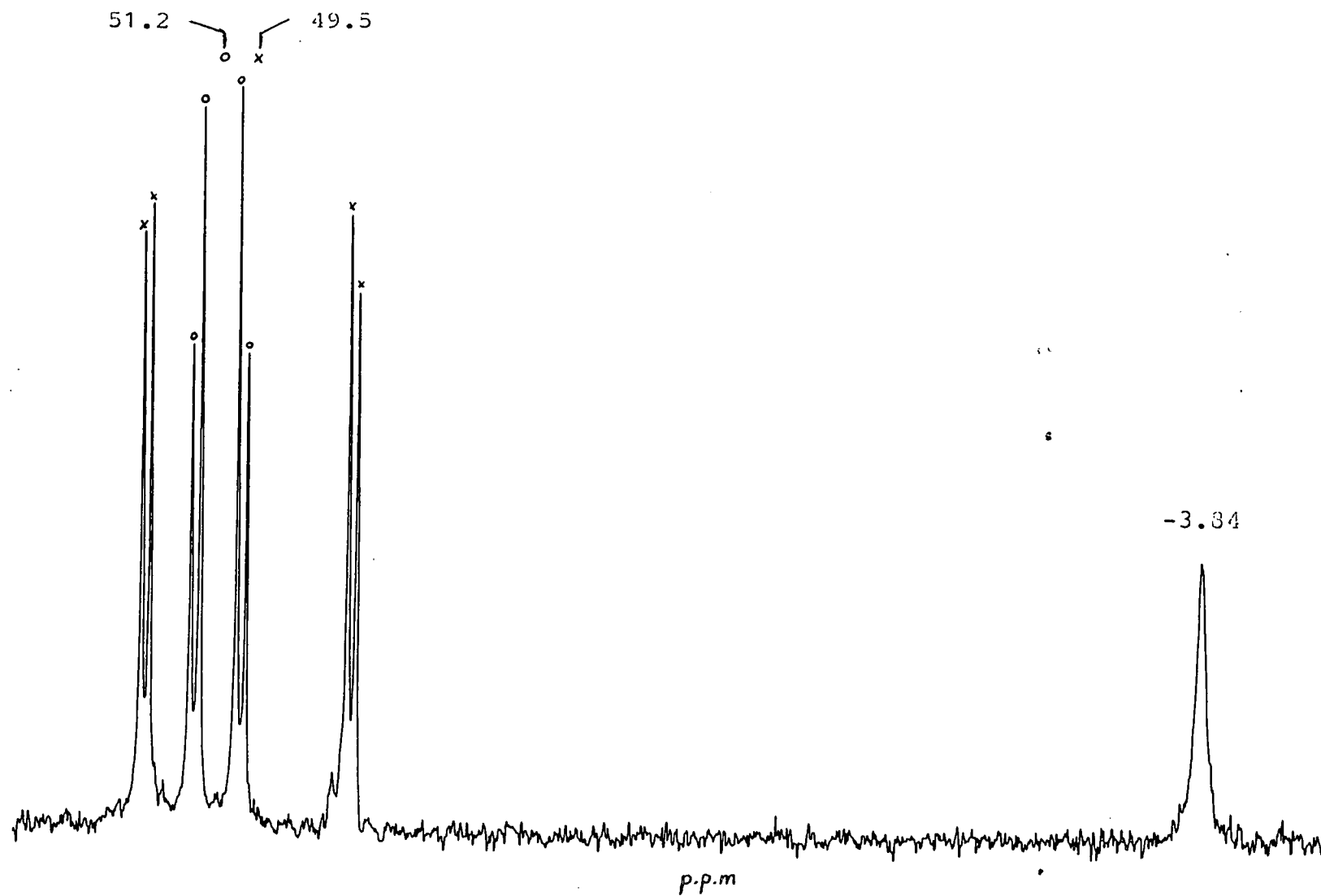
The aim of the present study was to synthesise further examples of these interesting species. As Easton and Stephenson had found that other Ru(II) chlorophosphine complexes did not react with AgCl, the present study concentrated on the variation of the  $d^{10}$  metal and the halide.

## 5.2 Results and Discussion

### 5.2.1 CuCl

Reaction of CuCl with two molar equivalents of  $\text{RuCl}_2(\text{PEtPh}_2)_3$  in MeOH yielded a salmon pink precipitate over a period of 3 hours. The product, recrystallised from a  $\text{CH}_2\text{Cl}_2/\text{MeOH}$  solvent system, analysed for  $\text{Ru}_2\text{Cl}_5(\text{PEtPh}_2)_4 \cdot \text{Cu}(\text{PEtPh}_2) \cdot \text{CH}_2\text{Cl}_2$ .

Figure 5.3:  $^{31}\text{P}$ -( $^1\text{H}$ ) n.m.r. Spectrum of  
 $\text{Ru}_2\text{Cl}_5(\text{PEtPh}_2)_4 \cdot \text{Cu}(\text{PEtPh}_2)_2$  at 184K in  $\text{CD}_2\text{Cl}_2$



The  $^{31}\text{P}$ -( $^1\text{H}$ ) n.m.r. spectrum of the complex at 184K (see Figure 5.3) exhibits two AB patterns for the Ru-bound  $\text{PEtPh}_2$  ligands, one centred at 51.2p.p.m. ( $J_{\text{AB}} = 42.5\text{Hz}$ ,  $\nu_{\text{AB}} = 205\text{Hz}$ ) and the other at 49.5p.p.m. ( $J_{\text{AB}} = 38.1\text{Hz}$ ,  $\nu_{\text{AB}} = 932\text{Hz}$ ). In addition a singlet at -3.84p.p.m. for the Cu-bound  $\text{PEtPh}_2$  ligand is also observed. Like the silver analogue the spectrum at ambient temperature consisted of a singlet (50.0p.p.m) for the magnetically equivalent Ru-bound  $\text{PEtPh}_2$  ligands, due to intra-and intermolecular fluxional processes.

The  $^{31}\text{P}$ -( $^1\text{H}$ )n.m.r. spectral data indicated that the solid state geometry of (64) would be analogous to the silver complex (63). However, it was of interest to see if there was any significant difference in the  $[(\text{PEtPh}_2)_2\text{ClRuCl}_3\text{RuCl}(\text{PEtPh}_2)_2]^-$  unit in (63) and (64) due to the different atomic radii of Ag(I) and Cu(I) (1.26 and 0.96 respectively)<sup>(3)</sup>.

Crystals suitable for a single crystal X-ray analysis could be grown by the slow diffusion of MeOH into a  $\text{CH}_2\text{Cl}_2$  solution of the complex. Details of the structural solution, which converged to give a final R factor of 5.57%, are given in the experimental section. An ortep plot of the structure (H's removed for clarity) is given in Figure 5.4 while selected bond lengths, bond angles and torsion angles are given in Tables 5.1-3.

Figure 5.4: Ortep Plot of  $\text{Ru}_2\text{Cl}_5(\text{PEtPh}_2)_4 \cdot \text{Cu}(\text{PEtPh}_2)_2$

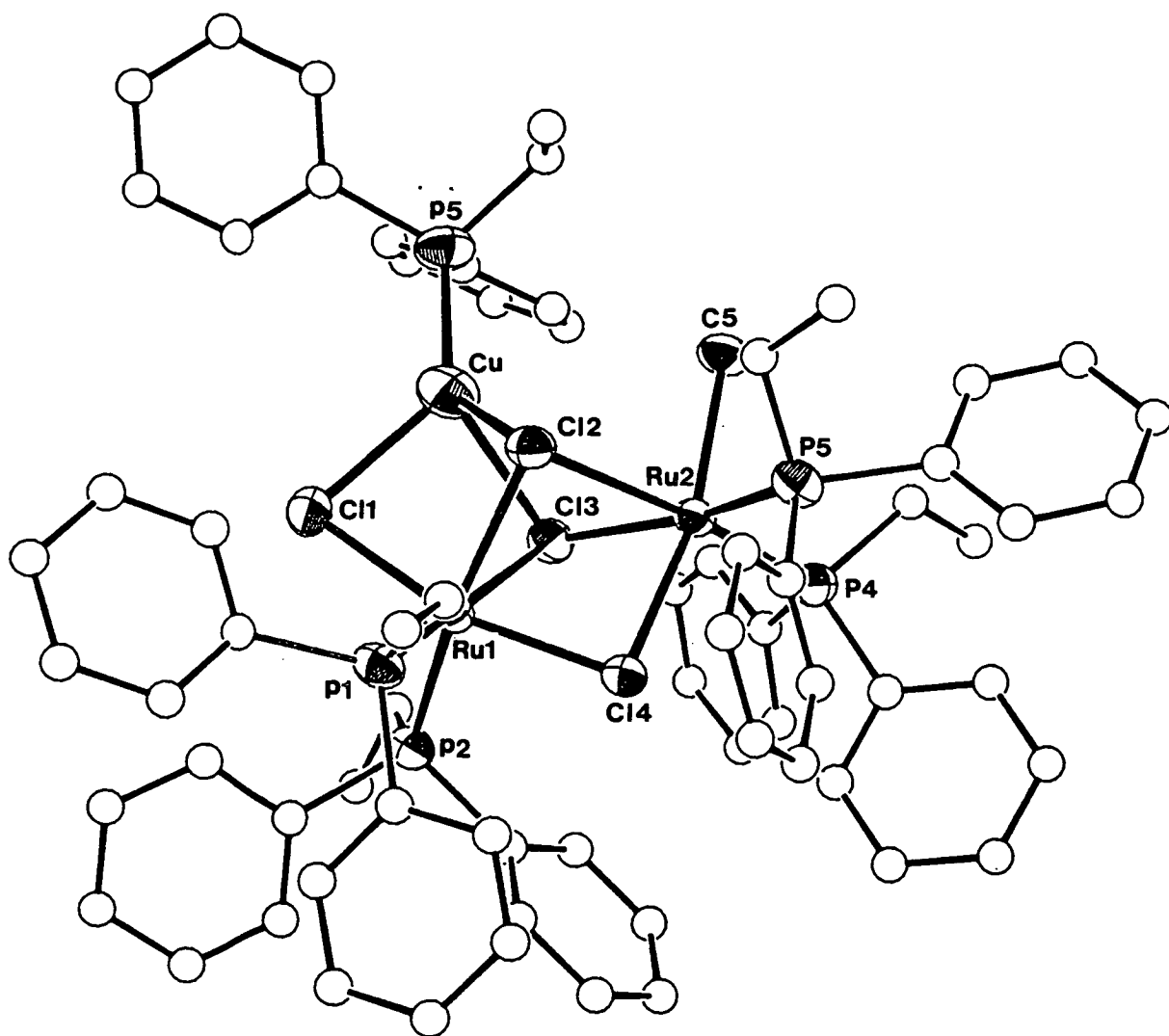


Table 5.1: Selected Bond Lengths (Å) with Standard Deviations

for  $\text{Ru}_2\text{Cl}_5(\text{PEtPh}_2)_4 \cdot \text{Cu}(\text{PEtPh}_2)$ 

Ru(1) -Ru(2)	3.3326( 8)	Ru(2) -Cl(3)	2.5823(18)
Ru(1) -Cu(1)	3.1509(12)	Ru(2) -Cl(4)	2.4112(18)
Ru(1) -Cl(1)	2.4376(21)	Ru(2) -Cl(5)	2.3959(20)
Ru(1) -Cl(2)	2.5047(18)	Ru(2) - P(3)	2.2715(21)
Ru(1) -Cl(3)	2.5504(18)	Ru(2) - P(4)	2.2645(21)
Ru(1) -Cl(4)	2.3731(18)	Cu(1) -Cl(1)	2.4071(22)
Ru(1) - P(1)	2.2560(20)	Cu(1) -Cl(2)	2.5188(20)
Ru(1) - P(2)	2.2869(20)	Cu(1) -Cl(3)	2.4423(20)
Ru(2) -Cl(2)	2.5028(18)	Cu(1) - P(5)	2.1768(25)

Table 5.2: Selected Bond Angles (°) with Standard Deviations

for  $\text{Ru}_2\text{Cl}_5(\text{PEtPh}_2)_4 \cdot \text{Cu}(\text{PEtPh}_2)$ 

Ru(2) -Ru(1) -Cu(1)	68.920(24)	Cl(2) -Ru(2) -Cl(3)	76.19( 6)
Ru(2) -Ru(1) -Cl(1)	117.67( 5)	Cl(2) -Ru(2) -Cl(4)	81.44( 6)
Ru(2) -Ru(1) -Cl(2)	48.25( 4)	Cl(2) -Ru(2) -Cl(5)	88.95( 6)
Ru(2) -Ru(1) -Cl(3)	49.93( 4)	Cl(2) -Ru(2) - P(3)	95.32( 7)
Ru(2) -Ru(1) -Cl(4)	46.32( 4)	Cl(2) -Ru(2) - P(4)	166.33( 7)
Ru(2) -Ru(1) - P(1)	118.94( 5)	Cl(3) -Ru(2) -Cl(4)	80.29( 6)
Ru(2) -Ru(1) - P(2)	122.70( 5)	Cl(3) -Ru(2) -Cl(5)	89.85( 6)
Cu(1) -Ru(1) -Cl(1)	49.01( 5)	Cl(3) -Ru(2) - P(3)	171.46( 7)
Cu(1) -Ru(1) -Cl(2)	51.35( 5)	Cl(3) -Ru(2) - P(4)	90.19( 7)
Cu(1) -Ru(1) -Cl(3)	49.36( 4)	Cl(4) -Ru(2) -Cl(5)	167.59( 7)
Cu(1) -Ru(1) -Cl(4)	115.17( 5)	Cl(4) -Ru(2) - P(3)	97.70( 7)
Cu(1) -Ru(1) - P(1)	123.48( 6)	Cl(4) -Ru(2) - P(4)	95.39( 7)
Cu(1) -Ru(1) - P(2)	124.90( 6)	Cl(5) -Ru(2) - P(3)	90.96( 7)
Cl(1) -Ru(1) -Cl(2)	83.98( 6)	Cl(5) -Ru(2) - P(4)	92.12( 7)
Cl(1) -Ru(1) -Cl(3)	87.26( 6)	P(3) -Ru(2) - P(4)	98.28( 7)
Cl(1) -Ru(1) -Cl(4)	163.91( 7)	Ru(1) -Cu(1) -Cl(1)	49.85( 5)
Cl(1) -Ru(1) - P(1)	93.99( 7)	Ru(1) -Cu(1) -Cl(2)	50.95( 5)
Cl(1) -Ru(1) - P(2)	99.54( 7)	Ru(1) -Cu(1) -Cl(3)	52.41( 5)
Cl(2) -Ru(1) -Cl(3)	76.74( 6)	Ru(1) -Cu(1) - P(5)	175.29( 7)
Cl(2) -Ru(1) -Cl(4)	82.15( 6)	Cl(1) -Cu(1) -Cl(2)	84.30( 7)
Cl(2) -Ru(1) - P(1)	90.39( 7)	Cl(1) -Cu(1) -Cl(3)	90.45( 7)
Cl(2) -Ru(1) - P(2)	170.18( 7)	Cl(1) -Cu(1) - P(5)	128.95( 9)
Cl(3) -Ru(1) -Cl(4)	81.67( 6)	Cl(2) -Cu(1) -Cl(3)	78.45( 6)
Cl(3) -Ru(1) - P(1)	166.88( 7)	Cl(2) -Cu(1) - P(5)	125.59( 8)
Cl(3) -Ru(1) - P(2)	94.20( 6)	Cl(3) -Cu(1) - P(5)	131.69( 9)
Cl(4) -Ru(1) - P(1)	94.22( 7)	Ru(1) -Cl(1) -Cu(1)	81.14( 7)
Cl(4) -Ru(1) - P(2)	92.91( 7)	Ru(1) -Cl(2) -Ru(2)	83.44( 6)
P(1) -Ru(1) - P(2)	98.46( 7)	Ru(1) -Cl(2) -Cu(1)	77.69( 6)
Ru(1) -Ru(2) -Cl(2)	48.30( 4)	Ru(2) -Cl(2) -Cu(1)	93.97( 6)
Ru(1) -Ru(2) -Cl(3)	49.10( 4)	Ru(1) -Cl(3) -Ru(2)	80.97( 5)
Ru(1) -Ru(2) -Cl(4)	45.38( 4)	Ru(1) -Cl(3) -Cu(1)	78.23( 6)
Ru(1) -Ru(2) -Cl(5)	122.22( 5)	Ru(2) -Cl(3) -Cu(1)	93.85( 6)
Ru(1) -Ru(2) - P(3)	124.13( 6)	Ru(1) -Cl(4) -Ru(2)	88.30( 6)
Ru(1) -Ru(2) - P(4)	121.05( 6)		



Table 5.3: Selected Torsion Angles ( $^{\circ}$ ) with Standard Deviations for  $\text{Ru}_2\text{Cl}_5(\text{PEtPh}_2)_4\cdot\text{Cu}(\text{PEtPh}_2)$

Cl(2) -Ru(1) -Cl(1) -Cu(1)	-42.25( 6)	P(3) -Ru(2) -Cl(2) -Ru(1)	132.20( 6)
Cl(3) -Ru(1) -Cl(1) -Cu(1)	34.70( 6)	P(3) -Ru(2) -Cl(2) -Cu(1)	-150.69( 7)
Cl(4) -Ru(1) -Cl(1) -Cu(1)	-11.7( 3)	P(4) -Ru(2) -Cl(2) -Ru(1)	-42.3( 3)
P(1) -Ru(1) -Cl(1) -Cu(1)	-132.22( 7)	P(4) -Ru(2) -Cl(2) -Cu(1)	34.8( 3)
P(2) -Ru(1) -Cl(1) -Cu(1)	128.49( 7)	Ru(1) -Ru(2) -Cl(3) -Cu(1)	-77.42( 6)
Cu(1) -Ru(1) -Cl(2) -Ru(2)	95.53( 6)	Cl(2) -Ru(2) -Cl(3) -Ru(1)	46.10( 5)
Cl(1) -Ru(1) -Cl(2) -Ru(2)	136.05( 6)	Cl(2) -Ru(2) -Cl(3) -Cu(1)	-31.32( 6)
Cl(1) -Ru(1) -Cl(2) -Cu(1)	40.52( 6)	Cl(4) -Ru(2) -Cl(3) -Ru(1)	-37.38( 5)
Cl(3) -Ru(1) -Cl(2) -Ru(2)	47.46( 5)	Cl(4) -Ru(2) -Cl(3) -Cu(1)	-114.81( 7)
Cl(3) -Ru(1) -Cl(2) -Cu(1)	-48.07( 5)	Cl(5) -Ru(2) -Cl(3) -Ru(1)	135.06( 6)
Cl(4) -Ru(1) -Cl(2) -Ru(2)	-35.77( 5)	Cl(5) -Ru(2) -Cl(3) -Cu(1)	57.63( 7)
Cl(4) -Ru(1) -Cl(2) -Cu(1)	-131.30( 6)	P(3) -Ru(2) -Cl(3) -Ru(1)	39.6( 5)
P(1) -Ru(1) -Cl(2) -Ru(2)	-129.98( 6)	P(3) -Ru(2) -Cl(3) -Cu(1)	-37.8( 5)
P(1) -Ru(1) -Cl(2) -Cu(1)	134.49( 6)	P(4) -Ru(2) -Cl(3) -Ru(1)	-132.82( 6)
P(2) -Ru(1) -Cl(2) -Ru(2)	24.5( 4)	P(4) -Ru(2) -Cl(3) -Cu(1)	149.76( 7)
P(2) -Ru(1) -Cl(2) -Cu(1)	-71.1( 4)	Cl(2) -Ru(2) -Cl(4) -Ru(1)	-37.20( 6)
Cl(1) -Ru(1) -Cl(3) -Ru(2)	-130.38( 6)	Cl(3) -Ru(2) -Cl(4) -Ru(1)	40.14( 6)
Cl(1) -Ru(1) -Cl(3) -Cu(1)	-34.49( 6)	Cl(5) -Ru(2) -Cl(4) -Ru(1)	2.4( 3)
Cl(2) -Ru(1) -Cl(3) -Ru(2)	-45.92( 5)	P(3) -Ru(2) -Cl(4) -Ru(1)	-131.46( 7)
Cl(2) -Ru(1) -Cl(3) -Cu(1)	49.97( 6)	P(4) -Ru(2) -Cl(4) -Ru(1)	129.41( 7)
Cl(4) -Ru(1) -Cl(3) -Ru(2)	37.92( 5)	Cl(2) -Cu(1) -Cl(1) -Ru(1)	41.93( 6)
Cl(4) -Ru(1) -Cl(3) -Cu(1)	133.81( 6)	Cl(3) -Cu(1) -Cl(1) -Ru(1)	-36.43( 6)
P(1) -Ru(1) -Cl(3) -Ru(2)	-34.6( 3)	P(5) -Cu(1) -Cl(1) -Ru(1)	174.09(10)
P(1) -Ru(1) -Cl(3) -Cu(1)	61.3( 3)	Ru(1) -Cu(1) -Cl(2) -Ru(2)	-82.40( 5)
P(2) -Ru(1) -Cl(3) -Ru(2)	130.25( 6)	Cl(1) -Cu(1) -Cl(2) -Ru(1)	-41.12( 6)
P(2) -Ru(1) -Cl(3) -Cu(1)	-133.86( 6)	Cl(1) -Cu(1) -Cl(2) -Ru(2)	-123.52( 7)
Cu(1) -Ru(1) -Cl(4) -Ru(2)	-3.33( 7)	Cl(3) -Cu(1) -Cl(2) -Ru(1)	50.51( 5)
Cl(1) -Ru(1) -Cl(4) -Ru(2)	6.4( 3)	Cl(3) -Cu(1) -Cl(2) -Ru(2)	-31.89( 6)
Cl(2) -Ru(1) -Cl(4) -Ru(2)	37.09( 6)	P(5) -Cu(1) -Cl(2) -Ru(1)	-175.98( 9)
Cl(3) -Ru(1) -Cl(4) -Ru(2)	-40.56( 6)	P(5) -Cu(1) -Cl(2) -Ru(2)	101.62(10)
P(1) -Ru(1) -Cl(4) -Ru(2)	126.90( 7)	Ru(1) -Cu(1) -Cl(3) -Ru(2)	79.94( 5)
P(2) -Ru(1) -Cl(4) -Ru(2)	-134.38( 6)	Cl(1) -Cu(1) -Cl(3) -Ru(1)	34.95( 6)
Cl(3) -Ru(2) -Cl(2) -Ru(1)	-46.84( 5)	Cl(1) -Cu(1) -Cl(3) -Ru(2)	114.88( 7)
Cl(3) -Ru(2) -Cl(2) -Cu(1)	30.27( 6)	Cl(2) -Cu(1) -Cl(3) -Ru(1)	-49.15( 5)
Cl(4) -Ru(2) -Cl(2) -Ru(1)	35.19( 5)	Cl(2) -Cu(1) -Cl(3) -Ru(2)	30.79( 6)
Cl(4) -Ru(2) -Cl(2) -Cu(1)	112.30( 7)	P(5) -Cu(1) -Cl(3) -Ru(1)	-176.98(10)
Cl(5) -Ru(2) -Cl(2) -Ru(1)	-136.94( 6)	P(5) -Cu(1) -Cl(3) -Ru(2)	-97.04(11)
Cl(5) -Ru(2) -Cl(2) -Cu(1)	-59.83( 7)		

The structure consists of a four-coordinate Cu(I) ion bound to one terminal and two bridging chloride ligands of the  $[(\text{PEtPh}_2)_2\text{ClRuCl}_3\text{RuCl}(\text{PEtPh}_2)_2]^-$  moiety as well as one PEtPh<sub>2</sub> ligand. The geometry about the Cu(I) centre is nearer tetrahedral than the corresponding Ag(I) centre. Moreover the difference between the Cu(I)-bridging chloride bond lengths of 0.077Å is smaller than that for the Ag(I) analogue (0.131Å).

- This might have been expected to lead to some significant distortion of the  $[(\text{PEtPh}_2)_2\text{ClRuCl}_3\text{RuCl}(\text{PEtPh}_2)_2]^-$  moiety however this is not found to be the case. Comparison of the bond lengths and angles of this unit with that in (63) (see Table 5.4) reveals that, although there are some slight changes, these do not lead to a significant change in the Ru-Ru vector (3.3326(8)Å for the Cu complex and 3.331(2)Å for the Ag complex).

### 5.2.2 HgCl<sub>2</sub>

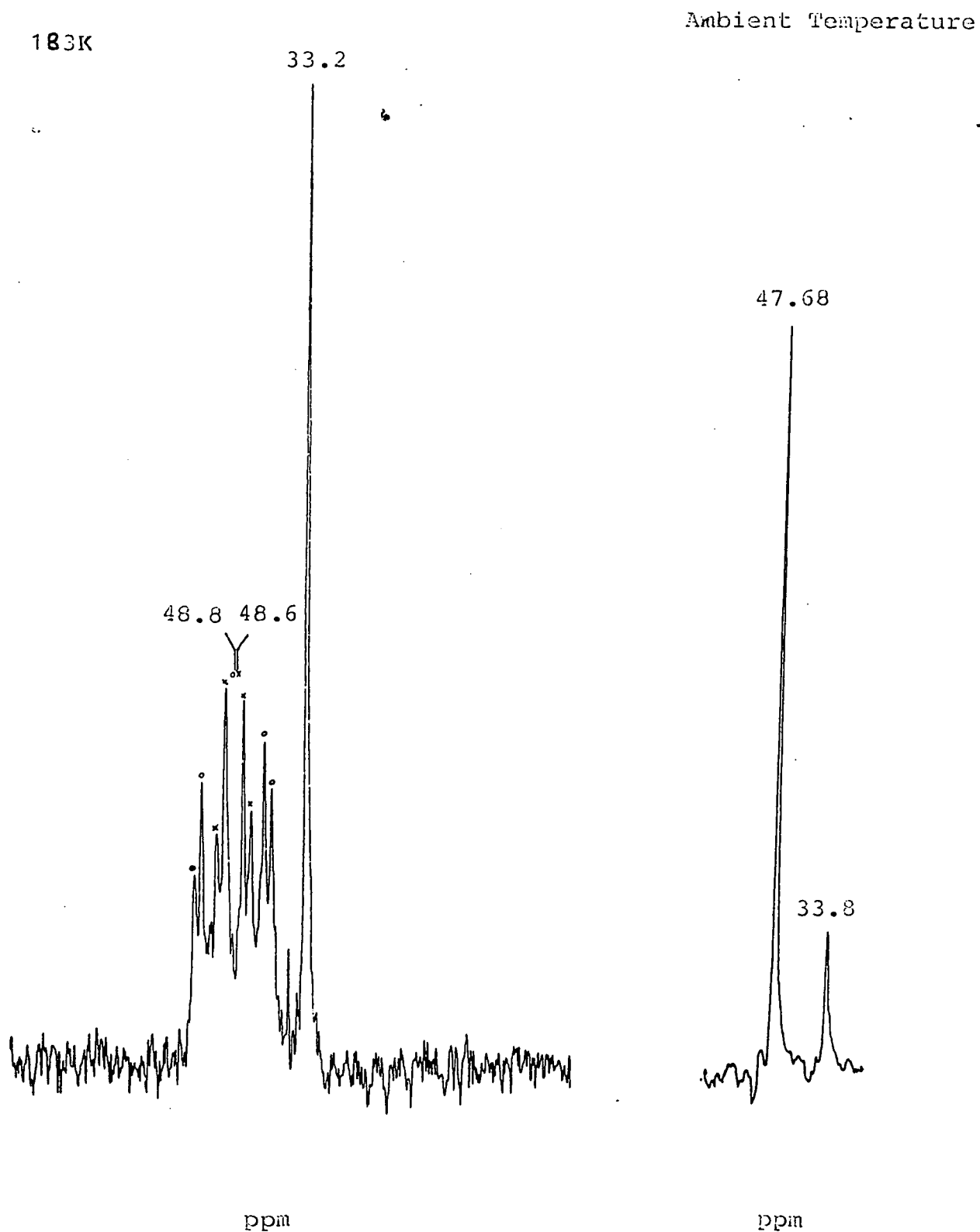
Reaction of HgCl<sub>2</sub> with two molar equivalents of RuCl<sub>2</sub>(PEtPh<sub>2</sub>)<sub>3</sub> in MeOH, over a period of 15 hours, also yielded a salmon pink precipitate.

This product analysed for Ru<sub>2</sub>Cl<sub>5</sub>(PEtPh<sub>2</sub>)<sub>4</sub>·HgCl(PEtPh<sub>2</sub>) (65). The <sup>31</sup>P-(<sup>1</sup>H)n.m.r. spectrum (see Figure 5.5) of the product at 183K exhibits two AB patterns for the PEtPh<sub>2</sub> ligands bound to ruthenium, one centred at 48.8p.p.m. (J<sub>AB</sub> = 36Hz, V<sub>AB</sub> = 366Hz) and the other at 48.6p.p.m. (J<sub>AB</sub> = 43Hz, V<sub>AB</sub> = 144Hz). A singlet at 33.2p.p.m. is also observed and is assigned as the mercury bound PEtPh<sub>2</sub> ligand.

Table 5.4: Selected Bond Lengths ( $\text{\AA}$ ) and Bond Angles ( $^\circ$ ) for $\text{Ru}_2\text{Cl}_5(\text{PEtPh}_2)_4 \cdot \text{M}(\text{PEtPH}_2)$  (M = Ag, Cu)

	Cu	Ag
Ru(1) -Ru(2)	3.3326( 8)	3.331( 2)
Ru(1) -Cl(1)	2.4376(21)	2.433( 6)
Ru(1) -Cl(2)	2.5047(18)	2.493( 5)
Ru(1) -Cl(3)	2.5504(18)	2.578( 5)
Ru(1) -Cl(4)	2.3731(18)	2.378( 5)
Ru(1) - P(1)	2.2560(20)	2.280( 6)
Ru(1) - P(2)	2.2869(20)	2.282( 5)
Ru(2) -Cl(2)	2.5028(18)	2.490( 5)
Ru(2) -Cl(3)	2.5823(18)	2.570( 5)
Ru(2) -Cl(4)	2.4112(18)	2.449( 5)
Ru(2) -Cl(5)	2.3959(20)	2.441( 5)
Ru(2) - P(3)	2.2715(21)	2.280( 6)
Ru(2) - P(4)	2.2645(21)	2.274( 6)
M(1) -Cl(1)	2.4071(22)	2.675( 6)
M(1) -Cl(2)	2.5188(20)	2.788( 5)
M(1) -Cl(3)	2.4423(20)	2.657( 5)
M(1) - P(5)	2.1768(25)	2.376( 6)
Ru(1) -Cl(2) -Ru(2)	83.44( 6)	83.91(15)
Ru(1) -Cl(3) -Ru(2)	80.97( 5)	80.65(15)
Ru(1) -Cl(4) -Ru(2)	88.30( 6)	87.26(17)

Figure 5.5:  $^{31}\text{P}$ -( $^1\text{H}$ )n.m.r. Spectrum of  $\text{Ru}_2\text{Cl}_5(\text{PEtPh}_2)_4 \cdot \text{HgCl}(\text{PEtPh}_2)$  at 183K and Ambient Temperature in  $\text{CD}_2\text{Cl}_2$

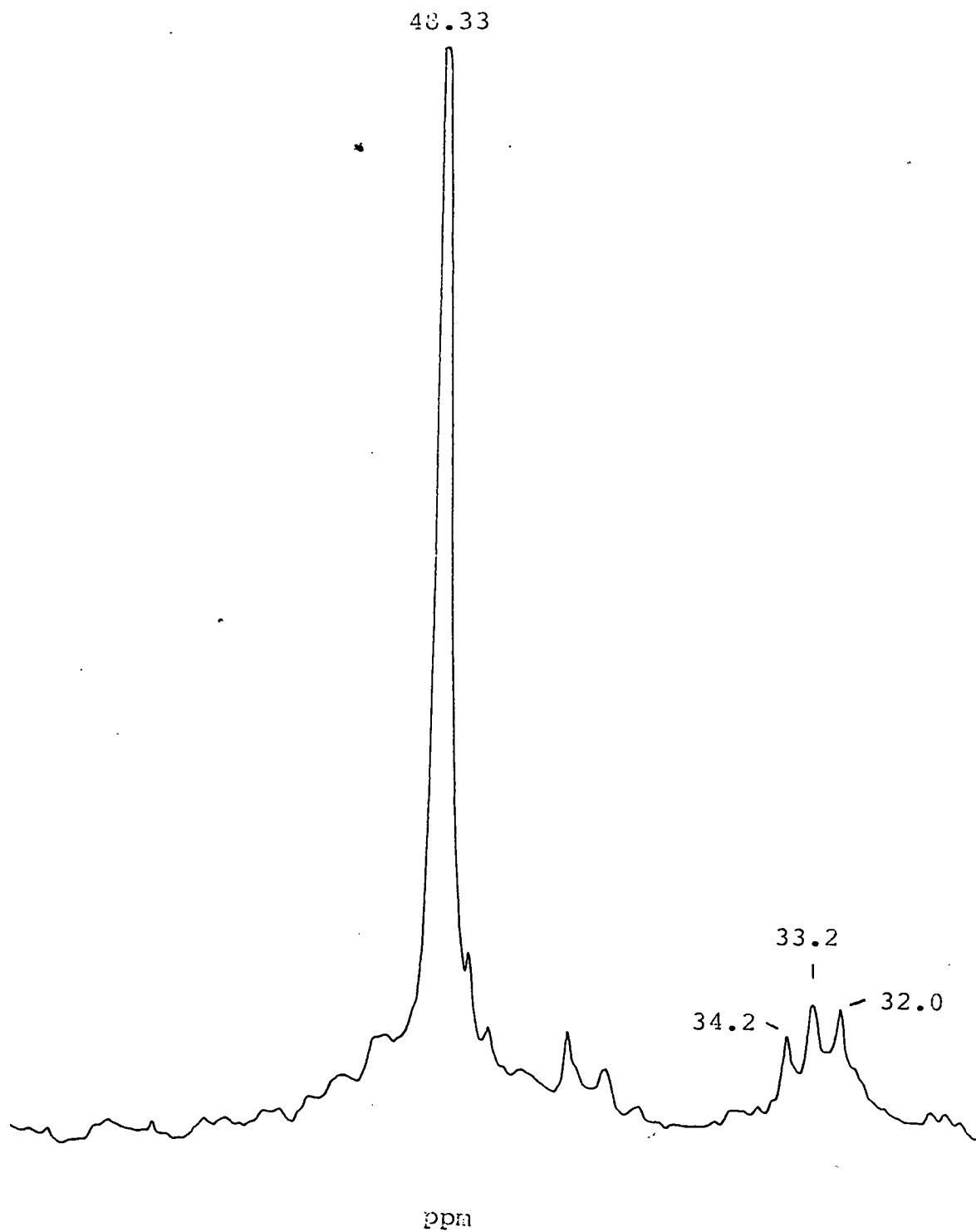


However, the expected satellites due to the spin 1/2 isotope  $^{199}\text{Hg}$  (17%) are not observed. At ambient temperature, the spectrum (see Figure 5.5) consists of two singlets, one at 47.68p.p.m. for the now magnetically equivalent Ru bound  $\text{PEtPh}_2$  ligands (i.e. an intramolecular exchange similar to that for (63) and (64) and the other at 33.80p.p.m. for the  $\text{PEtPh}_2$  ligand bound to mercury, though again no  $^{199}\text{Hg}$  satellites are observed.

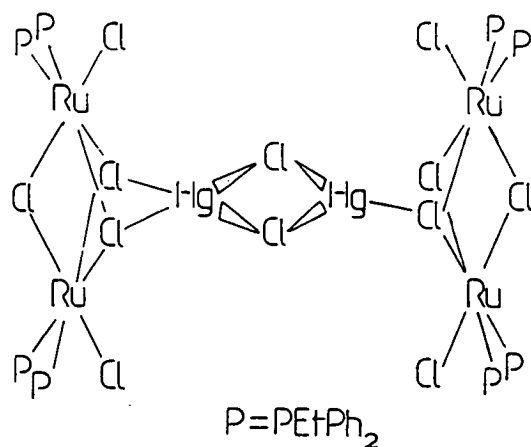
The apparent absence of the  $^{199}\text{Hg}$  satellites (typical  $J_{^{199}\text{Hg}^{31}\text{P}}$  coupling constants fall in the range 3000-7500Hz)<sup>(4)</sup> obviously requires further investigation. However, apart from this, the method of preparation and colour of the complex, its observed spectra along with the analytical data strongly suggests that the complex has been formulated correctly.

On leaving the solution at ambient temperature for 48 hours the  $^{31}\text{P}$ -( $^1\text{H}$ )n.m.r. spectrum at 183K reveals that further reaction takes place, which, after three weeks has neared completion (see Figure 5.6). The spectrum now consists predominantly of a singlet at 48.33p.p.m. In addition two new resonances are also observed at 34.2 and 32.0p.p.m. A similar spectrum is observed on warming to ambient temperature (see Figure 5.6).

Figure 5.6:  $^{31}\text{P}$ -( $^1\text{H}$ )n.m.r. Spectrum at 183K on Leaving  $\text{Ru}_2\text{Cl}_5(\text{PEtPh}_2)_4 \cdot \text{HgCl}(\text{PEtPh}_2)$  at Ambient Temperature for Three Weeks in  $\text{CD}_2\text{Cl}_2$



Although the identity of the species associated with the resonances at 34.2 and 32.0 p.p.m. remains unknown the complex associated with the resonance at 48.33 p.p.m. has been identified. This species was synthesised by treating  $\text{HgCl}_2$  with two molar equivalents of  $\text{RuCl}_2(\text{PEtPh}_2)_3$  in refluxing  $\text{CH}_2\text{Cl}_2/\text{MeOH}$  (3:1 v/v) for 3 hours, affording a red solution. The solid obtained on removal of the  $\text{CH}_2\text{Cl}_2$  was then refluxed in EtOH for 3 hours to afford a red solution from which the complex (66) may be isolated, as an orange solid, on removal of the solvent. This material analyses for  $\text{Ru}_2\text{Cl}_5(\text{PEtPh}_2)_4 \cdot \text{HgCl}$ . It seems unlikely that the formation of  $\text{Ru}_2\text{Cl}_5(\text{PEtPh}_2)_4 \cdot \text{HgCl}$  would lead to the observed magnetic equivalent of the ruthenium bound  $\text{PEtPh}_2$  ligands and thus a hexametalllic structure (66) is proposed i.e.  $[\text{Ru}_2\text{Cl}_5(\text{PEtPh}_2)_4 \cdot \text{HgCl}]_2$ .



### 5.2.3 AgBr

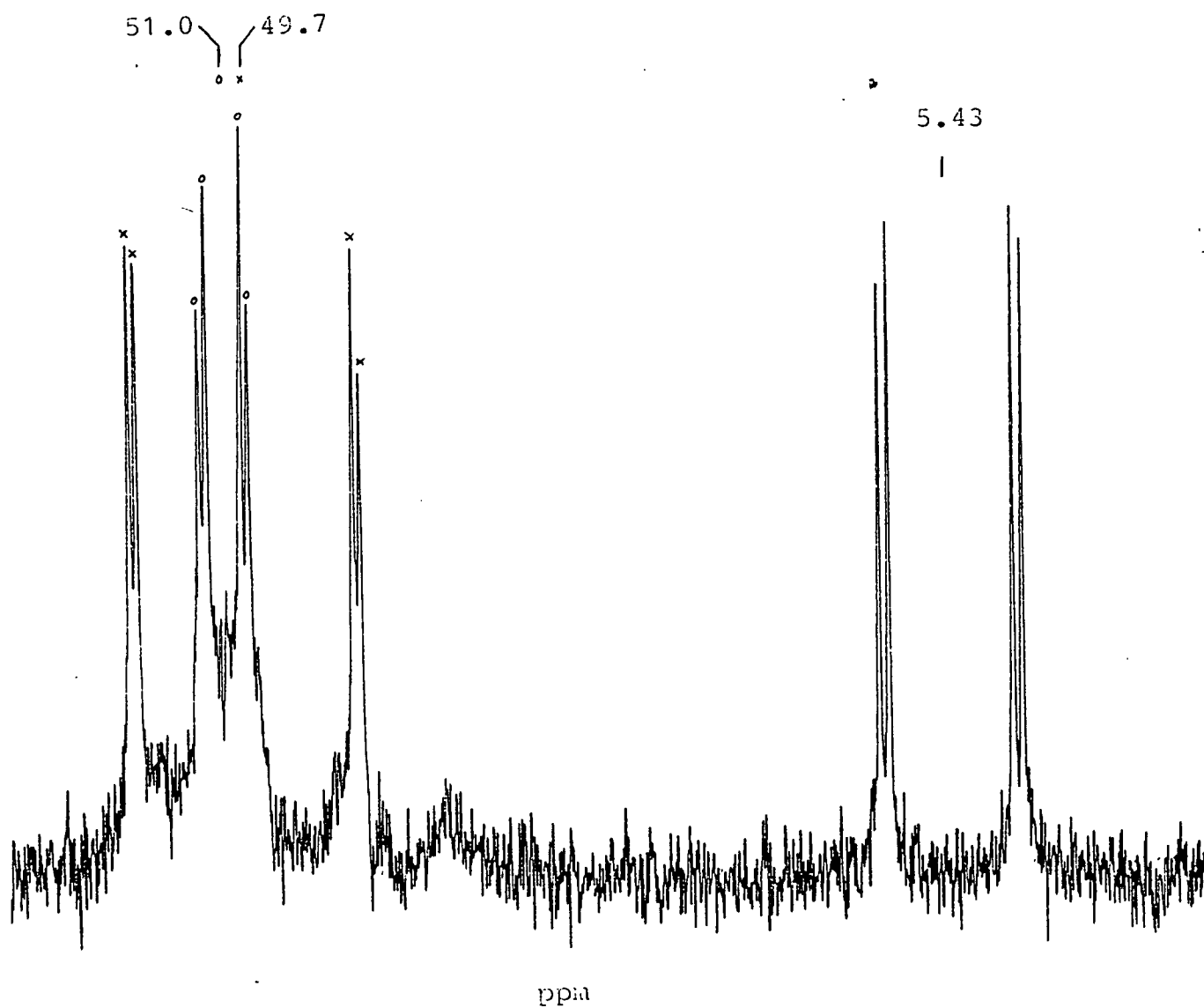
Unlike the analogous chloride reaction to form (63), no pink

precipitate is formed on treating AgBr with two molar equivalents of  $\text{RuCl}_2(\text{PEtPh}_2)_3$  in MeOH for 2 days. On refluxing the solution for 6 hours a very small amount of a salmon pink solid was formed. If, however, EtOH instead of MeOH is used as the solvent a high yield of the pink material may be obtained after refluxing for only 30 minutes. Elemental analysis indicated that the product, recrystallised from a  $\text{CH}_2\text{Cl}_2/\text{MeOH}$  solvent system, was  $\text{Ru}_2\text{Br}_5(\text{PEtPh}_2)_4 \cdot \text{Ag}(\text{PEtPh}_2) \cdot 2(\text{CH}_2\text{Cl}_2)$  (67).

The  $^{31}\text{P}$ -( $^1\text{H}$ ) n.m.r. spectrum of the complex (see Figure 5.7) at 182K, like  $\text{Ru}_2\text{Cl}_5(\text{PEtPh}_2)_4 \cdot \text{Ag}(\text{PEtPh}_2)$ , exhibits two AB patterns for the  $\text{PEtPh}_2$  ligands attached to ruthenium, one centred at 51.0p.p.m. ( $J_{\text{AB}} = 41\text{Hz}$ ,  $V_{\text{AB}} = 222\text{Hz}$ ) and the other at 49.7p.p.m. ( $J_{\text{AB}} = 35\text{Hz}$ ,  $V_{\text{AB}} = 1147\text{Hz}$ ) as well as two characteristic doublets centred at 5.43p.p.m. for the silver-bound  $\text{PEtPh}_2$  ligand ( $J_{109_{\text{Ag}}^{31}\text{p}} = 735\text{Hz}$ ,  $J_{107_{\text{Ag}}^{31}\text{p}} = 636\text{Hz}$ ). As for the chloride analogue the spectrum at ambient temperature consists of a singlet (49.75p.p.m.) for the magnetically equivalent Ru-bound  $\text{PEtPh}_2$  ligands, due to intra- and intermolecular fluxional processes.



Figure 5.7:  $^{31}\text{P}$ -( $^1\text{H}$ )n.m.r. Spectrum of  
 $\text{Ru}_2\text{Br}_5(\text{PEtPh}_2)_4 \cdot \text{Ag}(\text{PEtPh}_2)_2$  at 182K in  $\text{CD}_2\text{Cl}_2$



### 5.3 Conclusions

Although a full study has not been carried out, this work has shown that metals other than silver, and bromide as well as chloride may result in the formation of complexes analogous to that reported by Easton and Stephenson. At ambient temperature, the new complexes (64), (65) and (67) exhibit the same intramolecular switching between the two equivalent sites offered by the  $[(\text{PEtPh}_2)_2\text{ClRuCl}_3\text{RuCl}(\text{PEtPh}_2)_2]^-$  moiety. For the mercury complex (65) the presence of an additional chloride may explain the subsequent reaction to form  $[(\text{Ru}_2\text{Cl}_5(\text{PEtPh}_2)_4 \cdot \text{HgCl})_2]$  (66). Comparison of the two structures,  $\text{Ru}_2\text{Cl}_5(\text{PEtPh}_2)_4 \cdot \text{M}(\text{PEtPh}_2)$  ( $\text{M} = \text{Ag}, \text{Cu}$ ), reveals that the  $[(\text{PEtPh}_2)_2\text{ClRuCl}_3\text{RuCl}(\text{PEtPh}_2)_2]^-$  moiety is not significantly distorted ( $\text{Ru-Ru} = 3.3326(8)$  and  $3.331(2)\text{\AA}$  for the Cu and Ag complex respectively) even though the ionic radius of Cu(I) is smaller than that of Ag(I) (0.96 and 1.26\AA respectively).

Obviously, further investigation of this class of complex is required. Of particular interest is the isolation of the anionic moiety  $[(\text{PEtPh}_2)_2\text{XRuX}_3\text{RuX}(\text{PEtPh}_2)_2]^-$  and the ability to study the symmetric mixed-valence complex  $(\text{PEtPh}_2)_2\text{XRuX}_3\text{RuX}(\text{PEtPh}_2)_2$  ( $\text{X} = \text{Cl}^-, \text{Br}^-$ ) - cf Chapter 4.

## 5.4 Experimental

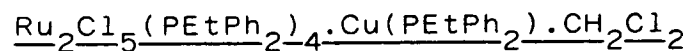
Physical measurements were performed as described in Chapter 2.

### Materials

The following were prepared using literature methods:



### Single Crystal Structure Determination of



Crystals were obtained by the diffusion of degassed MeOH into a degassed  $\text{CH}_2\text{Cl}_2$  solution of the complex.

### Crystal Data

$(\text{C}_{70}\text{H}_{75}\text{Cl}_5\text{P}_5\text{CuRu}_2) \cdot \text{CH}_2\text{Cl}_2$ ,  $M = 1599.12$  monoclinic  $a = 15.4887(29)$ ,  $b = 18.7700(47)$ ,  $c = 26.0218(79)\text{\AA}$ ,  $\alpha = 90$ ,  $\beta = 106.798(29)$ ,  $\gamma = 90^\circ$ ,  $V = 7242.3\text{\AA}^{-3}$  using 23 reflections measured at  $\pm \omega$  ( $2\theta = 38-39^\circ$ ),  $\lambda = 0.71073\text{\AA}$ , space group  $P2_{1/c}$ ,  $Z = 4$ ,  $D_{\text{calc}} = 1.466\text{g cm}^{-3}$ . Dark red plates. Crystal dimensions  $1.078 \times 0.693 \times 0.5775\text{mm}$ ,  $(\text{Mo-K}\alpha) = 11.04\text{cm}^{-1}$ .

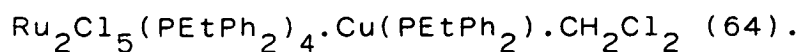
### Data Collection and Processing

Stoe STADI-4 four circle diffractometer,  $\text{Mo-K}\alpha$  X-radiation  $\omega-2\theta$

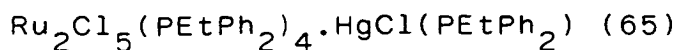
scan mode with  $\omega$  width  $(1.20 + 0.347 \tan \theta)^\circ$ ; 9783 reflections,  $(2.5 \leq \theta \leq 25^\circ, h -16 \rightarrow 16, k 0 \rightarrow 20, l 0 \rightarrow 28)$ , giving 1672 with  $F \gg 3 \sigma(F)$ .

### Structure Analysis and Refinement

Patterson synthesis (Ru) followed by iterative cycles of least squares refinement and difference Fourier synthesis revealed the positions of all non-H atoms. Full-matrix least squares with C (phenyl) and H atoms in calculated positions, C (solvent) constrained to an occupancy of 1 and anisotropic thermal parameters of Ru, C, P, Cu atoms. Final R,  $R_w$  and S values are 0.0557, 0.0722 and 1.164 for 302 parameters and the final  $\Delta F$  synthesis showed max. peak and min. trough of 1.23,  $-0.57 \text{eA}^{-3}$ . The weighting scheme  $w = 5.2806 / (\sigma^2(F) + 0.000240(F)^2)$  gave satisfactory agreement analysis.

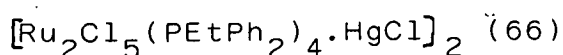


$\text{RuCl}_2(\text{PEtPh}_2)_3$  (148.2mg,  $1.8 \times 10^{-4}$  mmol) and  $\text{CuCl}$  ( $9 \times 10^{-5}$  mmol) were stirred for 3 hours in degassed MeOH (10ml) under  $\text{N}_2$ . The salmon-pink solid was filtered off and washed with MeOH. Red crystals of the  $\text{CH}_2\text{Cl}_2$  solution of the solid (95mg, 65%). Found: C 52.0, H 4.70; Calc for  $\text{Ru}_2\text{CuCl}_5\text{C}_{70}\text{H}_{75} \cdot \text{CH}_2\text{Cl}_2$  C 53.3, H 4.85%. I.R.  $\nu_{\text{Ru-Cl}}$   $320 \text{cm}^{-1}$ .

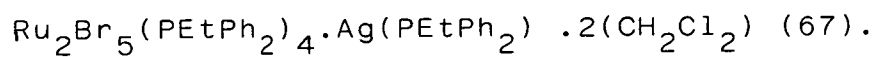


$\text{RuCl}_2(\text{PEtPh}_2)_3$  (141.6mg,  $1.74 \times 10^{-4}$  mmol) and  $\text{HgCl}_2$

( $8.7 \times 10^{-5}$  mmol) were stirred for 15 hours in degassed MeOH under  $N_2$ . The salmon-pink precipitate was filtered off and washed with MeOH. This was recrystallised via a degassed  $CH_2Cl_2$ /hexane solvent system and then dried in vacuo. (86.5mg, 59%). Found C 49.6, H 4.47; Calc for  $Ru_2HgCl_6P_5C_{70}H_{75}$  C 49.8, H 4.48%. I.R.  $\nu_{Ru-Cl}$   $330cm^{-1}$ .



$RuCl_2(PEtPh_2)_3$  (150.4mg,  $1.84 \times 10^{-4}$  mmol) and  $HgCl_2$  ( $9.2 \times 10^{-5}$  mmol) were refluxed in degassed  $CH_2Cl_2$ /MeOH (30ml 3:1) for 3 hours under  $N_2$  to yield a red solution. The solid obtained on removal of the solvent was then refluxed in degassed EtOH for a further 3 hours. After filtration of the red solution, and removal of the solvent, an orange material was isolated. This was recrystallised via a  $CH_2Cl_2$ /hexane solvent system and dried in vacuo. (112.5mg, 81%). Found C 46.3, H 4.09 Calc for  $Ru_4Hg_2Cl_{12}P_8C_{112}H_{120}$  C 45.7, H 4.11% I.R.  $\nu_{Ru-Cl}$   $320cm^{-1}$



$RuBr_2(PEtPh_2)_3$  (167.4mg,  $1.85 \times 10^{-4}$  mmol) and  $AgBr$  ( $9.3 \times 10^{-5}$  mmol) were refluxed in degassed EtOH (10ml) under  $N_2$  for 30 minutes. The salmon-pink solid was filtered off and washed with MeOH. Red crystals of the  $CH_2Cl_2$  solvate were obtained by the slow diffusion of MeOH into a degassed  $CH_2Cl_2$  solution of the complex. (108mg, 52%). Found: C 44.3, H 4.08

Calc for  $\text{Ru}_2\text{AgBr}_5\text{P}_4\text{C}_{70}\text{H}_{75} \cdot 2(\text{CH}_2\text{Cl}_2)$  C 44.6, H 4.00.

### References

1. T. Easton PhD Thesis, University of Edinburgh, 1986.
2. E. L. Muetterties and C. w. Alegranti, J. Am. Chem. Soc., 1970, 92, 4114; 1972 94, 6386.
3. "Handbook of Chemistry and Physics", 62nd Edition, 1981, CRC Press.
4. C. Brevard and P. Granger, "Handbook of High Resolution Multinuclear N.M.R.".
5. P. W. Armit, A. Boyd and T. A. Stephenson, J. Chem. Soc. Dalton Trans., 1975, 1663.

Appendix 1

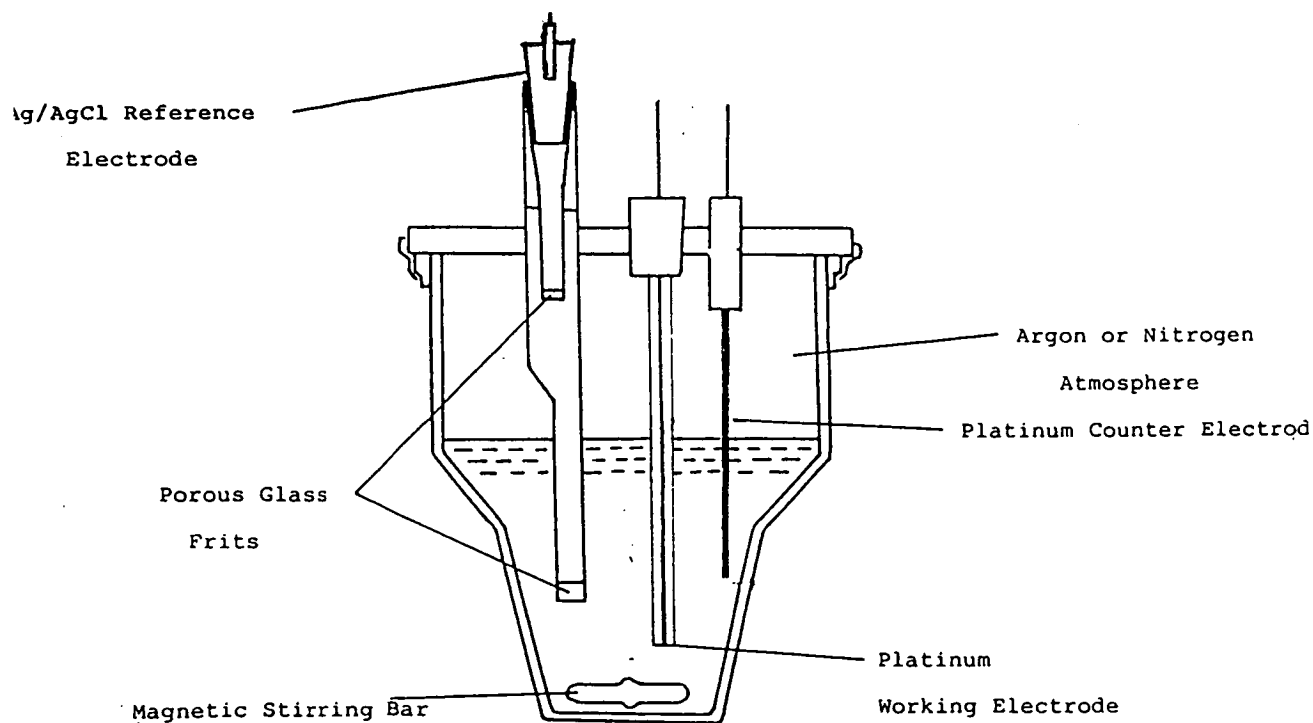
Electrochemical and Spectroelectrochemical Techniques

In Chapter 3 and 4 electrochemical and spectroelectrochemical techniques were employed to carry out in situ characterisation. A brief description of these techniques and the electrochemical cells used is given below.

### A.1 Electrochemical Techniques

For the techniques described below a three electrode configuration as outlined in Figure A.1 was employed.

Figure A.1: Standard Three-electrode Electrochemical Cell



### a/Cyclic Voltammetry (c.v.)

For linear sweep cyclic voltammetry (c.v.) the solution is quiet i.e. unstirred and thus the diffusion of reactants and products between the bulk solution and the solution/electrode



interface is the only means of mass transport.

The potential of the working electrode is varied at a finite rate, the "scan rate",  $V$ , as a linear function of time (50-500mVs<sup>-1</sup>). Upon reaching a preset value, the "switching potential", the voltage scan is reversed to its base potential at the same rate as the forward scan. Figure A.2 shows a typical current-potential response curves for both reversible and irreversible charge-transfer processes. The cyclic voltammetric scan rate is thus of critical importance since it effectively controls the time-scale of the experiment.

There are four measurable parameters that can be obtained for a reversible process; namely the net current ( $i_p^F$ ), the potential at the maximum of the forward curve ( $E_p^F$ ) and the corresponding parameters of the reverse curve ( $i_p^R$  and  $E_p^R$ ). These parameters can subsequently be used to identify the nature of the charge-transfer process. If the charge-transfer is "reversible" then the process occurs considerably faster than the diffusion rate. In contrast, a reaction in which the charge-transfer process is controlled by both diffusion and change-transfer kinetics is termed "quasi-reversible", while a reaction in which the charge transfer process is much slower than the diffusion rate is termed "irreversible" (see Table A.1).

Figure A.2: Cyclic and Stirred Linear Sweep Voltammograms of a Reversible and an Irreversible Charge Transfer Process

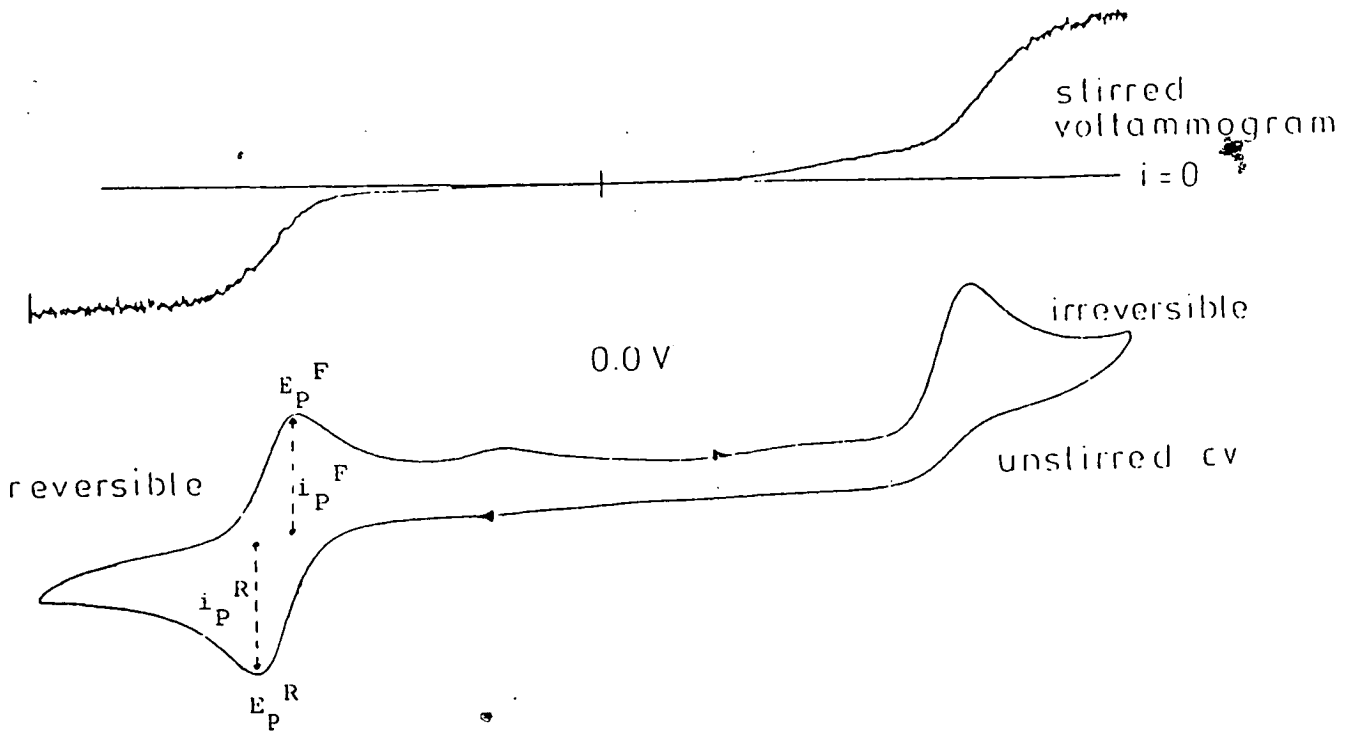


Table A.1: Cyclic Voltammetry Reversibility CriteriaReversible $E_p$  is independent of  $v$  $E_p^F - E_p^R = 0.297T/n$  and is independent of  $v$  $1/2[E_p^F + E_p^R] = E_{1/2}$ , independent of concentration $i_p/v^{1/2}$  (current function) is independent of  $v$  $i_p^R/i_p^F = 1$  and independent of  $v$ Quasi-reversible $E_p$  shifts with  $v$  $E_p^F - E_p^R$  increases as  $v$  increases $i_p/v^{1/2}$  is independent of  $v$  $i_p^R/i_p^F$  generally = 1Partially-reversible

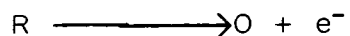
(i.e. Irreversible chemical reaction following charge transfer, E.C. mechanism)

 $E_p$  increases by  $30/n$  mv for a ten fold increase in  $v$ , at low  $v$ . $i_p/v^{1/2}$  is independent of  $v$  $i_p^R/i_p^F$  increases towards 1 as  $v$  increasesIrreversible $E_p$  shifts with  $v$  $i_p/v^{1/2}$  is independent of  $v$ 

There is no current on the reverse scan

 $v$  = sweep rate in  $\text{mvs}^{-1}$  $T$  = temperature (K) $n$  = number of electrons involved in the redox process

If the electrochemical process involves for example a one electron oxidation this may be written as



If on reversing the cell current the reaction is reversed (i.e. no new reaction takes place) the process is termed chemically reversible, though it may or may not be electrochemically reversible. It should, however, be noted that a chemically irreversible process will always be electrochemically irreversible.

#### b/Stirred Linear Sweep Voltammetry

For this technique the test solution is stirred whilst scanning ( $v = 10\text{mVs}^{-1}$ ) to increasingly more cathodic or anodic potentials (see Figure A.2). The technique allows oxidations (current under  $i = 0$  line) and reductions (current above  $i = 0$  line) to be distinguished. In addition, it is also possible to tell the number of electrons involved in the electrode process by comparison with limiting currents of known charge-transfer reactions.

#### c/Linear Sweep A.C. Voltammetry

This technique is complementary to cyclic voltammetry and involves the superposition of a small alternating potential upon a linearly scanning d.c. potential. The net alternating current is recorded as a function of the linear d.c. potential and, for a reversible redox step, is a symmetric peak centred

upon  $E_{1/2}$  of the corresponding d.c. polarogram as shown in Figure A.3. The superimposed voltage is usually sinusoidal (though other cyclic, small amplitude waveforms, such as sawtooth may be used) with an amplitude of 10mV and frequency,  $\omega$ , between 10-1000Hz.

In a simple model the a.c. wave may be considered as the "first derivative" of the d.c. wave. However although this correctly predicts the shape of the wave it disregards the kinetic information contained in the cell response to variation in the a.c. frequency,  $\omega$ . The value of  $\omega$  effectively controls the time-scale of the experiment and provides a particularly sensitive test of departure from reversibility (see Table A.2 for reversibility criteria). For "quasi-reversible" systems displacements similar to those seen in linear sweep cyclic voltammetry are observed (except where the electrode kinetics are sufficiently facile to maintain a reversible d.c. response, while none-the-less showing significant charge transfer resistance to the a.c. perturbation) (1).

A considerable advantage of a.c. voltammetry is the discrimination against the background "residual" or "capacitative" current. This is possible because of the differing phase relationships which the "faradic" and "capacitative" current components have with the applied voltage. Thus this phase sensitive technique lowers detection limits to include samples having analyte concentrations in the range  $10^{-6}$ - $10^{-7}$  mol dm<sup>-3</sup>.

Figure A.3: Linear Sweep A. C. Voltammogram

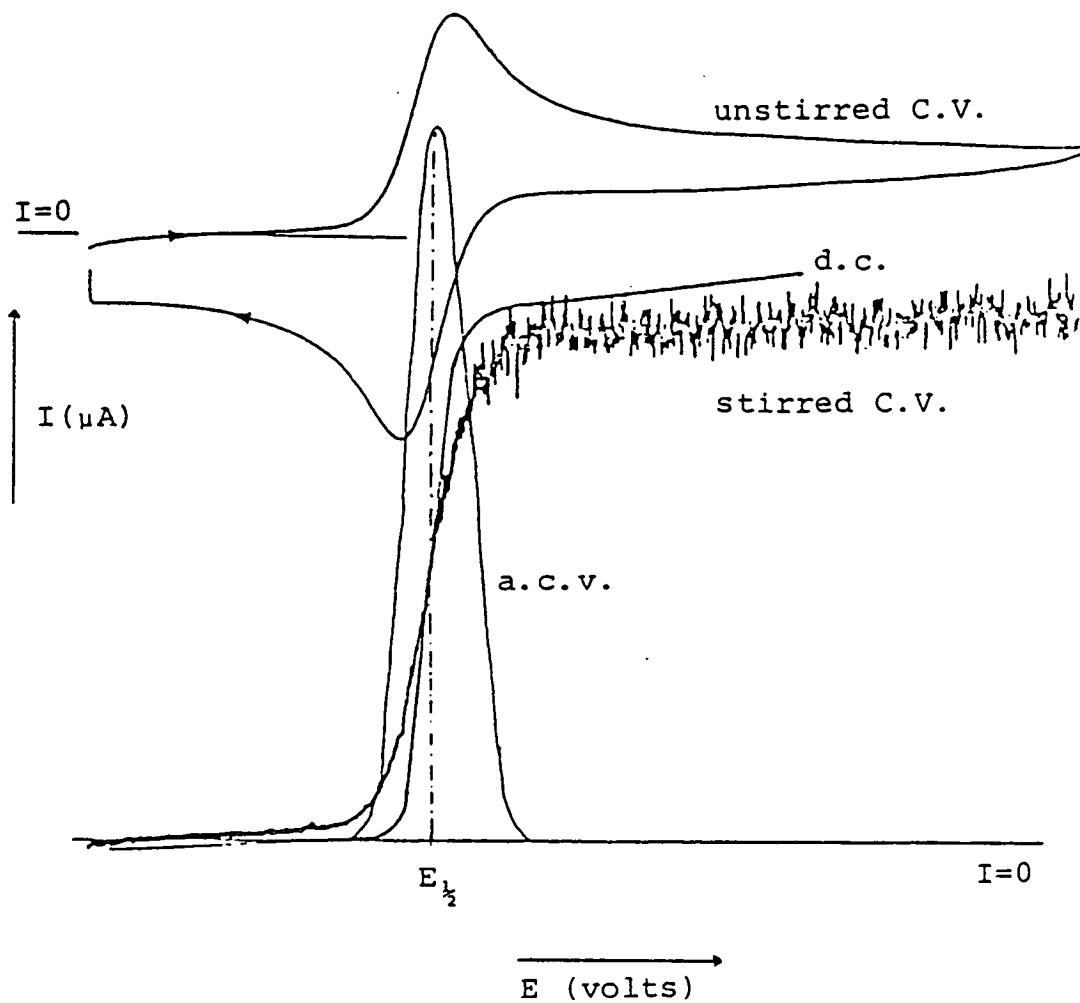


Table A.2: A. C. Voltammetry Reversibility Criteria

$E_p = E_{1/2}$  (d.c.), independent of concentration and  $w$

The wave is highly symmetrical with a width at half height of 90mV

$i_p/w^{1/2}$  gives a linear plot which passes through the origin

In addition a.c. voltammetry can accurately resolve two adjacent waves separated by only 80mV, which is small compared to cyclic voltammetry resolution (150V). Even closer a.c. waves (40mV) can be qualitatively distinguished; the degree of resolution increasing on decreasing the alternating voltage amplitude.

## A.2 Electrosynthesis

Preparative-scale electrosynthesis falls into two classes, namely controlled current (galvanostatic) and controlled-potential (potentiostatic). The latter technique, used in this work, simply involves allowing an electrochemical reaction to proceed at an electrode, the potential of which is held constant and at a value beyond  $E_{1/2}$  for the process. As the starting material is consumed the current decays exponentially with time as shown in Figure A.4. The area under curve gives the total quantity of electrical charge which has passed during the electrolysis. In order to maintain a smooth fall in the current during the electrolysis stirring should be kept steady and the electrodes not subject to fouling.

To prevent reoxidation/reduction of the reaction product a modified three-electrode cell is used in which the working (a Pt basket) and counter (a Pt gauze) electrodes are "isolated" from each other (see Figure A.5).

Figure A.4: Typical Electrogeneration Current/Time Plot

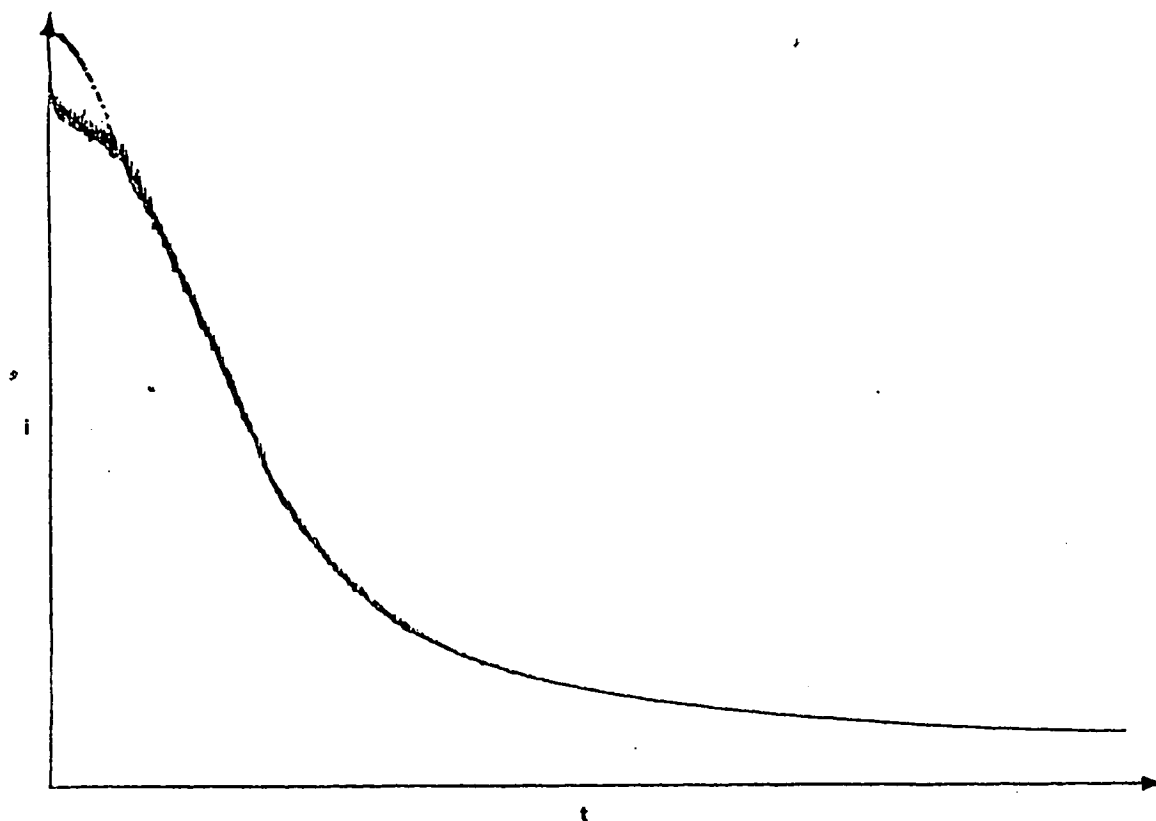
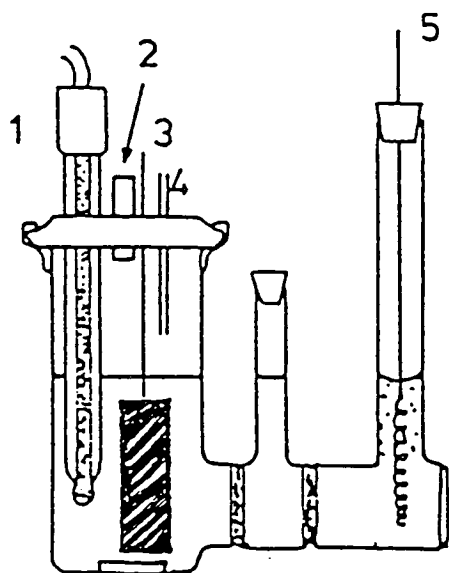


Figure A.5: Modified Three-electrode Cell Used for Preparative-scale Electrosynthesis



- 1 Reference Electrode
- 2 N<sub>2</sub> Inlet
- 3 Working Electrode
- 4 N<sub>2</sub> Outlet
- 5 Counter Electrode

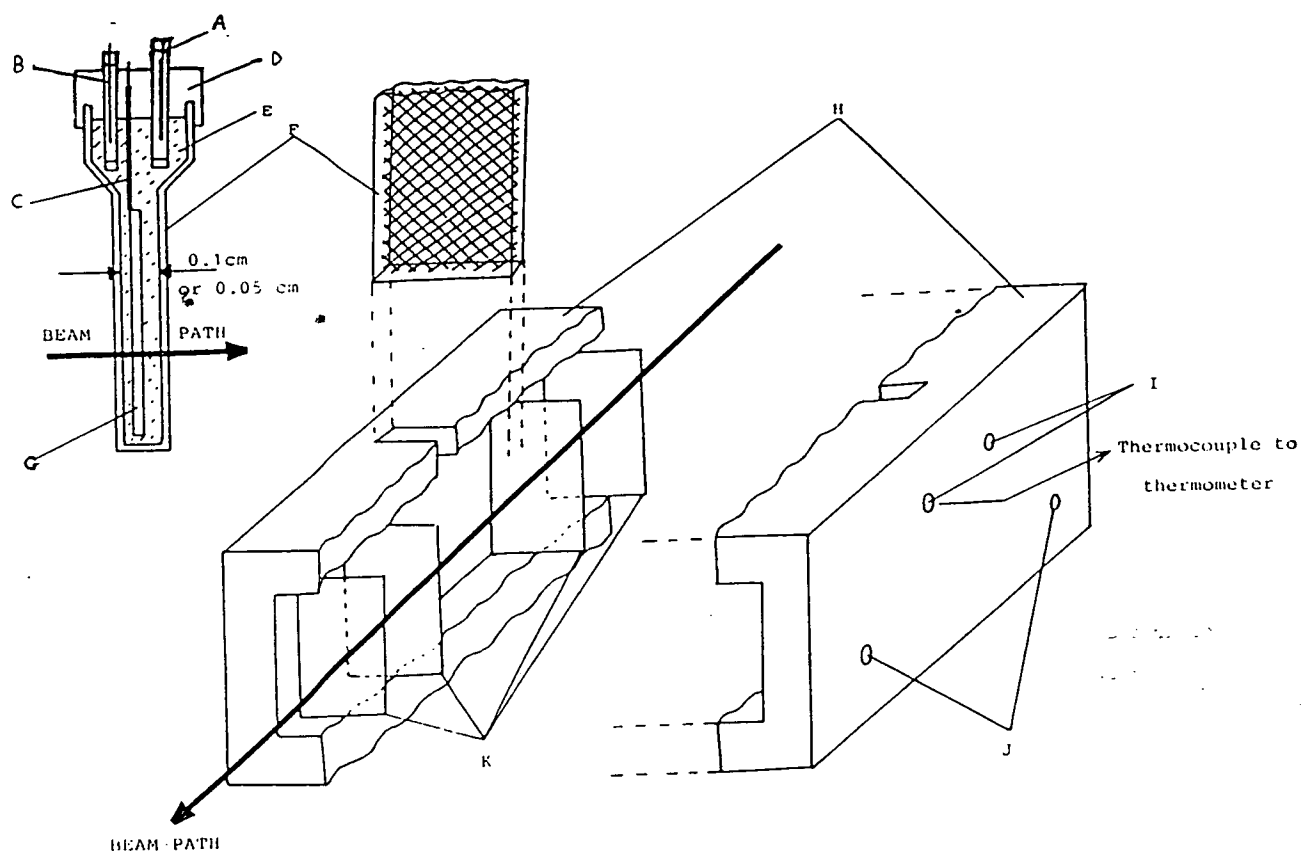


### A.3 Spectroelectrosynthesis

This technique is in effect a controlled-potential electro-synthesis in which spectroscopic data on the reaction product may be obtained directly. The Chilled Optically Transparent Thin Layer Electrode (O.T.T.L.E.) cell used was designed and built in the Department of Chemistry, University of Edinburgh, in accordance with the original principles of Murray et al <sup>(2)</sup>. The O.T.T.L.E. cell consists of a fine Pt gauze working electrode (transparency ca 40%) fitted into a standard infrasil quartz UV/Vis/NIR cell of 0.05cm pathlength. A quartz extension fitted to the top of the cell functions as a solution reservoir. The reservoir also contains a Pt wire auxiliary electrode and Ag/AgCl reference electrode, both protected from the bulk solution by a porous glass frit.

The assembly is fitted into a gas-tight poly(tetrafluoroethylene) double glazed cell block (see Figure A.6). Temperature control, monitored by a thermocouple/digital thermometer, is maintained by the passage of dry, pre-cooled nitrogen gas between the inner pair of quartz windows and the quartz cell assembly. The inner pair of quartz windows are prevented from fogging by the passage of dry nitrogen between the inner and outer windows, thus preventing contact of air with any cooled surface.

Figure A.6: O.T.T.L.E. Cell



- A Counter Electrode
- B Reference Electrode
- C Working Electrode connection protected from bulk solution by PTFE sleeve
- D PTFE cell cap
- E Test solution, deoxygenated with Ar or N<sub>2</sub>
- F 0.1cm Infrasil Quartz cell containing platinum grid working electrode
- G Platinum grid working electrode
- H PTFE cell block
- I Variable Temperature nitrogen inlet ports
- J Dry nitrogen inlet ports (to prevent fogging of inner quartz windows)
- K Infrasil Quartz cell block windows

Solutions of the test species are purged with dry nitrogen or argon and electrolysed at the Pt minigrad working electrode of the O.T.T.L.E. cell which is placed directly in the beam of the spectrophotometer. The progress of the electrolysis can be monitored both spectroscopically to the limiting absorption curve and by the decay of the current to a consistent residual value. A successful spectroelectrochemical experiment requires regeneration of the starting spectrum on reversal of the electrogenerating potential (i.e. a chemically reversible process).

#### References

1. A. J. Bard and L. R. Faulkner, "Electrochemical Methods", John Wiley & Sons Inc. (New York), 1980.
2. W. R. Heinemann, R. W. Murray and G. W. O'Dom, Anal. Chem., 1967, 39, 1666.

Appendix 2

Abbreviations

[9] aneS3	1,4,7 trithianonane
acac	acetylacetonate
bipy	2,2 <sup>1</sup> - bipyridine
COD	cyclooctadiene
DMF	dimethylformamide
DMSO	dimethylsulphoxide
dppb	(1,2-diphenylphosphine) butane
dppm	(1,2-diphenylphosphine) methane
en	ethylenediamine
e.s.r.	electron spin resonance
Et	ethyl
FAB	Fast Atom Bombardment
Fc	ferrocene
Hz	hertz
Me	methyl
NHE	Normal Hydrogen Electrode
NIR	near infra red
n.m.r.	nuclear magnetic resonance
OAc	acetate
Ph	phenyl
p.p.m.	parts per million
<sup>i</sup> Pr	iso propyl
Py	pyridine
pz	pyrdzine
sacsac	di-thioacetylacetonate
SCE	Standard Calomel Electrode
TBA	Tetrabutylammonium
THF	tetrahydrofuran

TMC	tetramethyl cyclam
p-tol	4-methylphenyl
UV	ultra violet
Vis	Visible

Lecture Courses and Meetings AttendedLectures

"The Electronic Structures of Inorganic Complexes"

Dr L. J. Yellowlees

"Lanthanides and Actinides", Dr S. Cradock

"Mass Spectrometry", Professor K. R. Jennings

"Multipulse N.M.R. Spectroscopy", Dr I. H. Sadler

"Recent Developments in Electrochemistry"

Drs H. H. Girault and G. A. Heath

"X-Ray Crystallography", Drs R. O. Gould and A. J. Blake

"Recent Developments in Electrochemistry"

Drs H. H. Girault and L. J. Yellowlees

Meetings

R. S. C. Dalton, Scottish Division Meeting ,

University of Strathclyde 1986, Heriot Watt

University 1987, St. Andrews University 1988.

Butler Meeting,

University of Edinburgh 1987, 1988.

R. C. C. Dalton Autumn Meeting,

Birmingham University 1938.

University of Strathclyde Inorganic Club Conferences,

1986, 1987.

Departmental and research seminars and colloquia.